Buckling of Woven Fibre and Graphene Platelet Reinforced Nanocomposite Laminates

Kiren Sewnath

In fulfilment of the academic requirements for the degree of Master of Science in Mechanical Engineering, College of Agriculture, Engineering and Science, University of KwaZulu-Natal.

Supervisor: Prof. Sarp Adali

Co-Supervisor: Dr. Georgios Drosopoulos

January 2021

DECLARATION 1 - PLAGIARISM

As the candidate's Supervisor, I agree to the submission of this thesis.

Signed: _____ Date: __30 December 2019_____

Professor Sarp Adali

As the candidate's Co-supervisor I agree/do not agree to the submission of this thesis.

Signed: _____ Date: __30 December 2019_____

Dr. Georgios Drosopoulos

I, Kiren Sewnath, declare that

1. The research reported in this thesis, except where otherwise indicated, is my original research.

2. This thesis has not been submitted for any degree or examination at any other university.

3. This thesis does not contain other persons' data, pictures, graphs or other information, unless specifically acknowledged as being sourced from other persons.

4. This thesis does not contain other persons' writing, unless specifically acknowledged as being sourced from other researchers. Where other written sources have been quoted, then:

a. Their words have been re-written but the general information attributed to them has been referenced

b. Where their exact words have been used, then their writing has been placed in italics and inside quotation marks, and referenced.

5. This thesis does not contain text, graphics or tables copied and pasted from the Internet, unless specifically acknowledged, and the source being detailed in the thesis and in the References sections.

Signed: _____ Date: _____

Mr. Kiren Sewnath

DECLARATION 2 – PUBLICATIONS

Details of contributions to publications that form part and/or include research presented in this thesis:

1. K Sewnath, G Drosopoulos, S Adali, Effect of graphene platelet reinforcement on the buckling load of laminated woven fabric composites, in preparation

2. K Sewnath, G Drosopoulos, S Adali, Effect of fibre orientation on the buckling of graphene platelet-woven fabric reinforced composites, in preparation

Signed: _____ Date: _____

Mr. Kiren Sewnath

Acknowledgements

I would like to thank my supervisor, Professor Sarp Adali, for making this study possible and for his immense effort, support and guidance since the very beginning. The experience and knowledge he has in his field has proven invaluable.

I would also like to thank my co-supervisor, Dr Georgois Drosopoulos, for his guidance and motivation and for assisting with the necessary tools that have made this report possible.

Finally, I would like to thank my family and friends for their love, continued encouragement and support throughout the duration of this study.

Abstract

Composite materials are known for exhibiting high specific stiffness, strength and light weight. Their properties can be optimized by designers for a specific application. They currently have many applications in various industries such as aerospace, automotive and building industries. Fibre reinforced polymer composites are a large portion of the composite material market. The use of such materials has many advantages. Recently, nanosized reinforcements such as carbon nanotubes and graphene nanoplatelets have also been used as filler materials in composites. Graphene is one of the strongest materials available today and exhibits excellent mechanical properties. The study presented here is an investigation into the buckling of a woven glass fibre and graphene nanoplatelet reinforced epoxy composite. A laminate analogy is utilised. The analytical equations governing these types of laminates are presented and incorporated into Matlab, a computer simulation software that makes use of matrix implementations. The programme is then used to investigate the effects of various design parameters on the buckling load, by generating 2D and 3D graphs.

In this study, a laminate analogy is used for the woven glass fibres whereby undulation of the fibres is neglected, and the composite is regarded as an assembly of cross-ply laminates with woven fibres orientated at 90° to each other. The Halpin-Tsai equations are used to incorporate the graphene nanoplatelets into the epoxy matrix. The laminate that is investigated consists of 4 plies, each reinforced by woven glass fibres and graphene nanoplatelets. The laminate is symmetric about its midpoint, such that the two outer layers are identical, and the two middle layers are identical. Layer thicknesses are non-uniform and the reinforcements are distributed non-uniformly in the layers. The thickness ratio of the laminate is defined as the ratio of the total width of the outer layers to the entire laminate thickness. The governing equations of classical laminate theory for buckling of a simply-supported rectangular plate under biaxial loading are used to predict the critical buckling load of the laminate. The bending-twisting coupling terms are neglected.

The results generated display the influence of various design parameters on the buckling load. The design parameters investigated are the woven glass fibre volume fraction, woven glass fibre orientation, woven glass fibre balancing coefficient, graphene platelet weight fraction, laminate thickness ratio and laminate aspect ratio. The results show that the graphene nanoplatelets have a greater effect on the buckling load than the woven glass fibres. High graphene content can obscure the effect of the woven fibre orientation and laminate aspect ratio on the buckling load. At low graphene contents, a more concentrated fibre distribution in a single direction (warp or weft) is preferred for the buckling load. At higher graphene content, a more evenly balanced distribution is preferred. Furthermore, for high thickness ratios, more focus must be placed in the reinforcements in the outer layer of the laminate for a cost-effective design.

Table of Contents

List of Tables

List of Figures

Nomenclature

a	Length
b	Width
E_{11}	Longitudinal Elastic Modulus
E_{22}	Transverse Elastic Modulus
e	Width of One Layer
e_{wf}	Width of Weft Layer
e_{wp}	Width of Warp Layer
G_{12}	Longitudinal Shear Modulus
G_{23}	Transverse Shear Modulus
H	Laminate Thickness
k_m	Woven Fibre Balancing Coefficient (Middle Layer)
k_o	Woven Fibre Balancing Coefficient (Outer Layer)
N_0	Non-dimensional Critical Buckling Load
N_{cr}	Critical Buckling Load
N_x	Compressive Force in x-direction
N_y	Compressive Force in y-direction
ρ	Density
R	Aspect Ratio
τ	Thickness Ratio
Vf	Volume Fraction
Vf_{total_m}	Total Fibre Volume Fraction (Middle Layer)
Vf_{total_o}	Total Fibre Volume Fraction (Outer Layer)

Vf_{wf_m}	Weft Fibre Volume Fraction (Middle Layer)
Vf_{wf_o}	Weft Fibre Volume Fraction (Outer Layer)
Vf_{wp_m}	Warp Fibre Volume Fraction (Middle Layer)
Vf_{wp_o}	Warp Fibre Volume Fraction (Outer Layer)
W	Weight Fraction
W_{gpl_m}	Graphene Platelet Weight Fraction (Middle Layer)
W_{gpl_o}	Graphene Platelet Weight Fraction (Outer Layer)

1 Introduction

Composite materials are multiphase materials, obtained by artificially combining different materials together to achieve properties that the individual constituents themselves do not exhibit [1]. They are known for their unique properties, such as high specific stiffness, high specific strength, light weight and the fact that their properties can be tailored by designers to suit a certain application [2]. Composite materials have been in existence since ancient times and mankind had found applications for such materials even many centuries ago. Currently, they have a wide variety of applications in several different industries. They are used in aerospace, sporting goods, medical equipment, electronic equipment, automotive and building materials, among others [3]. As a result, their properties and behaviour under different conditions is of importance. A large portion of composite materials in use in engineering currently are fibre reinforced composite materials [2]. Common fibre reinforcements include carbon fibres, glass fibres and aramid fibres. These fibres may also be present in a composite in the form of a weave, or fabric. The use of woven fabrics as a reinforcement material has several advantages, including thicker fibre forms, ease of handling and improved fracture toughness [4]. A composite may consist of fibre reinforcement as well as nanoscopic reinforcement, such as nanotubes or nanoplatelets. Recently, graphene platelet reinforced composites are of high interest. These graphene reinforced composites are known to exhibit enhanced mechanical properties at weight fractions of graphene as low as 0.1% [5]. Several processes have been developed to manufacture these fibre and graphene reinforced polymer composites [2]. Furthermore, the way in which the properties of these composites are predicted in the design process has evolved as well [6]. Generally, analytical tools or numerical methods are used to predict the behaviour of these materials. The most widely used numerical tool used is finite element analysis [7]. Currently, the analytical approach in predicting the behaviour of these composites involves multiscale methods, where the overall macroscopic behaviour is dependent on the micromechanical interactions of the constituents [7].

1.1 Background

Textile composites such as woven fabric composites primarily find applications within aerospace, marine, transportation, construction and power generation industries [8]. For example, glass and carbon fibre fabrics infused with a polymer are used in aircraft propellers, turbine blades for wind power generation employ glass fabric reinforcements infused with thermoplastic and woven glass fibres infused in polypropylene are used in impact structures such as bumper beams in automotive vehicles [8]. There has been an enormous amount of work in the field of woven fabrics, however, there currently is no widely accepted analytical model that accurately describes all the properties of woven fabric mechanical behaviour and several approaches exist [9]. While glass fibre reinforced polymer composites exhibit excellent strength and high stiffness and have been used in structural applications in low temperatures, the development of many industries, such as aerospace and cryogenic equipment, have called for an even improved performance of these composites [10]. As a result, research has been

conducted into the use of nanoscale reinforcements incorporated with glass fibres in polymer composites. The number of nanomaterial-based discoveries in the recent century has grown significantly [11]. In the composite material industry, many nanoparticles have been used with fibres and matrices to form nanocomposite materials [11]. Some particles are added to improve mechanical properties for specific applications while others add multifunctionality such as conductivity [11]. One candidate that has already been considered as an added reinforcement in glass fibre reinforced polymers is carbon-nanotubes, due to their high Young's modulus, tensile strength and thermal conductivity [10]. However, graphene nanoplatelets have attracted significant attention recently, owing to their excellent physical and electronic properties [12]. They are one of the strongest materials available today, with a Young's modulus in the region of $1\,TPa$ [12]. Graphene nanoplatelets as nanofillers in composite materials can have a dramatic effect on the materials mechanical and thermal properties, even at very low quantities [12]. The applications of graphene and graphene reinforced composites are currently expanding, and they are finding their way into several industries [13]. However, these applications are precarious and as a result, many theoretical and computational studies must be carried out as investigative research prior to fabricating these composites [13].

1.2 Problem statement and objectives

Composite materials are used in various structural applications [3]. In many instances, structures made from composites may undertake high compressive loading. Buckling occurs when deflection or fracture of the structure occurs under compressive loading [14]. In such a circumstance, the critical buckling load of the composite is of importance. Therefore, the critical buckling load of a composite must be optimized for composite materials undergoing such compressive loads. Various methods exist for predicting the critical buckling load of composite materials in the design process. Generally, these are analytical tools or numerical methods [7]. The macroscopic behaviour of a composite structure is normally predicted by analysing the composite material as a laminate [14]. Woven fabrics used in composite materials have already proven to have distinct advantages. Furthermore, glass fibre reinforced materials are commonly in use and are known to perform well under compressive loading [15]. Graphene nanoplatelet reinforced composites have also been the subject of recent research owing to their exceptional mechanical properties at low weight fractions in laminates [5]. A hybrid composite consisting of both woven glass fibres and graphene nanoplatelets will thus increase the tailoring capability of the laminate.

The objectives of this dissertation are therefore:

- To use existing analytical tools dealing with woven glass fibre and nanoplatelet reinforced nanocomposites to predict the critical buckling load of a woven fibre and graphene platelet reinforced laminate.

- To develop a computer programme using Matlab that incorporates these analytical equations and generates solutions of these equations under different design parameters.
- To study the behaviour of the woven glass fibre and graphene platelet reinforced laminate under these different design parameters.

1.3 Methodology

The methodology used in this dissertation is outlined here. In chapter 1, the reader is introduced to the topic of composite materials and their applications. The research objectives and dissertation outline are then presented. In chapter 2, literature relevant to fibre and nanoscale reinforced composites is reviewed. The concept of laminates in composite material theory is presented and different factors that influence the behaviour of these laminates are discussed. Different analytical approaches that currently exist in predicting the properties of composite materials are then presented. The governing equation for buckling that will be used in the computer simulations in chapter 4 is also then presented. Chapter 3 outlines the laminate properties that is investigated in this dissertation. Namely, its geometry, constituents, stiffness terms and stiffness matrices. In chapter 4, the framework for the Matlab computer programme that was developed is presented. The analytical equations that were inputted into the programme are discussed. In chapter 5, the results from the Matlab simulation are presented. The critical buckling load of the specified laminate is predicted for various design parameters. Chapter 6 concludes the results of chapter 5 and highlights key findings of the dissertation. Shortcomings of the research and recommendations for future work are discussed as well.

2 Literature review

This chapter delves into relevant literature relating to composite materials. The aim is to develop an understanding of the current topic. An overview of composite materials that currently exist are presented. The correct terminology required for the analysis of composite materials is developed. Comparisons are given for different matrix materials and reinforcement materials that are currently used in the composite material industry. A brief overview of some applications for composite materials is presented. Thereafter, the study process for analysing the mechanical behaviour of a composite structure is discussed. The concept of laminates is introduced. Different approaches in the micromechanical modelling of laminates are discussed. The woven fibre laminate analogy and the Halpin-Tsai equations for determining the engineering constants of a laminate are presented. Lastly, classical laminate theory is discussed and the governing equation for buckling of a simply-supported, rectangular plate under biaxial loading is presented.

2.1 Composite materials: Overview

Composite materials are macroscopic, heterogenous and can be naturally occurring (for example, wood) or man-made. They are composed of two or more materials with a discrete and recognizable interface separating them [16]. This macroscale composite exhibits advantages that its individual constituents do not. A composite material can exhibit better strength, stiffness, fatigue life, toughness and thermal insulation, among others, than its individual components [11]. The per unit-density mechanical properties of these materials, such as elastic modulus, is often much greater than standard engineering metallic materials [11]. Not all of these mechanical properties are improved at the same time, and there is usually a conflict between two or more where one is improved, and one is weakened [17]. A trade-off is made in the design process in order to suit the design application. Figure 2.1 shows some of the characteristics of composites compared to conventional, monolithic materials. Designers can target some of the properties to be optimized [11]. The demand for composite materials is expected to continue to increase steadily as seen in the non-linear timescale of figure 2.2 showing the relative importance of four different classes of materials in engineering.

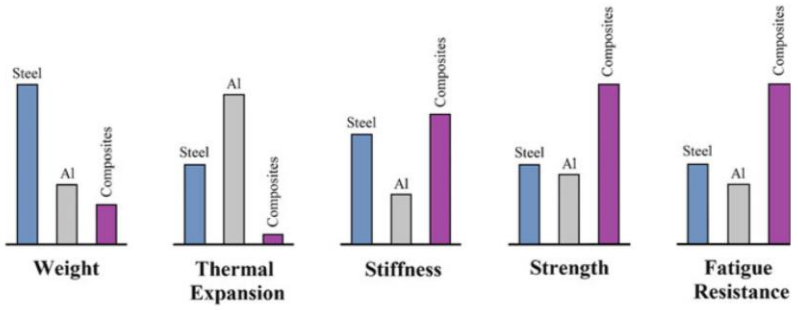

Figure 2.1: Conventional materials and composite materials [18]

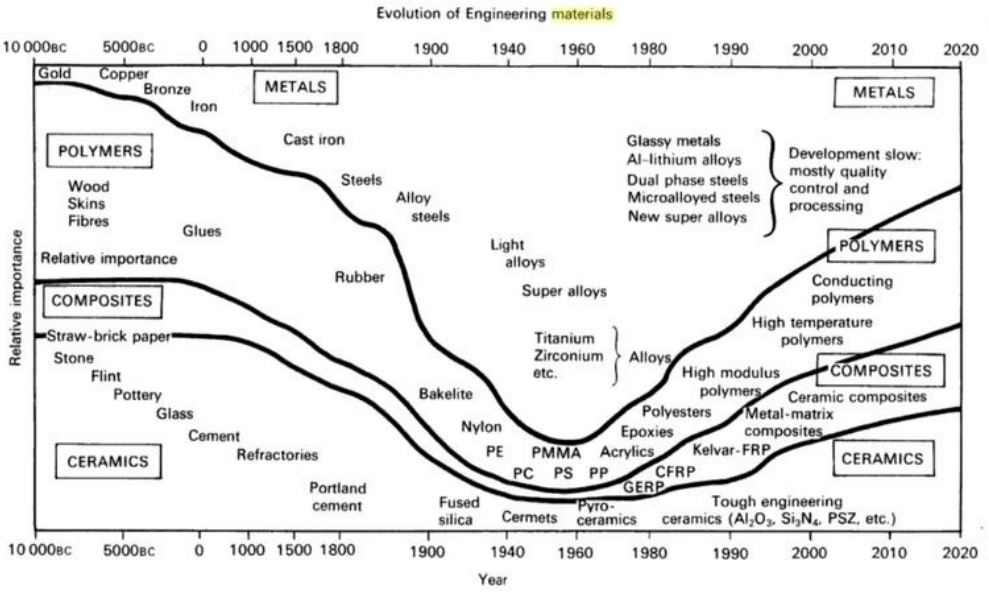

Figure 2.2: Relative importance of materials over time [19]

The composite materials constituents fall into two categories: the reinforcing phase and the matrix phase. The reinforcing phase material is usually in the form of fibres, particles or flakes and is embedded in the matrix material which is usually continuous [20]. The matrix material is usually present in a greater quantity than the reinforcement material in a composite [19]. Composite materials can thus be categorized into four types: fibrous composite materials that consist of fibre reinforcements in a matrix, laminated composite materials that consist of layers of materials, particulate composite materials that consist of particles in a matrix, or combinations of some or all of these [17]. Common types of reinforcement materials are long fibres of carbon or glass [21]. Polymeric and metallic fibres are also used commercially, and more recently, graphite fibres are of high interest in composite structures [17]. The matrix material may be ceramic, polymeric or metallic, however, the most prevalent type of matrix material in industrial applications are polymer-based. Resins are most common; however, thermoplastics are also used [21]. Composite materials which have their properties governed by the reinforcement material generally have better performance specifications than ones governed by the matrix material. The matrix serves to protect the reinforcement from environmental attack and transfer stresses [22].

2.1.1 Matrix phase

The matrix phase of a composite is generally of the ceramic, polymer, or metallic form.

2.1.1.1 Polymer matrix

Polymers have lower strength and elastic moduli than metals or ceramics and are generally used in lower temperature environments. They are, however, more resistant to chemicals than metals [18]. Common types of polymers used as matrix materials are thermosets and thermoplastics. Polyester and epoxy resins are common types of thermoset polymers used as matrices. Epoxy resins are generally

more expensive than polyesters but have lower shrinkage after curing, can be used under higher temperatures, are more resistant to moisture and have good adhesion with glass fibres [18]. Polyester is cheap and has good resistance to weathering, aging and chemicals. Polyester resins can shrink by up to 8% after curing [18]. Tests done on woven glass-fibre composites with epoxy and polyester resin matrices prove that epoxy resin matrix composites also exhibit less wear than polyester resin matrix composites under the same loading conditions [23]. [24] compares the characteristics of jute fibre reinforced composites that have been treated with NaOH using epoxy resins and polyester resins. The results in figure 2.3, show that epoxy resin composites exhibit better tensile strength and polyester resin composites exhibit better flexural strength.

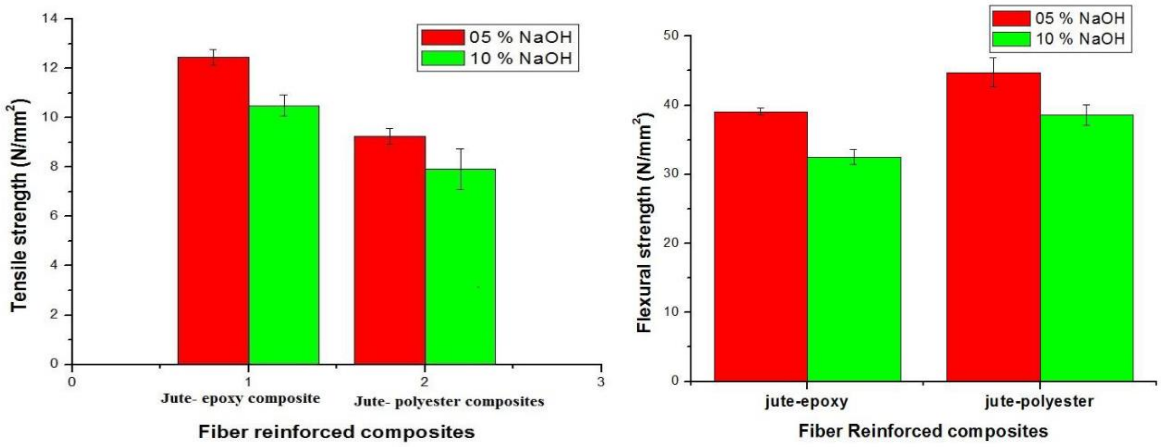

Figure 2.3: Tensile and flexural strength of epoxy and polyester resin composites [24]

2.1.1.2 Ceramic matrix

Ceramic materials have high elastic moduli and can withstand very high temperatures. They are also very hard and brittle. Ceramic matrices are generally used in fibre reinforced composites to improve fracture toughness [18]. Ceramic matrix composites only retain the monolithic ceramic's ability to withstand high temperatures if the reinforcements also have good high temperature properties [25]. Differences in coefficients of thermal expansion between the matrix and the reinforcement in ceramic matrix materials can also result in cracking of the matrix [25]. Figure 2.4 shows typical stress-strain curves for ceramic matrix composites compared to a monolithic ceramic. The area under the curves represent the energy of fracture and measures toughness. It can be concluded that both particle and fibre reinforced ceramic composites increase the toughness of the sample and that the fibre reinforced sample has a more desirable failure mode, as a significant load carrying capacity is maintained after failure occurs [25].

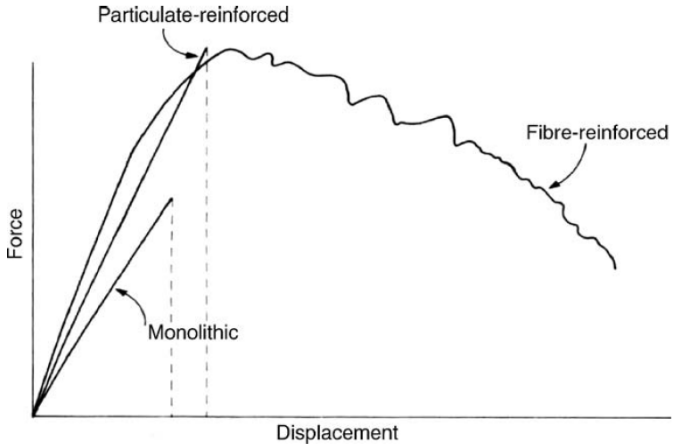

Figure 2.4: Stress-strain curves of ceramic matrix composites vs. monolithic ceramics [25]

2.1.1.3 Metallic matrix

Aluminium, magnesium, and titanium alloys are common materials used in metal matrix composites. Aluminium is the most common while titanium is used in applications where high performance is desired without regard to cost-effectiveness [25]. Reinforced materials rarely significantly improve stiffness of these composites, however, wear performance, resistance to thermal distortion and creep performance are important improvements that occur with metal matrix composites [21]. They also have higher specific moduli and specific strength than monolithic metals [25]. Metal matrix composites are attractive materials for aerospace and automotive industries [26]. Figure 2.5 shows the specific strength and specific elastic modulus of quasi-isotropic fibre reinforced composites with different metallic matrices, compared to monolithic metallic alloys.

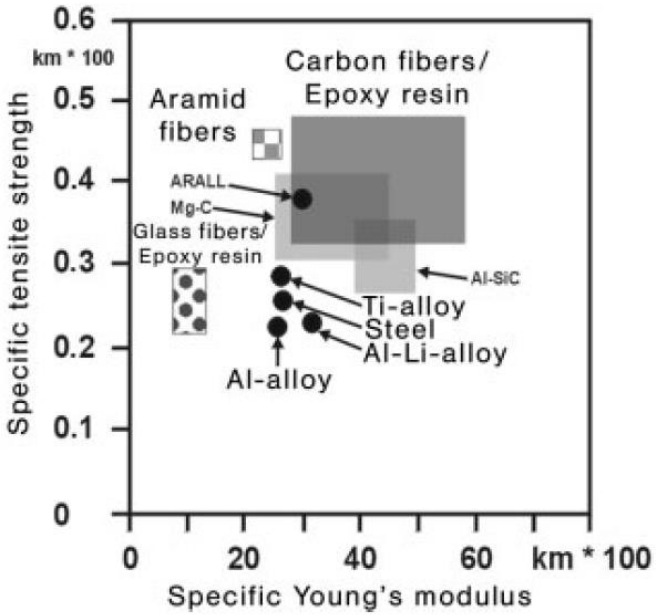

Figure 2.5: Specific strength and modulus of fibre reinforced metal matrix composites [27]

2.1.2 Reinforcement phase

Reinforcement materials in a composite can be in the form of particles, long fibres, short fibres, continuous fibres, flakes, whiskers, or sheets. Fibrous and nanoscopic reinforcement materials are discussed in the following sections.

2.1.2.1 Fibre-based reinforcements

Most reinforcements use a fibrous form as this is the strongest and stiffest form of materials [18]. Man-made reinforcement fibres include glass, Kevlar, boron, carbon, silicon carbide and alumina fibres [18]. Figure 2.6 shows the graph of Young's modulus vs tensile strength for some fibre reinforcement materials. The top right corner in this plot contains some high-performance fibres with high moduli and high tensile strength.

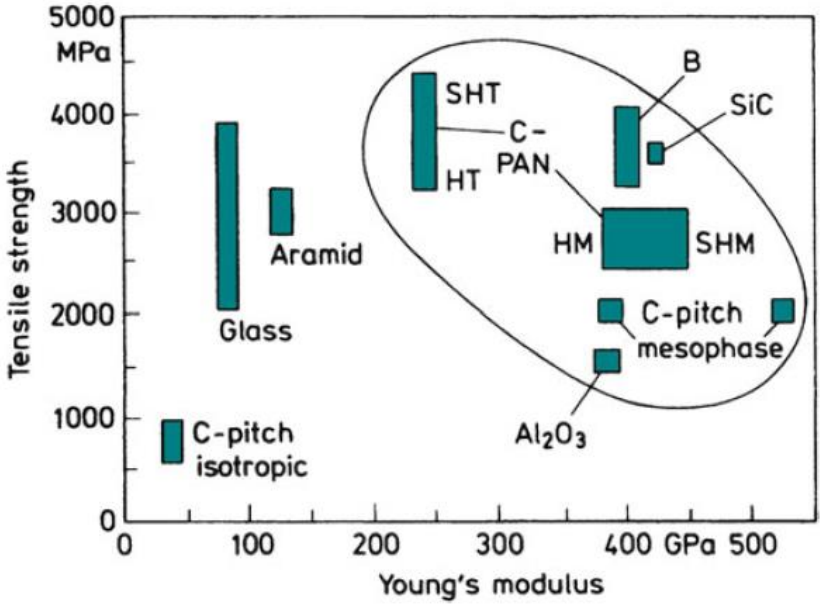

Figure 2.6: Young's modulus vs. Tensile strength for fibrous reinforcement materials [18]

Glass fibres are common. They are associated with low costs, simple production processes and excellent price/performance ratios [14]. Many different chemical compositions of glass fibres exist. Commonly, they are silica based and contain other oxides such as boron, calcium, sodium, iron and aluminium [18]. Industrial glass fibres are available as milled threads which have fibre lengths of about a few tenths of a millimetre, chopped strands which can be supplied in various different lengths, rovings or yarns, curly rovings, chopped strand mats and continuous strand mats and woven fabrics [14]. Glass fibres are commonly used in applications where low weight, high strength and high stiffness are important design parameters [28]. E glass fibres are good electrical insulators, C glass fibres have good chemical resistance and S glass fibres have high silica content and can withstand higher temperatures than other glass fibres [18]. E-glass fibres are the most widely used [14]. Table 2.1 gives the mechanical properties

of E-glass fibres and R-glass fibres. Glass fibres conserve their mechanical properties at temperatures up to 200°C, thus making them useful for reinforcing resins that have high thermal behaviour [14].

Table 2.1: Mechanical properties of E-glass fibres and R-glass fibres [14]

Characteristics	E-glass	R-glass
Density	$2600\ kg/m^3$	$2550\ kg/m^3$
Young's modulus	$73\ GPa$	$86\ GPa$
Tensile strength	$3400\ MPa$	$4400\ MPa$
Poisson's ratio	0.22	–

Carbon fibres are also common. They are found in numerous forms in industry, such as woven carbon fabrics, rovings and filaments [14]. Carbon in graphitic form can have an in-plane elastic modulus of 1000 GPa [18]. High modulus carbon fibres can be produced by carbonization of organic precursor fibres followed by graphitization [18]. Precursor fibres can be polyacrylonitrile (PAN), rayon, polyvinyl alcohol, polyamides and phenolics [18]. The resulting Young's modulus and tensile strength of the carbon fibre after graphitization depends on the temperature of the final heat treatment, seen in figure 2.7, with higher temperatures producing higher-modulus fibres [29].

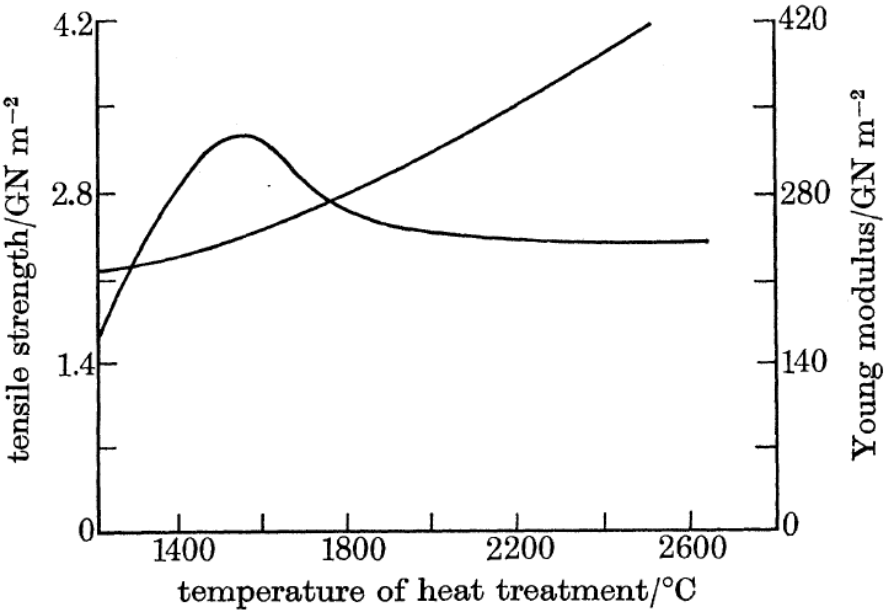

Figure 2.7: Strength and modulus of carbon fibres under different heat treatment temperatures [29]

Carbon fibres also exhibit a higher Young's modulus if the fibres are perfectly orientated (anisotropic) rather than isotropic. Figure 2.8 depicts the Young's modulus of various carbon fibres with different

precursors (Rayon-based, PAN-based and pitch-based fibres) under different orientation parameters, q. The parameter q is 1 for perfect orientation and 0 for isotropic fibres [18].

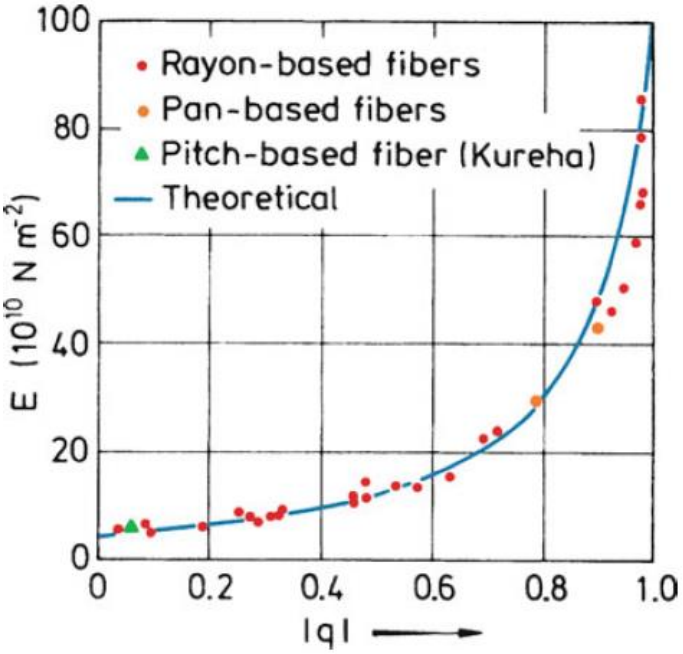

Figure 2.8: Young's modulus of carbon fibres under different orientation parameters [18]

Hybrid composites consisting of an incorporation of both carbon fibres and glass fibres in a single matrix also exist. The incorporation of both glass and carbon fibres in a composite can lead to improved impact resistance and increase the flexural modulus of the composite [30]. Aramid fibres, commonly known as Kevlar, are available as strands, woven fabrics and rovings and are known for their lightness, good resistance to shock and impact and damage tolerance [14]. They, however, exhibit low resistance to compression, buckling and bending. They are used as steel replacements in tires and pipes and for ballistic applications such as armoured jackets and helmets [14]. Boron fibres are known for their high cost compared to other fibres [18]. Because of their high-temperature manufacturing process, substrate materials that can be used to form the cores of boron fibres are limited to fine tungsten wires or carbon substrates [18]. Interest in strong, lightweight boron fibres has been exhibited by the aerospace industry, however these fibres face a lot of competition from more advanced carbon fibres [18].

2.1.2.2 Nanoscopic reinforcement

Any material can, in theory, be produced to a nano-scaled shape and size. Nanoscopic reinforcements help composites attain unique properties because of the reinforcement's nanometric dimensions [31]. Composites reinforced with microfibres and nanoscale reinforcements, such as nanotubes and nanoplatelets, are known as multiscale composites [32]. Carbon-nanotubes (CNT) are one such nanoscale reinforcement. They have excellent mechanical, electrical and thermal properties. They have a tensile strength of about 150 GPa, a Young's modulus of about 1000 GPa and are about three to five

times lighter than steel [33]. Tensile tests on a polymer matrix, CNT reinforced composite show that just 1.5% weight fraction of carbon-nanotubes in a laminate can increase the tensile modulus by 87% and increase the tensile strength by 69% [34]. Just 2% weight fraction of CNT in a woven glass fibre reinforced polymer matrix laminate can increase thermal conductivity of the composite by 42% [34]. In one study, adding just 0.3% of carbon-nanotubes to a polymer composite increased fracture toughness of the composite by 45% [35]. Combining carbon fibres with carbon-nanotubes in a polymer matrix composite material (CNTFRC) can lead to improved fibre/polymer interfacial load transfer [36]. Carbon-nanotube coated SiC woven fabric reinforced epoxy composites exhibit extremely enhanced out-of-plane mechanical and electrical properties [36]. Carbon nanotube, fibre reinforced polymer matrix composites under mechanical and electrical loading exhibit a significant decrease in deflection with a small percentage of carbon-nanotubes [32]. Graphene nanoplatelets (GNP) are another such nanosized reinforcement. Graphene is defined as short stacks of individual layers of graphite [37]. They can produce a dramatic improvement in composite material properties at low weight fractions. It has been shown that graphene-platelet enhanced epoxy composites have had their tensile modulus increased from 2.72 GPa to 3.36 GPa for just 6% weight fraction of graphene nanoplatelets in the composite [37]. [38] reports that, for 0.25% weight fraction of graphene in a graphene-nanoplatelet epoxy composite, tensile strength was increased by 17% and for 1% graphene weight fraction, tensile modulus was increased by 9.6%. A graphene-based polyvinyl alcohol composite had its Young's modulus increased nearly 10 times its original value by the addition of just 1.8% volume fraction of graphene nanosheets [39]. Composites reinforced with graphene nanoplatelets also exhibit enhanced compressive strength and in-plane shear properties [40]. Very small amounts of graphene platelets in a polymer matrix can greatly improve bending performance of nanocomposite beams [41]. Graphene nanofillers at low content can greatly improve the critical buckling loads of laminate plates. [42] reports that 1% of graphene platelet weight fraction in a functionally graded composite epoxy plate increased its critical buckling load by 555%. Small amounts of graphene platelets can also increase natural frequencies of composites and reduce forced vibration response [43]. Graphene platelets have higher specific surface area than carbon-nanotubes and exhibit enhanced nanoplatelet-matrix adhesion than carbon nanotubes, thus graphene platelets are superior nanoscale reinforcement materials in terms of enhancing tensile strength, Young's modulus, fracture energy, fracture toughness and resistance to fatigue crack growth than carbon nanotubes [44]. Hybrid graphene-carbon composites exist that combine graphene platelets and carbon-nanotubes in a single composite. One such composite prepared by [45] utilizes 0.1% weight fraction of carbon-nanotubes and 0.9% weight fraction of graphene nanoplatelets to improve the tensile strength of the epoxy by 35.4%, compared to an increase of only 0.9% in the tensile strength of the same composite without carbon-nanotubes. Another such carbon-nanotube and graphene platelet hybrid epoxy composite showed a 40% increase in tensile modulus and 36% increase in tensile strength of the composite compared to the neat epoxy [46].

2.1.3 Applications

Composite materials have a wide range of applications in several industries such as aerospace, electronics, biomedical automotive industries, civil and building industries [3]. It is possible that, at the going rate, carbon fibre reinforced plastics will contribute to more than 50% of the structural mass of aircraft [47]. E-glass fibre composites and hemp fibre composites have found an application in helicopter interiors, replacing steel electronic racks resulting in weight savings and lower disposal costs [48]. Polyether ether ketone matrix composites with 60% volume of carbon fibres are extensively used in aerospace applications [21]. There have proven to be various advantages of using polymer composites in various biomedical applications [49]. E-glass fibre reinforced composites are used in dentistry to substitute for metallic restorations because of they are biocompatible, have good chemical resistance and low cost [50]. Composite materials are also used in naval ships, space vehicles and re-entry vehicles [51]. Woven glass fibre polypropylene composites have found an application in the floor structure of automotive vehicles because of their weight savings compared to conventional metal structures [52]. Carbon composites and glass composites can be used as a replacement for marine steel in ship hulls [53]. Woven glass fibre epoxy composites can be used for multilayer circuit board materials [54]. Because of their unique and tailorable properties, composite materials are used in cryogenic applications such as support structures, vessels or insulation [55]. A breakdown of the markets for one type of composite material, namely glass fibre reinforced plastic, is shown in figure 2.9 [3].

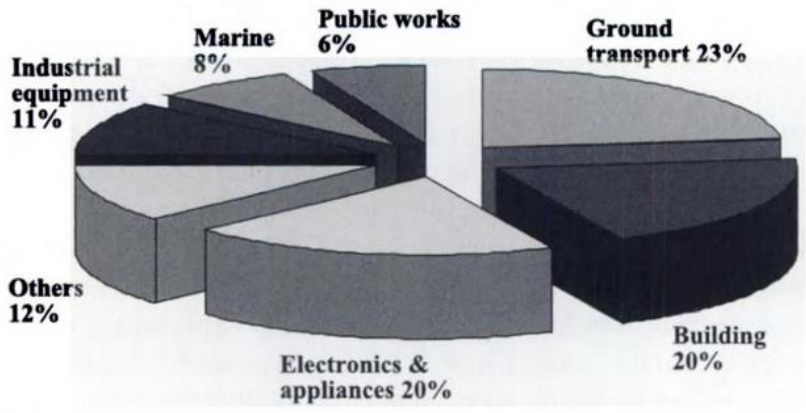

Figure 2.9: Breakdown of the market for glass fibre reinforced plastics [3]

2.2 Laminates

To study the behaviour of a composite material, one must study the behaviour of laminates. Laminates consist of layers, called laminae or plies, containing reinforcements and impregnated with resins that are stacked together in a predetermined arrangement [21]. The process of studying the behaviour of a laminate, called the macroscopic behaviour of the composite, involves first studying the micromechanical behaviour, or microscopic behaviour, of one layer of the laminate. Thereafter, classical tools of structural analysis can be adapted to study the macroscopic behaviour of composites.

Simple structures, such as beams or plates, can be analysed using analytical methods and complex structures can be analysed using finite element methods [14]. The process of analysing a composite structure is summarized in the schematic diagram in figure 2.10.

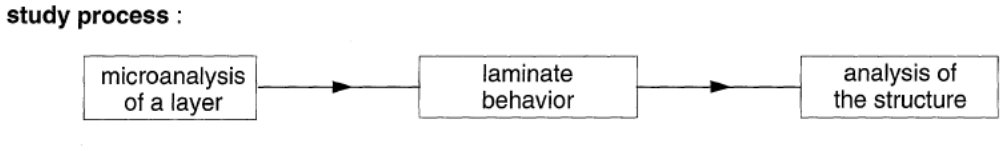

Figure 2.10: Process of analysing the mechanical behaviour of composite structures [14]

In theory, every type of laminate can be reduced to a basic laminate consisting of unidirectional fibres or cloth embedded in a matrix [14]. Laminates can be identified by using a common type of orientation code. Each layer is designated by the fibre orientation in the layer with respect to the x axis. Successive layers are separated with a "/" and successive layers of the same fibre orientation are represented by a numerical index [21]. The laminate in figure 2.11 is represented by the code [30/90_2/45/0/45] [14]. "S" can be used in the notation to designate the point of symmetry. Hybrid laminates use index symbols such as C or G to represent layers containing different materials, such as carbon and glass. Laminates containing layers of different thicknesses use indexed numerical values to indicate the thickness of each layer. $[30_G/90_C/0_{K0.25}]_S$ designates a symmetric laminate of 6 layers, with glass, carbon and Kevlar fibres orientated at 30°, 90° and 0° and with the Kevlar layer at a thickness a quarter the thickness of the other layers. The sequence $[0/90]_n$ is called a cross-ply laminate. Angle-ply laminates have plies of equal thicknesses with fibre orientations at $+\theta$ and $-\theta$ alternatively, such as [30/-30/-60/60].

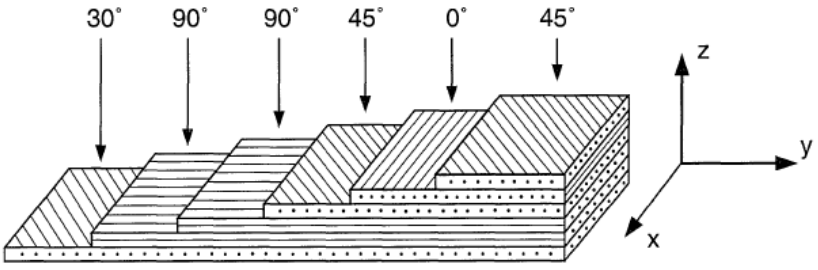

Figure 2.11: [30/90_2/45/0/45] stacked laminate [14]

2.2.1 Influencing factors on the mechanical properties of laminates

The factors discussed here, namely the laminate stacking sequence, fibre orientation and fibre volume fraction influence the mechanical properties of laminates and are areas that can be considered for optimization in the design of composite structures.

2.2.1.1 Stacking sequence

In practical applications, the ply orientations are limited to 0°, 90° and ±45° orientations and the lamina thicknesses are limited to integer multiples of the overall laminate thickness [56]. Thus, the stacking sequence of the laminate is an important design consideration and can alter the critical buckling load, tensile strength and delamination properties of a laminate [57]. Porosity of the laminate is also dependant on the stacking sequence [58]. Because the transverse properties of a unidirectional laminate are usually dominated by the matrix, they are usually unsatisfactory [59]. In fact, a laminate with more layers but a poor stacking sequence arrangement may perform worse, strength-wise, than a laminate with fewer layers but a good stacking sequence. Using an optimum ply stacking sequence can help strengthen these laminates. Methods used to optimize the stacking sequence include genetic algorithms, finite element analysis and integer programming. Buckling tests done on a theoretical 16 ply graphite epoxy laminate plate conclude that the optimal ply stacking sequence for low aspect ratios of the plate is when ply angles are 0° for uniaxial and biaxial loading and 90° for high aspect ratios and biaxial loading [56]. Another study used genetic algorithms to optimize the ply stacking sequence for buckling loads using a balanced symmetric graphite-epoxy laminate [60]. One buckling analysis study on laminated composite plates proved that laminates with the sequence $[0/\pm45/90]_S$ have lower buckling loads than laminates with the sequence $[0\pm<40|25|45>]_{2S}$ [61]. Tests done on a uniaxially loaded 8-ply carbon fibre reinforced plastic laminate with the stacking sequence equal to $[0_2/\pm45]_s$ and $[\pm45/0_2]_s$ proved that the greatest strength of the laminate was exhibited when fibres were orientated at 0° in the outer layers, parallel to the applied load, and the least strength was exhibited when fibres in the interior of the laminate were orientated at 0° to the applied load [62].

2.2.1.2 Fibre orientation

The orientation of the reinforcement in a composite, θ, alters its isotropy [19]. Since practical applications of fibre reinforced composites often require that the material undergo loading in different directions that are not always parallel to the fibres, fibre orientations in combination with the stacking sequence of a laminate can affect its tensile strength, critical buckling load, natural frequency and fracture toughness among other mechanical properties [63]. A study into the effect of fibre orientation on the fatigue behaviour of glass fibre reinforced polymer composites showed that increasing fibre angle with respect to the longitudinal axis of the composites resulted in a lower fatigue strength of the laminates [64]. Even slight fibre orientations, at $\theta = 1.2°$, were shown to influence the fracture toughness of fibre reinforced composites [65]. Numerous studies have been devoted to optimizing fibre orientations in laminates to maximize tensile strength or buckling loads. Figure 2.12, taken from a report on tests done on aluminium composites reinforced with steel wires and silica fibres show that fibre orientation (x-axis) can drastically affect tensile strength (y-axis) and the failure modes of composites [63]. A study on the effect of fibre orientation on the critical buckling load of simply-supported angle-ply laminate plates under axial and biaxial compression showed that a constant ply-angle throughout

all plies resulted in the maximum buckling loads [66]. Fibre orientation in a laminate also affects its thermal conductivity, with one study proving that higher fibre orientations decrease thermal conductivity of carbon fibre reinforced, glass matrix composites [67].

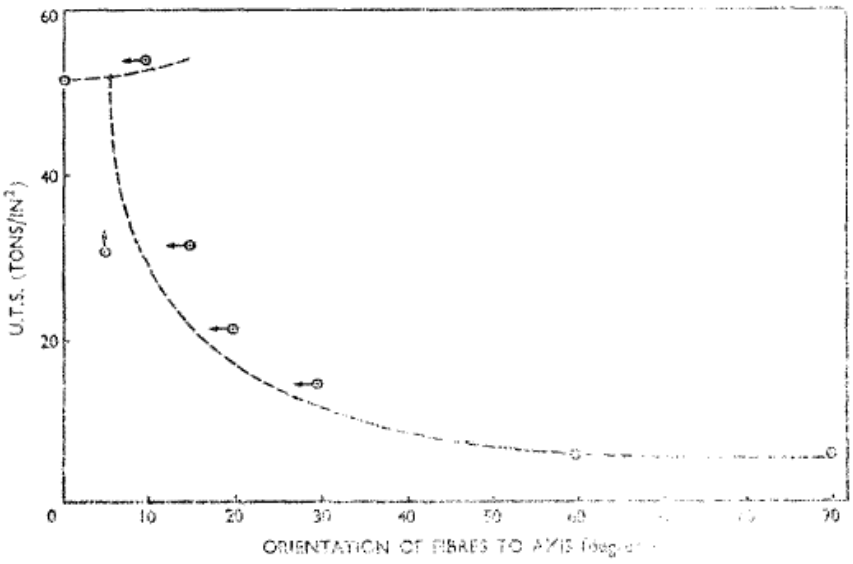

Figure 2.12: Effect of fibre orientation on the ultimate tensile strength of a composite [63]

2.2.1.3 Fibre volume fraction

Because the mechanical properties of composite materials are largely dominated by the reinforcement material properties, it is natural that the volume fraction of the reinforcement in the laminate alters its properties drastically. The volume fraction of a reinforcement material, Vf, consisting of fibres represents the ratio of the total volume of fibres in the composite, v_f, to the total composite volume, v_c [14]:

$$Vf = \frac{v_f}{v_c}$$

Eq. 2.1

The volume fraction of the reinforcement can also be expressed as a weight fraction, W. Weight fractions are easier to measure when the materials are being manufactured while volume fractions appear in theoretical models describing the behaviour of the material [14]. The weight fraction is defined as the ratio of the density of the reinforcement, ρ_f, to the density of the composite, ρ_c, multiplied by the volume fraction of the reinforcement, Vf [14]:

$$W = \frac{\rho_f}{\rho_c} Vf$$

Eq. 2.2

The fibre volume fraction of a laminate alters its tensile strength, buckling load, fatigue behaviour, thermal conductivity and its elastic and thermoelastic behaviour, among other properties. Optimization of this factor is thus a crucial part of the design process of a composite material and since, unintuitively, optimum values of mechanical properties may be exhibited at lower fibre volume fractions rather than higher ones, optimization of the fibre volume fraction can also result in cost-savings when designing composite materials [68]. In one study, higher glass fibre volume fractions (up to 45%) in a polymer composite resulted in higher fatigue strength [69]. Testing on glass fibre reinforced epoxy revealed that fracture toughness increased for lower glass fibre volume fractions [70]. A study on the effect of fibre volume fraction on the tensile strength of a natural fibre composite proved that the tensile strength of the composite varied between approximately 20-60 MPa for increasing fibre volume fractions from 0 to 0.5 [71]. The effect of fibre packing problems such as bunching, or clustering, of fibres during the manufacturing process is an important consideration. Delamination of the laminate may also occur under higher fibre volume fractions [72]. Because of this, it is sometimes difficult to achieve volume fractions above 0.7 in reality [21]. A study into the influence of fibre concentration on glass fibre reinforced polymer composites proved that the elastic modulus of the laminate increases linearly with fibre weight fraction up to 40%, and thereafter improvement in the modulus was considerably less, possibly due to fibre packing issues [73]. Further proving that more fibres may not always be beneficial than less fibres, a tensile strength on Kevlar-reinforced epoxy laminates proved that for fibre volume fractions up to 25%, tensile strength increased proportionally with fibre volume fraction, however for fibre volume fractions between 25% and 60%, the tensile strength remained independent of fibre volume fraction and for fibre volume fractions above 65%, tensile strength exhibited inverse proportionality to fibre volume content [74]. Testing done a hybrid Sic-particle and carbon fibre reinforced laminate for fibre volume fractions up to 60% proved that the maximum longitudinal tensile strength was exhibited when fibre volume fraction was at 33%, rather than higher values [68].

2.3 Micromechanics

A generalized Hooke's Law gives the relation between stress, σ, and strain, ε, in a medium by using a stiffness matrix, $\boldsymbol{C}$:

$$\sigma = \boldsymbol{C}\varepsilon$$

Eq. 2.3

For a unidirectional material, this relation reduces to [14]:

$$\begin{bmatrix}\sigma_1\\ \sigma_2\\ \sigma_3\\ \sigma_4\\ \sigma_5\\ \sigma_6\end{bmatrix} = \begin{bmatrix} C_{11} & C_{12} & C_{12} & 0 & 0 & 0 \\ C_{12} & C_{22} & C_{23} & 0 & 0 & 0 \\ C_{12} & C_{23} & C_{22} & 0 & 0 & 0 \\ 0 & 0 & 0 & \frac{1}{2}(C_{22}-C_{23}) & 0 & 0 \\ 0 & 0 & 0 & 0 & C_{66} & 0 \\ 0 & 0 & 0 & 0 & 0 & C_{66} \end{bmatrix} \begin{bmatrix}\varepsilon_1\\ \varepsilon_2\\ \varepsilon_3\\ \varepsilon_4\\ \varepsilon_5\\ \varepsilon_6\end{bmatrix}$$

Eq. 2.4

The engineering constants that are usually of concern in practice are the elastic modulus in the longitudinal direction E_{11}, elastic modulus in the transverse direction, E_{22}, Poisson's ratio for longitudinal tension, ν_{12}, longitudinal shear modulus, G_{12}, and transverse shear modulus G_{23}. These are given as functions of the stiffness terms in $\boldsymbol{C}$ [14]:

$$E_{11} = C_{11} - \frac{2C_{12}^2}{C_{22}+C_{23}}$$

Eq. 2.5

$$E_{22} = C_{22} + \frac{C_{12}^2(C_{22}-2C_{23}) + C_{11}C_{23}^2}{C_{12}^2 - C_{11}C_{22}}$$

Eq. 2.6

$$\nu_{12} = \frac{C_{12}}{C_{22}+C_{23}}$$

Eq. 2.7

$$G_{12} = C_{66}$$

Eq. 2.8

$$G_{23} = \frac{1}{2}(C_{22}-C_{23})$$

Eq. 2.9

The aim of the microanalysis of a laminate, which is the first step in analysing the behaviour a composite structure, is to determine these engineering constants of a single layer of a laminate as a function of the mechanical and geometric properties of the constituents of the laminate. Properties of the constituents of the laminate include the elastic moduli of the fibres and the matrix, E_f and E_m, Poisson's ratio of the fibres and the matrix, ν_f and ν_m, shear modulus of the fibres and the matrix, G_f and G_m, lateral compression modulus of the fibres and the matrix, K_f and K_m and the volume fractions of the fibres and the matrix, Vf_f and Vf_m. Different approaches exist, each with their own merits. One approach that has been studied previously consists of analysing the elastic field of an ellipsoidal inclusion in a matrix [75]. In a different approach, the evaluation of bounds approach, upper and lower bounds of engineering

constants are developed [18]. An approach based on fibre reinforced materials, resulted in bounds for the lateral compression modulus, K_{23}, the transverse shear modulus, G_{23}, and the longitudinal shear modulus, G_{12} [76]. A similar approach resulted in bounds for the longitudinal elastic modulus, E_{11}, and Poisson's ratio for longitudinal tension, ν_{12} [77]. When the bounds of these properties are equal, they give the exact solutions of the engineering constants. When they are equal or close enough to equal, they can be safely used to describe the material properties, however, they are often well separated [18].

2.3.1 Cylindrical cell approach

An exact solution approach exists for a particular arrangement of fibres by considering a cylindrical elementary cell representing the fibre, in a cylindrical cell representing the matrix, subject to uniform tension [78]. This approach leads to the following expressions for the longitudinal elastic modulus, E_{11}, Poisson's ratio, ν_{12}, longitudinal shear modulus, G_{12}, and lateral compression modulus, K_{23} [14]:

$$E_{11} = E_f V f_f + E_m(1 - V f_f)$$

Eq. 2.10

$$\nu_{12} = \nu_f V f_f + \nu_m\left(1 - V f_f\right)$$

Eq. 2.11

$$G_{12} = G_m \frac{G_f\left(1 + V f_f\right) + G_m\left(1 - V f_f\right)}{G_f\left(1 - V f_f\right) + G_m\left(1 + V f_f\right)}$$

Eq. 2.12

$$K_{23} = K_m + \frac{V f_f}{\frac{1}{k_f - k_m + \frac{1}{3}(G_f - G_m)} + \frac{1 - V f_f}{k_m + \frac{4}{3}G_m}}$$

Eq. 2.13

The expressions k_m and k_f are the bulk moduli of the matrix and the fibre, respectively. They are related to the elastic modulus, E, and Poisson's ratio, ν, as follows [14]:

$$k_m = \frac{E_m}{3(1 - 2\nu_m)}$$

Eq. 2.14

$$k_f = \frac{E_f}{3\left(1 - 2\nu_f\right)}$$

Eq. 2.15

A similar model, except considering a 3-phase cylinder consisting of the matrix, fibres and the equivalent homogenous material surrounding them, leads to the expression for the transverse shear modulus, G_{23} [79]:

$$G_{23} = G_m \left(1 + \frac{V f_f}{\frac{G_m}{G_f - G_m} + \frac{k_m + \frac{7}{3}G_m}{2k_m + \frac{8}{3}G_m}\left(1 - V f_f\right)} \right)$$

Eq. 2.16

For glass and carbon fibre composites, the transverse elastic modulus, E_{22}, is well approximated by [14]:

$$E_{22} = \frac{2}{\frac{1}{2K_{23}} + \frac{1}{2G_{23}} + \frac{2\nu_{12}^2}{E_{11}}}$$

Eq. 2.17

2.3.2 Halpin-Tsai equations

Using the cylindrical cell approach and the law of mixtures to ascertain the longitudinal elastic modulus, E_{11}, and the Poisson's ratio, ν_{12}, a generalized formula has been developed to determine the transverse elastic modulus, E_{22}, and other engineering moduli [80]:

$$\frac{M}{M_m} = \frac{1 + \xi\eta V f_f}{1 - \eta V f_f}$$

Eq. 2.18

M is the modulus to be evaluated (E_{22}, in this case), and M_m is the modulus of the matrix (E_m, in this case). The coefficient η is evaluated by:

$$\eta = \frac{\left(\frac{M_f}{M_m}\right) - 1}{\left(\frac{M_f}{M_m}\right) + \xi}$$

Eq. 2.19

M_f is the value of M corresponding to the fibres (E_f, in this case) and ξ is a factor determined by the geometry and arrangement of the fibres and the modulus being evaluated [14]. Because ξ depends on the geometry of the reinforcement phase, its value changes in cases where the reinforcements are square fibres, rectangular fibres, or platelets and hence the Halpin-Tsai equation takes into account the influence of the geometry of the reinforcement on the engineering moduli [81].

2.3.3 Woven fabrics laminate analogy

Several methods for investigating the elastic properties of woven fabric composites exist. The fibre undulation model considers the undulation of fibres in the analysis of the elastic properties of woven fabrics [82]. The bridging model is used for satin-weave fabrics, where undulation and continuity of fibres is taken into consideration along the loading direction [83]. The mosaic model, which treats the fabric composite as an assembly of cross-ply laminates (laminates whose plies consists of fibres alternating between 0° and 90° orientation) is a simple model which neglects the undulation of fibres [82]. Figure 2.13 depicts the laminate analogy of a woven fabric deconstructed into plies containing fibres at 0° and 90° orientation with respect to the longitudinal axis, L [14]. The fibres aligned in the longitudinal direction, L, are called the warp fibres and the fibres aligned in the transverse direction, T, are called the weft fibres. The thicknesses of the warp layer and the weft layer are denoted e_{wp} and e_{wf} respectively:

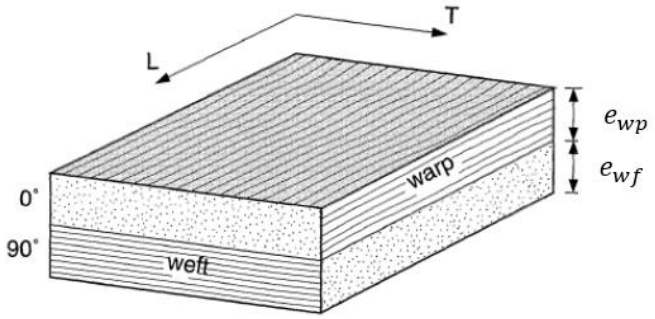

Figure 2.13: One layer of a woven fabric decomposed to the warp and weft layers [14]

The methods described in chapter 2.3.1, using the cylindrical cell approach, can be used to determine the engineering constants of each layer (warp and weft) [84]. The warp layer is thus described by its longitudinal elastic modulus, $E_{11_{wp}}$, transverse elastic modulus, $E_{22_{wp}}$, Poisson's ratio for longitudinal tension, $\nu_{12_{wp}}$, and longitudinal shear modulus, $G_{12_{wp}}$. Similarly, the weft layer is described by its longitudinal elastic modulus, $E_{11_{wf}}$, transverse elastic modulus, $E_{22_{wf}}$, Poisson's ratio for longitudinal tension, $\nu_{12_{wf}}$, and longitudinal shear modulus, $G_{12_{wf}}$. A balancing coefficient, k, gives the ratio of threads in the warp direction to threads in the weft direction by their volume, v_{wp} and v_{wf} [14]:

$$k = \frac{v_{wp}}{v_{wp} + v_{wf}}$$

Eq. 2.20

For a woven fabric with $k = 0.5$, the fabric contains equal volumes of fibres in the warp and weft direction and is balanced with respect to the warp and weft fibres [14]. The thickness of the warp and weft layers, e_{wp} and e_{wf}, is a function of the woven fibre balancing coefficient, k, and the total lamina thickness, e:

$$e_{wp} = ke$$

Eq. 2.21

$$e_{wf} = (1-k)e$$

Eq. 2.22

The volume fraction of the warp layer, V_{wp}, is the ratio of the volume of the warp fibres to the total volume of the entire lamina (containing both warp and weft fibres). The volume fraction of the weft layer, V_{wf}, is the ratio of the weft fibres to the volume of the entire lamina. Thus $V_{ftot} = V_{wp} + V_{wf}$ is the total volume fraction of all fibres (both the warp and weft fibres) for the lamina. By defining the parameters α_{wp} and α_{wf} such that:

$$\alpha_{wp} = \frac{1}{1 - \left(\frac{E_{22_{wp}}}{E_{11_{wp}}}\right)\nu_{12_{wp}}^2}$$

Eq. 2.23

$$\alpha_{wf} = \frac{1}{1 - \left(\frac{E_{22_{wf}}}{E_{11_{wf}}}\right)\nu_{12_{wf}}^2}$$

Eq. 2.24

Then the expressions for the in-plane moduli of a lamina of woven fabric, E_{11}, E_{22}, ν_{12} and G_{12}, are expressed as functions of $E_{11_{wp}}$, $E_{22_{wp}}$, $E_{11_{wf}}$, $E_{22_{wf}}$, $\nu_{12_{wp}}$, $\nu_{12_{wf}}$, $G_{12_{wp}}$, $G_{12_{wf}}$, and k [14]:

$$E_{11} = (1-\alpha)\left(k\alpha_{wp}E_{11_{wp}} + (1-k)\alpha_{wf}E_{22_{wf}}\right)$$

Eq. 2.25

$$E_{22} = (1-\alpha)\left(k\alpha_{wp}E_{22_{wp}} + (1-k)\alpha_{wf}E_{11_{wf}}\right)$$

Eq. 2.26

$$\nu_{12} = \frac{k\alpha_{wp}\nu_{12_{wp}}E_{22_{wp}} + (1-k)\alpha_{wf}\nu_{12_{wf}}E_{22_{wf}}}{k\alpha_{wp}E_{22_{wp}} + (1-k)\alpha_{wf}E_{11_{wf}}}$$

Eq. 2.27

$$G_{12} = kG_{12_{wp}} + (1-k)G_{12_{wf}}$$

Eq. 2.28

The parameter α is calculated by [14]:

$$\alpha = \frac{\left[k\alpha_{wp}v_{12_{wp}}E_{22_{wp}} + (1-k)\alpha_{wf}v_{12_{wf}}E_{22_{wf}}\right]^2}{\left[k\alpha_{wp}E_{11_{wp}} + (1-k)\alpha_{wf}E_{22_{wf}}\right]\left[k\alpha_{wp}E_{22_{wp}} + (1-k)\alpha_{wf}E_{11_{wf}}\right]}$$

Eq. 2.29

Curvature of the threads and misalignment of the threads are not taken into consideration by these formulae [14].

2.4 Classical laminate theory

The classical laminate theory is based on a first order model of the displacement field of a laminate plate and allows for the elastic behaviour of a multi-layered orthotropic material to be calculated by using the properties of a single layer [85]. Classical laminate theory neglects the effects of transverse shear [14].

2.4.1 Reduced stiffness matrix

The reduced stiffness matrix in the principal directions of a laminate for the k^{th} layer is [86]:

$$Q_k = \begin{bmatrix} Q_{11} & Q_{12} & 0 \\ Q_{12} & Q_{22} & 0 \\ 0 & 0 & Q_{66} \end{bmatrix}$$

Eq. 2.30

The terms inside this matrix are expressed as functions of the layer's longitudinal elastic modulus, E_{11}, transverse elastic modulus, E_{22}, Poisson's ratio, ν_{12}, and longitudinal shear modulus, G_{12} [14]:

$$Q_{11} = \frac{E_{11}}{1 - \left(\frac{E_{22}}{E_{11}}\right)\nu_{12}^2}$$

Eq. 2.31

$$Q_{22} = \frac{E_{22}}{1 - \left(\frac{E_{22}}{E_{11}}\right)\nu_{12}^2}$$

Eq. 2.32

$$Q_{12} = \nu_{12}Q_{22}$$

Eq. 2.33

$$Q_{66} = G_{12}$$

Eq. 2.34

These reduced stiffness terms referred to a separate set of axes that do not coincide with the principal axes and that make an angle θ with the principal axes is given by [14]:

$$\bar{Q}_{11} = Q_{11}\cos^4\theta + Q_{22}\sin^4\theta + 2(Q_{12} + 2Q_{66})\sin^2\theta\cos^2\theta$$

Eq. 2.35

$$\bar{Q}_{22} = Q_{11}\sin^4\theta + 2(Q_{12} + 2Q_{66})\sin^2\theta\cos^2\theta + Q_{22}\cos^4\theta$$

Eq. 2.36

$$\bar{Q}_{12} = (Q_{11} + Q_{22} - 4Q_{66})\sin^2\theta\cos^2\theta + Q_{12}(\cos^4\theta + \sin^4\theta)$$

Eq. 2.37

$$\bar{Q}_{66} = \big(Q_{11} + Q_{22} - 2(Q_{12} + 2Q_{66})\big)\sin^2\theta\cos^2\theta + Q_{66}(\sin^4\theta + \cos^4\theta)$$

Eq. 2.38

2.4.2 Constitutive equation

The constitutive equation of a laminated plate gives the relationship between the applied forces, N_x, N_y and N_{xy}, and the moments, M_x, M_y and M_{xy} and the midplane strains, ε^0_{xx}, ε^0_{yy} and γ^0_{xy} and the midplane curvatures, κ_x, κ_y and κ_{xy} [14]:

$$\begin{bmatrix} N_x \\ N_y \\ N_{xy} \\ M_x \\ M_y \\ M_{xy} \end{bmatrix} = \begin{bmatrix} A_{11} & A_{12} & A_{16} & B_{11} & B_{12} & B_{16} \\ A_{12} & A_{22} & A_{26} & B_{12} & B_{22} & B_{26} \\ A_{16} & A_{26} & A_{66} & B_{16} & B_{26} & B_{66} \\ B_{11} & B_{12} & B_{16} & D_{11} & D_{12} & D_{16} \\ B_{12} & B_{22} & B_{26} & D_{12} & D_{22} & D_{26} \\ B_{16} & B_{26} & B_{66} & D_{16} & D_{26} & D_{66} \end{bmatrix} \begin{bmatrix} \varepsilon^0_{xx} \\ \varepsilon^0_{yy} \\ \gamma^0_{xy} \\ \kappa_x \\ \kappa_y \\ \kappa_{xy} \end{bmatrix}$$

Eq. 2.39

Grouping the force, moments, strains and curvature terms into matrices:

$$\begin{bmatrix} \boldsymbol{N} \\ - \\ \boldsymbol{M} \end{bmatrix} = \begin{bmatrix} \boldsymbol{A} & | & \boldsymbol{B} \\ - & - & - \\ \boldsymbol{B} & | & \boldsymbol{D} \end{bmatrix} \begin{bmatrix} \varepsilon^0 \\ - \\ \kappa \end{bmatrix}$$

Eq. 2.40

Matrix $\boldsymbol{A}$ is the stretching stiffness matrix, matrix $\boldsymbol{B}$ is the coupling stiffness matrix and matrix $\boldsymbol{D}$ is the bending stiffness matrix [14]. The coupling stiffness matrix $\boldsymbol{B} = 0$ when the laminate is geometrically symmetric of its mechanical properties and orientations [14]. The terms A_{16} and A_{26} induce tension-shear couplings and D_{16} and D_{26} induce bending-twisting couplings [14]. In the case where $A_{16} = A_{26} = 0$, the laminate is said to be balanced [87]. In the case where the laminate consists of orthotropic or isotropic plies and the principal material axes are parallel to the laminate plate axes, then $D_{16} = D_{26} = 0$, and the laminate being considered is termed specially orthotropic [88]. The inclusion of the D_{16} and D_{26} terms when they are non-zero complicates the analysis of the laminate and they are often neglected from the analysis [88]. For example, in the case of symmetric laminates, neglecting the bending-twisting coupling results in simple expressions for the buckling load and deformation [89]. By

defining h_n as the distance from the midpoint of the laminate to the top of the n_{th} layer, the $\boldsymbol{A}$, $\boldsymbol{B}$ and $\boldsymbol{D}$ matrices are evaluated as follows for a laminate of k layers:

$$A_{ij} = \sum_{n=1}^{k} (h_n - h_{n-1})\left(Q_{ij}\right)_n$$

Eq. 2.41

$$B_{ij} = \frac{1}{2}\sum_{n=1}^{k} (h_n^2 - h_{n-1}^2)\left(Q_{ij}\right)_n$$

Eq. 2.42

$$D_{ij} = \frac{1}{3}\sum_{n=1}^{k} (h_n^3 - h_{n-1}^3)\left(Q_{ij}\right)_n$$

Eq. 2.43

2.5 Buckling

The phenomenon of buckling occurs when a loaded beam or plate undergoes a compressive load such that fracture or a large deflection of the beam or plate occurs [14]. The governing equations of classical laminate theory apply to the analysis of buckling of a laminate. Unique solutions of the governing equations are given for different boundary conditions of a laminate plate [14]. A laminate plate may be simply supported, clamped or free at its edges. Laminates with different edge conditions have different buckling strengths [90]. A laminate plate may have each of its edges in a different boundary condition, such two clamped edges, one simply supported edge and one free edge [91].

2.5.1 Simply-supported rectangular plate under biaxial loading

Assuming the bending-twisting coupling terms D_{16} and D_{26} are negligible and neglecting shear ($N_{xy} = 0$), the governing equation based on classical laminate theory for a symmetric laminate simply supported on all its edges under biaxial loading (N_x and N_y) is given by [87]:

$$D_{11}\partial^4 w_o + 2(D_{12} + 2D_{66})\frac{\partial^4 w_o}{\partial x^2 \partial y^2} + D_{22}\frac{\partial^4 w_o}{dy^4} = N_x\frac{\partial^2 w_o}{dx^2} + N_y\frac{\partial^2 w_o}{dy^2}$$

Eq. 2.44

For a plate with width a and length b, the solution for w that satisfies all boundary conditions is [14]:

$$w_o(x, y) = A_{mn}\sin\left(\frac{m\pi x}{a}\right)\sin\left(\frac{n\pi y}{b}\right)$$

Eq. 2.45

The buckling load is thus a function of m and n, which are the number of half-waves in the x and y direction respectively [87]. By defining the aspect ratio of the rectangular plate as $R = a/b$, and the buckling ratio as $\alpha_b = N_y/N_x$, then the critical buckling load $N_{cr} = -N_x$ is given by [87]:

$$N_{cr} = \frac{\pi^2(D_{11}m^4 + 2(D_{12} + 2D_{66})m^2n^2R^2 + D_{22}n^4R^4)}{a^2(m^2 + \alpha_b n^2R^2)}$$

Eq. 2.46

The values of m and n determine the mode of buckling, and the buckling load of interest is the one that corresponds to the values of m and n that lead to the lowest values of N_{cr} [14].

3 Laminate description

The laminate under consideration for this dissertation is a 4-ply, woven glass fibre and graphene platelet reinforced symmetric nanocomposite. The reinforcements are non-uniformly distributed in the layers and the layer thicknesses are non-uniform as well. In this chapter, a detailed description of the laminate is presented. The geometry of the laminate is discussed, and the relevant terminology is developed. Equations for the reduced stiffness terms, stretching stiffness matrix, coupling stiffness matrix and bending stiffness matrix of the laminate are developed. Lastly, the compressive loading of the laminate is discussed.

3.1 Geometry

The symmetric woven fibre and graphene reinforced composite plate consists of four layers, shown in figure 3.1: two middle layers (shown in red) that are identical and two outer layers (shown in blue) that are identical. The layers are labelled from $n = 1$ to $n = 4$, starting from the bottom most layer. The layers are depicted with their corresponding warp and weft fibres. Because the two middle layers are identical, the fibre content, graphene content and fibre orientation in these layers are the same and thus they are referred to collectively as the middle layer. The same applies for the two outer layers and they are referred to collectively as the outer layer. Thickness of the laminate is denoted by H, thickness of one outer layer as e_o and thickness of one middle layer as e_m. Thus, $H = 2e_o + 2e_m$. The fibre orientation in the outer layers are is denoted as θ_o and the fibre orientation in the middle layers is denoted as θ_m.

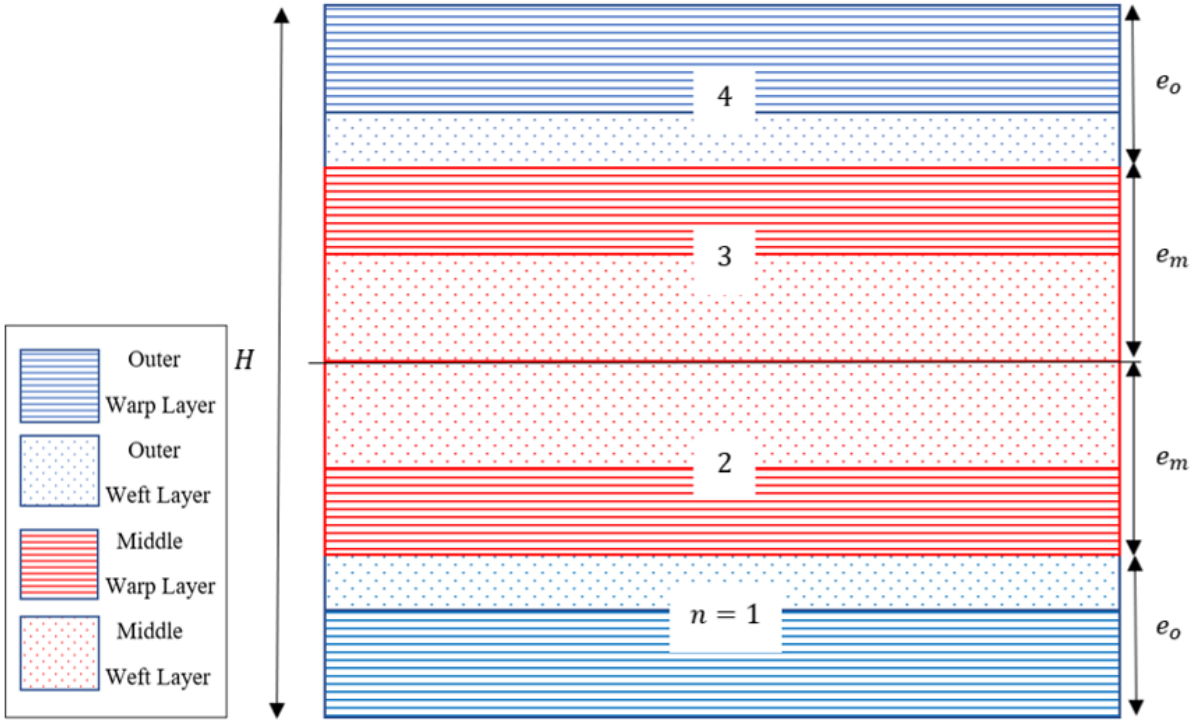

Figure 3.1: Four-layer, symmetric, woven fibre and graphene platelet reinforced laminate plate

The thickness ratio, τ, is a measure of the thickness of the outer surface layers compared to the laminate thickness:

$$\tau = \frac{2e_o}{H}$$

Eq. 3.1

Therefore, $\tau = 1$ corresponds to a laminate of only outer layers. $\tau = 0$ corresponds to a laminate with middle layers only. Thus, $0 \leq \tau \leq 1$.

3.2 Reduced stiffness terms

Let Q_{ijn} denote the reduced stiffness terms in the n^{th} layer ($n = 1,2,3,4$). Since the two outer layers are identical and the two middle layers are identical, let $p = o$ or m denote the outer and middle layers respectively. The reduced stiffness terms are then [14]:

$$Q_{11p} = \alpha_p E_{11p} \quad Q_{12p} = \alpha_p \nu_{12p} E_{22p} \quad Q_{16p} = Q_{26p} = 0 \quad Q_{22p} = \alpha_p E_{22p}$$

Eq. 3.2

$$Q_{66p} = G_{12p}$$

Eq. 3.3

$$where\ \alpha_p = \frac{1}{1 - \frac{E_{22p}}{E_{11p}} \nu_{12p}^2}$$

Eq. 3.4

The fibre orientations in the outer and middle layers, θ_o and θ_m, are depicted in figure 3.2. The reduced stiffness constants, $\bar{Q}_{ijo}$ and $\bar{Q}_{ijm}$, referred to the angles of fibre orientation in the outer and middle layer, θ_o and θ_m, are given by the equations for the reduced stiffness constants of a unidirectional or orthotropic composite off its principal directions [14]:

$$\bar{Q}_{11p} = Q_{11p} \cos^4 \theta_p + Q_{22p} \sin^4 \theta_p + 2\left(Q_{12p} + 2Q_{66p}\right) \sin^2 \theta_p \cos^2 \theta_p$$

Eq. 3.5

$$\bar{Q}_{12p} = \left(Q_{11p} + Q_{22p} - 4Q_{66p}\right) \sin^2 \theta_p \cos^2 \theta_p + Q_{12p}(\cos^4 \theta_p + \sin^4 \theta_p)$$

Eq. 3.6

$$\bar{Q}_{22} = Q_{11p} \sin^4 \theta_p + 2\left(Q_{12p} + 2Q_{66p}\right) \sin^2 \theta_p \cos^2 \theta_p + Q_{22p} \cos^4 \theta_p$$

Eq. 3.7

$$\bar{Q}_{66} = \left(Q_{11p} + Q_{22p} - 2\left(Q_{12p} + 2Q_{66p}\right)\right) \sin^2 \theta_p \cos^2 \theta_p + Q_{66p}(\sin^4 \theta_p + \cos^4 \theta_p)$$

Eq. 3.8

3.3 Stretching stiffness matrix

The stretching stiff matrix, $\boldsymbol{A}$, of the constitutive equation of a 4-layer laminate plate, with h_n denoting the distance from the midpoint of the laminate to the top of n^{th} layer is given by:

$$A_{ij} = \sum_{n=1}^{4} (h_n - h_{n-1})(Q_{ij})_n$$

Eq. 3.9

In figure 3.2, the formulae for the widths of each sublayer (warp and weft layer of each lamina) are shown on the left. The subscripts wp and wf denote the warp and weft layer respectively, and the subscripts o and m denote the outer and middle layers respectively. The woven fibre balancing coefficient, k_o or k_m, dictates the width of each sublayer. Since the laminate is symmetric about the midpoint, it has two outer layers whose widths are e_o and balancing coefficient k_o, and two middle layers with e_m and k_m. Introduce $c = e_m$ as the distance from the midpoint to the top of the middle layer, above the midpoint. Since the laminate is symmetric about the midpoint, this is the same distance to the top of the outer layer below the midpoint.

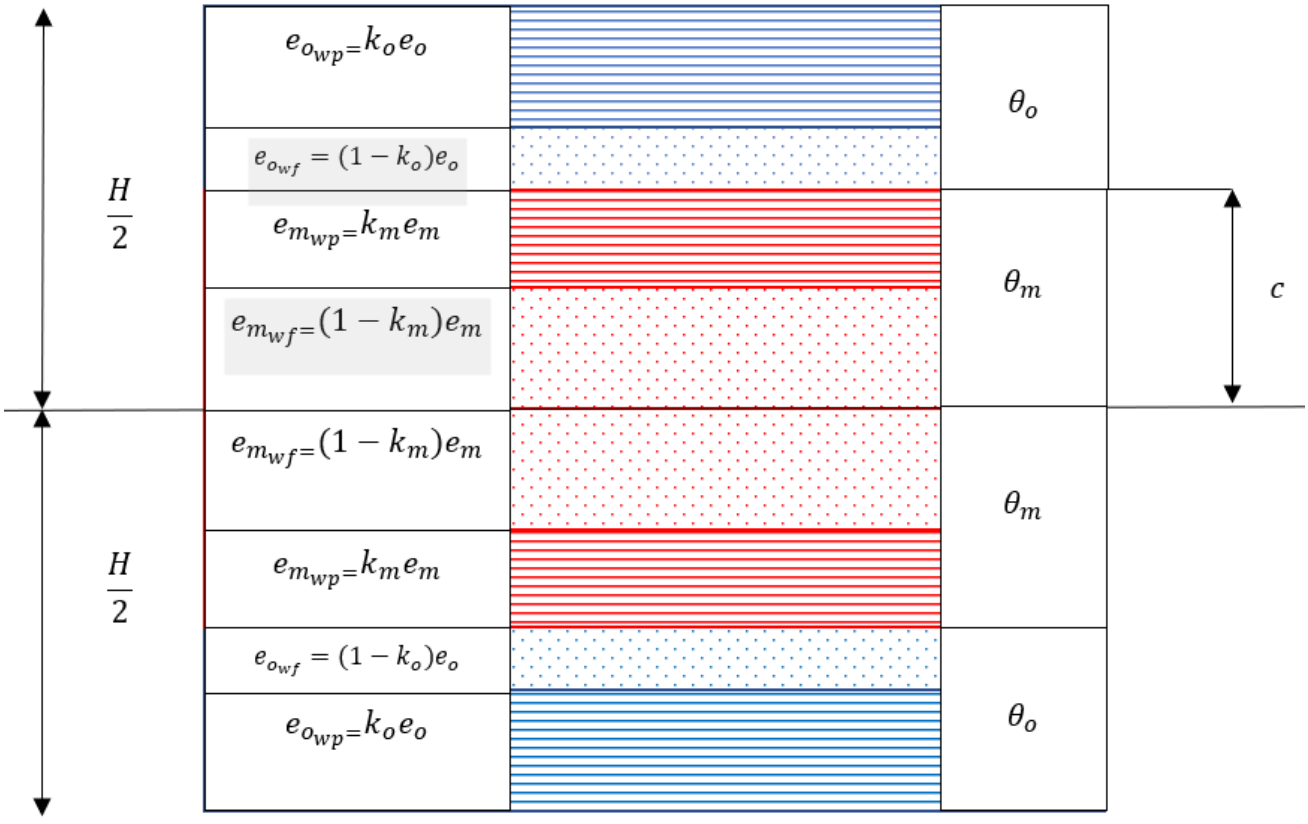

Figure 3.2: Widths of sublayers and orientation of fibres

The stretching stiffness matrix is thus:

$$A_{ij} = \left(\bar{Q}_{ijo} \left((-c) - \left(-\frac{H}{2} \right) \right) + \bar{Q}_{ijm}(-(-c)) + \bar{Q}_{ijm}(c) + \bar{Q}_{ijo} \left(\left(\frac{H}{2} \right) - (c) \right) \right)$$

Eq. 3.10

$$A_{ij} = \left(\bar{Q}_{ijo} \left((-c) - \left(-\frac{H}{2} \right) \right) + 2\bar{Q}_{ijm}(c) + \bar{Q}_{ijo} \left(\left(\frac{H}{2} \right) - (c) \right) \right)$$

Eq. 3.11

$$A_{ij} = \left(2\bar{Q}_{ijo} \left(\left(\frac{H}{2} \right) - (c) \right) + 2\bar{Q}_{ijm}(c) \right)$$

Eq. 3.12

By introducing the constants a_1 and a_2 such that:

$$a_1 = \left(\frac{H}{2} \right) - (c)$$

Eq. 3.13

$$a_2 = c = e_m$$

Eq. 3.14

Then:

$$A_{ij} = \left(2\bar{Q}_{ijo}(a_1) + 2\bar{Q}_{ijm}(a_2) \right)$$

Eq. 3.15

3.4 Coupling stiffness matrix

Since the laminate under consideration is symmetric, the coupling stiffness matrix, $\boldsymbol{B} = 0$. This can be proved by calculating $\boldsymbol{B}$ using the equation:

$$B_{ij} = \frac{1}{2} \sum_{n=1}^{n} (h_n^2 - h_{n-1}^2) \left(Q_{ij} \right)_n$$

Eq. 3.16

Thus, using figure 3.2 and the dimensions c and H:

$$B_{ij} = \frac{1}{2} \left(\bar{Q}_{ijo} \left((-c)^2 - \left(-\frac{H}{2} \right)^2 \right) + \bar{Q}_{ijm}(-(-c)^2) + \bar{Q}_{ijm}(c^2) + \bar{Q}_{ijo} \left(\left(\frac{H}{2} \right)^2 - (c)^2 \right) \right) = 0$$

Eq. 3.17

3.5 Bending stiffness matrix

The bending stiffness matrix, $\boldsymbol{D}$, of the constitutive equation of a 4-layer laminated plate, with h_n denoting the distance from the midpoint of the laminate to the top of n^{th} layer is given by:

$$D_{ij} = \frac{1}{3}\sum_{n=1}^{4} \bar{Q}_{ijn}\left(h_n^3 - h_{(n-1)}^3\right)$$

Eq. 3.18

Using figure 3.2 and the dimensions c and H, the $\boldsymbol{D}$ matrix of the constitutive equation is thus:

$$D_{ij} = \frac{1}{3}\left(\bar{Q}_{ijo}\left((-c)^3 - \left(-\frac{H}{2}\right)^3\right) + \bar{Q}_{ijm}(-(-c)^3) + \bar{Q}_{ijm}(c^3) + \bar{Q}_{ijo}\left(\left(\frac{H}{2}\right)^3 - (c)^3\right)\right)$$

Eq. 3.19

$$D_{ij} = \frac{1}{3}\left(\bar{Q}_{ijo}\left((-c)^3 - \left(-\frac{H}{2}\right)^3\right) + 2\bar{Q}_{ijm}(c^3) + \bar{Q}_{ijo}\left(\left(\frac{H}{2}\right)^3 - (c)^3\right)\right)$$

Eq. 3.20

$$D_{ij} = \frac{1}{3}\left(2\bar{Q}_{ijo}\left((-c)^3 - \left(-\frac{H}{2}\right)^3\right) + 2\bar{Q}_{ijm}(c^3)\right)$$

Eq. 3.21

By introducing the constants d_1 and d_2 such that:

$$d_1 = (-c)^3 - \left(-\frac{H}{2}\right)^3$$

Eq. 3.22

$$d_2 = c^3 = e_m^3$$

Eq. 3.23

Then:

$$D_{ij} = \frac{1}{3}\left(2\bar{Q}_{ijo}(d_1) + 2\bar{Q}_{ijm}(d_2)\right)$$

Eq. 3.24

3.6 Loading of the laminate plate

The laminate plate is modelled as a rectangular plate simply supported along its four edges. The plate is subjected to uniform compression on each edge, with in plane loads N_x and N_y along the x and y axes respectively (figure 3.3). The laminate has dimensions a and b along the x and y axes:

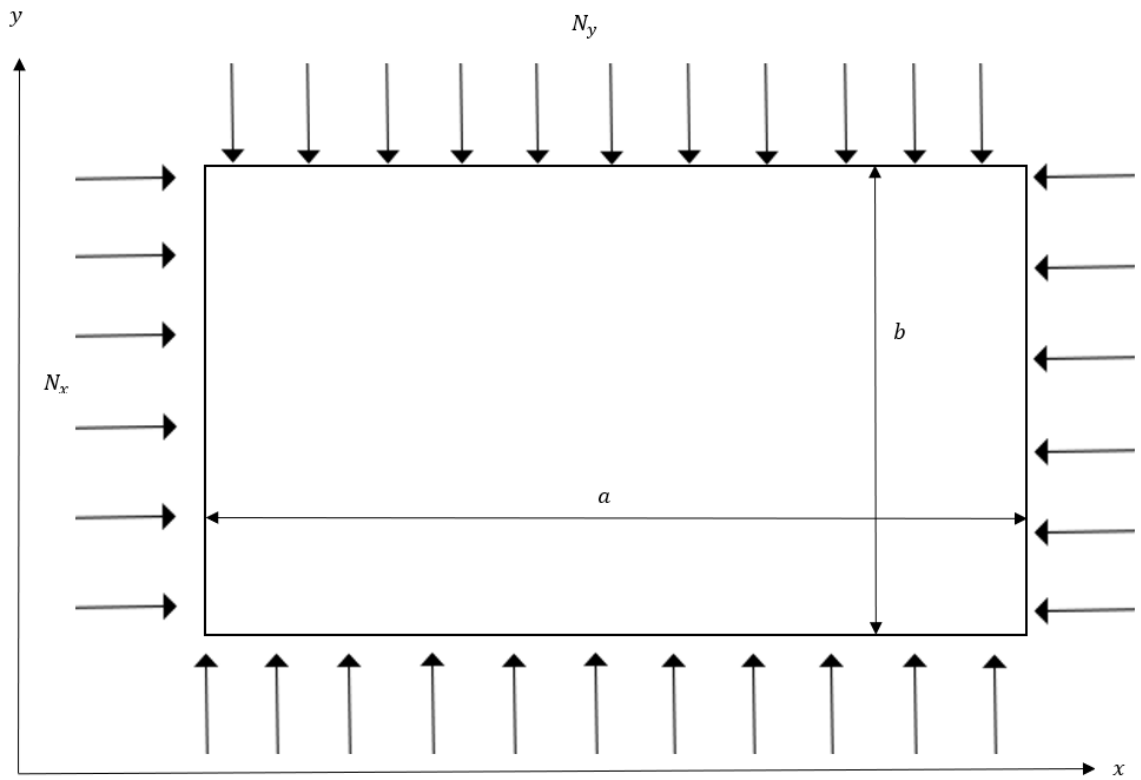

Figure 3.3: Loading conditions of the simply-supported rectangular laminate plate

4 Simulation framework

Simulation of the 4-ply symmetric woven glass fibre and graphene nanoplatelet nanocomposite under biaxial compression was performed using the Matlab software package. Matlab is a high-level programming language commonly used in engineering and science and developed by MathWorks, Inc [92]. The software makes use of matrix implementations and produces graphics suitable for publication purposes [93]. The simulation incorporates the micromechanical model of a graphene reinforced nanocomposite, the micromechanical model of a woven fabric reinforced composite and the governing equation of classical laminate theory for a simply-supported rectangular plate under biaxial compression to produce 2-dimensional line graphs and 3-dimensional contour-plots of the critical buckling load versus the fibre volume fraction, fibre orientation, graphene weight fraction, laminate aspect ratio, laminate thickness ratio and woven fibre balancing coefficient. The analytical models that were programmed into the software are presented in this chapter.

4.1 Micromechanics

The analysis procedure in predicting the material properties of a symmetric woven fibre composite with a graphene reinforced matrix is twofold. First, graphene nanoplatelets are added to the polymer matrix using suitable micromechanical equations. The graphene platelets are assumed to be uniformly distributed in the matrix. The resulting properties of the matrix are then used in the micromechanical equations for woven fibre reinforced laminates. Each layer in the woven fibre composite is treated as a layer comprised of two integral unidirectional layers – the warp and weft layers, orientated at 90° to each other.

4.1.1 Graphene platelet reinforced matrix

Graphene platelets are added to the polymer matrix as reinforcement. The platelets are assumed to be uniformly distributed. Let $p = o$ or m denote the outer and middle layers of the laminate respectively. Defining the volume fraction of the graphene platelets in the outer and middle lamina as V_{gpl_o} and V_{gpl_m}, and the Young's modulus of the matrix material as E_m, then, using the Halpin-Tsai approach, the Young's modulus of the graphene reinforced matrix in the outer and middle layers, E_{gm_o} and E_{gm_m}, is given by [94]:

$$E_{gm_p} = \left(\frac{3}{8}\frac{1+\xi_L\eta_L V_{gpl_p}}{1-\eta_L V_{gpl_p}} + \frac{5}{8}\frac{1+\xi_W\eta_W V_{gpl_p}}{1-\eta_W V_{gpl_p}}\right) \times E_m$$

Eq. 4.1

The geometry factors ξ_L and ξ_W are expressed in terms of the graphene platelets length l_{gpl}, width w_{gpl}, and thickness h_{gpl}:

$$\xi_L = 2\frac{l_{gpl}}{h_{gpl}};\ \xi_W = 2\frac{w_{gpl}}{h_{gpl}}$$

Eq. 4.2

The coefficients η_L and η_W are expressed in terms of the Young's moduli of the graphene, E_{gpl}, and of the matrix, E_m:

$$\eta_L = \frac{\left(\frac{E_{gpl}}{E_m}\right) - 1}{\left(\frac{E_{gpl}}{E_m}\right) + \xi_L};\ \eta_W = \frac{\left(\frac{E_{gpl}}{E_m}\right) - 1}{\left(\frac{E_{gpl}}{E_m}\right) + \xi_W}$$

Eq. 4.3

Using the mass density of the graphene platelets, ρ_{gpl}, and the mass density of the matrix, ρ_m, the graphene volume fraction can be expressed in terms of its weight fraction, W_{gpl}:

$$V_{gpl_p} = \frac{W_{gpl_p}}{W_{gpl_p} + (\frac{\rho_{gpl}}{\rho_m})(1 - W_{gpl_p})}$$

Eq. 4.4

Denoting ν_{gpl} as the Poisson's ratio of the graphene platelets and ν_m as the Poisson's ratio of the matrix then the Poisson's ratio, ν_{gm}, and shear modulus, G_{gm}, of the graphene reinforced matrix is given by:

$$\nu_{gm_p} = \nu_{gpl}V_{gpl_p} + \nu_m\left(1 - V_{gpl_p}\right)$$

Eq. 4.5

$$G_{gm_p} = \frac{E_{gm_p}}{2\left(1 + \nu_{gm_p}\right)}$$

Eq. 4.6

Figure 4.1 shows the graphene platelet reinforced 4-layer laminate prior to the addition of woven glass fibres. The corresponding characteristics of each layer (E_{gm_o}, E_{gm_m}, ν_{gm_o}, ν_{gm_m}, G_{gm_o} and G_{gm_m}) is depicted in each layer.

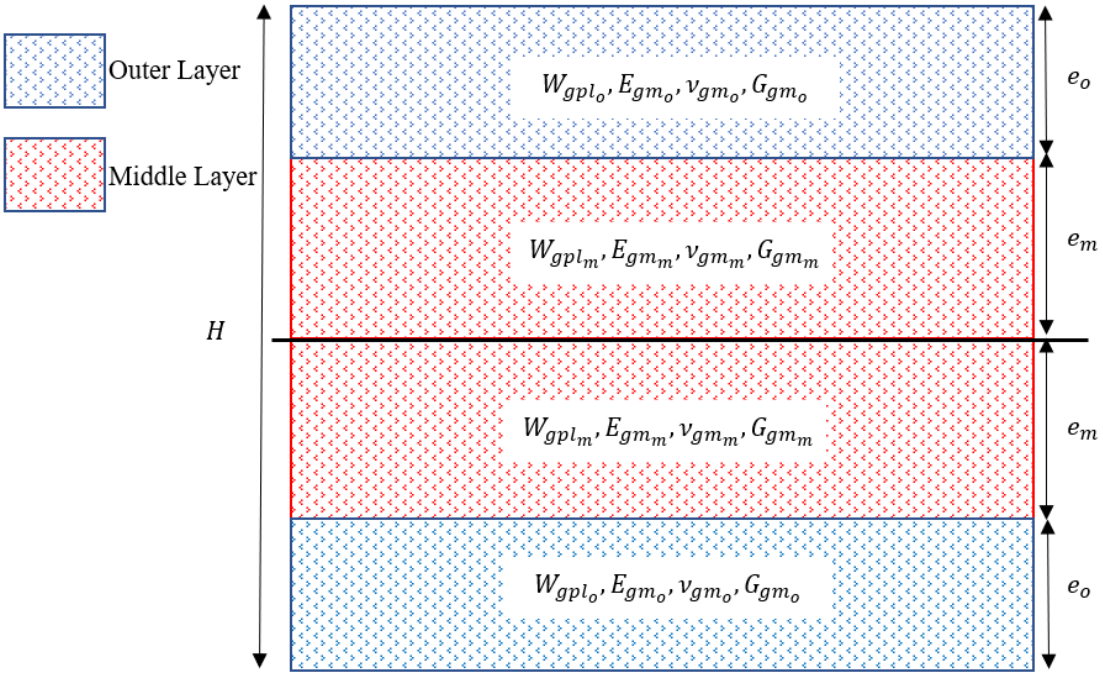

Figure 4.1:Engineering constants of the laminate with graphene nanoplatelet reinforcement

4.1.2 Woven fibre and graphene platelet reinforced matrix

The next step is to add woven fibres to the graphene reinforced polymer matrix. The methods used to determine the warp layer engineering constants ($E_{11_{wp}}$, $E_{22_{wp}}$, $\nu_{12_{wp}}$ and $G_{12_{wp}}$) and the weft layer engineering constants ($E_{11_{wf}}$, $E_{22_{wf}}$, $\nu_{12_{wf}}$ and $G_{12_{wf}}$) in a lamina are the law of mixtures and the cylindrical cell approach described in chapter 2.3. Woven fibre laminate theory is then used to determine the overall lamina engineering constants (E_{11}, E_{22}, ν_{12} and G_{12}). The method is described here for one layer. The same method is used for all four layers of the 4-ply, symmetric laminate.

4.1.2.1 Warp and weft layers

The longitudinal Young's modulus, E_{11}, of one layer (either warp or weft) is calculated from the law of mixtures. Let the subscript $l = wp$ denote the warp layer and $l = wf$ denote the weft layer, E_l denote the Young's modulus of the fibres in the warp or weft direction, and Vf_l denote the volume fraction of the warp and weft fibres present in the lamina. Then $E_{11_{wp}}$ and $E_{11_{wf}}$ can be calculated using the law of mixtures:

$$E_{11_l} = E_l Vf_l + E_{gm}(1 - Vf_l)$$

Eq. 4.7

Let ν_l denote the longitudinal Poisson's ratio of the warp and weft fibres. The longitudinal Poisson's ratios, $\upsilon_{12_{wp}}$ and $\upsilon_{12_{wf}}$, are then similarly calculated from the law of mixtures:

$$\nu_{12l} = \nu_l Vf_l + \nu_{gm}(1 - Vf_l)$$

Eq. 4.8

Let G_l denote the shear moduli of the warp and weft fibres. The longitudinal shear moduli, $G_{12_{wp}}$ and $G_{12_{wf}}$, are found from the cylindrical-cell approach [14]:

$$G_{12_l} = G_{gm}\left(\frac{G_l(1 + Vf_l) + G_{gm}(1 - Vf_l)}{G_l(1 - Vf_l) + G_{gm}(1 + Vf_l)}\right)$$

Eq. 4.9

The lateral compression modulus of the warp and weft layers, $K_{23_{wp}}$ and $K_{23_{wf}}$, are found using the cylindrical-cell approach [14]:

$$K_{23_l} = \frac{E_{gm}}{2(1 - 2\nu_{gm})(1 + \nu_{gm})} + \frac{Vf_l}{\frac{1}{k_l - k_{gm} + \frac{1}{3}(G_l - G_{gm})} + \frac{1 - Vf_l}{k_{gm} + \frac{4}{3}G_{gm}}}$$

Eq. 4.10

The bulk moduli of the graphene reinforced matrix, k_{gm}, the warp layer, k_{wp}, and the weft layer, k_{wf}, are calculated from [14]:

$$k_{gm} = \frac{E_{gm}}{3(1 - 2\nu_{gm})}$$

Eq. 4.11

$$k_l = \frac{E_l}{3(1 - 2\nu_l)}$$

Eq. 4.12

The transverse shear modulus of the warp and weft layers, $G_{23_{wp}}$ and $G_{23_{wf}}$, is calculated using the 3-phase cylindrical-cell approach [79]:

$$G_{23_l} = G_{gm}\left(1 + \frac{Vf_l}{\frac{G_{gm}}{G_l - G_{gm}} + \frac{k_{gm} + \frac{7}{3}G_{gm}}{2k_{gm} + \frac{8}{3}G_{gm}}(1 - Vf_l)}\right)$$

Eq. 4.13

Thus the transverse Young's moduli of the warp and weft layers, $E_{22_{wp}}$ and $E_{22_{wf}}$, is given by [14]:

$$E_{22_l} = \frac{2}{\frac{1}{2K_{23_l}} + \frac{1}{2G_{23_l}} + \frac{2\nu_{12_l}^2}{E_{11_l}}}$$

Eq. 4.14

4.1.2.2 Single layer

Since the 4-ply laminate is symmetric, the two outer layers have identical properties and the two middle layers have identical properties. Let $p = o$ or m denote the outer and middle layers respectively. The in-plane longitudinal Young's modulus, E_{11_p}, transverse Young's modulus, E_{22_p}, Poisson's ratio, ν_{12_p} and shear modulus, G_{12_p} of each layer (outer or middle) is given by [14]:

$$E_{11_p} = (1 - \alpha_p)\left(k_p \alpha_{wp_p} E_{11_{wp_p}} + (1 - k_p)\alpha_{wf_p} E_{22_{wf_p}}\right)$$

Eq. 4.15

$$E_{22} = (1 - \alpha_p)\left(k_p \alpha_{wp_p} E_{22_{wp_p}} + (1 - k_p)\alpha_{wf_p} E_{11_{wf_p}}\right)$$

Eq. 4.16

$$\nu_{12_p} = \frac{k_p \alpha_{wp_p} \nu_{12_{wp_p}} E_{22_{wp_p}} + (1 - k_p)\alpha_{wf_p} \nu_{12_{wf_p}} E_{22_{wf_p}}}{k_p \alpha_{wp_p} E_{22_{wp_p}} + (1 - k_p)\alpha_{wf_p} E_{11_{wf_p}}}$$

Eq. 4.17

$$G_{12_p} = k_p G_{12_{wp_p}} + (1 - k_p) G_{12_{wf_p}}$$

Eq. 4.18

The parameters α_{wp_p} and α_{wf_p} are calculated using the Young's moduli and Poisson's ratio of the warp and weft layers of each layer:

$$\alpha_{wp_p} = \frac{1}{1 - \left(\frac{E_{22_{wp_p}}}{E_{11_{wp_p}}}\right)\nu_{12_{wp_p}}^2}; \; \alpha_{wf} = \frac{1}{1 - \left(\frac{E_{22_{wf_p}}}{E_{11_{wf_p}}}\right)\nu_{12_{wf_p}}^2}$$

Eq. 4.19

The parameter α_p is given by:

$$\alpha_p = \frac{\left[k_p \alpha_{wp_p} \nu_{12_{wp_p}} E_{22_{wp_p}} + (1 - k_p)\alpha_{wf} \nu_{12_{wf_p}} E_{22_{wf_p}}\right]^2}{k_p \alpha_{wp} E_{11_{wp_p}} + (1 - k_p)\alpha_{wf} E_{22_{wf_p}} + k_p \alpha_{wp} E_{22_{wp_p}} + (1 - k_p)\alpha_{wf} E_{11_{wf_p}}}$$

Eq. 4.20

Figure 4.2 shows the woven glass fibre and graphene platelet reinforced 4-layer laminate with the corresponding characteristics of each layer (E_{11_o}, E_{22_o}, ν_{12_o}, G_{12_o}, E_{11_m}, E_{22_m}, ν_{12_m}, G_{12_m}).

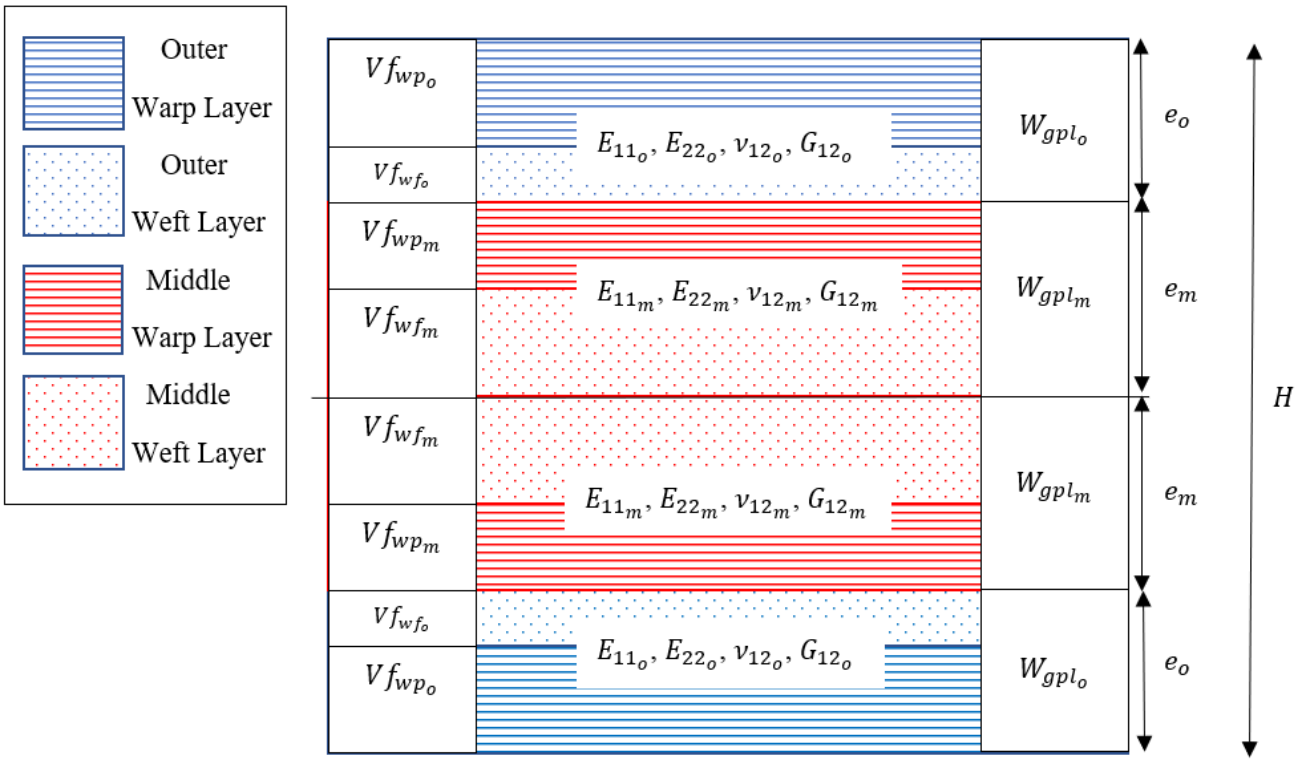

Figure 4.2: Engineering constants of the laminate with woven glass fibres and graphene nanoplatelets

4.2 Buckling

The governing equation for buckling taken from classical laminate theory used to predict the critical buckling load of the 4-ply, symmetric laminate is, with a as the width of the laminate plate, b as the length and $R = a/b$ [87]:

$$N_{cr} = \frac{\pi^2(D_{11}m^4 + 2(D_{12} + 2D_{66})m^2n^2R^2 + D_{22}n^4R^4)}{a^2(m^2 + \alpha_b n^2R^2)}$$

Eq. 4.21

A non-dimensional load, N_0, is often used by setting $E_o = 1\ GPa$ [95]:

$$N_0 = \frac{b^2N_{cr}}{E_oH^3}$$

Eq. 4.22

5 Numerical results

The results from the Matlab simulation incorporating the equations presented in chapter 4 are presented and discussed in this chapter. The results are categorized as either part of the woven fibre analysis or the graphene platelets analysis. In the woven fibre analysis, the graphs presented have the woven glass fibre properties presented on the x-axis. In the graphene platelet analysis, the graphs have the graphene platelet weight fraction presented on the x-axis. However, both these sections discuss the influence of the combination of these reinforcements on the buckling load. Table 5.1 gives the material properties of the epoxy matrix [96], the graphene platelets [94] and the glass fibres used for the analysis of the laminate [97]. The length, width and thickness of the graphene platelets are taken as $l_{gpl} = 2.5 \times 10^{-6}m$, $w_{gpl} = 1.5 \times 10^{-6}m$ and $h_{gpl} = 1.5 \times 10^{-9}m$ [94].

Table 5.1: Material properties of 4-ply, symmetric laminate

Material	E_{11}(GPa)	E_{22} (GPa)	ν_{12}
Graphene	1010	1010	0.186
Glass fibre	72.4	72.4	0.2
Matrix	3.5	3.5	0.35

5.1 Woven fibre analysis

In this section, the effect of the specifications of the woven glass fibres in the four-layer symmetric woven fibre and graphene platelet reinforced laminate is investigated.

5.1.1 Woven fibre volume fraction

In this section, the effect of the woven glass fibre volume fraction on the non-dimensional critical buckling load, N_0, is investigated for different laminate specifications. This section deals with how different volume fractions of woven glass fibres combined with various other laminate specifications (such as the woven glass fibre concentration in the warp and weft directions, Vf_{wp_o} and Vf_{wf_o}, the woven glass fibre balancing coefficient, k_o, the weight fraction of graphene in the outer and middle layers of the laminate, W_{gpl_o} and W_{gpl_m}, the woven glass fibre orientation in the outer layer, θ_o, the laminate thickness ratio, τ, and the laminate aspect ratio, $\frac{a}{b}$) influence the non-dimensional critical bucking load.

5.1.1.1 $\mathbf{Vf_{wp_o}}$ vs. $\mathbf{N_0}$ vs. $\mathbf{Vf_{wf_o}}$

Figure 5.1 shows the relationship between the non-dimensional critical buckling load, N_0, and the woven glass fibre volume fraction in the warp direction of the outer layers, Vf_{wp_o}, for different percentages of woven glass fibre content in the weft direction in the outer layers, Vf_{wf_o}. The buckling

load ratio is set to $\alpha_b = 1$, for uniform biaxial loading. At approximately 35% and 45% of warp fibre content, the 10% weft fibre line intersects the 20% and 30% line respectively. Thus, for warp fibre content of above 45%, a weft fibre content of 10% is more beneficial for the critical buckling load than a weft fibre content of 30% or lower, under these laminate specifications. Furthermore, at higher weft-fibre volumes, increasing the warp-fibre volume can have a detrimental effect on the buckling load. When $Vf_{wf_o} = 30\%$, for example, approximately the same buckling load can be achieved with either $Vf_{wp_o} = 0$ or $Vf_{wp_o} = 0.25$. For cost-effective designing, the lower value of Vf_{wp_o} is then preferred. A script detailing the order of the functions programmed into the software for this investigation is available in appendix A. Other investigations conducted in this study utilize a similar script with certain variables and functions altered as necessary.

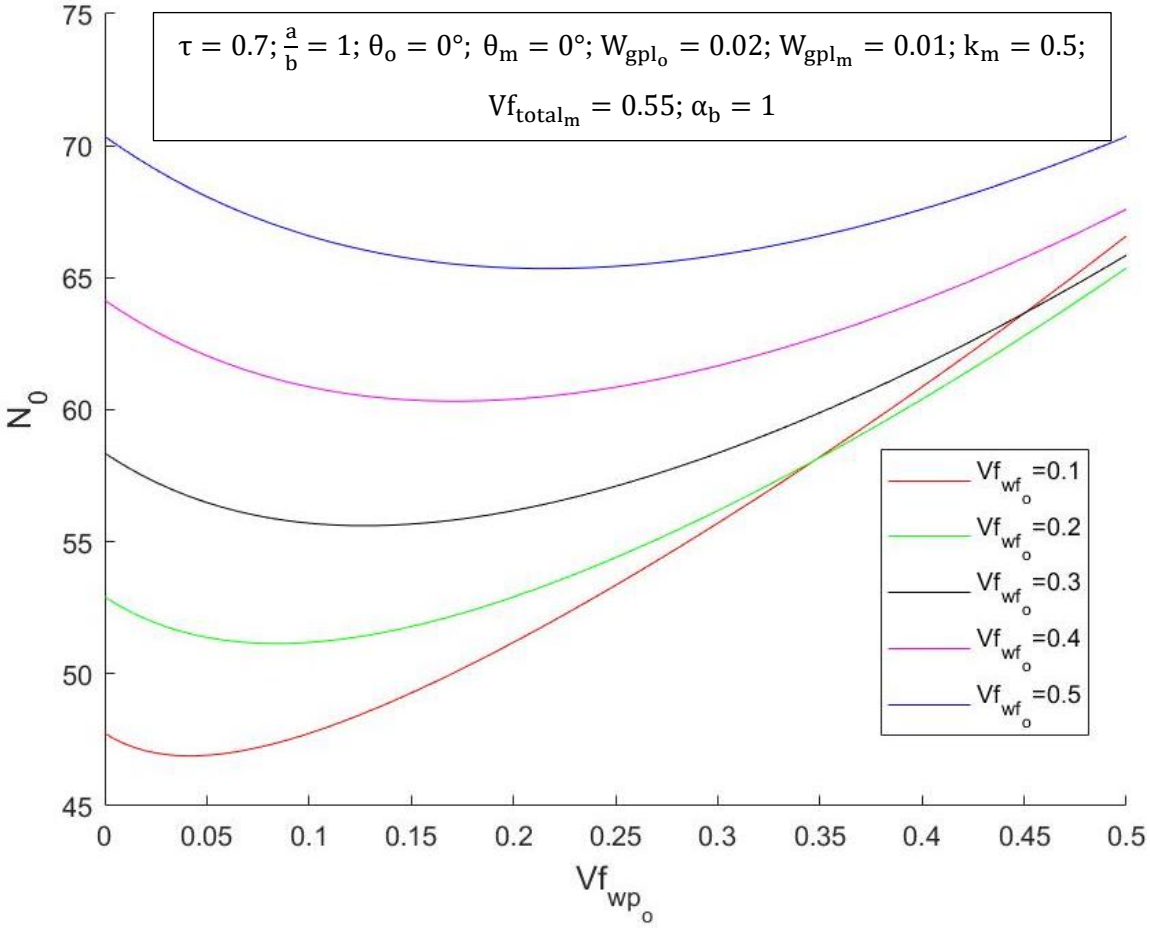

Figure 5.1: Critical buckling load vs. Vf_{wp_o} for different values of Vf_{wf_o}

5.1.1.2 Vf_{total} vs. N_0 vs. W_{gpl_o}

Figure 5.2(a) shows the variation in non-dimensional critical buckling load, N_0, with different values of the total fibre volume content in the outer layers, Vf_{total_o}, and different values of the graphene weight fraction in the outer layers, W_{gpl_o}. While the buckling load is directly proportional to both these variables, it is far more sensitive to the graphene platelet content. For 0% graphene weight percentage and 50% woven glass fibres volume content, the non-dimensional critical buckling load is

approximately 15. For the same amount of woven glass fibres but 4% graphene weight percentage, the buckling load is approximately 90 (75 more, 5 times larger). Whereas for any amount of graphene, increasing the total fibre content in the outer layer by 50% results in an increase of approximately 10 in the buckling load. This is visualized in the contour plot in figure 5.3. Figure 5.2(b) shows that the variation of the critical buckling load with respect to the total woven glass fibre volume content in the middle layer, Vf_{total_m}, is negligible for $\tau = 0.7$, which is when 70% of the laminate is comprised of the outer layer. Thus, more focus should be directed to the reinforcements in the outer layer for a cost-effective laminate.

$$\tau = 0.7; \frac{a}{b} = 1; \theta_o = 0°; \theta_m = 0°; W_{gpl_m} = 0.01; k_o = 0.5; k_m = 0.5; \alpha_b = 1$$

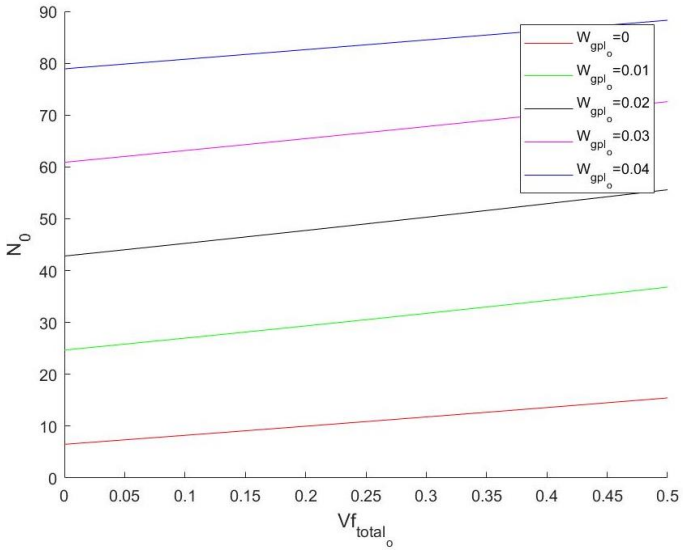

Figure 5.2 (a) $Vf_{total_m} = 0.55$

$$\tau = 0.7; \frac{a}{b} = 1; \theta_o = 0°; \theta_m = 0°; W_{gpl_m} = 0.01; k_o = 0.5; k_m = 0.5; \alpha_b = 1$$

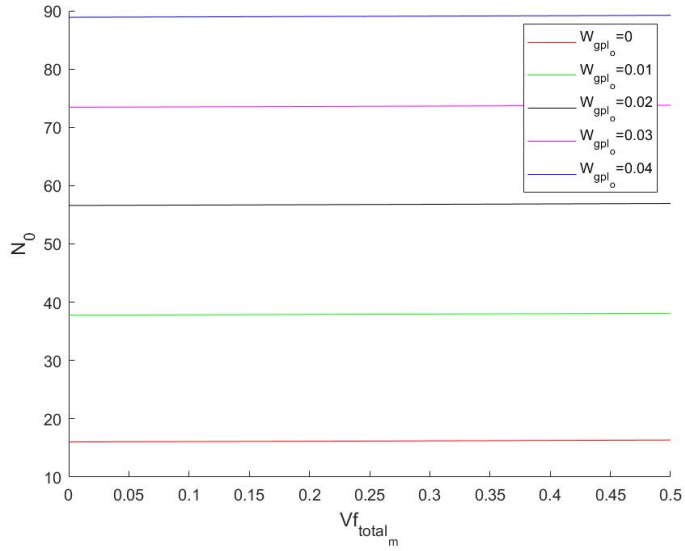

Figure 5.2 (b) $Vf_{total_o} = 0.55$

Figure 5.2: Critical buckling load vs. Vf_{total_o} *for different values of* W_{gpl_o}

$\tau = 0.7; \frac{a}{b} = 1; \theta_o = 0°; \theta_m = 0°; W_{gpl_m} = 0.01; k_o = 0.5; k_m = 0.5; Vf_{total_m} = 0.55; \alpha_b = 1$

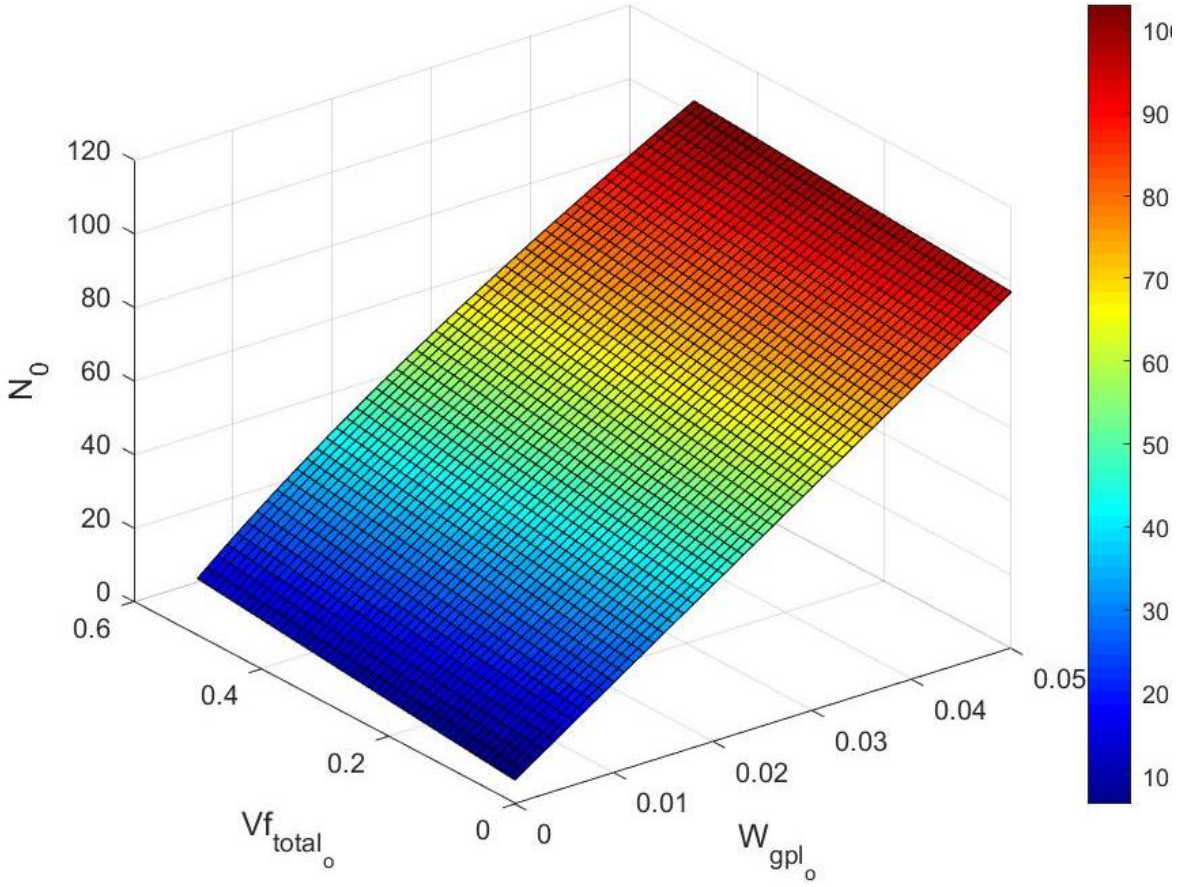

Figure 5.3: Contour plot of critical buckling load vs. Vf_{total_o} for different values of W_{gpl_o}

5.1.1.3 Vf_{wp_o} vs. N_0 vs. W_{gpl_o}

Figures 5.4(a) and 5.4(b) show the change in non-dimensional critical buckling load, N_0, with respect to the woven glass fibres volume fraction in only the warp direction in the outer layers, Vf_{wp_o}, for small values and large values of graphene weight percentage, W_{gpl_o}, respectively. Figure 5.4(b) shows that, up to a certain point of graphene content, increasing the warp fibre content can have a detrimental effect on the buckling load. For these laminate specifications, this occurs somewhere between $W_{gpl_o} = 6\%$ and $W_{gpl_o} = 10\%$. When $W_{gpl_o} = 15\%$, increasing Vf_{wp_o} from 0 to approximately 0.05 increases the buckling load, however, increasing it any further diminishes the buckling load. The influence of this phenomenon increases even further if the graphene weight percentage is further increased, as can be seen in the $W_{gpl_o} = 0.2$ line in figure 5.4(b). The influence of the laminate aspect ratio, $\frac{a}{b}$, is shown in figures 5.5(a) and 5.5(b). To remove the domineering effect of the graphene, graphene weight percentage W_{gpl_o} is set to 0%. The weft fibre volume percentage, Vf_{wf_o}, is set to 27.5%. From $\frac{a}{b} = 0.5$ to $\frac{a}{b} = 1$, increasing the volume percentage of fibres in the warp layer is beneficial for the critical buckling load. Between $\frac{a}{b} = 1$ and $\frac{a}{b} = 3$, seen in figure 5.5(b), the fibre percentage lines crossover each

other such that lower warp fibre volume percentages may be more beneficial for the critical buckling load, than higher ones. Eventually, at $\frac{a}{b} \approx 3$ for these laminate conditions, a lower fibre volume fraction in the warp layer is beneficial for the critical buckling load.

$\tau = 0.7; \frac{a}{b} = 1; \theta_o = 0°; \theta_m = 0°; W_{gpl_m} = 0.01; Vf_{wf_o} = 0.275; k_m = 0.5; Vf_{total_m} = 0.55; \alpha_b = 1$

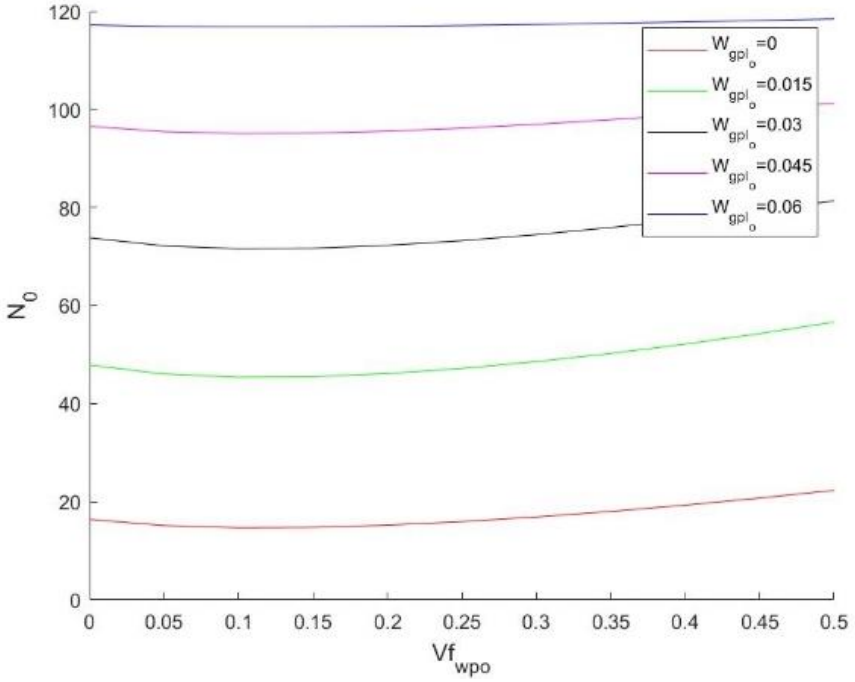

Figure 5.4 (a) $0 \leq W_{gpl_o} \leq 0.06$

$\tau = 0.7; \frac{a}{b} = 1; \theta_o = 0°; \theta_m = 0°; W_{gpl_m} = 0.01; Vf_{wf_o} = 0.275; k_m = 0.5; Vf_{total_m} = 0.55; \alpha_b = 1$

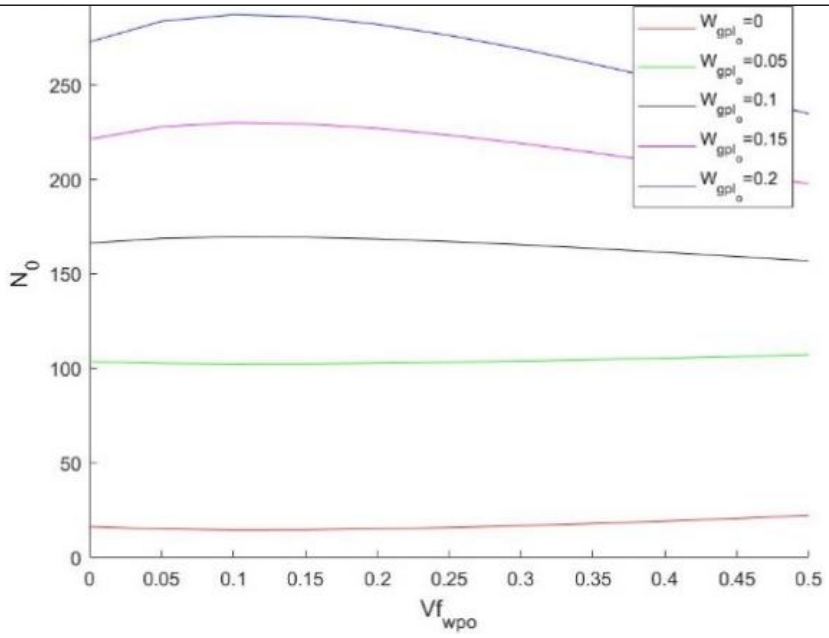

Figure 5.4 (b) $0 \leq W_{gpl_o} \leq 0.2$

Figure 5.4: Critical buckling load vs. Vf_{wp_o} *for different values of* W_{gpl_o}

$\tau = 0.7; \theta_o = 0°; \ \theta_m = 0°; W_{gpl_o} = 0; \ W_{gpl_m} = 0; Vf_{wf_o} = 0.275; k_m = 0.5; Vf_{total_m} = 0.55; \alpha_b = 1$

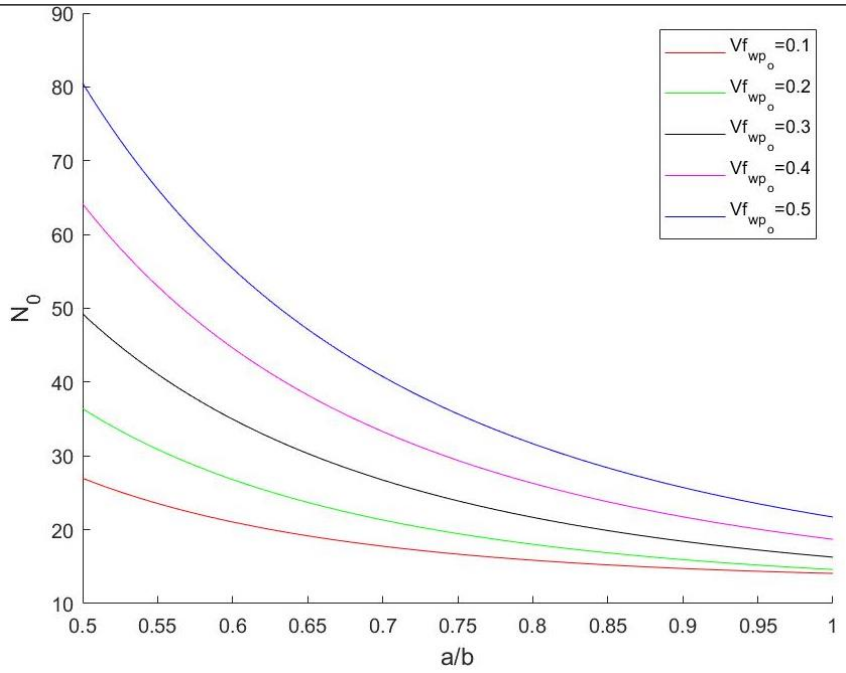

Figure 5.5 (a) $0.5 \leq a/b \leq 1$

$\tau = 0.7; \theta_o = 0°; \ \theta_m = 0°; W_{gpl_o} = 0; \ W_{gpl_m} = 0; Vf_{wf_o} = 0.275; k_m = 0.5; Vf_{total_m} = 0.55; \alpha_b = 1$

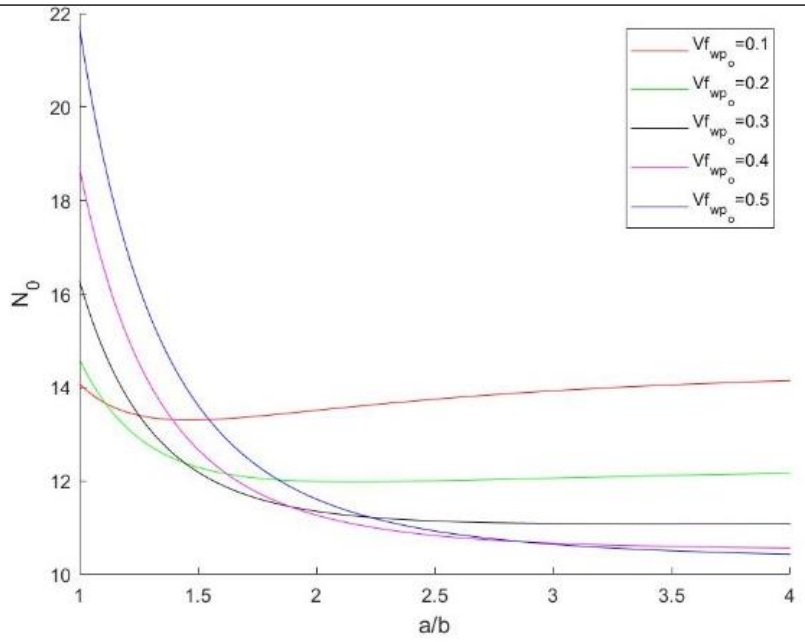

Figure 5.5 (b) $1 \leq a/b \leq 4$

Figure 5.5:Critical buckling load vs. a/b *for different values of* Vf_{wp_o}

If graphene is present however, this effect is no longer applicable. In figure 5.6, with $W_{gpl_o} = 2\%$, only the 10% warp fibre volume percentage line crosses over the 20% and 30% lines for aspect ratios $\frac{a}{b} = 1$

to $\frac{a}{b} = 100$. The effect of graphene in the laminate is thus to increase the critical buckling load and obscure the influence of the aspect ratio.

$\tau = 0.7;\ \theta_o = 0°;\ \theta_m = 0°;\ W_{gpl_o} = 0.02;\ W_{gpl_m} = 0;\ Vf_{wf_o} = 0.275;\ k_m = 0.5;\ Vf_{total_m} = 0.55;\ \alpha_b = 1$

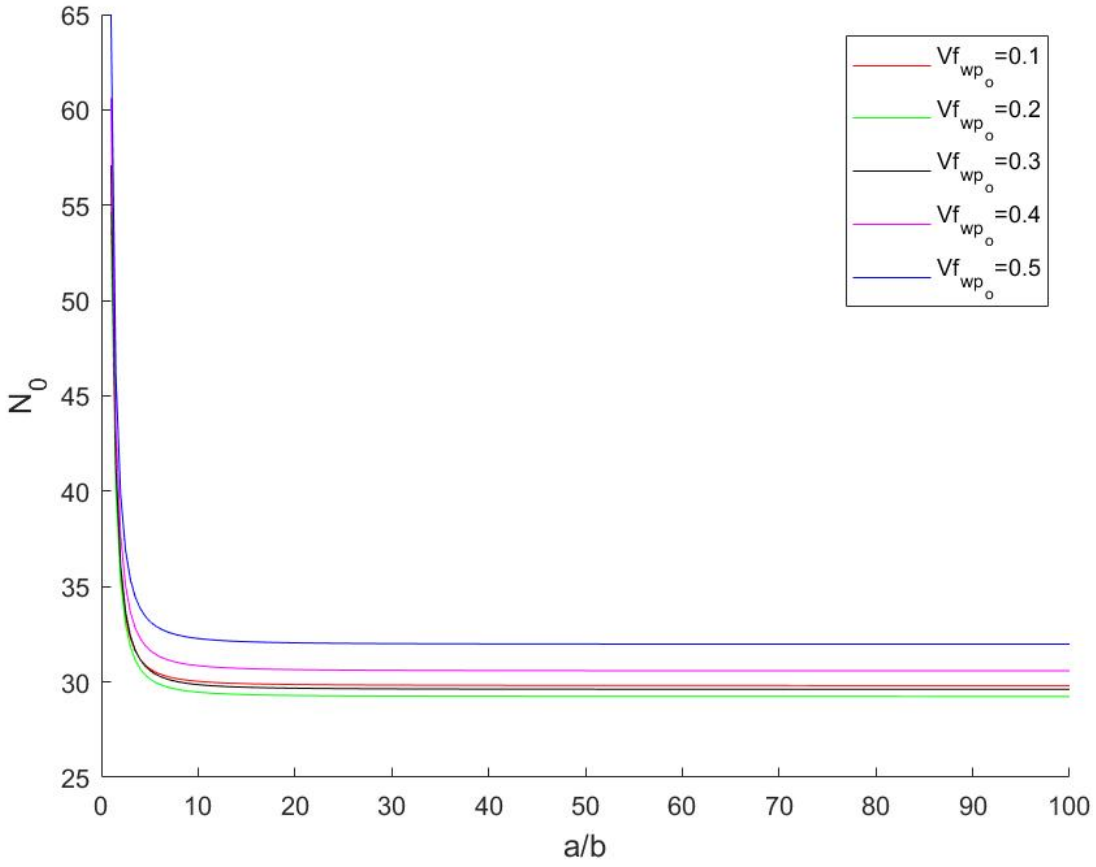

Figure 5.6: Critical buckling load vs. a/b for different values of Vf_{wp_o}

5.1.1.4 Vf_{wp_o} vs. N_0 vs. θ_o

Figure 5.7(a) shows the relationship between the non-dimensional critical buckling load, N_0, and the warp fibre volume fraction, Vf_{wp_o}, for different woven glass fibre orientations in the outer layer, θ_o. Graphene weight fractions in the outer and middle layers are set to $W_{gpl_o} = 0.01$ and $W_{gpl_m} = 0.01$. Figure 5.7(b) more clearly shows what happens between 25% and 30% of warp fibre content. Between these two percentages, the curves intersect, and the ideal woven glass fibre orientation is not clearly defined – it depends on the volume percentage of the woven glass fibres. For the laminate specifications in figure 5.7, for small values of Vf_{wp_o} up to approximately 26%, fibre orientation closer to 90° is preferred for a higher buckling load. After $Vf_{wp_o} \approx 0.275$, fibre orientation at 0° is preferred for a higher buckling load. For $Vf_{wp_o} > 28\%$, fibre orientation at 90° is the least preferred. The crossing point region is influenced by the woven glass fibre balancing co-efficient, k_o. It can be seen in figure 5.8 that for the same laminate specifications as in figure 5.7, the crossing point where $\theta_o = 90°$

intersects $\theta_o = 0°$ occurs when $k_o = 0.5$. In figure 5.7(a), the crossing point occurs at $Vf_{wp_o} = 0.275$, which is when $k_o = 0.5$. The graph of $k_o\ vs. N_0\ vs. \theta_o$ is altered with the addition of graphene platelets in the laminate. This effect is discussed in chapter 5.1.2.

$\tau = 0.7; \frac{a}{b} = 0.4; \theta_m = 0°; W_{gpl_o} = 0.01; W_{gpl_m} = 0.01;\ Vf_{wf_o} = 0.275; k_m = 0.5; Vf_{total_m} = 0.55; \alpha_b = 1$

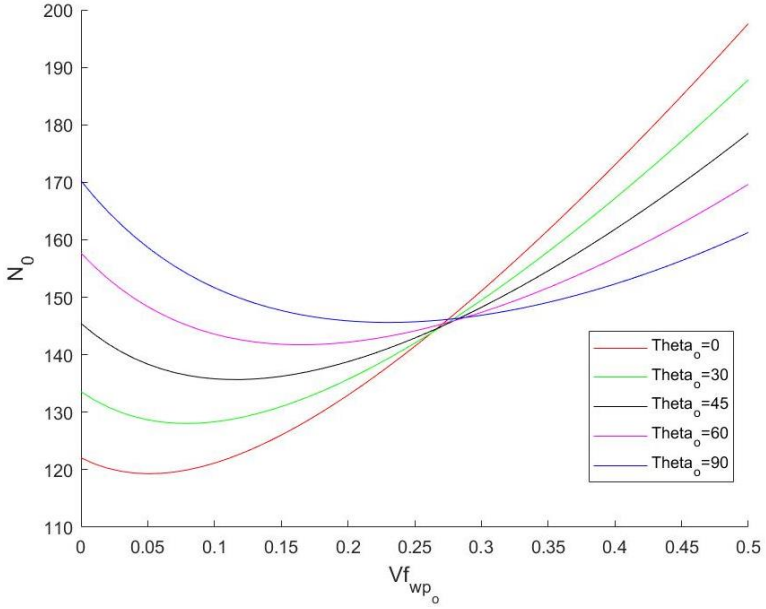

Figure 5.7 (a) $0 \leq Vf_{wp_o} \leq 0.5$

$\tau = 0.7; \frac{a}{b} = 0.4; \theta_m = 0°; W_{gpl_o} = 0.01; W_{gpl_m} = 0.01;\ Vf_{wf_o} = 0.275; k_m = 0.5; Vf_{total_m} = 0.55; \alpha_b = 1$

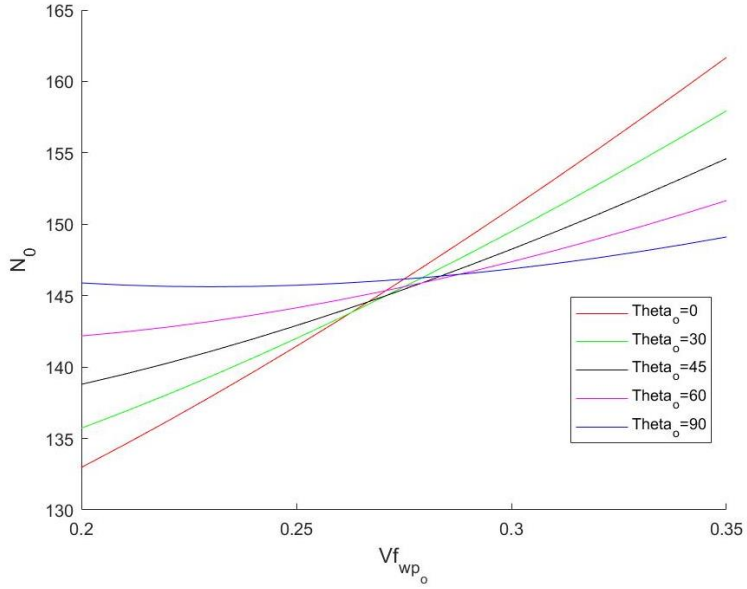

Figure 5.7 (b) $0.2 \leq Vf_{wp_o} \leq 0.35$

Figure 5.7: Critical buckling load vs. Vf_{wp_o} *for different values of* θ_o

$\tau = 0.7; \frac{a}{b} = 0.4; \theta_m = 0°; W_{gpl_o} = 0.01; W_{gpl_m} = 0.01; Vf_{total_o} = 0.55;$
$k_m = 0.5; Vf_{total_m} = 0.55; \alpha_b = 1$

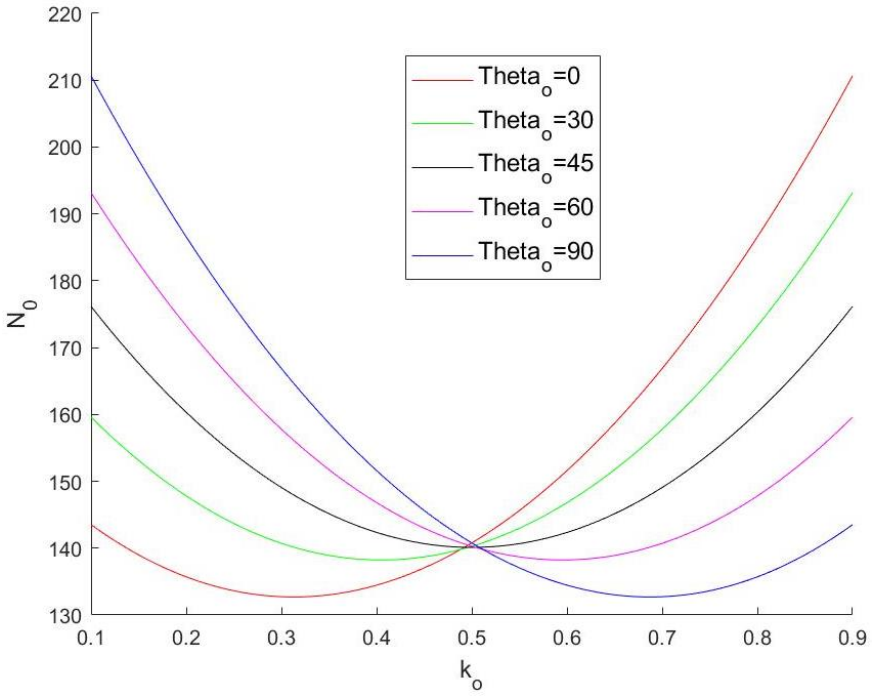

Figure 5.8: Critical buckling load vs. k_o for different values of θ_o

The woven glass fibre orientation, θ_o, that is ideal for the critical buckling load when $Vf_{wp_o} <$ the intersection point ($Vf_{wp_o} < 27.5\%$ in the case in figure 5.7) is influenced by the aspect ratio of the laminate. In figure 5.9, the effect of the aspect ratio is depicted for a laminate with the same specifications as figure 5.7. When $\frac{a}{b} = 0.4$, $\theta_o = 90°$ is ideal for the critical buckling load. Thus, for laminates with $\frac{a}{b} = 0.4$, such as in figure 5.7(a), $\theta_o = 90°$ is preferred when the fibre volume fraction is less than the intersection point.

$\tau = 0.7$; $\theta_m = 0°$; $W_{gpl_o} = 0.01$; $W_{gpl_m} = 0.01$; $Vf_{wp_o} = 0.15$; $Vf_{wf_o} = 0.275$; $k_m = 0.5$; $Vf_{total_m} = 0.55$; $\alpha_b = 1$

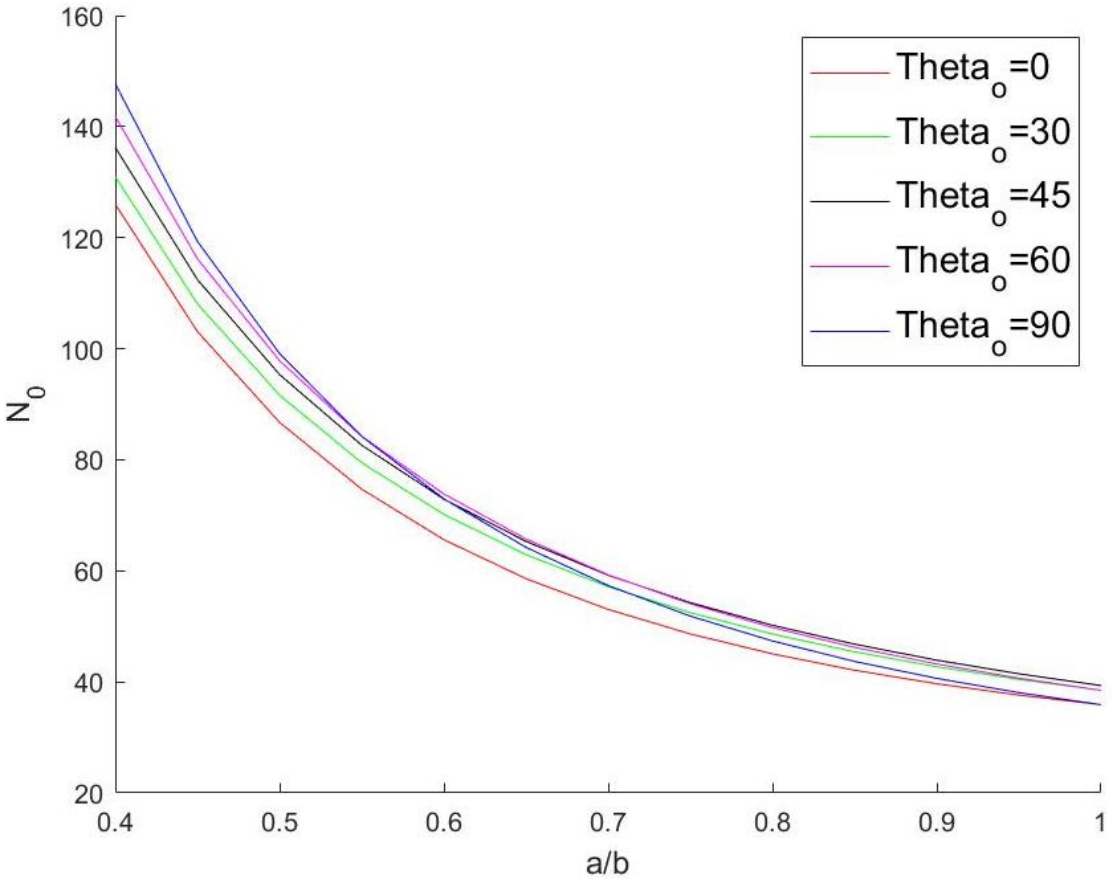

Figure 5.9: Critical buckling load vs. a/b for different values of θ_o

5.1.1.5 Vf_{wp_o} vs. N_0 vs. τ

Figures 5.10(a) and 5.10(b) show the relationship between the warp fibre volume in the outer layer, Vf_{wp_o}, and the non-dimensional critical buckling load, N_0, for different values of the thickness ratio, τ. In figure 5.10(a), no graphene is present in any layer ($W_{gpl_o} = W_{gpl_m} = 0$). The buckling load then favours a smaller thickness ratio up until $Vf_{wp_o} = 27.5\%$. At this point, $k_o = 0.5$. Increasing Vf_{wp_o} beyond this point causes a higher thickness ratio to be favourable for the critical buckling load. This is because when $k_o > 0.5$, there are more fibres in the warp direction than in the weft direction in the outer layer. Hence, the outer layer has its fibres more concentrated in one direction. For biaxial, uniform loading, at low graphene content, having the fibres more concentrated in a single direction is more beneficial for the buckling load ($k_o = 1$ or 0, depending on the aspect ratio and fibre orientation) than having the fibres balanced ($k_o = 0.5$). This is further discussed in chapter 5.1.3. When 1% of graphene platelet weight is added to the outer layer, in figure 5.10(b), the buckling load always favours a higher thickness ratio (hence thicker outer layers than middle layers) as the graphene has a more influential effect on the buckling load than the glass fibres. In figures 5.10(a) and 5.10(b), it is important to note

that there is not much difference in the critical buckling load for laminates with $\tau = 0.75$ and $\tau = 1$. Thus, for any fibre volume, it is more practical and cost effective to keep the thickness ratio below or equal to 0.75. Increasing τ above this value practically causes no difference to the buckling load.

The aspect ratio of the laminate, $\frac{a}{b}$, also influences the effect of the thickness ratio, τ, on the critical buckling load, N_0. In figure 5.11, the effect of the aspect ratio is depicted for the same laminate specifications as in figure 5.10. For $\frac{a}{b} = 1$, a higher thickness ratio is preferred. Therefore, in figure 5.10(a) where $\frac{a}{b} = 1$, a higher thickness ratio is preferred after the crossing point. For a different $\frac{a}{b}$, for example $\frac{a}{b} = 2.4$, a lower thickness ratio would be preferred under the same conditions.

The influence of the balancing coefficient, k_o, and the aspect ratio, $\frac{a}{b}$, on the critical buckling load is further discussed in chapter 5.1.2.

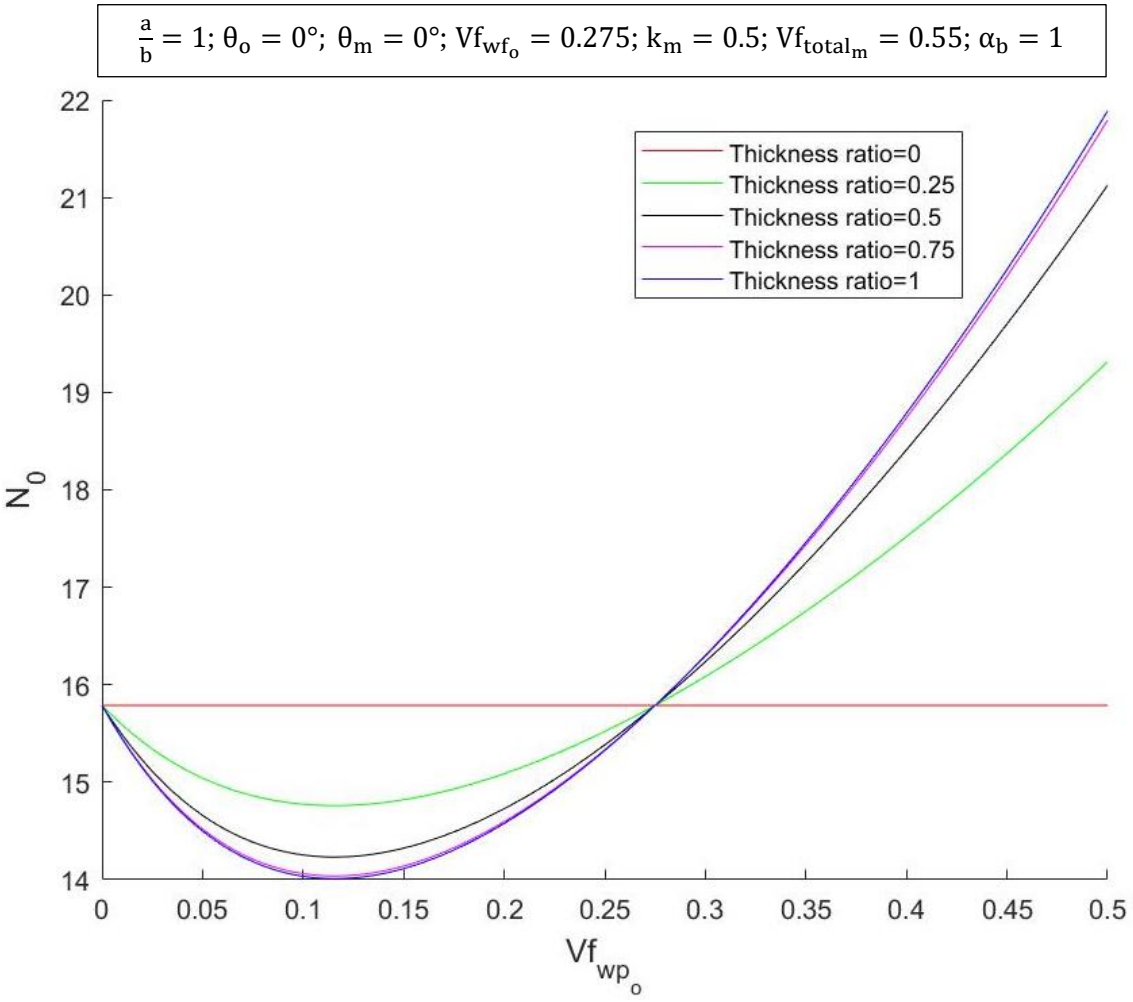

Figure 5.10 (a) $W_{gpl_o} = 0$; $W_{gpl_m} = 0$

$\frac{a}{b} = 1;\ \theta_o = 0°;\ \theta_m = 0°;\ Vf_{wf_o} = 0.275;\ k_m = 0.5;\ Vf_{total_m} = 0.55;\ \alpha_b = 1$

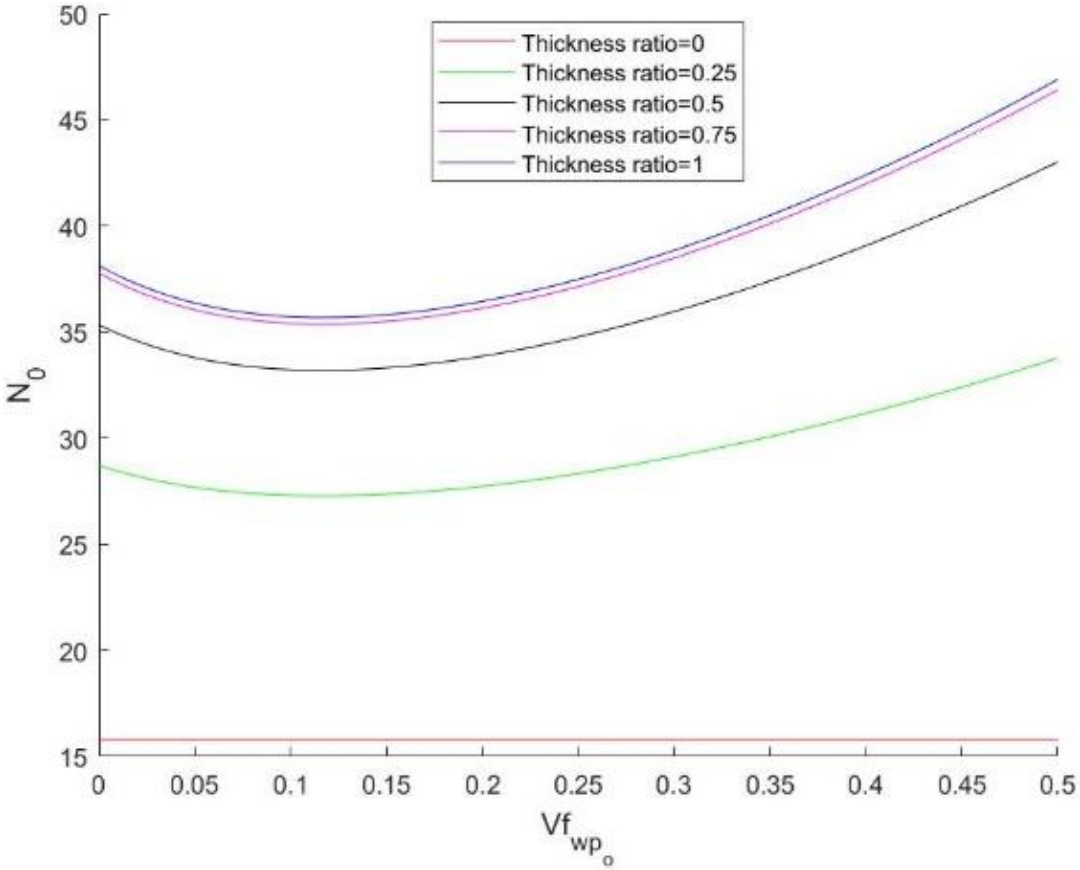

Figure 5.80 (b) $W_{gpl_o} = 0.01;\ W_{gpl_m} = 0$

Figure 5.10: Critical buckling load vs. Vf_{wp_o} *for different values of* τ

$\theta_o = 0°;\ \theta_m = 0°;\ W_{gpl_o} = W_{gpl_m} = 0;\ Vf_{wpo_o} = 0.4;\ Vf_{wf_o} = 0.275;\ k_m = 0.5;\ Vf_{total_m} = 0.55;\ \alpha_b = 1$

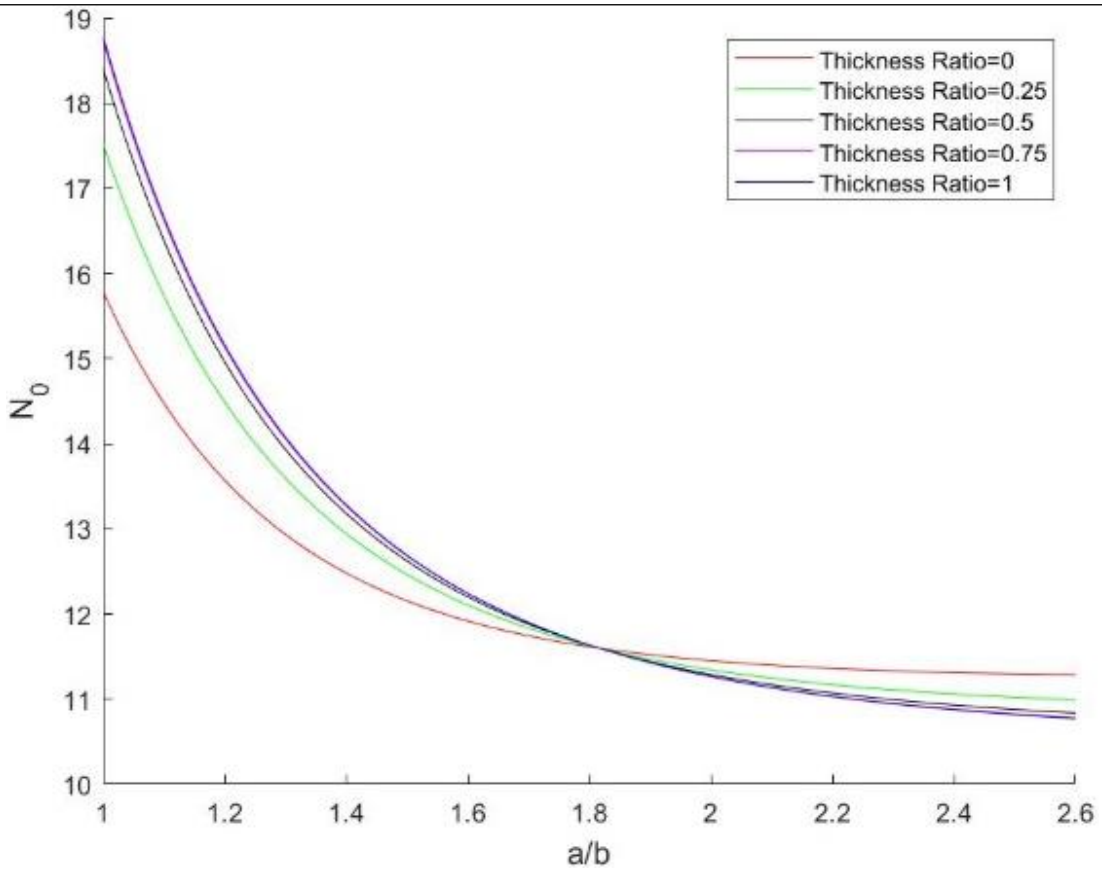

Figure 5.11: Critical buckling load vs. a/b for different values of τ

5.1.1.6 Vf_{total_o} vs. N_0 vs. τ

The intersection point in figure 5.10(a) is influenced by the total volume fraction of fibre in each layer, Vf_{total_o} and Vf_{total_m}, and the woven glass fibre balancing coefficient of each layer, k_o and k_m. In the absence of graphene, a thickness ratio that serves to increase the thickness of the layer with more fibres is more beneficial for the buckling load, provided that the woven glass fibre balancing coefficient in each layer is equal. In figure 5.12(a), the balancing coefficient of each layer is equal. The crossing point then occurs when $Vf_{total_o} = Vf_{total_m}$ (50% in figure 5.12(a)). However, changing the concentration of the woven glass fibres in either the warp or weft direction can influence this crossing point. For the same conditions as figure 5.12(a), but with k_m now 0.8 (keeping the fibre volume percentage constant but concentrating them in the warp direction), the crossing point changes to approximately $Vf_{total_o} = 70\%$ (figure 5.12(b)). This effect can be seen in figure 5.13. In figure 5.13, both layers have the same fibre volume content (55%), however the middle layer has the fibres more concentrated in the weft direction ($k_m = 0.36$). Therefore, when k_o is close to 0.5 (hence more balanced and less concentrated in any direction in the outer layer) a lower thickness ratio is preferred.

More figures depicting the combined effect of the woven glass fibre balancing coefficient, k_o, and the laminate thickness ratio, τ, on the non-dimensional critical buckling load, N_0 are included in appendix B, for $\frac{a}{b} = 1, 0.4$ and 4 and different values of W_{gpl_o} and W_{gpl_m}.

$\frac{a}{b} = 1;\ \theta_o = 0°;\ \theta_m = 0°;\ W_{gpl_o} = W_{gpl_m} = 0;\ k_o = 0.5;\ Vf_{total_m} = 0.5;\ \alpha_b = 1$

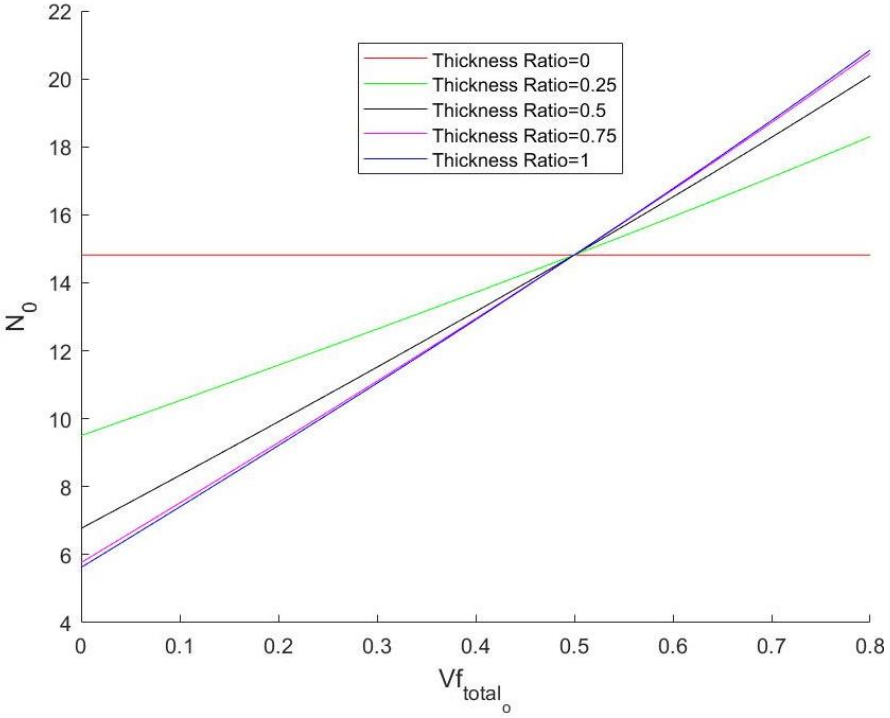

Figure 5.12 (a) $k_m = 0.5$

$\frac{a}{b} = 1;\ \theta_o = 0°;\ \theta_m = 0°;\ W_{gpl_o} = W_{gpl_m} = 0;\ k_o = 0.5;\ Vf_{total_m} = 0.5;\ \alpha_b = 1$

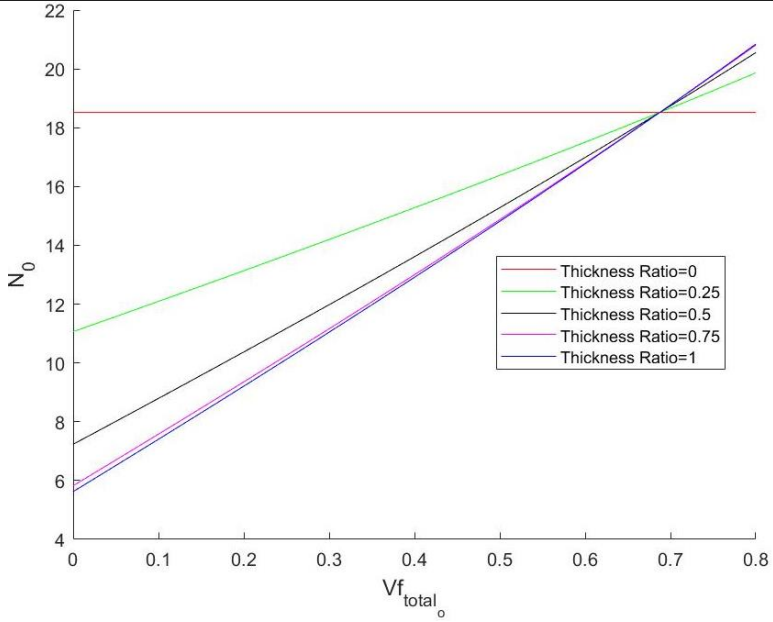

Figure 5.12 (b) $k_m = 0.8$

Figure 5.12: Critical buckling load vs. Vf_{total_o} for different values of τ

$\frac{a}{b} = 1;\ \theta_o = 0°;\ \theta_m = 0°;\ W_{gpl_o} = W_{gpl_m} = 0;\ Vf_{total_o} = 0.55;\ k_m = 0.36;\ Vf_{total_m} = 0.55;\ \alpha_b = 1$

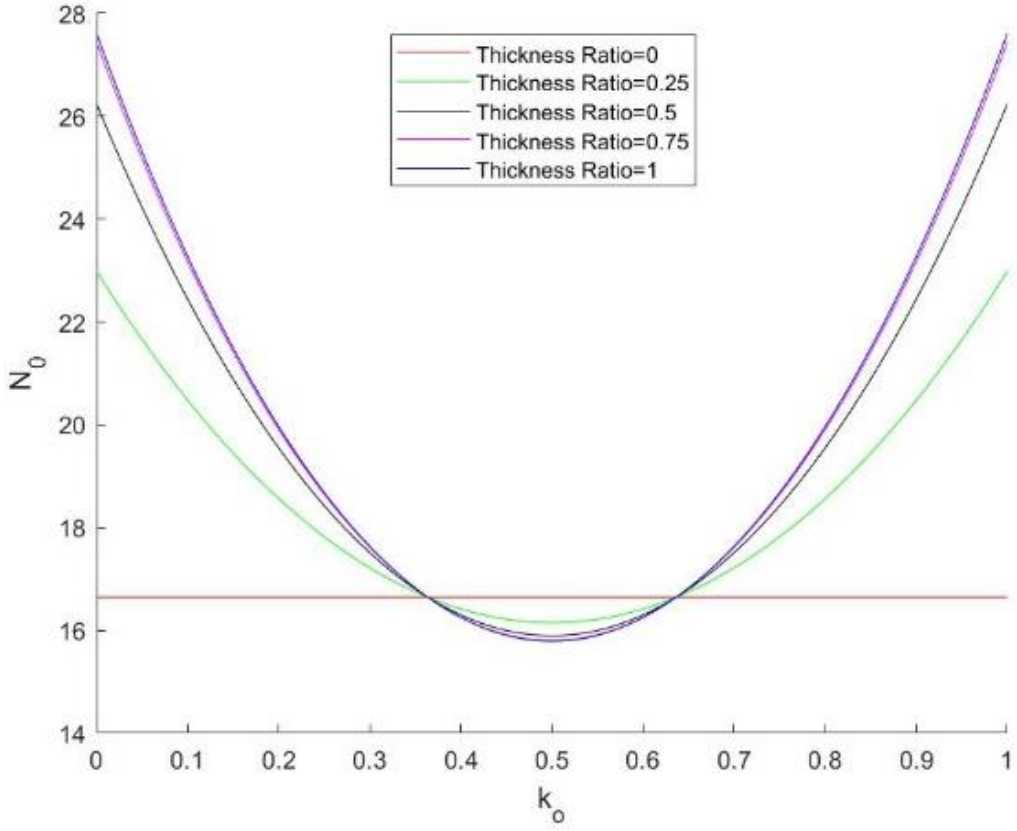

Figure 5.9: Critical buckling load vs. k_o for different values of τ

5.1.1.7 $\mathbf{Vf_{wp_o}}$ vs. $\mathbf{N_0}$ vs. $\frac{\mathbf{a}}{\mathbf{b}}$

In figures 5.14(a), 5.14(b) and 5.14(c), the relationship between the critical buckling load, N_0, and the warp fibre volume fraction in the outer layer, Vf_{wp_o}, is shown for different aspect ratios of the laminate, $\frac{a}{b}$, and increasing graphene platelet weight percentage, W_{gpl_o}. For each amount of W_{gpl_o} from 0% to 2%, buckling load greatly increases as aspect ratio diminishes. This proportion at which the buckling load increases also increases as the aspect ratio diminishes. The effect of the graphene on the influence of the woven glass fibre volume is also shown here. The curves gradually decrease in gradient as W_{gpl_o} increases. The effect of the graphene is thus to increase the critical buckling load and to obscure the influence of the woven glass fibre volume fraction, as discussed in chapter 5.1.1.

$\tau = 0.7;\ \theta_o = 0°;\ \theta_m = 0°;\ W_{gpl_m} = 0;\ Vf_{wf_o} = 0.275;\ k_m = 0.5;\ Vf_{total_m} = 0.55;\ \alpha_b = 1$

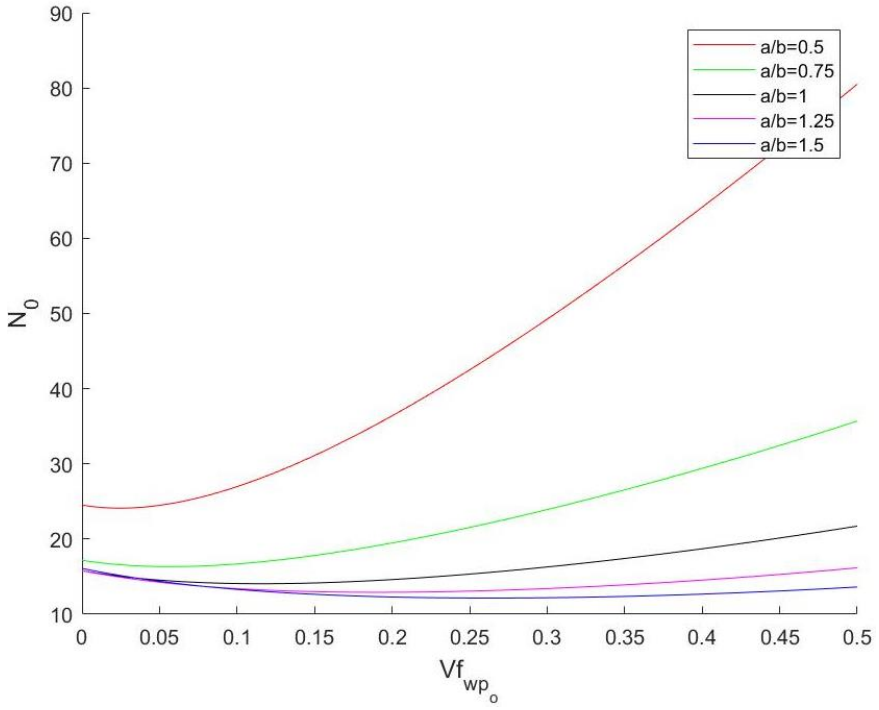

Figure 5.10 (a) $W_{gpl_o} = 0$

$\tau = 0.7;\ \theta_o = 0°;\ \theta_m = 0°;\ W_{gpl_m} = 0;\ Vf_{wf_o} = 0.275;\ k_m = 0.5;\ Vf_{total_m} = 0.55;\ \alpha_b = 1$

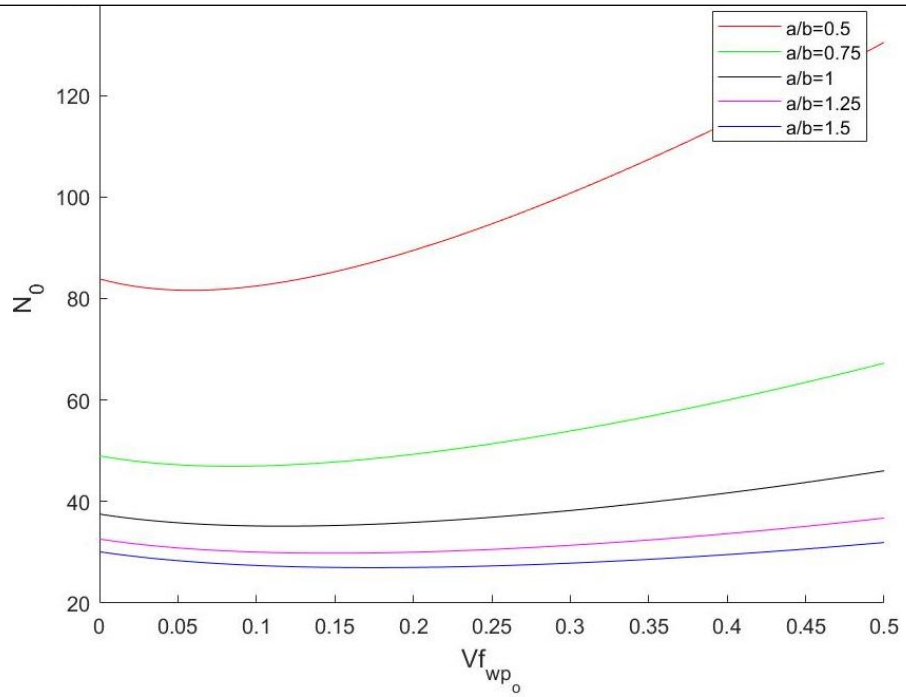

Figure 5.1411 (b) $W_{gpl_o} = 0.01$

$\tau = 0.7;\ \theta_o = 0°;\ \theta_m = 0°;\ W_{gpl_m} = 0;\ Vf_{wf_o} = 0.275;\ k_m = 0.5;\ Vf_{total_m} = 0.55;\ \alpha_b = 1$

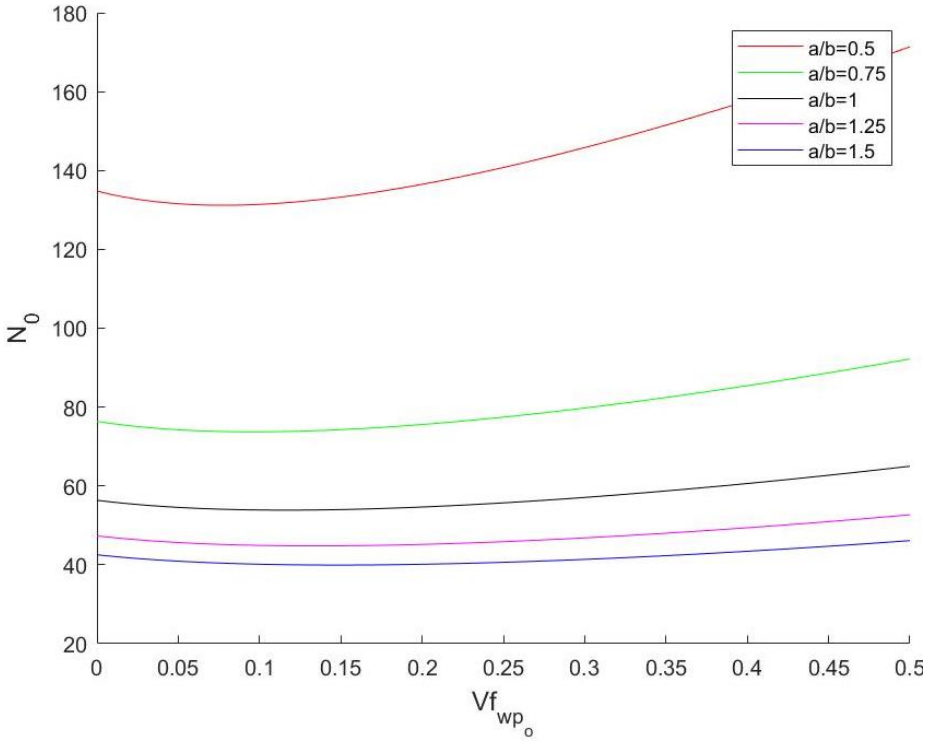

Figure 5.14 (c) $W_{gpl_o} = 0.02$

Figure 5.14: : Critical buckling load vs. Vf_{wp_o} *for different values of a/b*

5.1.2 Woven fibre balancing co-efficient

In this section, the effect of the woven glass fibre balancing coefficient in the outer layer of the woven glass fibre and graphene reinforced laminate, k_o, on the non-dimensional critical buckling load, N_0, is investigated. The section deals with the behaviour of the critical buckling load under different values of k_o and the how the combination of the woven glass fibre balancing coefficient with other laminate specifications (such as total woven glass fibre volume fraction, Vf_{total_o}, woven glass fibre orientation, θ_o, and laminate thickness ratio, τ) influences the critical buckling load.

5.1.2.1 $\mathbf{k_o}$ vs. $\mathbf{N_0}$ vs. $\mathbf{Vf_{total_o}}$

Figure 5.15 shows the relationship between the non-dimensional critical buckling load, N_0, and the woven glass fibre balancing coefficient in the outer layers, k_o, for different woven glass fibre volume fractions in the outer layers, Vf_{total_o}. At a certain k_o, the critical buckling load is at its lowest possible value. For $\frac{a}{b} = 2$ in figure 5.15, this low point occurs somewhere between $k_o = 0.6$ and $k_o = 0.8$. For low graphene content, the highest critical buckling load is always when the woven glass fibres are more concentrated in one direction (in either the warp or weft direction) rather than balanced. Thus either $k_o = 1$ or 0 is preferred, depending on the aspect ratio of the laminate. In figure 5.15, for $\frac{a}{b} = 2$, the critical buckling load favours a laminate with fibres more concentrated in the weft direction ($k_o = 0$).

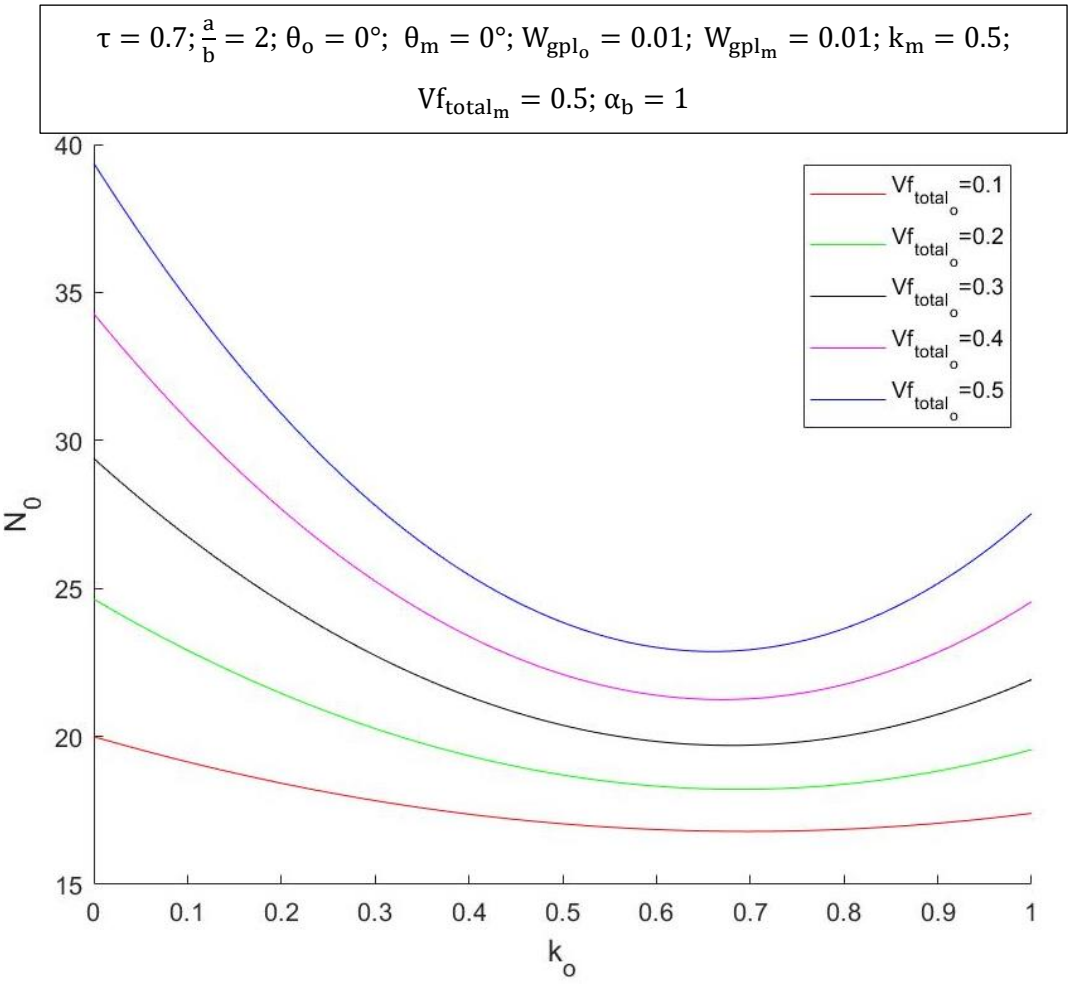

Figure 5.15: Critical buckling load vs. k_o for different values of Vf_{total_o}

Figure 5.16 shows the combined influence of the aspect ratio, $\frac{a}{b}$, and the outer layer woven glass fibre balancing coefficient, k_o, on the non-dimensional critical buckling load, N_0. For $\frac{a}{b} = 2$, $k_o = 0$ yields a higher critical buckling load. If $\frac{a}{b} = 1$, $k_o = 1$ yields a higher critical buckling load. Between $\frac{a}{b} = 0.4$ and $\frac{a}{b} = 2$, with $W_{gpl_o} = W_{gpl_m} = 0.01$, a more concentrated fibre distribution in one direction (either more warp or more weft concentrated, with either $k_o = 1$ or 0) is always the ideal scenario for the critical buckling load.

$\tau = 0.7$; $\theta_o = 0°$; $\theta_m = 0°$; $W_{gpl_o} = 0.01$; $W_{gpl_m} = 0.01$; $Vf_{total_o} = 0.5$; $k_m = 0.5$; $Vf_{total_m} = 0.5$; $\alpha_b = 1$

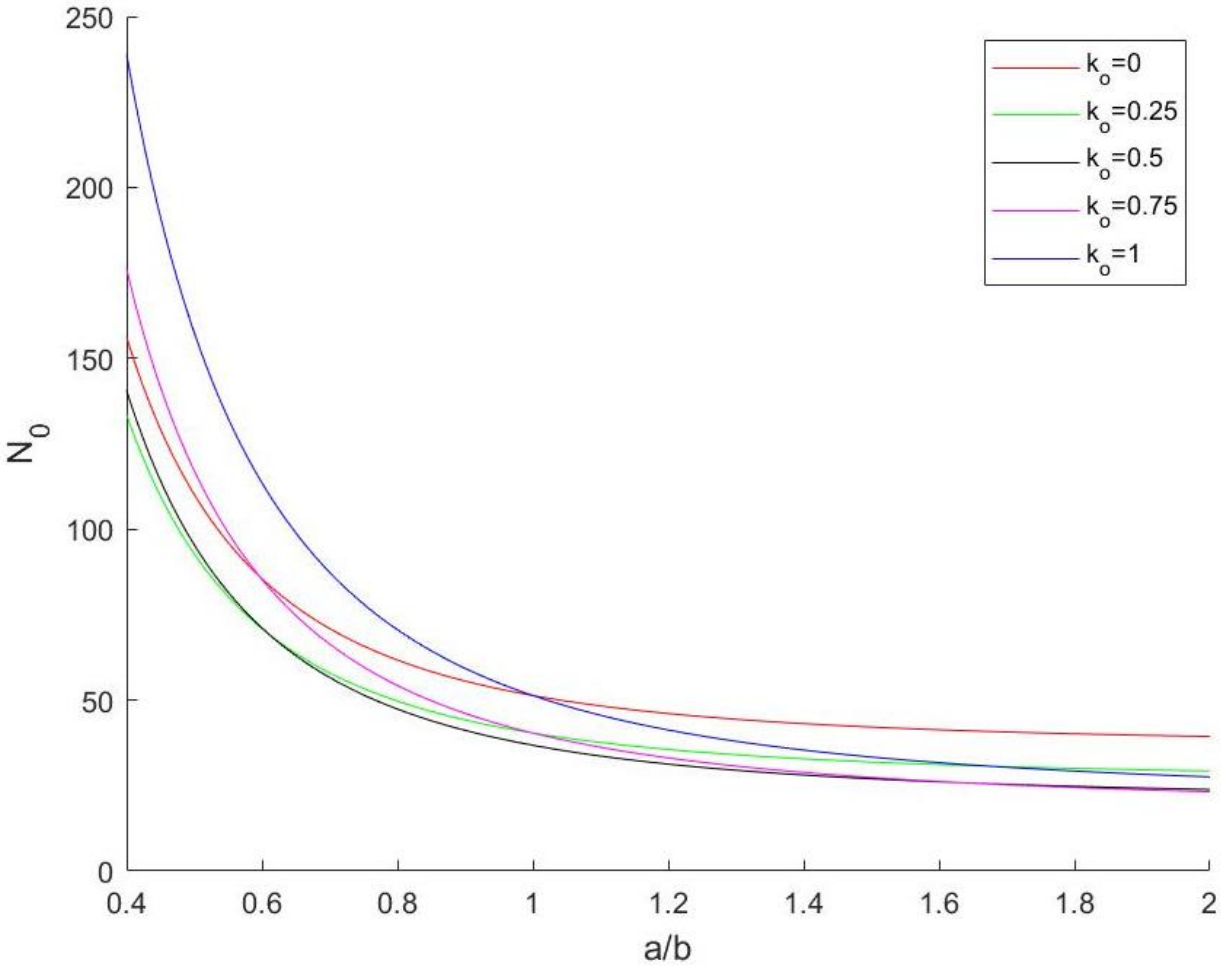

Figure 5.16: Critical buckling load vs. a/b for different values k_o

5.1.2.2 k_o vs. N_0 vs. θ_o

Figure 5.17 shows the relationship between the non-dimensional critical buckling load, N_0, and the woven glass fibre balancing coefficient in the outer layer, k_o, for different fibre orientations in the outer layer, θ_o, and for increasing graphene content in the outer layer, W_{gpl_o}. In figure 5.17(a), with no graphene present, the critical buckling load favours $\theta_o = 90°$ for $k_o < 0.5$. At $k_o = 0.5$, the curves intersect, and a crossover point occurs. For $k_o > 0.5$, a fibre orientation closer to or equal to 0° is more beneficial. In figures 5.17(a), 5.17(b) and 5.17(c), $\frac{a}{b}$ is set to equal 0.4. For $k_o < 0.5$ and low graphene content (up to approximately 6%), a fibre orientation closer to or equal to 90° is more beneficial. However, in figure 5.17(d) for $W_{gpl_o} = 6\%$ and above, the converse is true: for $k_o < 0.5$, $\theta_o = 0°$ yields the highest critical buckling load. The obscured effect of the fibre orientation on the buckling load as graphene content increases should also be kept in mind, however. At $W_{gpl_o} = 6\%$ in figure 5.17(d), the non-dimensional critical buckling load only varies between 422 and 428 for $0° \leq \theta_o \leq 90$. This is effect is discussed further in chapter 5.1.3.

The value of θ_o that yields the maximum critical buckling load on either side of the crossover point depends on the aspect ratio. In figure 5.18, the effect of the laminate aspect ratio, $\frac{a}{b}$, is depicted. For $\frac{a}{b} = 0.4$, maximum critical buckling load is when $\theta_o = 0°$. Hence, in figures 5.17(a), 5.17(b) and 5.17(c), the maximum critical buckling load after the crossover point ($k_o > 0.5$) is when $\theta_o = 0°$. If $\frac{a}{b} = 1$, for example, the maximum critical buckling load after the crossover point would be when $\theta_o = 45°$.

$\tau = 0.7;\ \frac{a}{b} = 0.4;\ \theta_m = 0°;\ W_{gpl_m} = 0;\ Vf_{total_o} = 0.5;\ k_m = 0.5;\ Vf_{total_m} = 0.55;\ \alpha_b = 1$

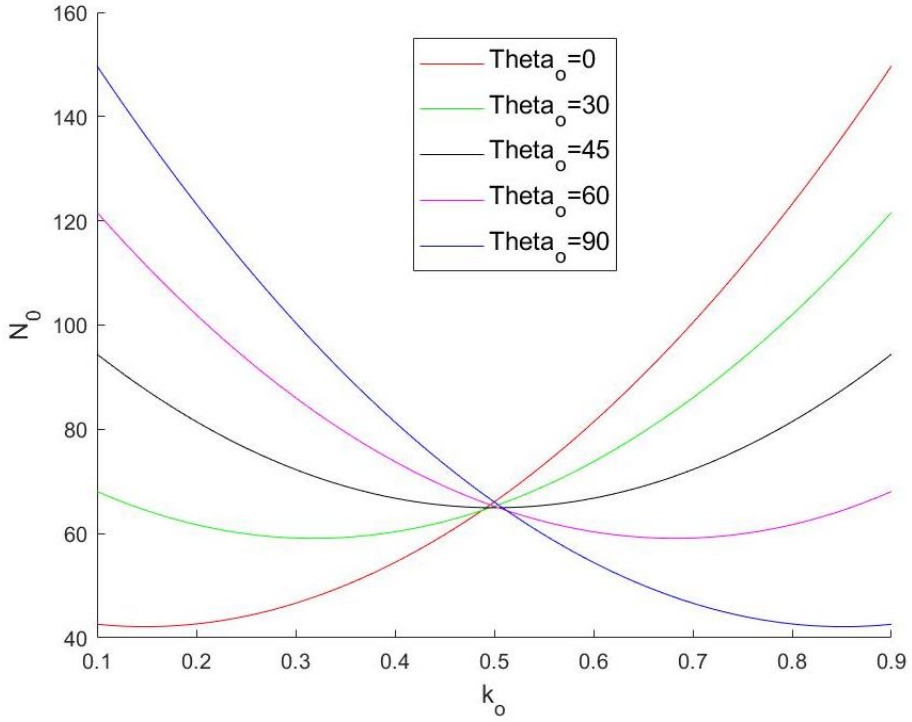

Figure 5.17 (a) $W_{gpl_o} = 0$

$\tau = 0.7;\ \frac{a}{b} = 0.4;\ \theta_m = 0°;\ W_{gpl_m} = 0;\ Vf_{total_o} = 0.5;\ k_m = 0.5;\ Vf_{total_m} = 0.55;\ \alpha_b = 1$

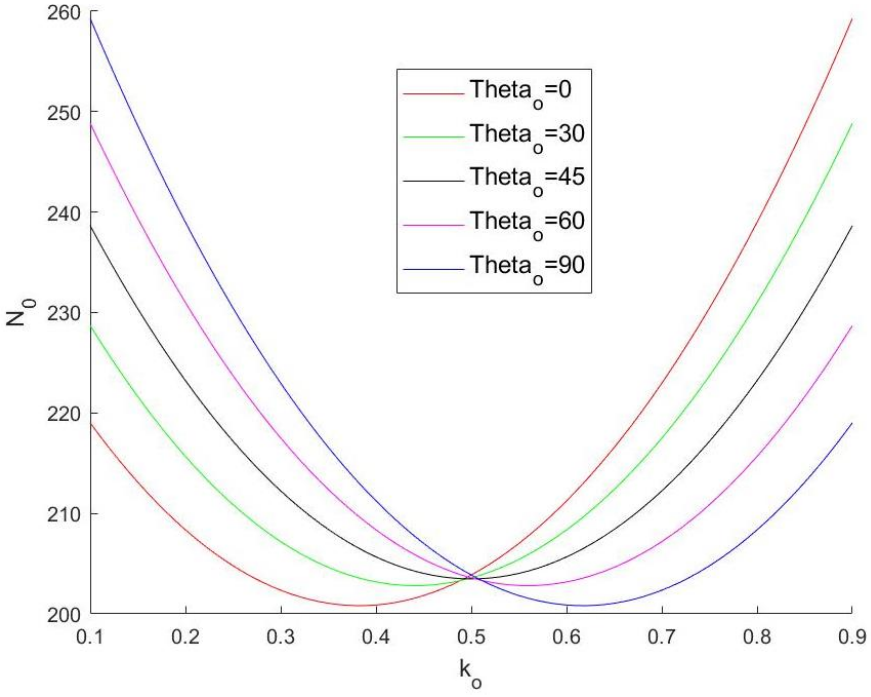

Figure 5.127 (b) $W_{gpl_o} = 0.02$

$\tau = 0.7;\ \frac{a}{b} = 0.4;\ \theta_m = 0°;\ W_{gpl_m} = 0;\ Vf_{total_o} = 0.5;\ k_m = 0.5;\ Vf_{total_m} = 0.55;\ \alpha_b = 1$

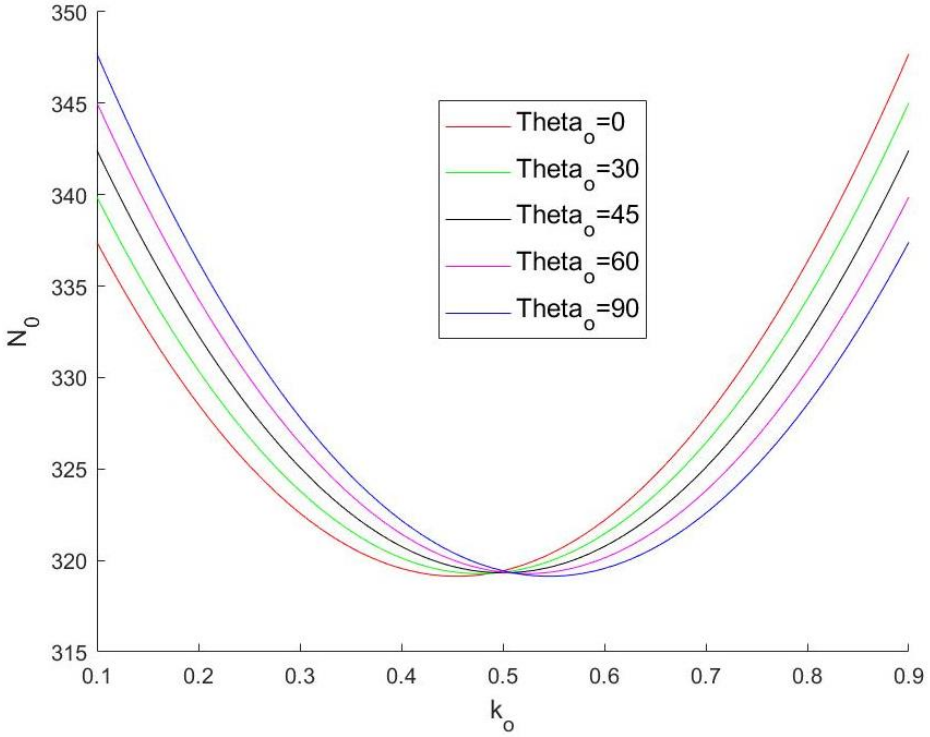

Figure 5.17 (c) $W_{gpl_o} = 0.04$

$\tau = 0.7;\ \frac{a}{b} = 0.4;\ \theta_m = 0°;\ W_{gpl_m} = 0;\ Vf_{total_o} = 0.5;\ k_m = 0.5;\ Vf_{total_m} = 0.55;\ \alpha_b = 1$

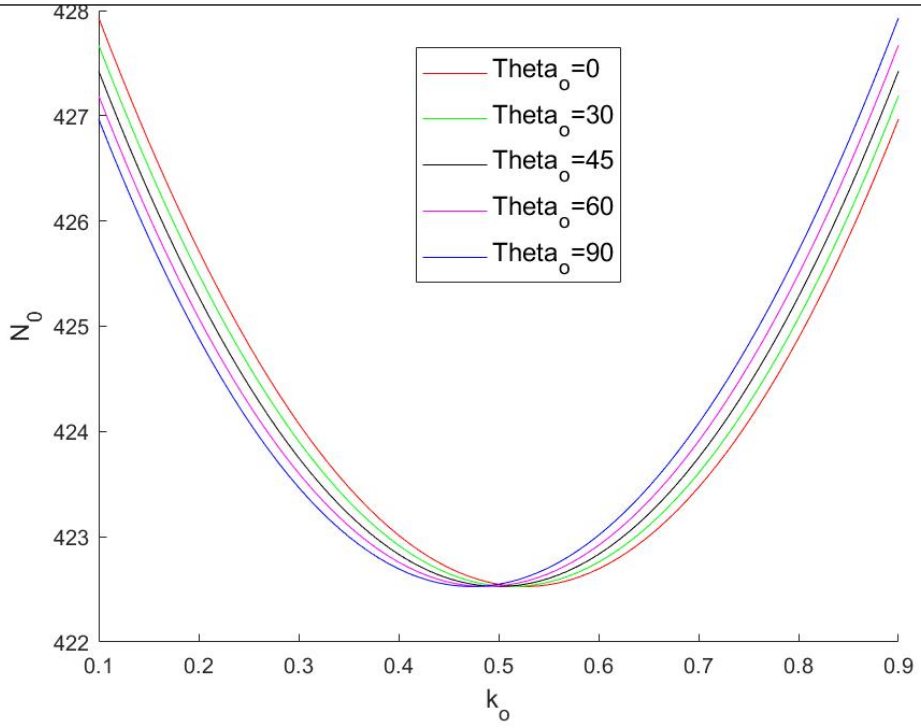

Figure 5.17 (d) $W_{gpl_o} = 0.06$

Figure 5.17: Critical buckling load vs. k_o *for different values of* θ_o

$\tau = 0.7;\ \theta_m = 0°; W_{gpl_o} = W_{gpl_m} = 0; k_o = 0.6; Vf_{total_o} = 0.5; k_m = 0.5; Vf_{total_m} = 0.55; \alpha_b = 1$

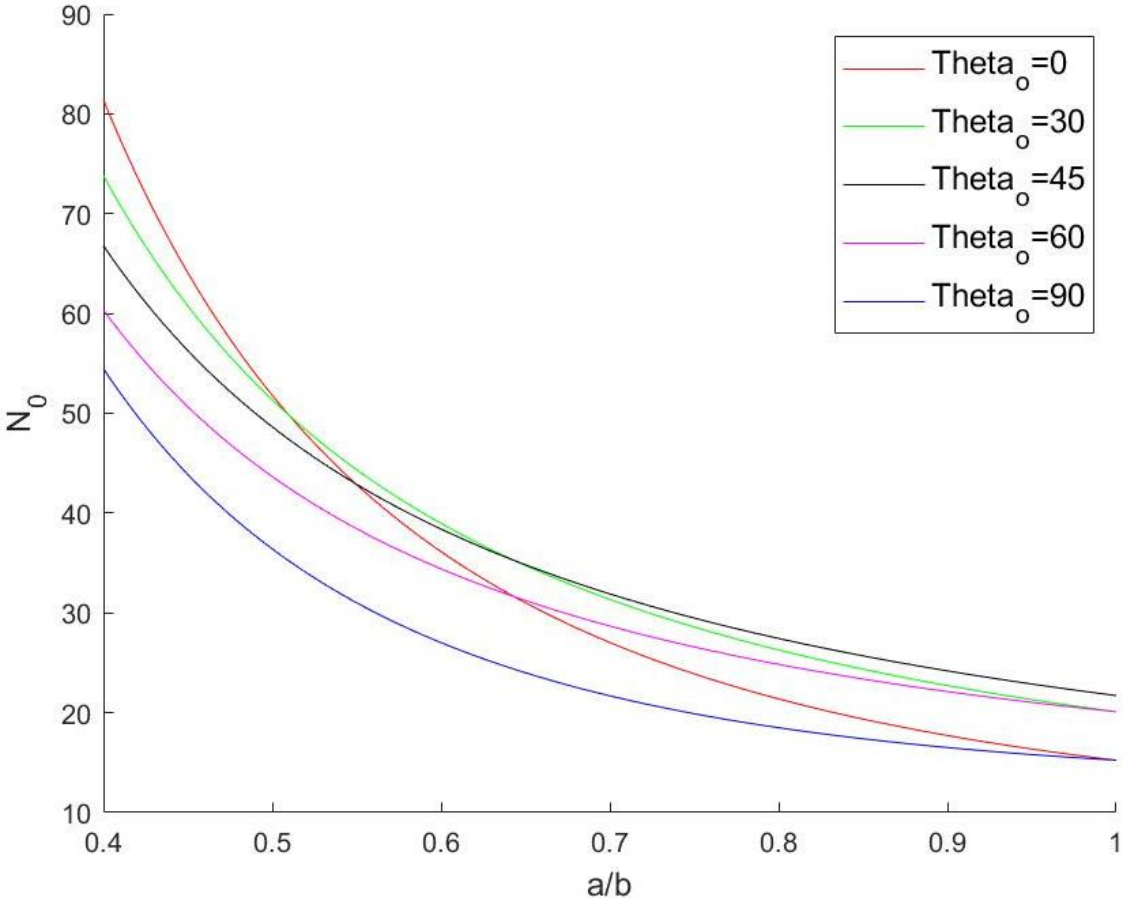

Figure 5.18: Critical buckling load vs. a/b for different values of θ_o

5.1.2.3 k_o vs. N_0 vs. τ

Figures 5.19 and 5.20 show the effect of the woven glass fibre balancing coefficient in the outer layer, k_o, for different values of the thickness ratio, τ. Figure 5.19(a) shows this relationship without the presence of graphene ($W_{gpl_o} = W_{gpl_m} = 0$). With equal volume fractions of fibres in the middle and outer layers, and with no graphene, a higher thickness ratio only yields the highest buckling load when the fibres are more concentrated in the weft or warp direction in the outer layer (when k_o is close to 0 or 1). A lower thickness ratio yields the highest critical buckling load if the fibres are more concentrated in one direction in the middle layer. In figure 5.19(a), with $\frac{a}{b} = 1$, when k_o is less than 0.35 and greater than 0.65, a higher thickness ratio yields the highest buckling load even though $Vf_{total_o} < Vf_{total_m}$. This is because the fibres in the outer layer are more concentrated in a single direction for these values of k_o. A lower thickness ratio is more ideal for the critical buckling load between $k_o = 0.35$ and $k_o = 0.65$. This is because the fibres in the outer layer are close to balanced at these values, less concentration occurs in either the warp or weft direction in the outer layer and more fibre volume is present in the

middle layer ($Vf_{total_m} = 0.55$ whereas $Vf_{total_o} = 0.5$). The maximum critical buckling load occurs at either $k_o = 0$ or $k_o = 1$. The effect of the graphene nanoplatelets is to obscure the influence of the woven glass fibre balancing coefficient, as can be seen in figures 5.19(b) and 5.20(b). With $W_{gpl_o} = 3\%$, a higher thickness ratio is always preferred as the graphene in the outer layer has a greater influence on the critical buckling load than the woven glass fibres.

$\frac{a}{b} = 1$; $\theta_o = 0°$; $\theta_m = 0°$; $W_{gpl_m} = 0$; $Vf_{total_o} = 0.5$; $k_m = 0.5$; $Vf_{total_m} = 0.55$; $\alpha_b = 1$

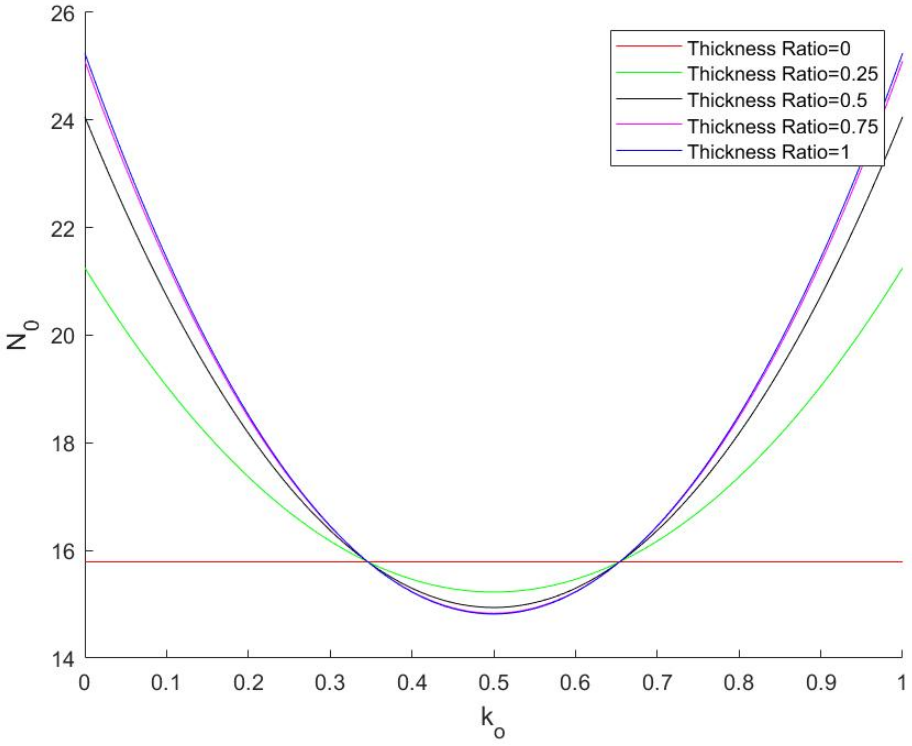

Figure 5.19 (a) $W_{gpl_o} = 0$

$\frac{a}{b} = 1; \theta_o = 0°; \theta_m = 0°; W_{gpl_m} = 0; Vf_{total_o} = 0.5; k_m = 0.5; Vf_{total_m} = 0.55; \alpha_b = 1$

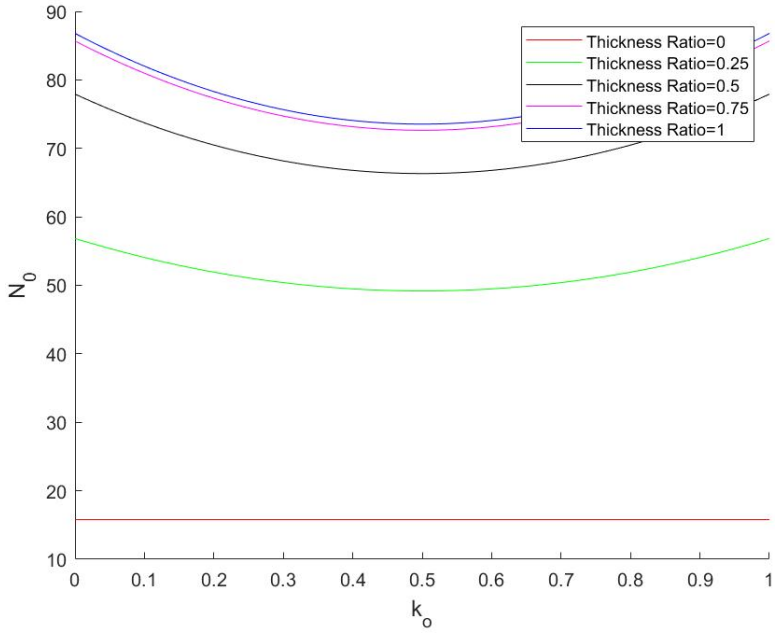

Figure 5.19 (b) $W_{gpl_o} = 0.03$

Figure 5.19: Critical buckling load vs. k_o *for different values of* τ

$\frac{a}{b} = 0.4; \theta_o = 0°; \theta_m = 0°; W_{gpl_m} = 0; Vf_{total_o} = 0.5; k_m = 0.5; Vf_{total_m} = 0.55; \alpha_b = 1$

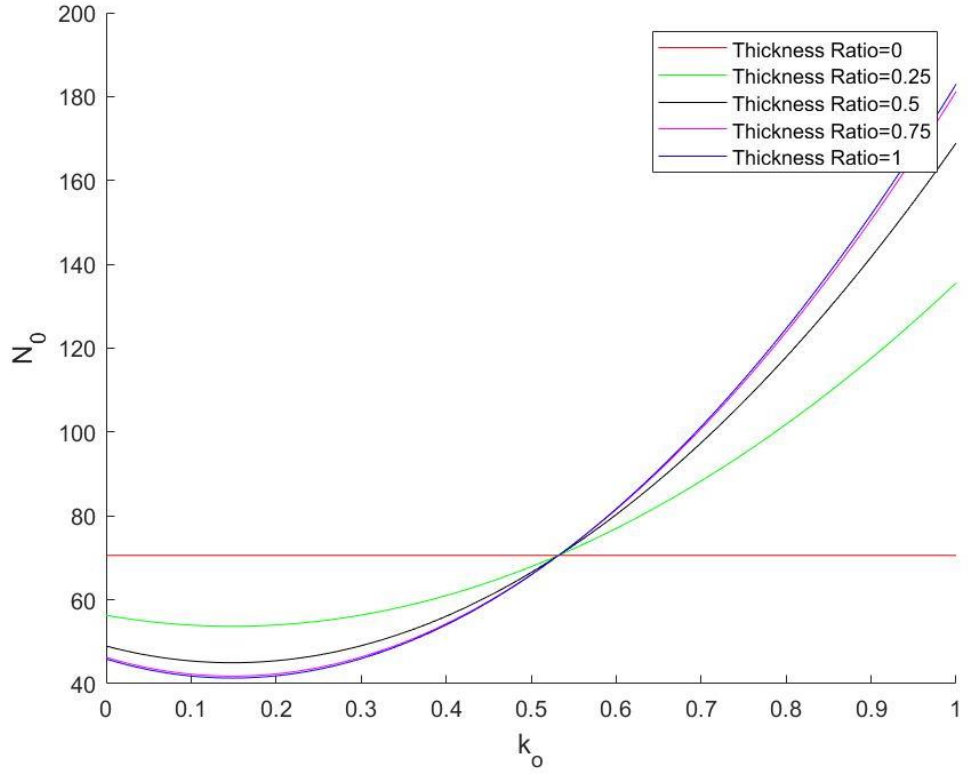

Figure 5.20 (a) $W_{gpl_o} = 0$

$\frac{a}{b} = 0.4$; $\theta_o = 0°$; $\theta_m = 0°$; $W_{gpl_m} = 0$; $Vf_{total_o} = 0.5$; $k_m = 0.5$; $Vf_{total_m} = 0.55$; $\alpha_b = 1$

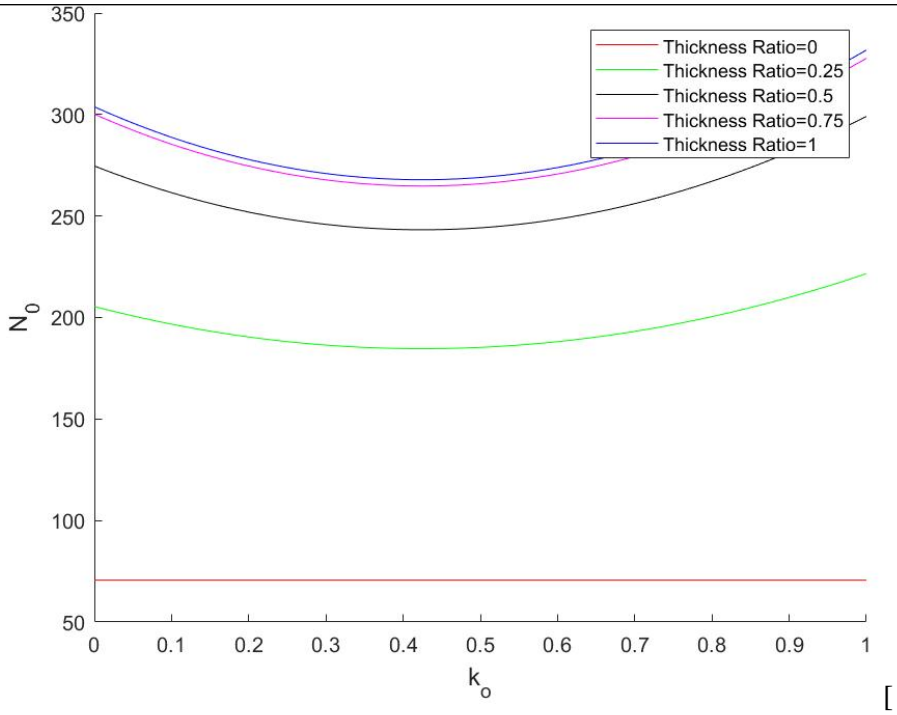

Figure 5.20 (b) $W_{gpl_o} = 0.03$

Figure 5.20: Critical buckling load vs. k_o *for different values of* τ

The values of k_o at which a lower thickness ratio will yield a higher critical buckling load is determined by the aspect ratio, $\frac{a}{b}$. In figure 5.19(a), $\frac{a}{b} = 1$. Here, a lower thickness ratio yields the maximum buckling load when $0.35 \leq k_o \leq 0.65$. In figure 5.20(a), $\frac{a}{b} = 0.4$. Here, a lower thickness ratio yields a higher critical buckling load when approximately $k_o < 0.53$. Figure 5.21 more clearly illustrates the effect of the aspect ratio. In figure 5.21, for $\frac{a}{b} = 1$, $k_o = 0.5$ yields the lowest critical buckling load.

This is verified in figure 5.19(a). For $\frac{a}{b} = 0.4$ in figure 5.21, k_o close to 0.25 yields the lowest critical buckling load. This is verified in figure 20(a).

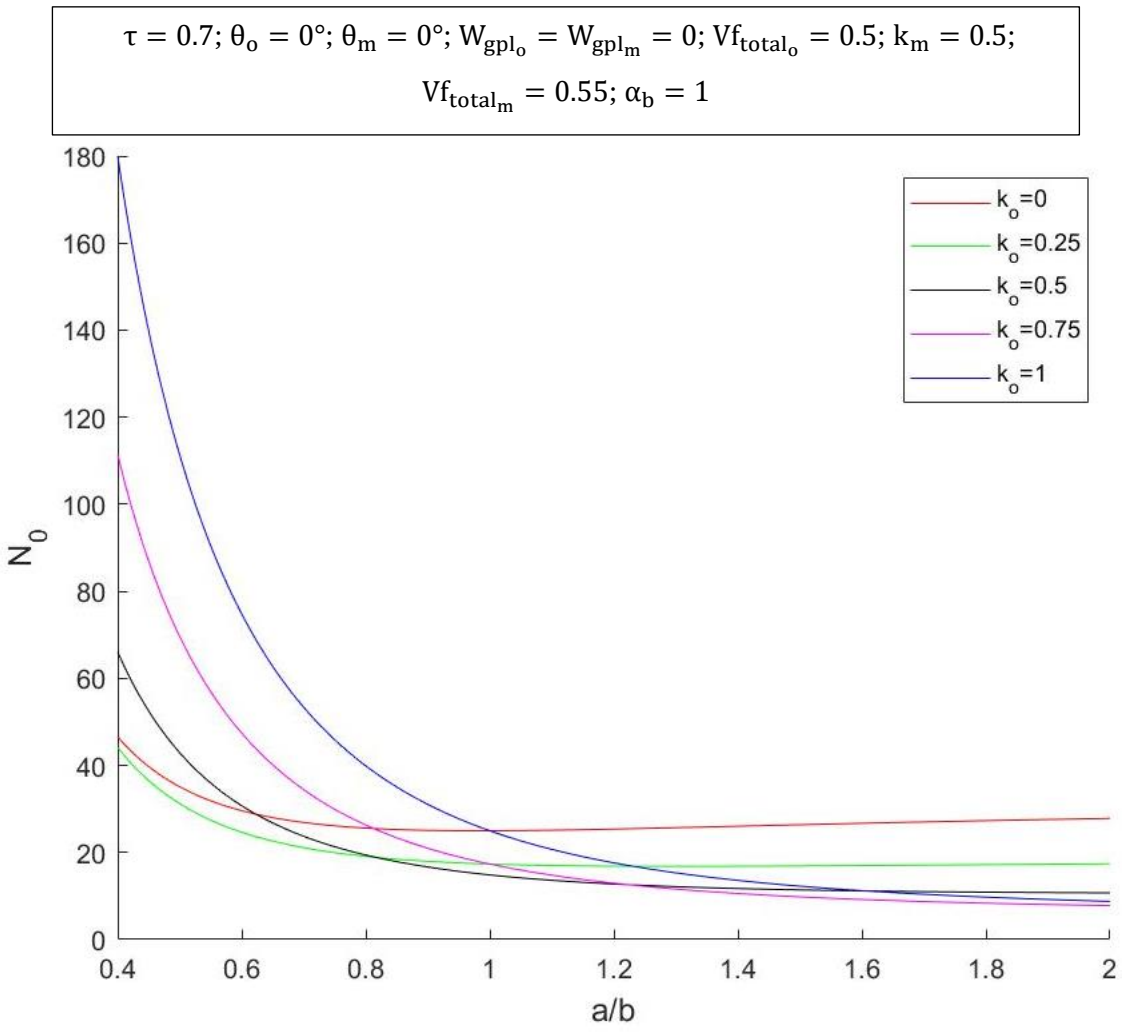

Figure 5.21:Critical buckling load vs. a/b for different values of k_o

5.1.3 Woven fibre orientation

In this section, the effect of the woven glass fibre orientation in the outer layer of the woven fibre and graphene reinforced laminate, θ_o, on the non-dimensional critical buckling load, N_0, is investigated. This section deals with the behaviour of the critical buckling load under different values of θ_o and the how the combination of the woven fibre orientation with other laminate specifications (such as woven glass fibre warp volume fraction, Vf_{wp_o}, graphene weight fraction, W_{gpl_o}, laminate thickness ratio, τ, and laminate aspect ratio, $\frac{a}{b}$) influences the critical buckling load.

5.1.3.1 θ_o vs. N_0 vs. Vf_{wp_o}

Figure 5.22 shows the relationship between the non-dimensional critical buckling load, N_0, and the woven glass fibre orientation in the outer layer, θ_o, for different values of the fibre volume fraction in

the warp direction in the outer layer, Vf_{wp_o}, and increasing graphene weight fraction, W_{gpl_o}. In figure 5.22(a), no graphene is present ($W_{gpl_o} = W_{gpl_m} = 0$). The critical buckling load varies between approximately 39 and 129 for $0° \leq \theta_o \leq 90°$ and $0.1 \leq Vf_{wp_o} \leq 0.5$. The woven glass fibre orientation, θ_o, at which the critical buckling load is at its maximum then heavily depends on the fibre volume fraction in the outer layer, Vf_{wp_o}. For $Vf_{wp_o} = 10\%$, maximum critical buckling load occurs when $\theta_o = 90°$. For $Vf_{wp_o} = 50\%$, however, maximum critical buckling load occurs when $\theta_o = 0°$.

At certain points in figure 5.22(a), the curves intersect. At these intersection points, two different values of Vf_{wp_o} at the same orientation, θ_o, will yield the same critical buckling load. For example, at $\theta \approx 60°$, a warp fibre volume fraction of 10% and a warp fibre volume fraction of 40% will both yield the same critical buckling load. The conservative approach would then be to design the laminate with the lower fibre volume fraction ($Vf_{wp_o} = 10\%$ in this case). Furthermore, two different combinations of Vf_{wp_o} and θ_o can yield the same critical buckling load, N_0. For example, when $\theta = 50°$ and $Vf_{wp_o} = 50\%$, $N_0 \approx 90$. However, if $\theta_o \approx 33°$ and $Vf_{wp_o} = 40\%$, N_0 still equals 90.

The buckling load is also influenced by the outer layer woven glass fibre balancing coefficient, k_o. For k_o values close to balanced ($k_o \approx 0.5$), the fibre orientation, θ_o, has negligible effect on the critical buckling load. In figure 5.22(a), this is when $Vf_{wp_o} = Vf_{wf_o} = 0.275$. This is depicted in the $Vf_{wp_o} = 0.3$ line, which has a gradient close to 0. The combined effect of the woven glass fibre balancing coefficient and the woven glass fibre orientation on the buckling load is further discussed in chapter 5.1.2 and chapter 5.1.3.4.

In figure 5.22(b), the laminate specifications are identical to figure 5.22(a), except $W_{gpl_o} = 1\%$. With the addition, of 1% graphene platelet weight fraction, there are now fewer intersection points of the curves than in figure 5.22(a). The critical buckling load now varies between approximately 120 and 195 for $0° \leq \theta_o \leq 90°$ and $0.1 \leq Vf_{wp_o} 0.5$. The gradients of the curves also decrease with the addition of graphene. This can be seen in figures 5.22(b) – 5.22(f), where graphene weight fraction, W_{gpl_o}, is increased in each figure in increments of 1%. Eventually, at $W_{gpl_o} = 0.04$ in figure 5.22(e), there are no intersection points. In figure 5.22(f), $W_{gpl_o} = 0.05$. The effect of the woven glass fibre orientation, θ_o, is negligible on the critical buckling load as the gradients of the curves are almost 0. The effect of graphene is thus to increase the critical buckling load and obscure the influence of the woven glass fibre orientation. The critical buckling load also loses sensitivity to the woven glass fibre volume fraction as graphene weight fraction is increased. In figure 5.22(a), with no graphene, the non-dimensional critical buckling load, N_0, ranges from 39 to 129 for $0° \leq \theta_o \leq 90°$ and $0.1 \leq Vf_{wp_o} 0.5$. In figure 5.22(f), however, $W_{gpl_o} = 5\%$ and the critical buckling load varies between approximately 370 and 388 for $0° \leq \theta_o \leq 90°$ and $0.1 \leq Vf_{wp_o} \leq 0.5$. This effect was discussed in chapter 5.1.1.

$\tau = 0.7;\ \frac{a}{b} = 0.4;\ \theta_m = 0°;\ W_{gpl_m} = 0;\ Vf_{wf_o} = 0.275;\ k_m = 0.5;\ Vf_{total_m} = 0.55;\ \alpha_b = 1$

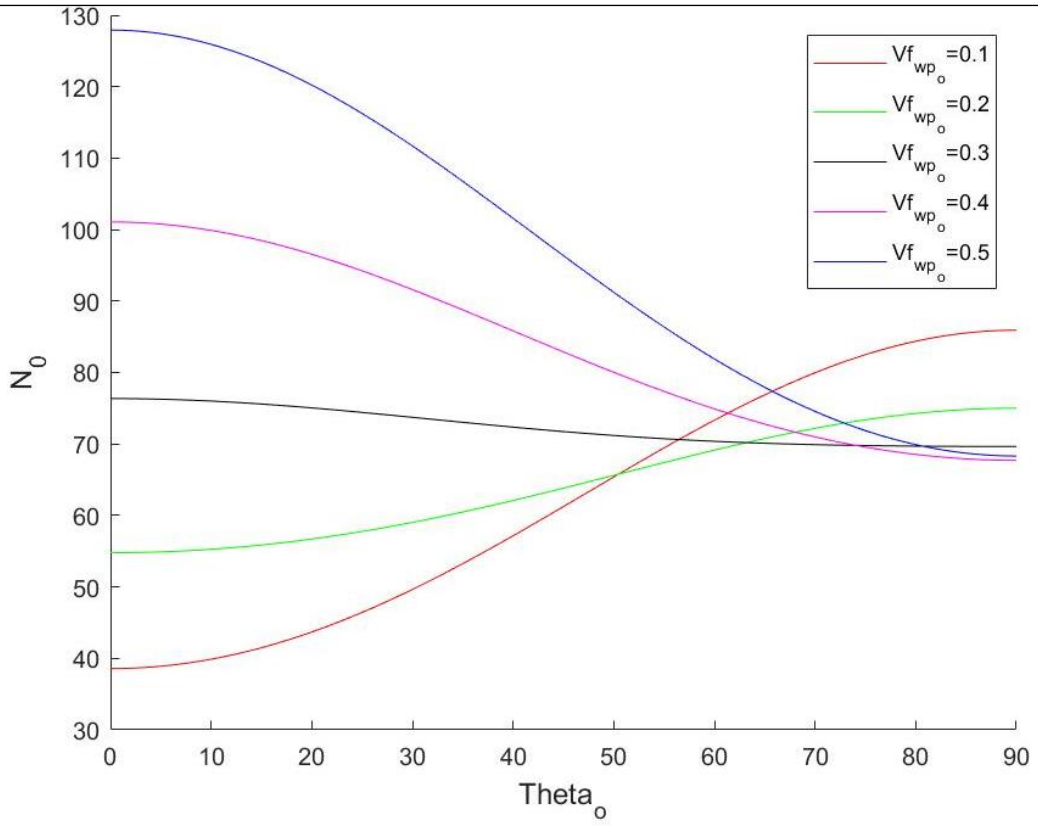

Figure 5.13 (a) $W_{gpl_o} = 0$

$\tau = 0.7;\ \frac{a}{b} = 0.4;\ \theta_m = 0°;\ W_{gpl_m} = 0;\ Vf_{wf_o} = 0.275;\ k_m = 0.5;\ Vf_{total_m} = 0.55;\ \alpha_b = 1$

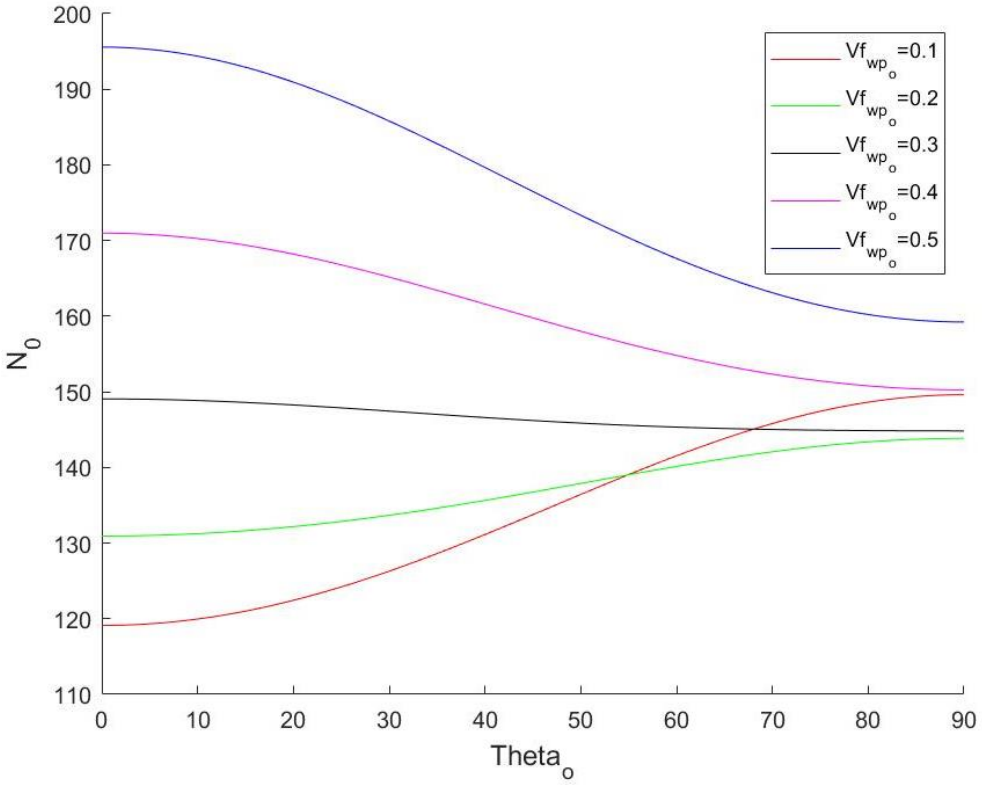

Figure 5.22 (b) $W_{gpl_o} = 0.01$

$\tau = 0.7;\ \frac{a}{b} = 0.4;\ \theta_m = 0°;\ W_{gpl_m} = 0;\ Vf_{wf_o} = 0.275;\ k_m = 0.5;\ Vf_{total_m} = 0.55;\ \alpha_b = 1$

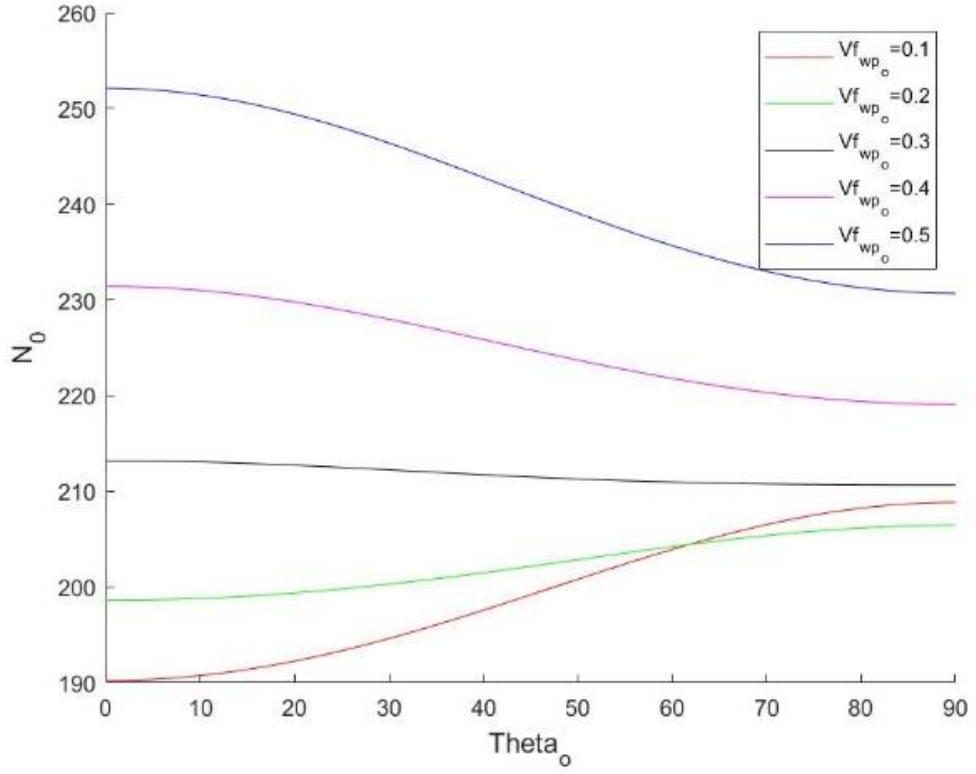

Figure 5.22 (c) $W_{gpl_o} = 0.02$

$\tau = 0.7;\ \frac{a}{b} = 0.4;\ \theta_m = 0°;\ W_{gpl_m} = 0;\ Vf_{wf_o} = 0.275;\ k_m = 0.5;\ Vf_{total_m} = 0.55;\ \alpha_b = 1$

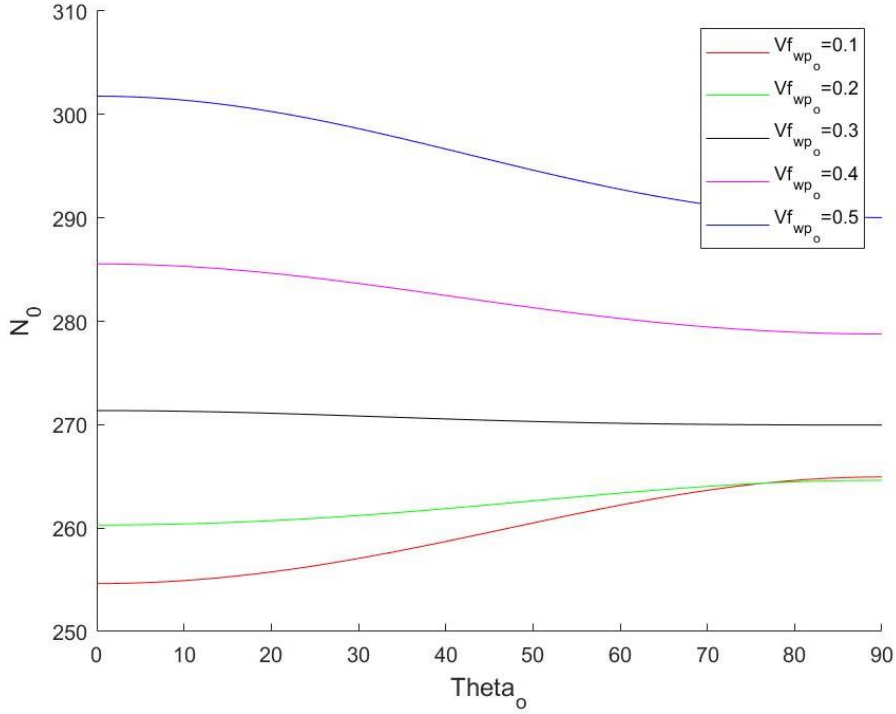

Figure 5.22 (d) $W_{gpl_o} = 0.03$

$\tau = 0.7;\ \frac{a}{b} = 0.4;\ \theta_m = 0°;\ W_{gpl_m} = 0;\ Vf_{wf_o} = 0.275;\ k_m = 0.5;\ Vf_{total_m} = 0.55;\ \alpha_b = 1$

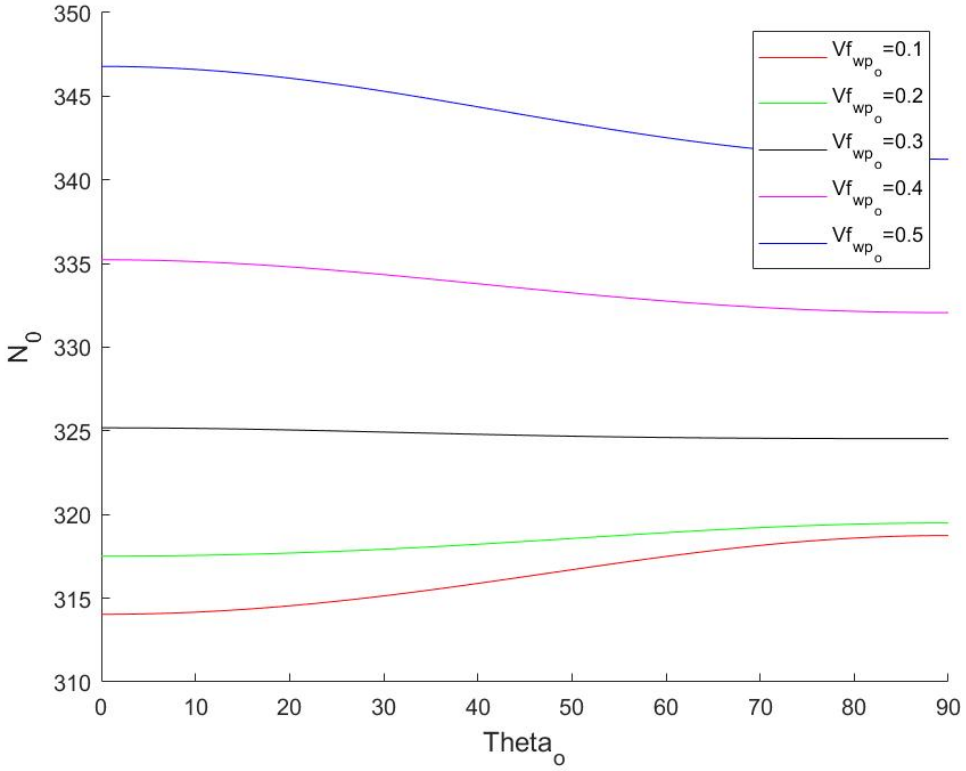

Figure 5.22 (e) $W_{gpl_o} = 0.04$

$\tau = 0.7;\ \frac{a}{b} = 0.4;\ \theta_m = 0°;\ W_{gpl_m} = 0;\ Vf_{wf_o} = 0.275;\ k_m = 0.5;\ Vf_{total_m} = 0.55;\ \alpha_b = 1$

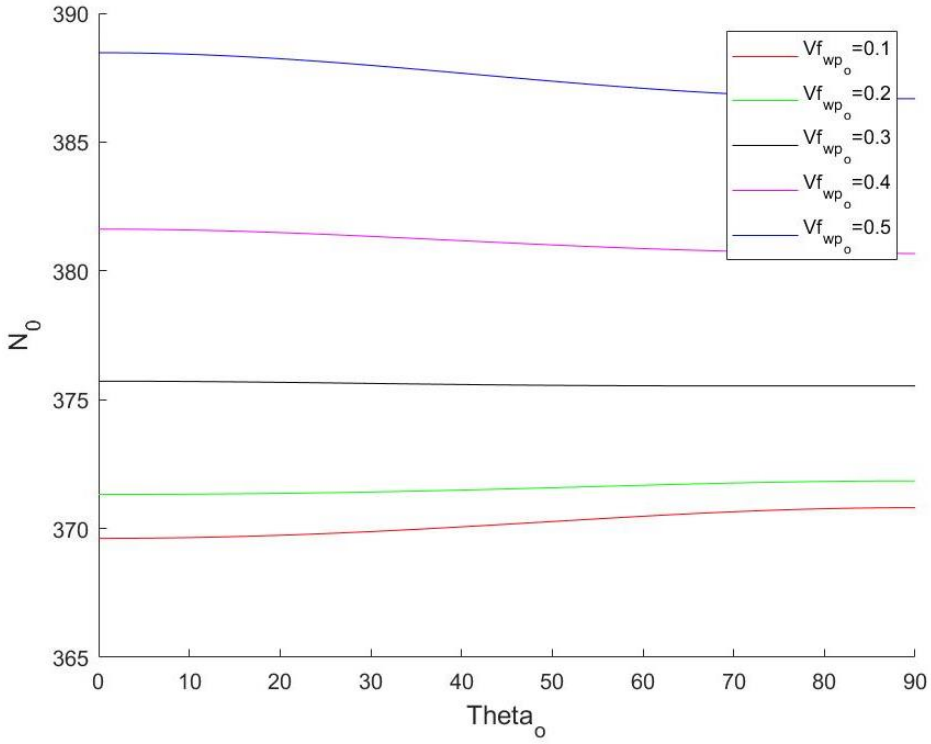

Figure 5.22 (f) $W_{gpl_o} = 0.05$

Figure 5.22: Critical buckling load vs. θ_o *for different values of* Vf_{wp_o}

Naturally, the buckling load for the same amount of warp fibre volume in figure 5.22(b) is higher than in figure 5.22(a). For $\theta_o = 0°$ and $Vf_{wp_o} = 0.2$ in figure 5.22(b), the non-dimensional critical buckling load is approximately 130. In figure 5.22(a), without the presence of graphene, this non-dimensional critical buckling load would be approximately 55. For $\theta_o = 50°$ and $Vf_{wp_o} = 40\%$ in figure 5.22(b), $N_0 \approx 160$. In figure 5.22(a), with no graphene, this result would be $N_0 \approx 85$. Thus, when $\frac{a}{b} = 0.4$, increasing W_{gpl_o} from 0% to 1% results in an approximate increase of 75 in the non-dimensional critical buckling load.

The effect of the woven glass fibre orientation in the outer layer, θ_o, on the non-dimensional critical buckling load, N_0, is also dependant on the aspect ratio, $\frac{a}{b}$, of the laminate. The same woven glass fibre orientation and woven glass fibre volume fraction may yield greatly different critical buckling loads at different aspect ratios. The woven glass fibre orientation, θ_o, at which the critical buckling load, N_0, is at a maximum or a minimum is also dependant on the aspect ratio, $\frac{a}{b}$. Figures 5.23-5.26 depict the effect of the woven glass fibre orientation, θ_o, on the non-dimensional critical buckling load, N_0, at $\frac{a}{b} = 1, 2, 3$

and 4 respectively. In each of these figures, the effect of increasing the graphene platelet weight fraction, W_{gpl_o}, in the laminate is also explored.

In figure 5.23(a)-(f), with laminate aspect ratio $\frac{a}{b} = 1$, the maximum critical buckling load always occurs at $\theta_o = 45°$. Unlike with figure 5.22, there are no intersection points. For $\frac{a}{b} = 1$, at any woven glass fibre orientation, increasing woven glass fibre volume fraction Vf_{wp_o} always results in an increased critical buckling load. The proportion at which the increased critical buckling load increases as woven fibre volume fraction is increased also increases as Vf_{wp_o} increases. In figure 5.23(a), for $\theta_o = 0°$, increasing Vf_{wp_o} from 10% to 20% results in an increase of the non-dimensional critical buckling load, N_0, from 14 to approximately 14.5. However, increasing Vf_{wp_o} from 40% to 50% results in an increase of N_0 from 19 to 22.

In figures 5.23(b)-(f), graphene weight fraction, W_{gpl_o}, is increased in increments of 1%. The gradients of the curves are gradually reduced with the addition of graphene. As with figure 5.22, increasing W_{gpl_o} in the laminate serves to increase the critical buckling load and obscure the effect of the woven glass fibre orientation. This is true for any aspect ratio, as can be seen in figures 5.22-5.26. In figure 5.23(a), with no graphene present, at $\theta_o = 0°$ and $Vf_{wp_o} = 30\%$, the critical buckling load, N_0 is approximately 16. In figure 5.23(b), for the same specifications but with $W_{gpl_o} = 1\%$, the critical buckling load is approximately 38. In general, it can be noted from figure 5.23(a) and 5.23(b) that for $\frac{a}{b} = 1$, increasing W_{gpl_o} from 0% to 1% results in an increase of the critical buckling load in the region of 20-25.

$\tau = 0.7;\ \frac{a}{b} = 1;\ \theta_m = 0°;\ W_{gpl_m} = 0;\ Vf_{wf_o} = 0.275;\ k_m = 0.5;\ Vf_{total_m} = 0.55;\ \alpha_b = 1$

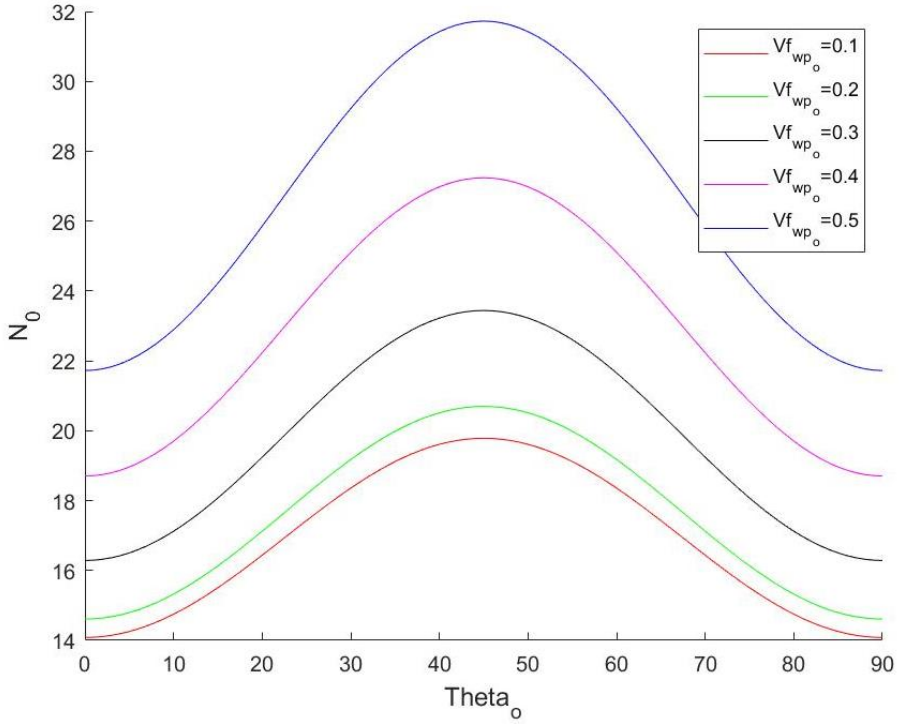

Figure 5.23 (a) $W_{gpl_o} = 0$

$\tau = 0.7;\ \frac{a}{b} = 1;\ \theta_m = 0°;\ W_{gpl_m} = 0;\ Vf_{wf_o} = 0.275;\ k_m = 0.5;\ Vf_{total_m} = 0.55;\ \alpha_b = 1$

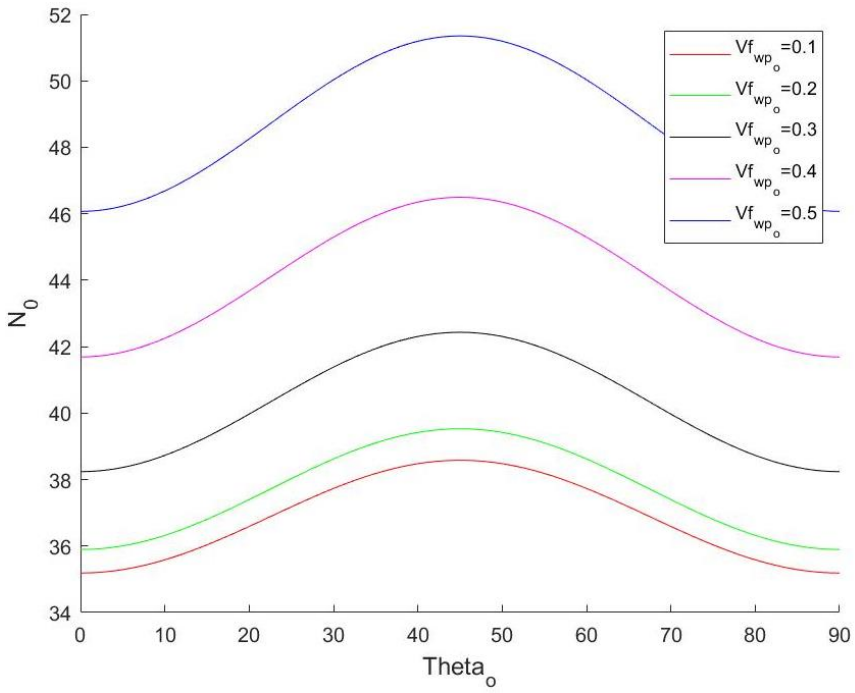

Figure 5.23 (b) $W_{gpl_o} = 0.01$

$\tau = 0.7;\ \frac{a}{b} = 1;\ \theta_m = 0°;\ W_{gpl_m} = 0;\ Vf_{wf_o} = 0.275;\ k_m = 0.5;\ Vf_{total_m} = 0.55;\ \alpha_b = 1$

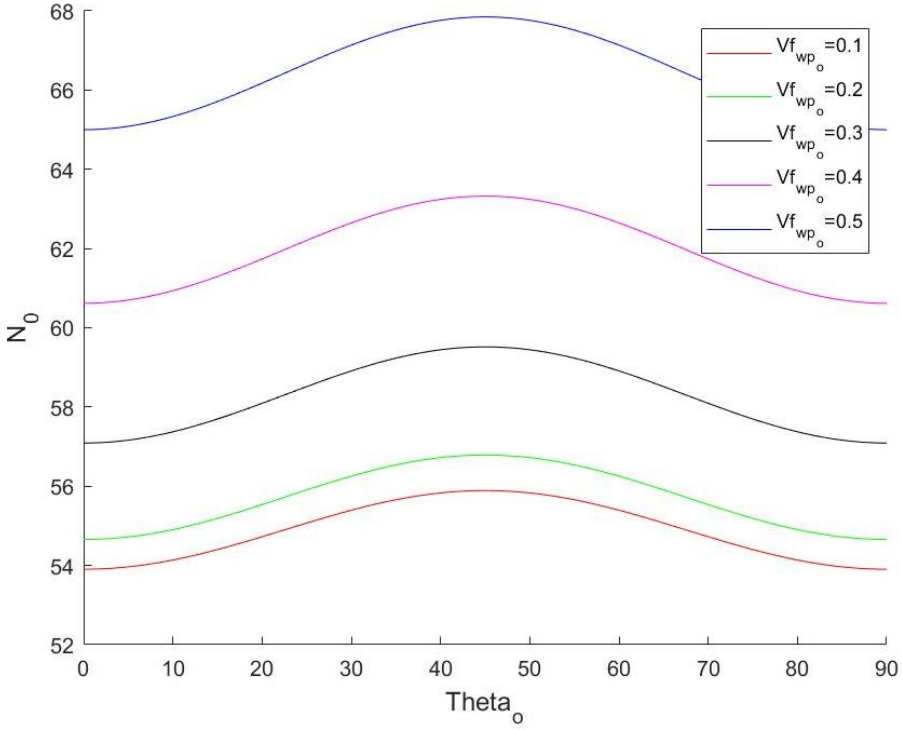

Figure 5.23 (c) $W_{gpl_o} = 0.02$

$\tau = 0.7;\ \frac{a}{b} = 1;\ \theta_m = 0°;\ W_{gpl_m} = 0;\ Vf_{wf_o} = 0.275;\ k_m = 0.5;\ Vf_{total_m} = 0.55;\ \alpha_b = 1$

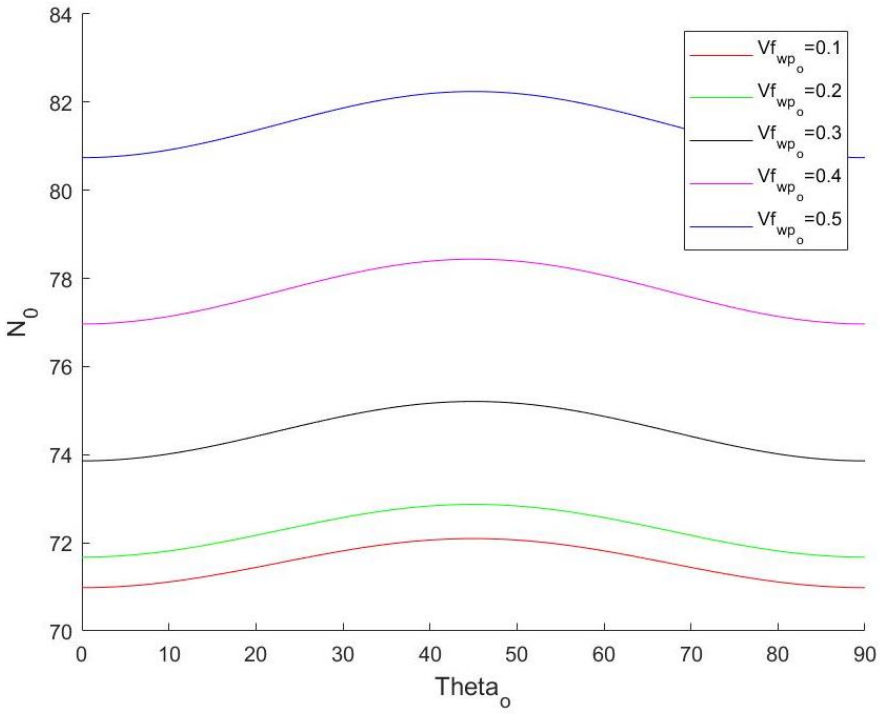

Figure 5.23 (d) $W_{gpl_o} = 0.03$

$\tau = 0.7;\ \frac{a}{b} = 1;\ \theta_m = 0°;\ W_{gpl_m} = 0;\ Vf_{wf_o} = 0.275;\ k_m = 0.5;\ Vf_{total_m} = 0.55;\ \alpha_b = 1$

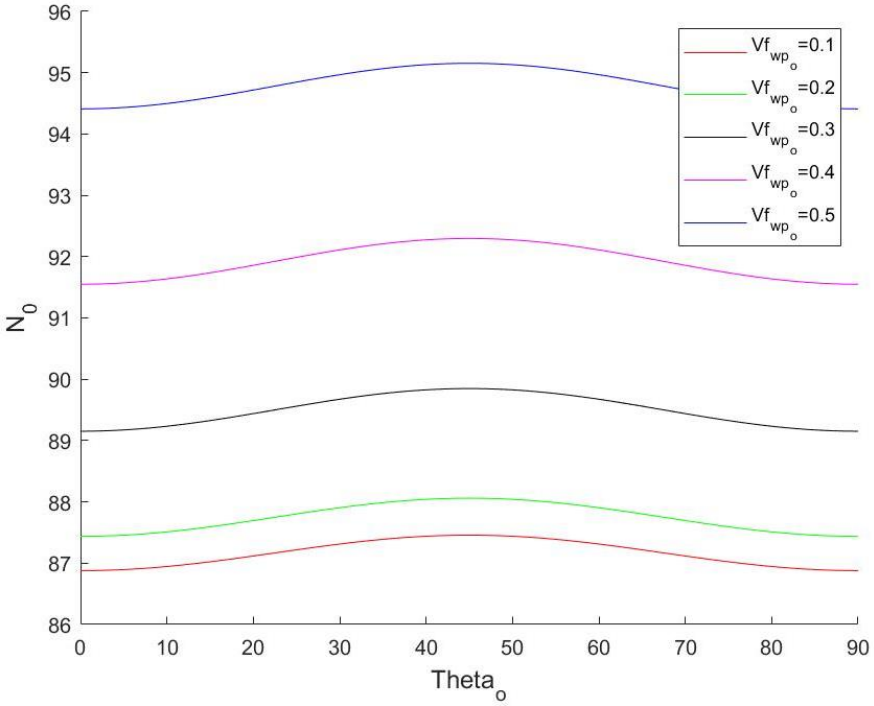

Figure 5.23 (e) $W_{gpl_o} = 0.04$

$\tau = 0.7;\ \frac{a}{b} = 1;\ \theta_m = 0°;\ W_{gpl_m} = 0;\ Vf_{wf_o} = 0.275;\ k_m = 0.5;\ Vf_{total_m} = 0.55;\ \alpha_b = 1$

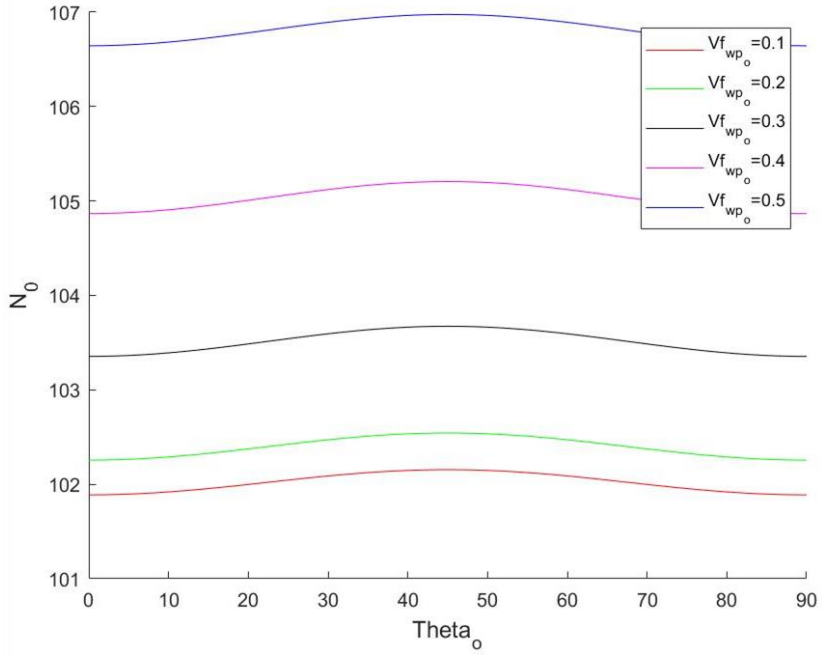

Figure 5.23 (f) $W_{gpl_o} = 0.05$

Figure 5.23: Critical buckling load vs. θ_o *for different values of* Vf_{wp_o}

Figure 5.24 shows the effect of the woven glass fibre orientation in the outer layer, θ_o, on the non-dimensional critical buckling load, N_0, for aspect ratio $\frac{a}{b} = 2$. Like figure 5.22(a), in figure 5.24(a) with no graphene present, there are points where the Vf_{wp_o} curves intersect. Thus, for $\frac{a}{b} = 2$, at certain θ_o values a lower warp fibre volume fraction, Vf_{wp_o}, may be more beneficial than a higher one. For example, at $\theta_o = 0°$, $Vf_{wp_o} = 10\%$ yields a higher critical buckling load than $Vf_{wp_o} = 50\%$.

Again, the woven glass fibre balancing coefficient, k_o, also influences the effect of the woven glass fibre orientation, θ_o. At values of Vf_{wp_o} where k_o is close to or equal to 0.5, the effect of the woven glass fibre orientation is negligible. This can be seen in the $Vf_{wp_o} = 30\%$ line in figure 5.24(a), where the gradient is close to 0.

In figure 5.24(a), with no graphene present, for a woven glass fibre orientation of $\theta_o = 0$ and a woven glass fibre volume fraction in the warp direction of $Vf_{wp_o} = 10\%$, the non-dimensional critical buckling load is approximately 13.5. In figure 5.24(b), for the same specifications but with $W_{gpl_o} = 1\%$, $N_0 \approx 25$. In general, for $\frac{a}{b} = 2$, increasing W_{gpl_o} from 0% to 1% results in an increase of N_0 in the region of 11-15. The effect of graphene is to increase the critical buckling load and obscure the effect of the woven glass fibre orientation and woven glass fibre volume fraction. In figures 5.24(a)-(f), W_{gpl_o} is increased in increments of 1%. In figure 5.24(b), the number of intersection points seen in figure 5.24(a) are reduced and the gradient of the curves are reduced. Eventually, at $W_{gpl_o} = 4\%$, there are no intersection points and a higher woven fibre volume fraction, Vf_{wp_o} will always yield a higher critical buckling load. However, in figure 5.24(f), where $W_{gpl_o} = 5\%$, the critical buckling load varies between approximately 63 and 67 for $0° \leq \theta_o \leq 90°$ and $0.1 \leq Vf_{wp_o} \leq 0.5$. Increasing Vf_{wp_o} from 10% to 50% results in an increase of only 2 in the non-dimensional critical buckling load.

In figures 5.25 and 5.26, the effect of θ_o on the non-dimensional critical buckling load, N_0 is shown for aspect ratios $\frac{a}{b} = 3$ and 4 respectively. The effect of increasing W_{gpl_o} is also depicted here. As shown in figures 5.22-5.24, the effect of graphene is to increase the critical buckling load and obscure the effect of the woven glass fibre orientation, θ_o, and woven glass fibre volume fraction, Vf_{wp_o}, on the critical buckling load. In figure 5.25(a), with no graphene present, at $\theta_o = 0°$ and $Vf_{wp_o} = 10\%$, $N_0 = 14$. For the same specifications in figure 5.25(b) but with $W_{gpl_o} = 1\%$, $N_0 \approx 23.5$. in general, for $\frac{a}{b} = 3$, increasing W_{gpl_o} from 0% to 1% results in an increase of N_0 in the region of 9-13. In figure 5.26(a), with $\frac{a}{b} = 4$ and no graphene present, the critical buckling load varies between approximately 5 and 21 for $0° \leq \theta_o \leq 90°$ and $0.1 \leq Vf_{wp_o} \leq 0.5$. At $\theta_o = 0°$ and $Vf_{wp_o} = 10\%$, $N_0 \approx 14$. For the same specifications but with $W_{gpl_o} = 1\%$, $N_0 \approx 23$ in figure 5.26(b). In general, for $\frac{a}{b} = 4$, increasing W_{gpl_o} from 0% to 1% results in an increase of N_0 in the region of 9-15.

$\tau = 0.7;\ \frac{a}{b} = 2;\ \theta_m = 0°;\ W_{gpl_m} = 0;\ Vf_{wf_o} = 0.275;\ k_m = 0.5;\ Vf_{total_m} = 0.55;\ \alpha_b = 1$

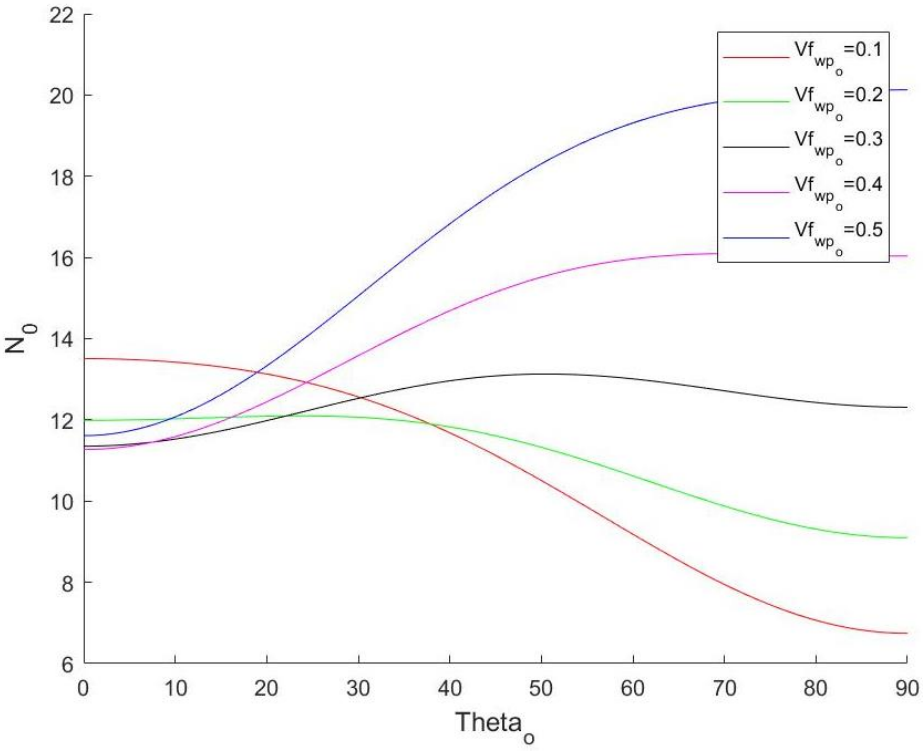

Figure 5.24 (a) $W_{gpl_o} = 0$

$\tau = 0.7;\ \frac{a}{b} = 2;\ \theta_m = 0°;\ W_{gpl_m} = 0;\ Vf_{wf_o} = 0.275;\ k_m = 0.5;\ Vf_{total_m} = 0.55;\ \alpha_b = 1$

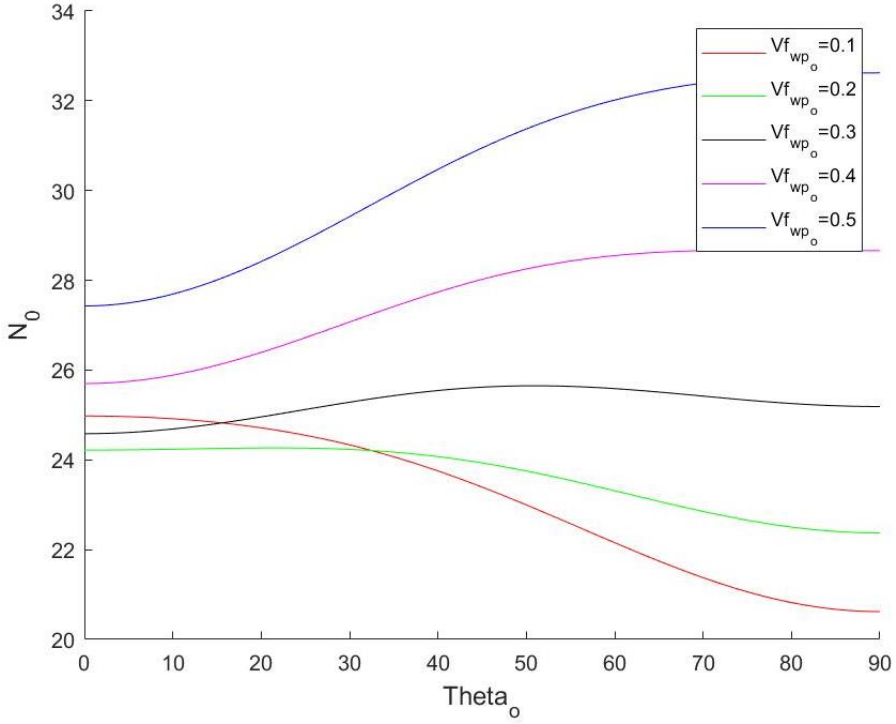

Figure 5.24 (b) $W_{gpl_o} = 0.01$

$\tau = 0.7;\ \frac{a}{b} = 2;\ \theta_m = 0°;\ W_{gpl_m} = 0;\ Vf_{wf_o} = 0.275;\ k_m = 0.5;\ Vf_{total_m} = 0.55;\ \alpha_b = 1$

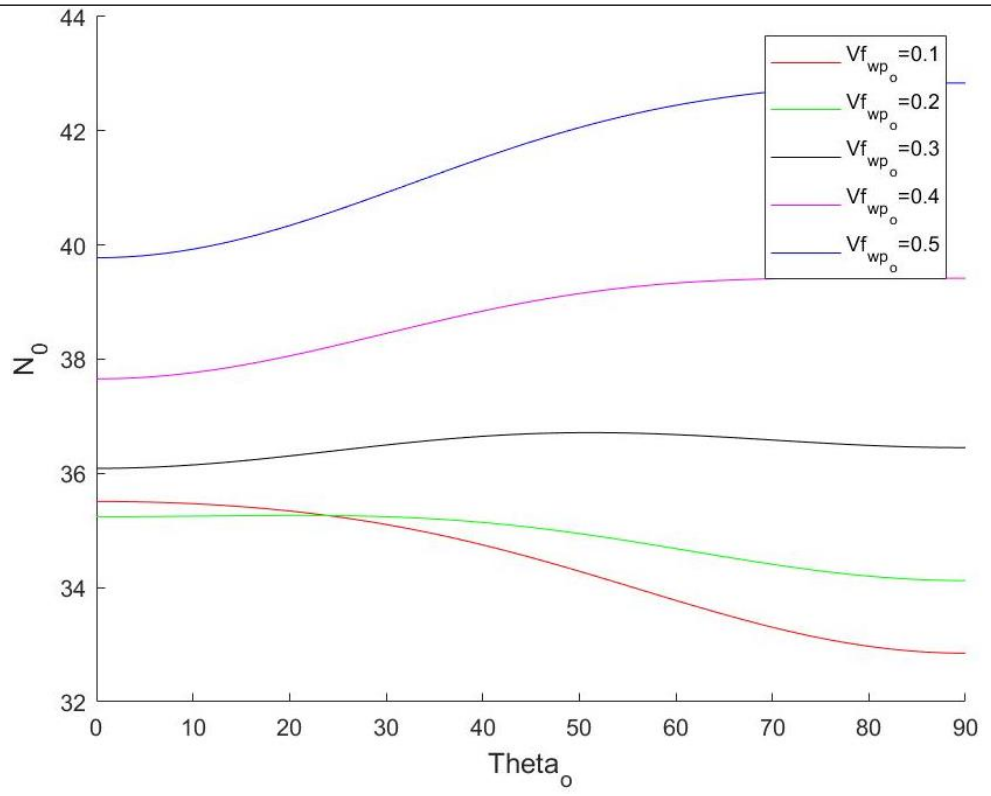

Figure 5.24 (c) $W_{gpl_o} = 0.02$

$\tau = 0.7;\ \frac{a}{b} = 2;\ \theta_m = 0°;\ W_{gpl_m} = 0;\ Vf_{wf_o} = 0.275;\ k_m = 0.5;\ Vf_{total_m} = 0.55;\ \alpha_b = 1$

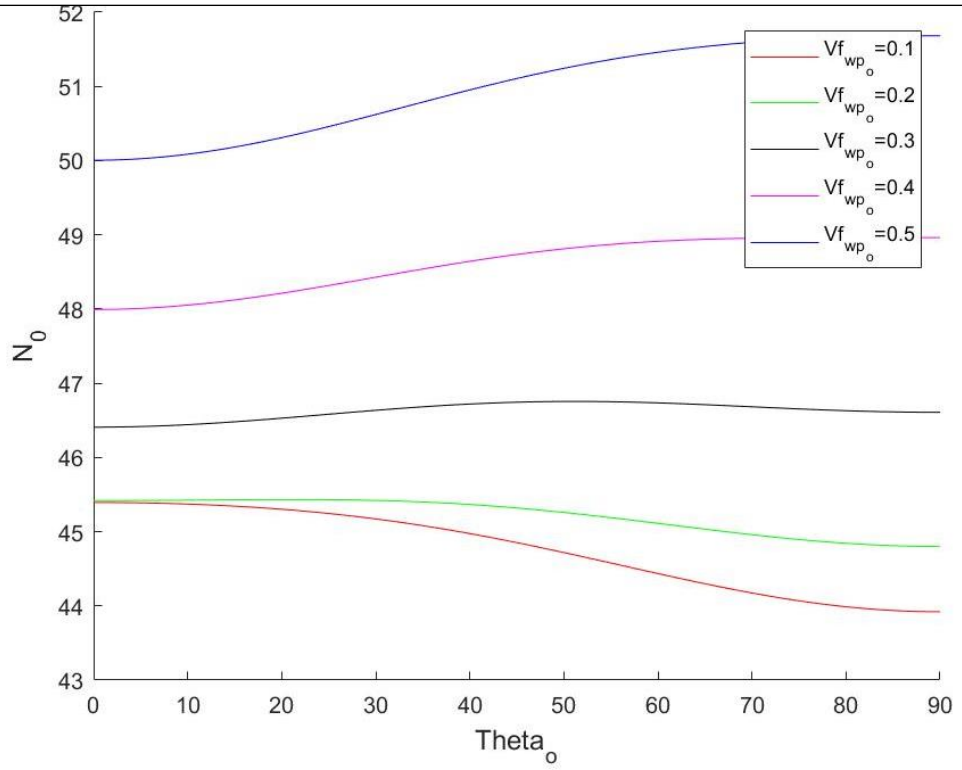

Figure 5.24 (d) $W_{gpl_o} = 0.03$

$\tau = 0.7;\ \frac{a}{b} = 2;\ \theta_m = 0°;\ W_{gpl_m} = 0;\ Vf_{wf_o} = 0.275;\ k_m = 0.5;\ Vf_{total_m} = 0.55;\ \alpha_b = 1$

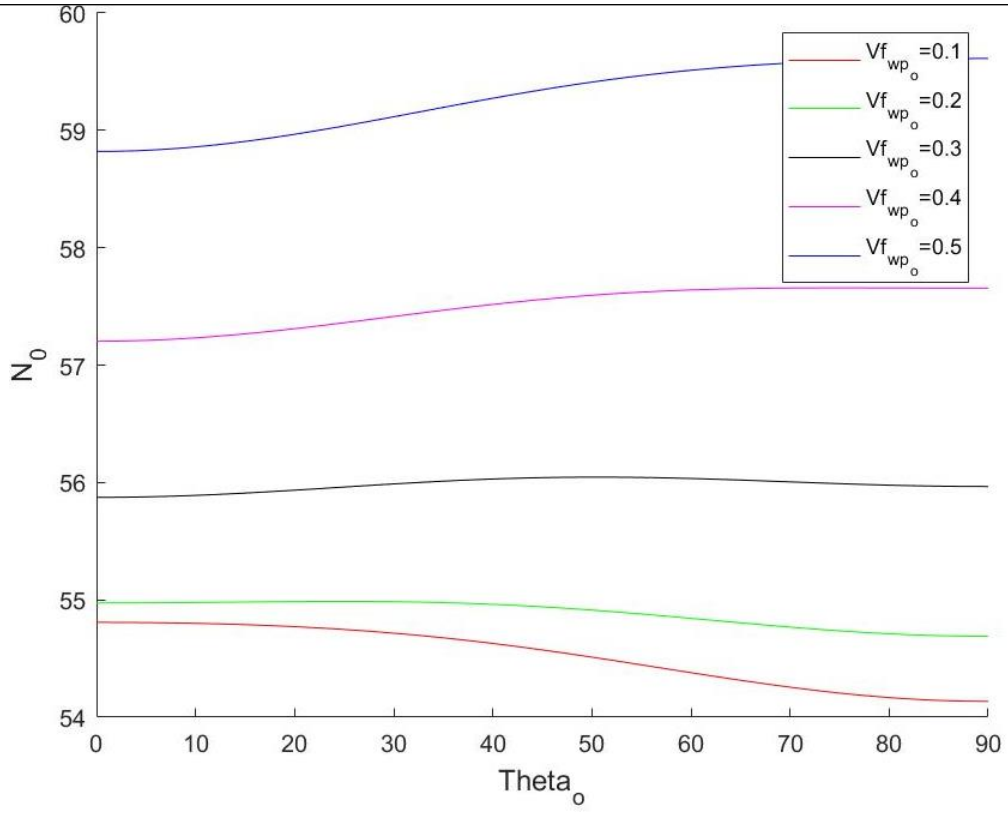

Figure 5.24 (e) $W_{gpl_o} = 0.04$

$\tau = 0.7;\ \frac{a}{b} = 2;\ \theta_m = 0°;\ W_{gpl_m} = 0;\ Vf_{wf_o} = 0.275;\ k_m = 0.5;\ Vf_{total_m} = 0.55;\ \alpha_b = 1$

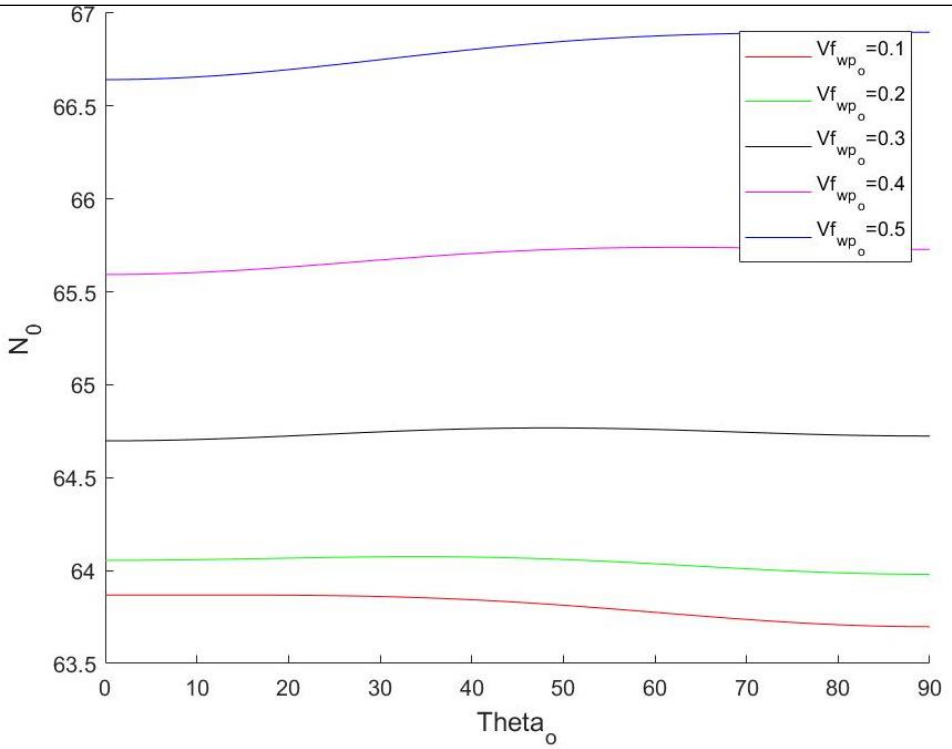

Figure 5.24 (f) $W_{gpl_o} = 0.05$

Figure 5.24: Critical buckling load vs. θ_o *for different values of* Vf_{wp_o}

$\tau = 0.7;\ \frac{a}{b} = 3;\ \theta_m = 0°;\ W_{gpl_m} = 0;\ Vf_{wf_o} = 0.275;\ k_m = 0.5;\ Vf_{total_m} = 0.55;\ \alpha_b = 1$

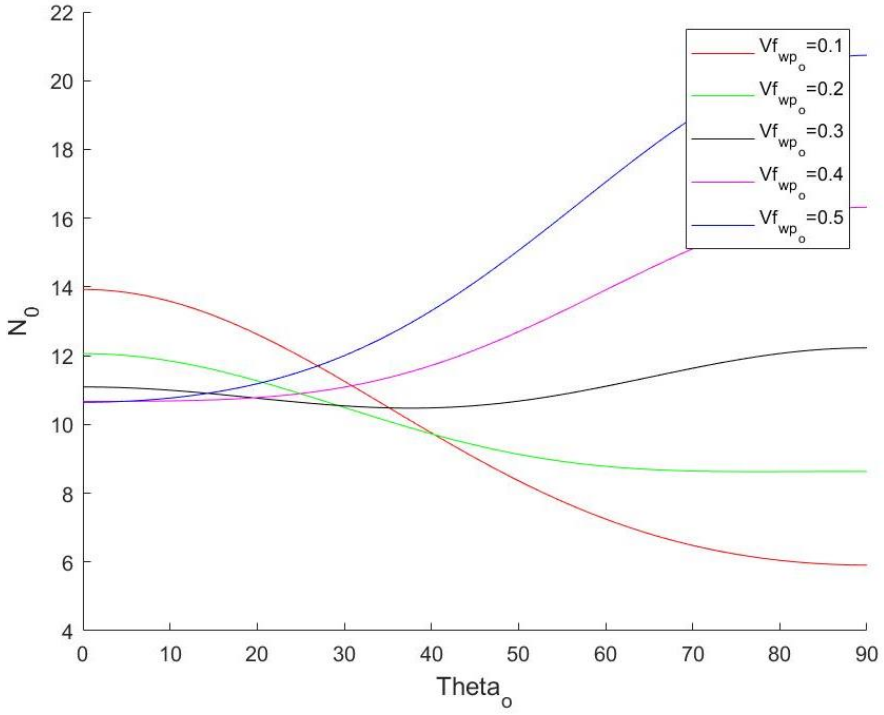

Figure 5.25 (a) $W_{gpl_o} = 0$

$\tau = 0.7;\ \frac{a}{b} = 3;\ \theta_m = 0°;\ W_{gpl_m} = 0;\ Vf_{wf_o} = 0.275;\ k_m = 0.5;\ Vf_{total_m} = 0.55;\ \alpha_b = 1$

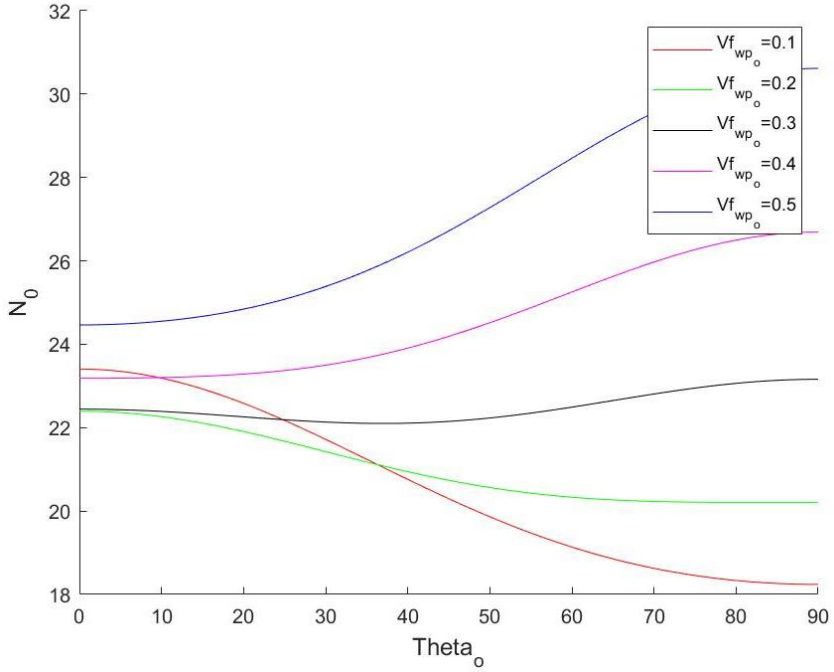

Figure 5.14 (b) $W_{gpl_o} = 0.01$

$\tau = 0.7;\ \frac{a}{b} = 3;\ \theta_m = 0°;\ W_{gpl_m} = 0;\ Vf_{wf_o} = 0.275;\ k_m = 0.5;\ Vf_{total_m} = 0.55;\ \alpha_b = 1$

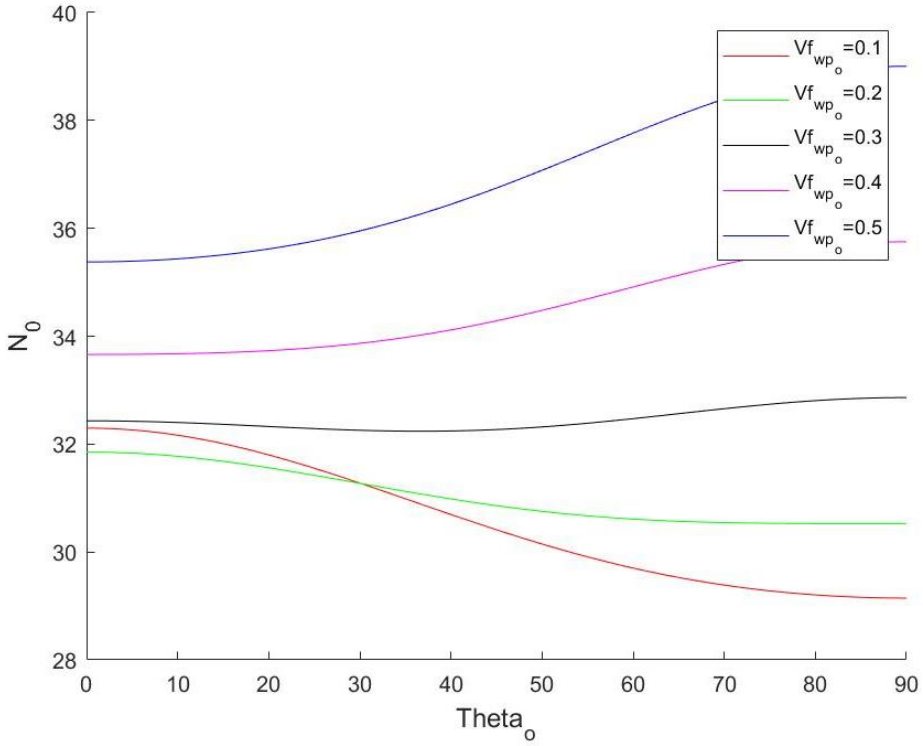

Figure 5.25 (c) $W_{gpl_o} = 0.02$

$\tau = 0.7;\ \frac{a}{b} = 3;\ \theta_m = 0°;\ W_{gpl_m} = 0;\ Vf_{wf_o} = 0.275;\ k_m = 0.5;\ Vf_{total_m} = 0.55;\ \alpha_b = 1$

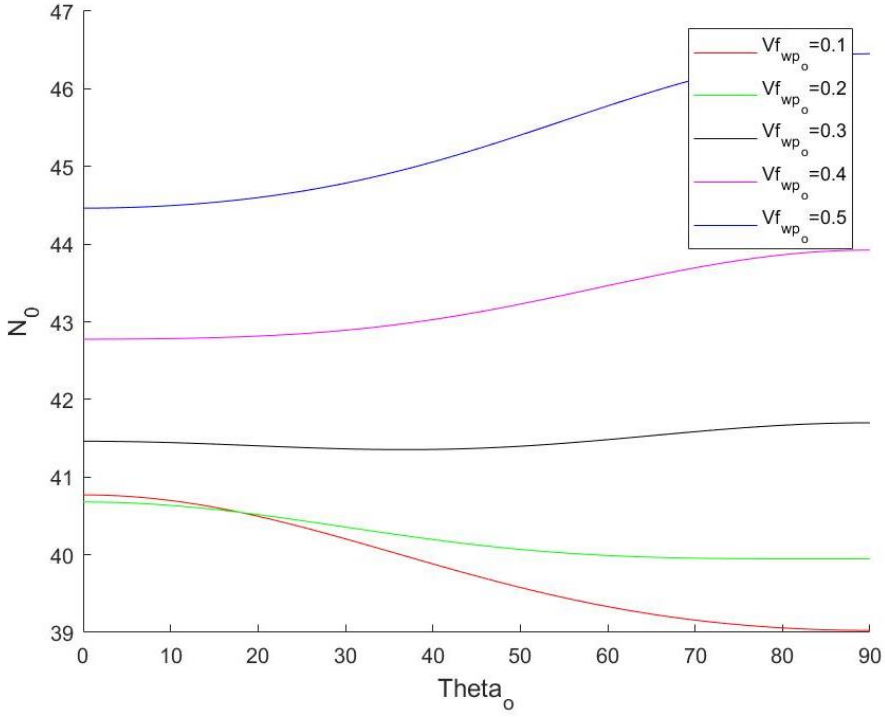

Figure 5.25 (d) $W_{gpl_o} = 0.03$

$\tau = 0.7;\ \frac{a}{b} = 3;\ \theta_m = 0°;\ W_{gpl_m} = 0;\ Vf_{wf_o} = 0.275;\ k_m = 0.5;\ Vf_{total_m} = 0.55;\ \alpha_b = 1$

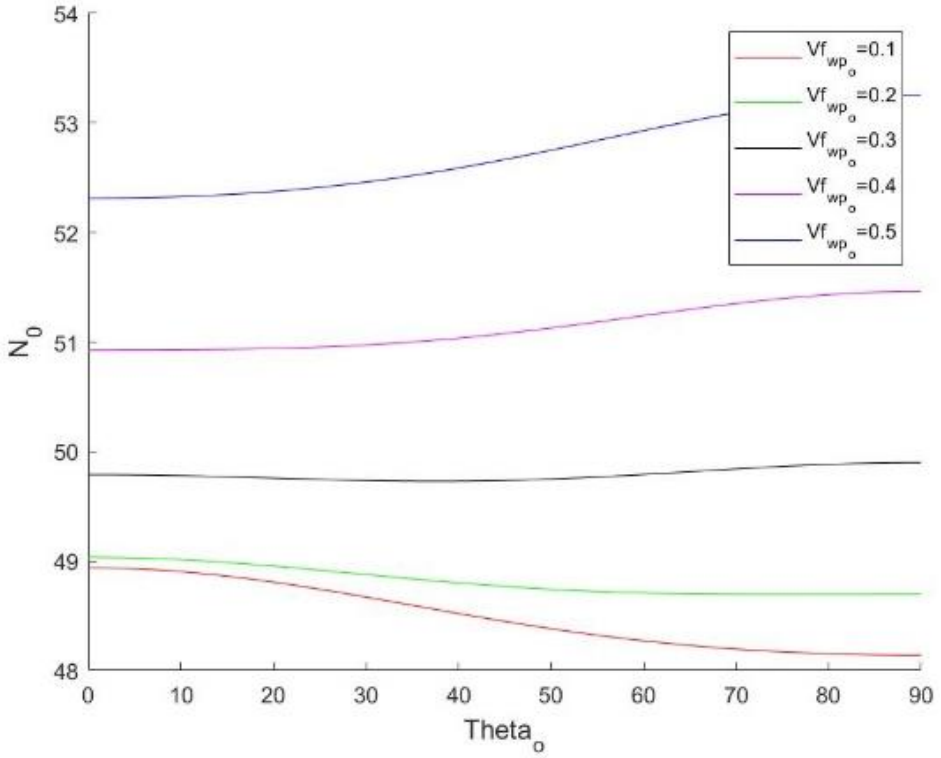

Figure 5.25 (e) $W_{gpl_o} = 0.04$

$\tau = 0.7;\ \frac{a}{b} = 3;\ \theta_m = 0°;\ W_{gpl_m} = 0;\ Vf_{wf_o} = 0.275;\ k_m = 0.5;\ Vf_{total_m} = 0.55;\ \alpha_b = 1$

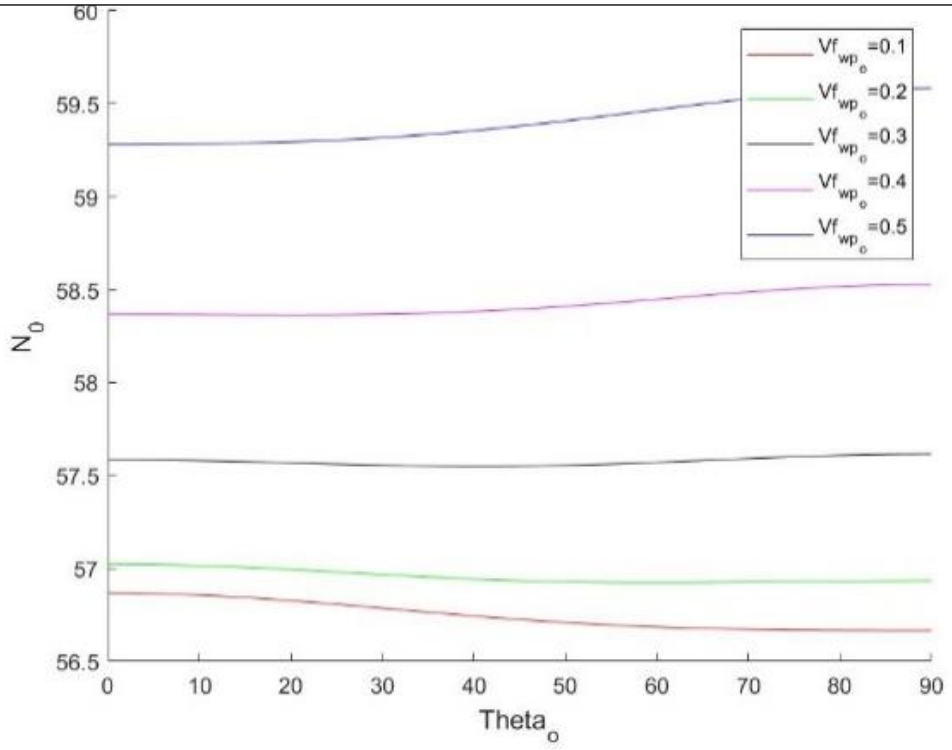

Figure 5.25 (f) $W_{gpl_o} = 0.05$

Figure 5.25: Critical buckling load vs. θ_o *for different values of* Vf_{wp_o}

$\tau = 0.7;\ \frac{a}{b} = 4;\ \theta_m = 0°;\ W_{gpl_m} = 0;\ Vf_{wf_o} = 0.275;\ k_m = 0.5;\ Vf_{total_m} = 0.55;\ \alpha_b = 1$

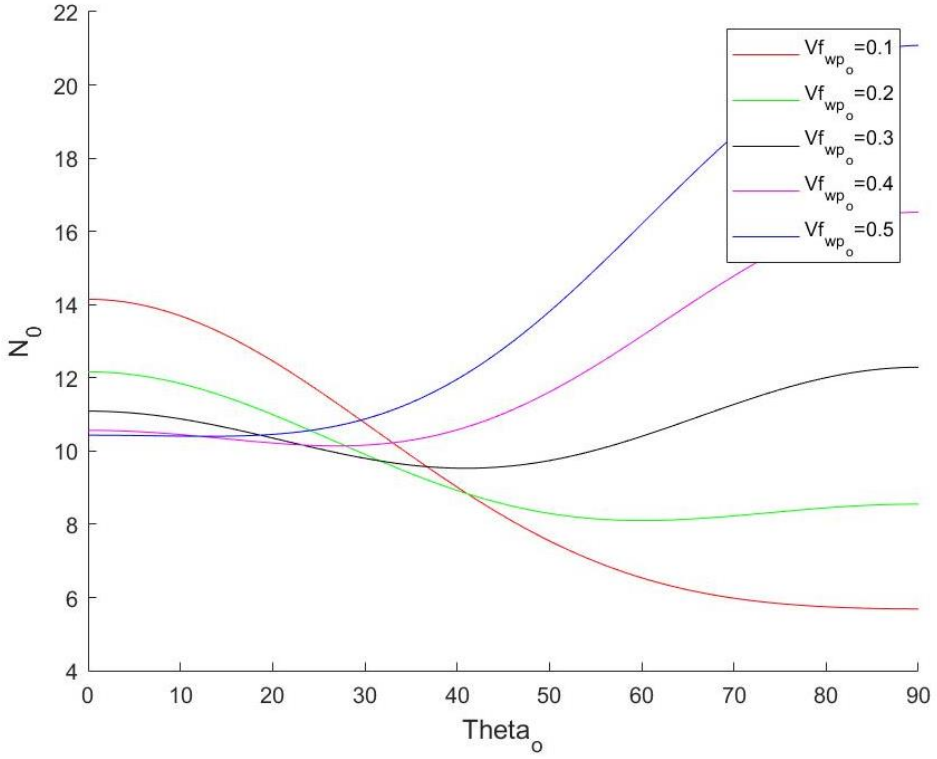

Figure 5.26 (a) $W_{gpl_o} = 0$

$\tau = 0.7;\ \frac{a}{b} = 4;\ \theta_m = 0°;\ W_{gpl_m} = 0;\ Vf_{wf_o} = 0.275;\ k_m = 0.5;\ Vf_{total_m} = 0.55;\ \alpha_b = 1$

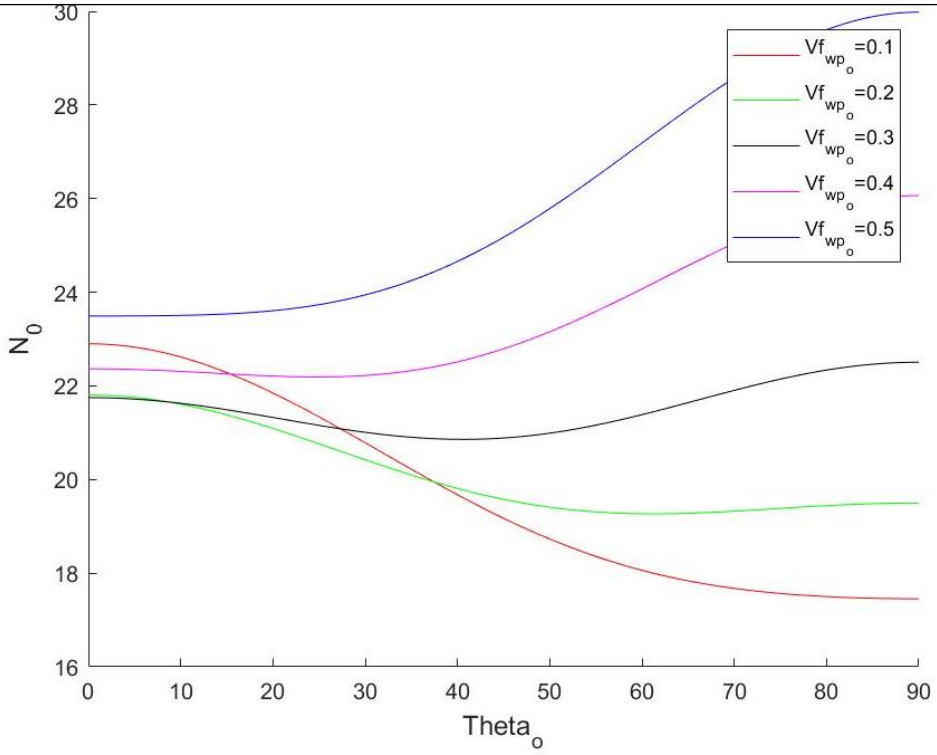

Figure 5.26 (b) $W_{gpl_o} = 0.01$

$\tau = 0.7;\ \frac{a}{b} = 4;\ \theta_m = 0°;\ W_{gpl_m} = 0;\ Vf_{wf_o} = 0.275;\ k_m = 0.5;\ Vf_{total_m} = 0.55;\ \alpha_b = 1$

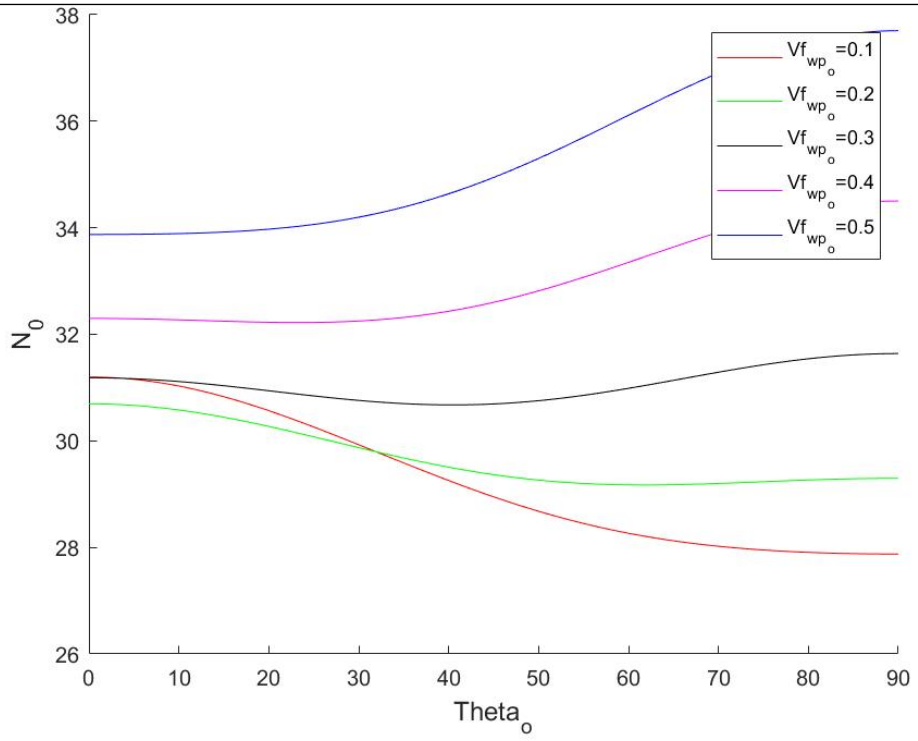

Figure 5.26 (c) $W_{gpl_o} = 0.02$

$\tau = 0.7;\ \frac{a}{b} = 4;\ \theta_m = 0°;\ W_{gpl_m} = 0;\ Vf_{wf_o} = 0.275;\ k_m = 0.5;\ Vf_{total_m} = 0.55;\ \alpha_b = 1$

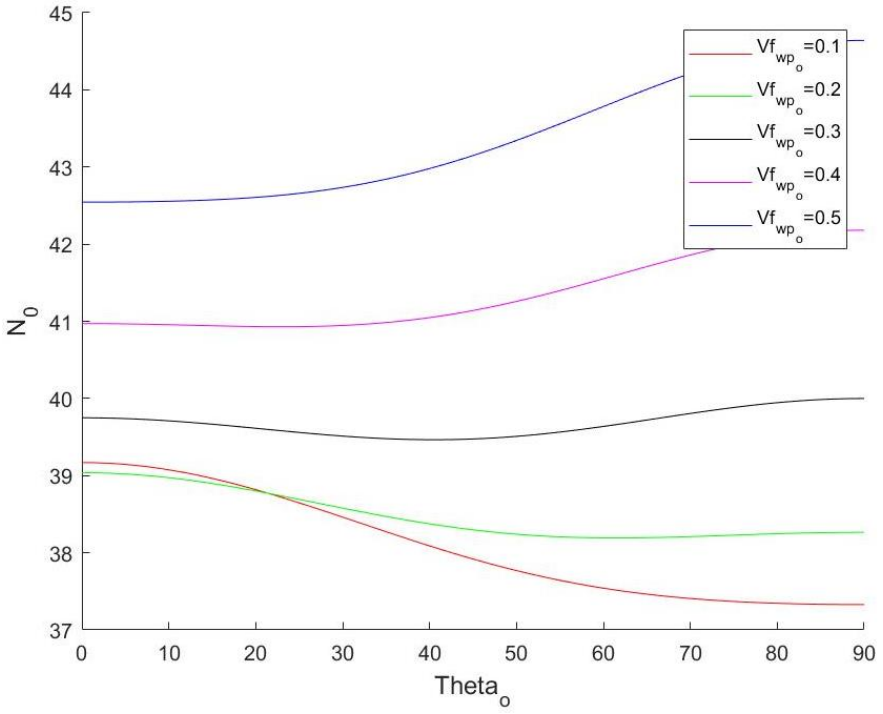

Figure 5.26 (d) $W_{gpl_o} = 0.03$

$\tau = 0.7;\ \frac{a}{b} = 4;\ \theta_m = 0°;\ W_{gpl_m} = 0;\ Vf_{wf_o} = 0.275;\ k_m = 0.5;\ Vf_{total_m} = 0.55;\ \alpha_b = 1$

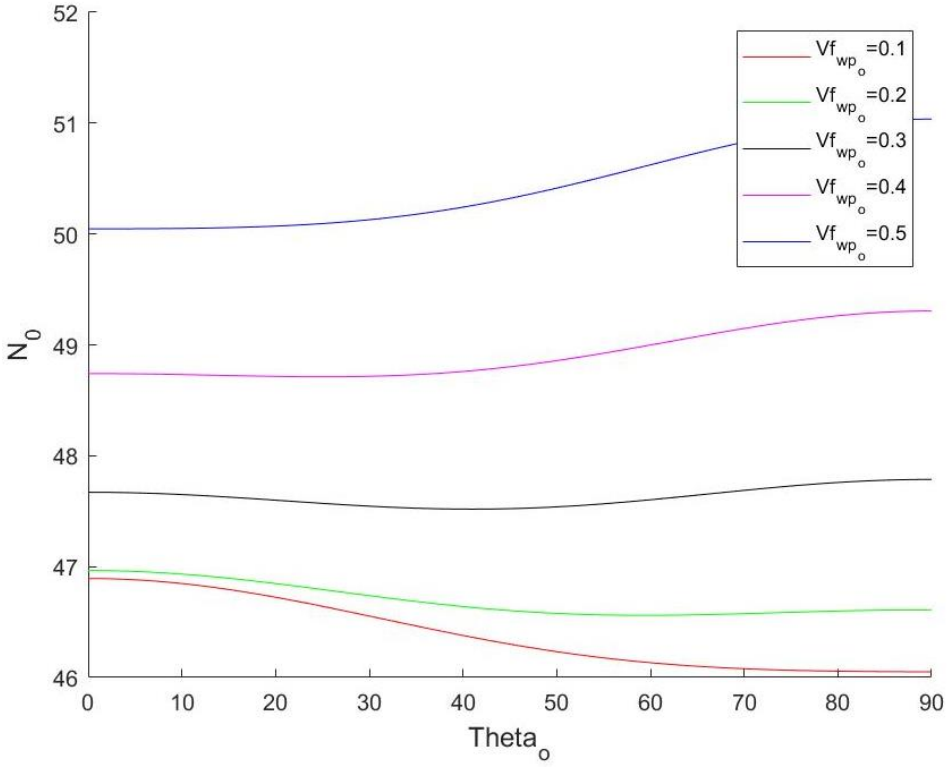

Figure 5.26 (e) $W_{gpl_o} = 0.04$

$\tau = 0.7;\ \frac{a}{b} = 4;\ \theta_m = 0°;\ W_{gpl_m} = 0;\ Vf_{wf_o} = 0.275;\ k_m = 0.5;\ Vf_{total_m} = 0.55;\ \alpha_b = 1$

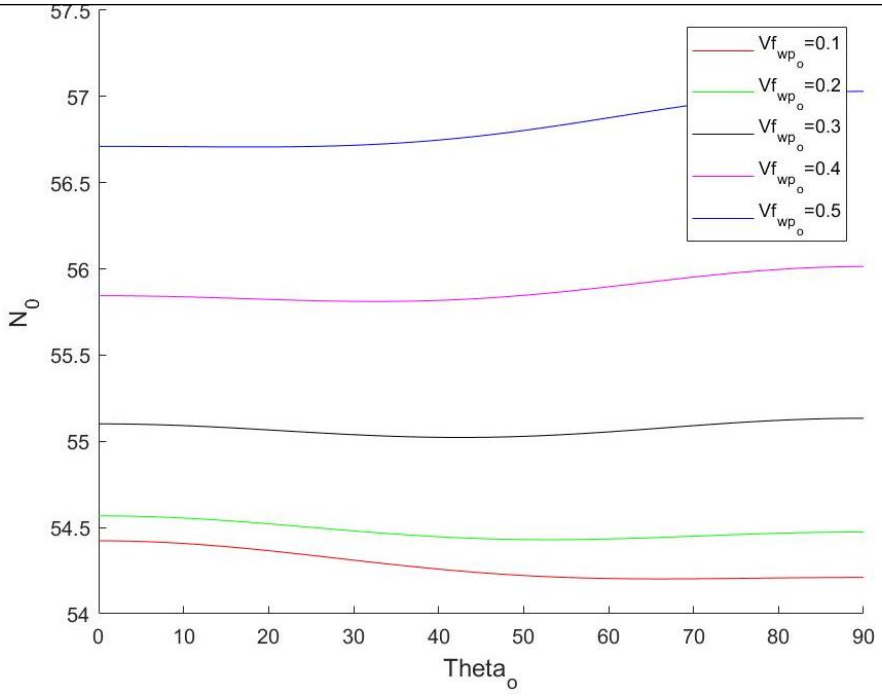

Figure 5.26 (f) $W_{gpl_o} = 0.05$

Figure 5.26: Critical buckling load vs. θ_o *for different values of* Vf_{wp_o}

More figures showing the combined effect of the aspect ratio, $\frac{a}{b}$, and the woven glass fibre orientation in the outer layer, θ_o, on the non-dimensional critical buckling load, N_0, with $Vf_{wp_o} = 0.5$ and $Vf_{wf_o} = 0.275$ and $0 \leq W_{gpl_o} \leq 0.02$ are included in appendix C.

Figures showing the combined effect of the laminate aspect ratio, $\frac{a}{b}$, and the warp fibre volume fraction in the outer layer of the laminate, Vf_{wp_o}, on the non-dimensional critical buckling load, N_0, for different woven glass fibre orientations in the outer layer are included in appendix D for $\theta = 0°, 30°, 60°$ and $90°$ respectively for each figure. In each figure, $\frac{a}{b}$ ranges from 0.4 to 4.

5.1.3.2 $\boldsymbol{\theta_o}$ vs. $\boldsymbol{N_0}$ vs. $\boldsymbol{W_{gpl_o}}$

Figure 5.27 shows the effect of the woven glass fibre orientation in the outer layer, θ_o, on the non-dimensional critical buckling load, N_0, for different values of the graphene platelet weight fraction. In figure 5.27(a) the aspect ratio $\frac{a}{b} = 1$ and in figure 5.27(b), $\frac{a}{b} = 4$. Both these figures show that increasing W_{gpl_o} reduces the effect of the woven glass fibre orientation such that it is eventually practically negligible. In figure 5.27(a), $\frac{a}{b} = 1$, and the maximum critical buckling load when $W_{gpl_o} = 0\%$ is at $\theta_o = 45°$. In figure 5.27(b), $\frac{a}{b} = 4$. For $W_{gpl_o} = 0\%$, maximum critical buckling load occurs when $\theta_o = 0°$ or $45°$. When $W_{gpl_o} = 3\%$, the critical buckling load, N_0, effectively remains constant as the woven glass fibre orientation, θ_o, changes. This is true for any aspect ratio, and the effect is seen in both figure 5.27(a), where $\frac{a}{b} = 1$, and figure 5.27(b), where $\frac{a}{b} = 4$.

$\tau = 0.7;\ \frac{a}{b} = 1;\ \theta_m = 0°;\ W_{gpl_m} = 0.01;\ k_o = 0.5;\ Vf_{total_o} = 0.55;\ k_m = 0.5;\ Vf_{total_m} = 0.55;\ \alpha_b = 1$

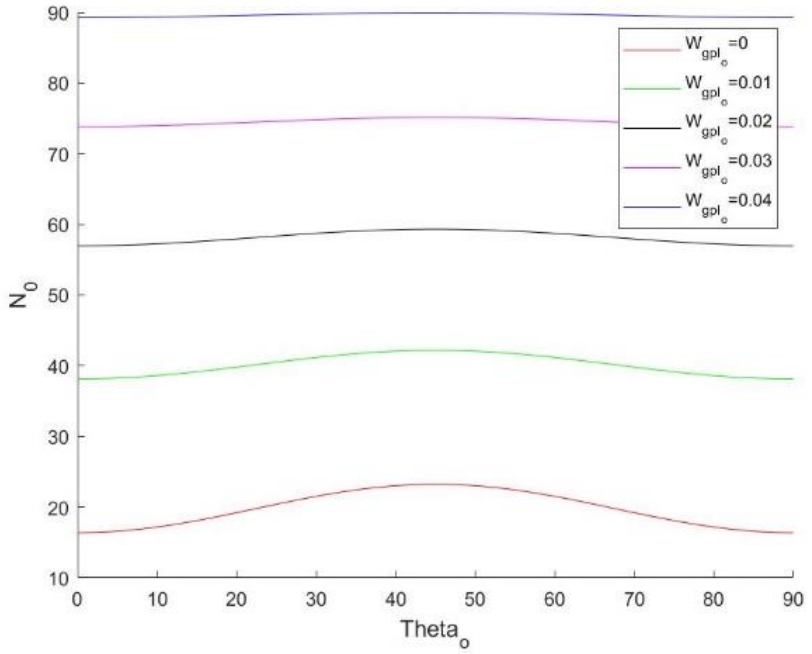

Figure 5.27 (a) $\frac{a}{b} = 1$

$\tau = 0.7;\ \frac{a}{b} = 1;\ \theta_m = 0°;\ W_{gpl_m} = 0.01;\ k_o = 0.5;\ Vf_{total_o} = 0.55;\ k_m = 0.5;\ Vf_{total_m} = 0.55;\ \alpha_b = 1$

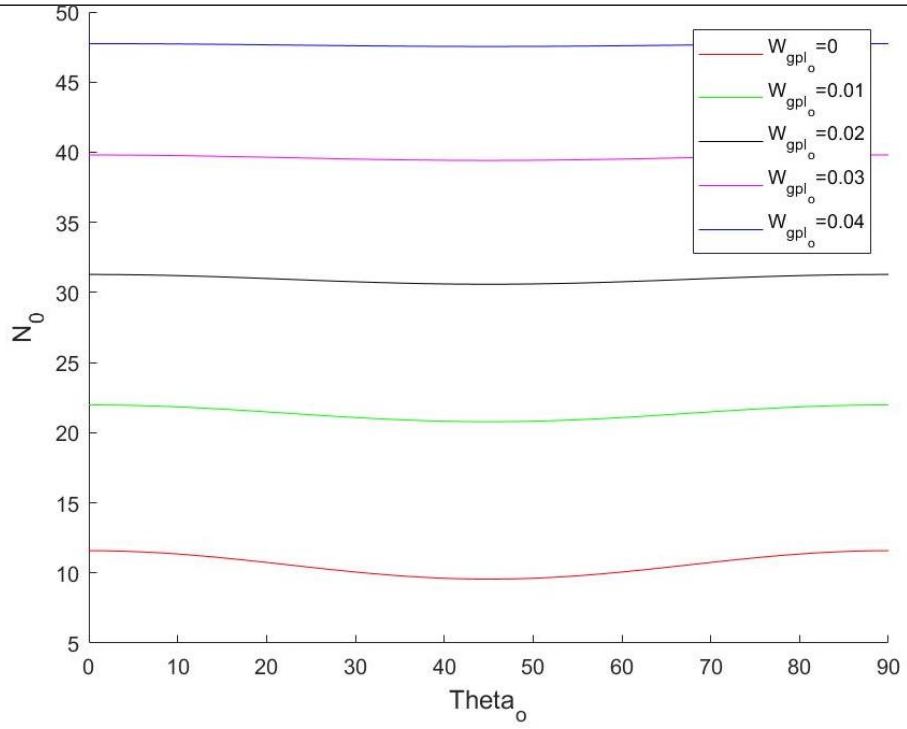

Figure 5.27 (b) $\frac{a}{b} = 4$

Figure 5.27: Critical buckling load vs. θ_o *for different values of* Vf_{wp_o}

5.1.3.3 θ_o vs. N_0 vs. τ

Figure 5.28 shows the combined effect of the woven glass fibre orientation in the outer layer, θ_o, and the thickness ratio of the laminate, τ, on the non-dimensional critical buckling load, N_0, for increasing graphene platelet weight fraction, W_{gpl_o}. For these graphs, $\frac{a}{b} = 1$. In figure 5.28(a), with no graphene present, the laminate has maximum critical buckling load at $\theta_o = 45°$ and minimum critical buckling load at $\theta_o = 0°$ and 90°. Furthermore, a higher thickness ratio always increases the maximum critical buckling load, and $\tau = 1$ is ideal. In figure 5.28(b), with $W_{gpl_o} = 3\%$, the effect of the woven glass fibre orientation, θ_o, on the critical buckling load, N_0 is greatly reduced. The graphene is more influential on the buckling load than the woven glass fibre orientation. The effect of graphene is thus to increase the critical buckling load and obscure the effect of the woven glass fibre orientation on the critical buckling load. This can be visualized in the contour plots of figure 5.29.

$\frac{a}{b} = 1$; $\theta_m = 0°$; $W_{gpl_m} = 0$; $k_o = 0.5$; $Vf_{total_o} = 0.55$; $k_m = 0.5$; $Vf_{total_m} = 0.55$; $\alpha_b = 1$

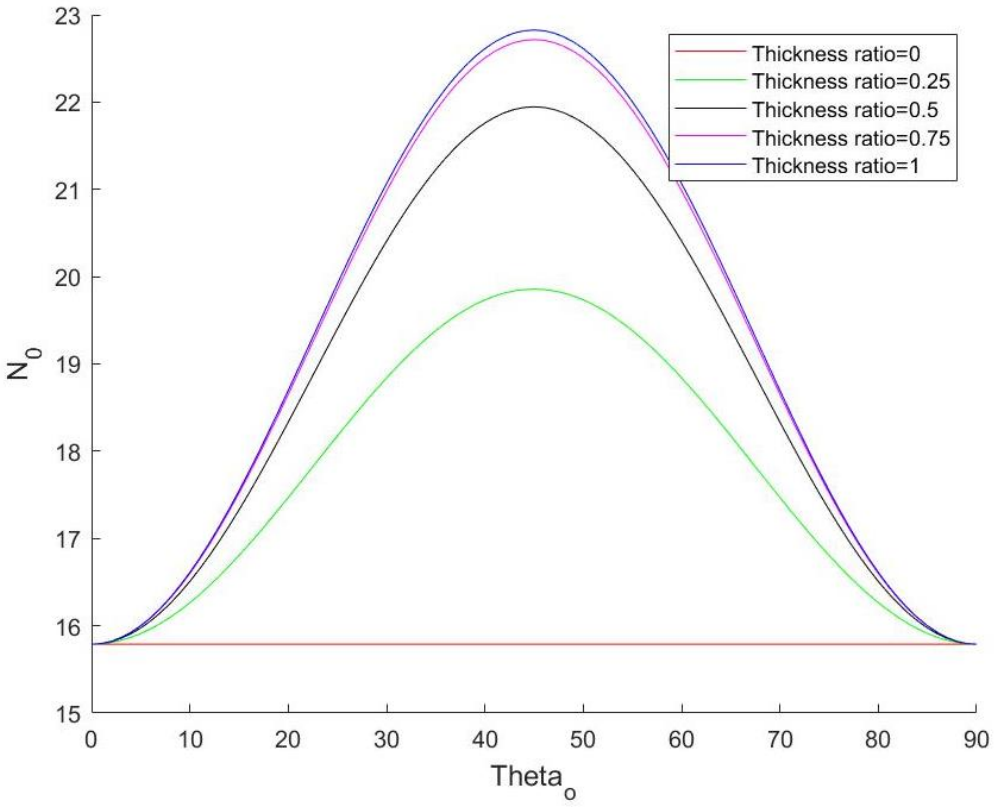

Figure 5.28 (a) $W_{gpl_o} = 0$

$\frac{a}{h} = 1$; $\theta_m = 0°$; $W_{gpl_m} = 0$; $k_o = 0.5$; $Vf_{total_o} = 0.55$; $k_m = 0.5$; $Vf_{total_m} = 0.55$; $\alpha_b = 1$

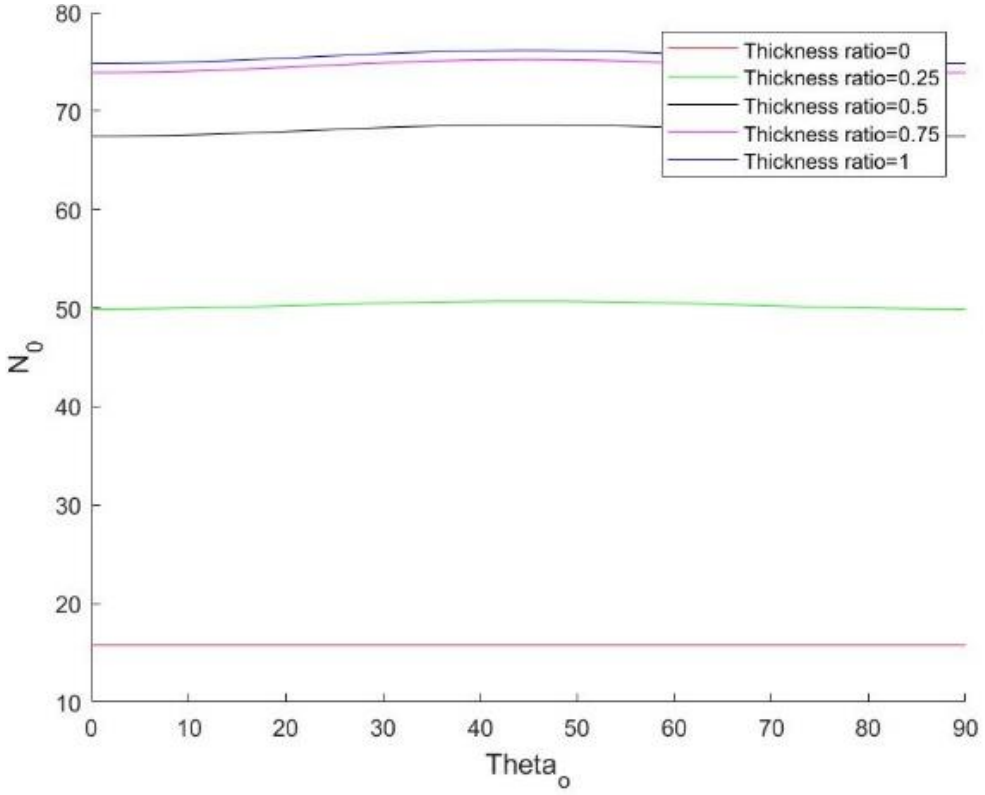

Figure 5.28 (b) $W_{gpl_o} = 0.03$

Figure 5.28: Critical buckling load vs. θ_o *for different values of* τ

$\frac{a}{b} = 1; \theta_m = 0°; k_o = 0.5; Vf_{total_o} = 0.55; k_m = 0.5; Vf_{total_m} = 0.55; \alpha_b = 1$

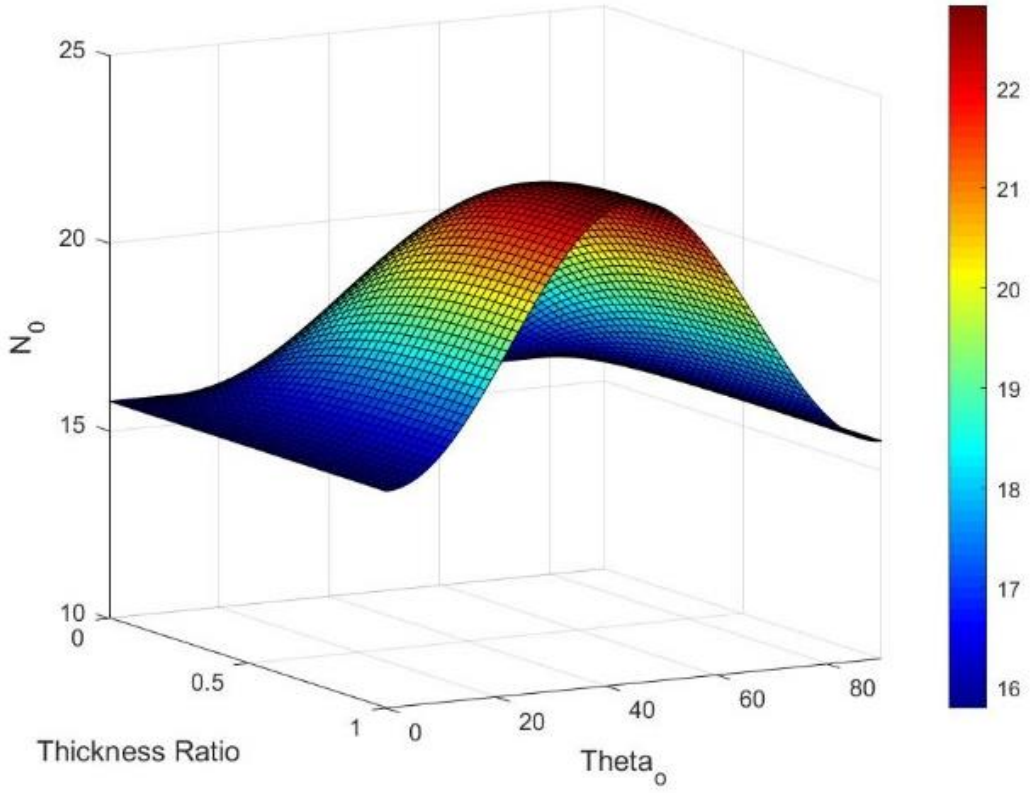

Figure 5.29 (a) $W_{gpl_o} = 0; W_{gpl_m} = 0$

$\frac{a}{b} = 1; \theta_m = 0°; k_o = 0.5; Vf_{total_o} = 0.55; k_m = 0.5; Vf_{total_m} = 0.55; \alpha_b = 1$

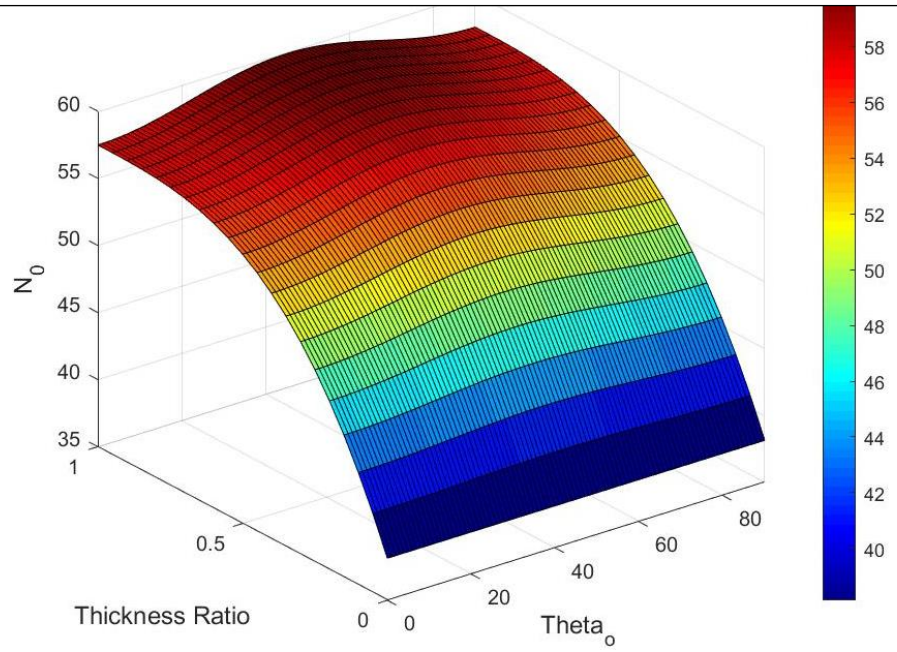

Figure 5.29 (b) $W_{gpl_o} = 0.02; W_{gpl_m} = 0.01$

Figure 5.29: Contour plot of critical buckling load vs. θ_o *for different values of* τ

In figure 5.29(a), there is variation in the buckling load for $0° \leq \theta_o \leq 90°$ and $0 \leq \tau \leq 1$. In figure 5.29(b), with $W_{gpl_o} = 2\%$ and $W_{gpl_m} = 1\%$, there is more variation on the critical buckling load, N_0 with increasing thickness ratio, τ, than there is with woven glass fibre orientation, θ_o.

In figures 5.30 and 5.31, $\frac{a}{b} = 0.2$. In figure 5.30(a), no graphene is present. The maximum critical buckling load, N_0, occurs when $\theta_o = 0°$ and 90°. The minimum critical buckling load occurs when $\theta_o = 45°$. This is contrary to figure 5.28. The aspect ratio thus has an influence on the critical buckling load. Figure 5.32 shows the combined effect of the aspect ratio, $\frac{a}{b}$, and the woven glass fibre orientation in the outer layer, θ_o, on the non-dimensional critical buckling load, N_0. In this figure, the $\theta_o = 0°$ line intersects the $\theta_o = 90°$ line at all points, hence these two curves are superimposed. The same applies for the $\theta_o = 30°$ line and the $\theta_o = 60°$ line. This is because $k_o = 0.5$ in this figure, hence the glass fibres are balanced in the warp and weft direction. For $\frac{a}{b} = 1$, maximum N_0 is when $\theta_o = 45°$. This is verified in figure 5.28. For $\frac{a}{b} = 0.2$, maximum buckling load is when $\theta_o = 0°$ or 90°. This is verified in figure 5.30. In figure 5.30(b), $W_{gpl_o} = 3\%$. The efect of the woven glass fibre orientation on the critical buckling load is greatly reduced. Because the graphene has a more influential effect on the

critical buckling load than the woven glass fibres, increasing the graphene content in the outer layer results in higher thickness ratios yielding a higher critical buckling load.

$\frac{a}{b} = 0.2; \theta_m = 0°; W_{gpl_m} = 0; k_o = 0.5; Vf_{total_o} = 0.55; k_m = 0.5; Vf_{total_m} = 0.55; \alpha_b = 1$

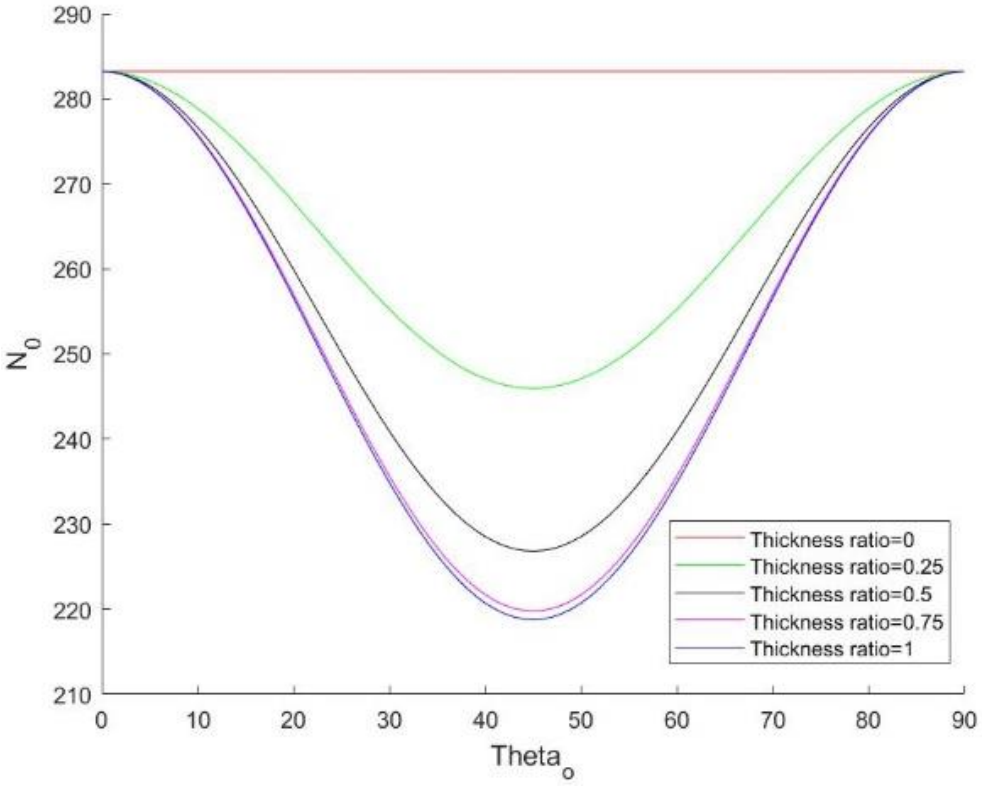

Figure 5.30 (a) $W_{gpl_o} = 0$

$\frac{a}{b} = 0.2; \theta_m = 0°; W_{gpl_m} = 0; k_o = 0.5; Vf_{total_o} = 0.55; k_m = 0.5; Vf_{total_m} = 0.55; \alpha_b = 1$

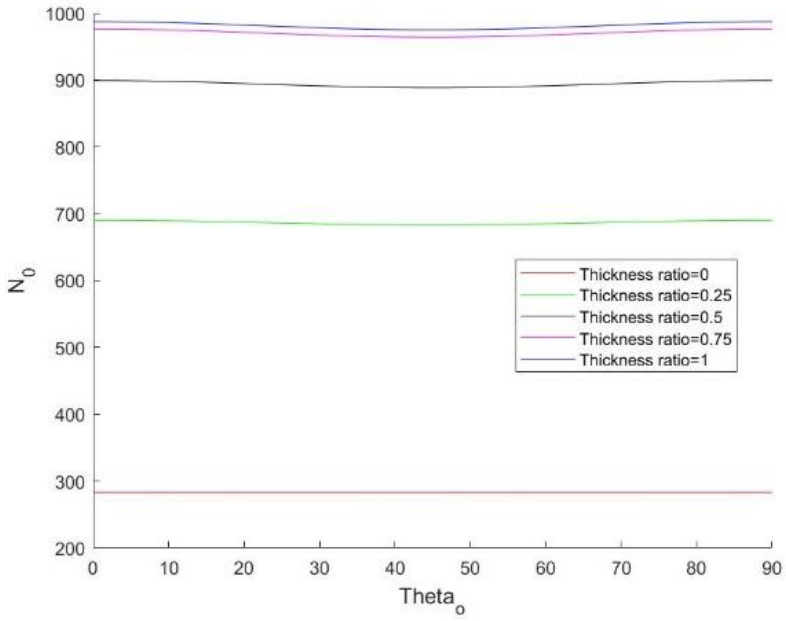

Figure 5.30 (b) $W_{gpl_o} = 0.03$

Figure 5.30: Critical buckling load vs. θ_o *for different values of* τ

In figure 5.31(b), the contour plot shows that when $W_{gpl_o} = 2\%$ and $W_{gpl_m} = 1\%$, there is more variation in the critical buckling load, N_0, as thickness ratio, τ, increases than there is as woven glass fibre orientation, θ_o increases.

$\frac{a}{b} = 0.2; \theta_m = 0°; k_o = 0.5; Vf_{total_o} = 0.55; k_m = 0.5; Vf_{total_m} = 0.55; \alpha_b = 1$

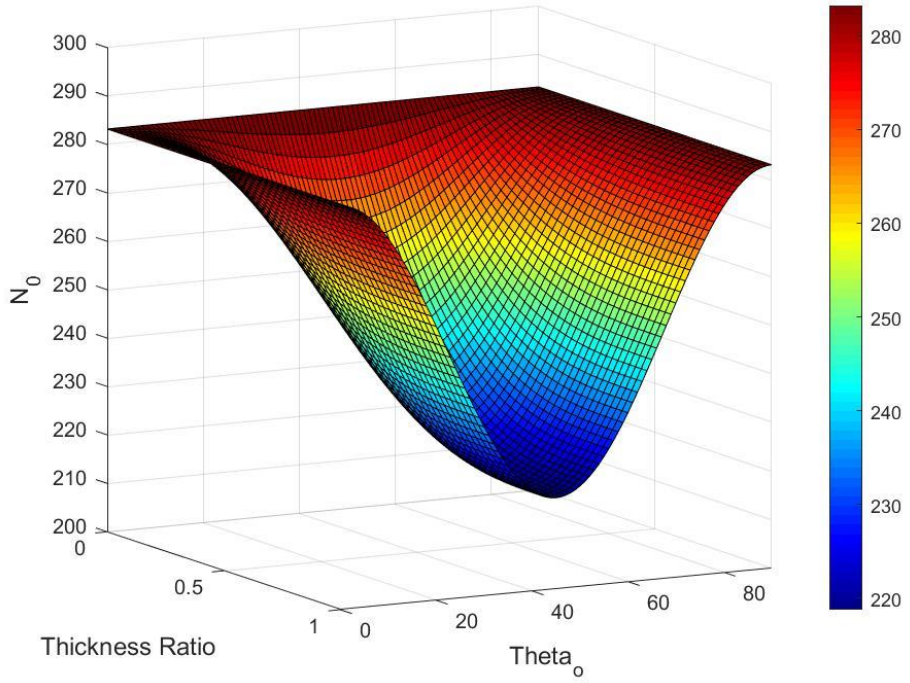

Figure 5.31 (a) $W_{gpl_o} = 0; W_{gpl_m} = 0$

$\frac{a}{b} = 0.2; \theta_m = 0°; k_o = 0.5; Vf_{total_o} = 0.55; k_m = 0.5; Vf_{total_m} = 0.55; \alpha_b = 1$

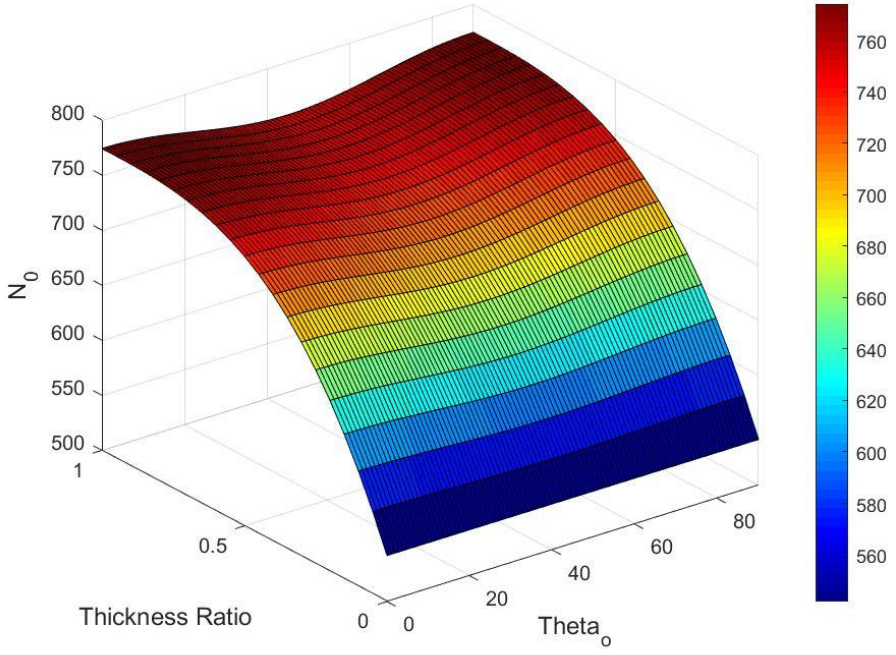

Figure 5.15 (b) $W_{gpl_o} = 0.02; W_{gpl_m} = 0.01$

Figure 5.31: Contour plot of critical buckling load vs. θ_o *for different values of* τ

$\theta_m = 0°$; $W_{gpl_o} = W_{gpl_m} = 0$; $k_o = 0.5$; $Vf_{total_o} = 0.55$; $k_m = 0.5$; $Vf_{total_m} = 0.55$; $\alpha_b = 1$

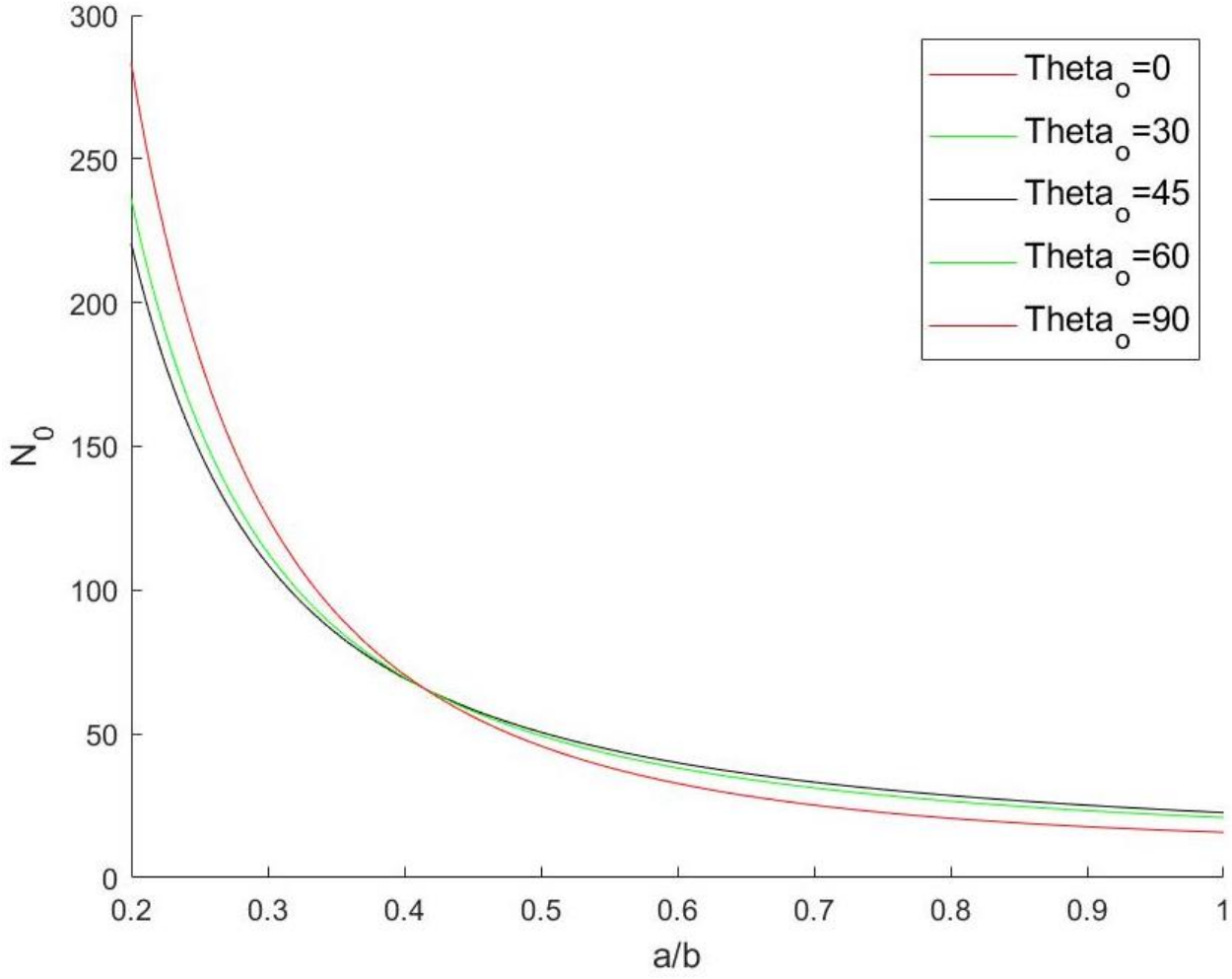

Figure 5.32: Critical buckling load vs. a/b for different values of θ_o

5.1.3.4 θ_o vs. N_0 vs. $\frac{a}{b}$

Figures 5.33-5.37 show the relation between the non-dimensional critical buckling load, N_0, and the woven glass fibre orientation in the outer layer, θ_o for different aspect ratios, $\frac{a}{b}$, and increasing graphene weight fractions, W_{gpl_o}. In figures 5.33-5.37, the woven glass fibre balancing coefficient, $k_o = 0.1, 0.3, 0.5, 0.7$ and 0.9 respectively. The total fibre volume fraction, Vf_{total_o}, is kept constant at 50%. In figure 5.33(a), with no graphene present ($W_{gpl_o} = W_{gpl_m} = 0\%$), the critical buckling load varies between approximately 10 and 100 for $0° \leq \theta_o \leq 90°$ and $0.5 \leq \frac{a}{b} \leq 1.5$. The value of θ_o at which the

critical buckling load is maximum depends on the aspect ratio. For $\frac{a}{b} = 0.5$, maximum N_0 is when $\theta_o = 90°$. For $\frac{a}{b} = 1$, however, maximum N_0 is when $\theta_o = 45°$.

The effect of graphene in the laminate is to increase N_0 and obscure the effect of θ_o on the critical buckling load. In figures 5.33(b)-(d), W_{gpl_o} is increased in increments of 0.02, from 0.01 to 0.05. the gradients of the curves are gradually reduced.

In figure 5.35, $k_o = 0.5$. In figure 5.35(a), no graphene is present, and the maximum critical buckling load occurs when $\theta_o = 45°$. This remains true for all aspect ratios, when $k_o = 0.5$.

In figure 5.37, $k_o = 0.9$. Contrary to figures 5.33 and 5.34, when $\frac{a}{b} = 0.5$ the maximum critical buckling load, N_0, is when $\theta_o = 0°$. The effect of the woven glass fibre balancing coefficient, k_o, on the critical buckling load is more clearly seen in figure 5.38. At different k_o values, maximum critical buckling load occurs at different woven glass fibre orientations, θ_o. In figure 5.38, $\frac{a}{b} = 0.5$. At $k_o = 0.9$ in this figure, the maximum critical buckling load occurs when $\theta_o = 0°$. This is verified in the $\frac{a}{b} = 0.5$ line in figure 5.37(a). Figure 5.38 similarly verifies the results in figures 5.33(a), 5.34(a), 5.35(a) and 5.36(a).

$\tau = 0.7;\ \theta_m = 0°;\ W_{gpl_m} = 0.01;\ k_o = 0.1;\ Vf_{total_o} = 0.5;\ k_m = 0.5;\ Vf_{total_m} = 0.55;\ \alpha_b = 1$

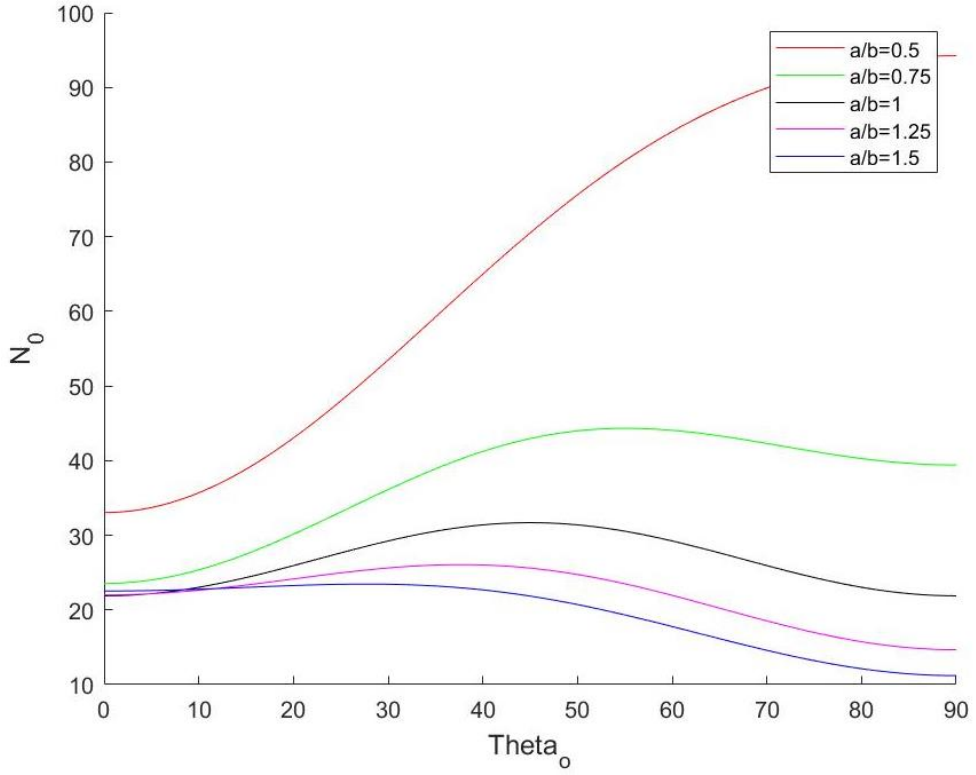

Figure 5.33 (a) $W_{gpl_o} = 0$

$\tau = 0.7;\ \theta_m = 0°;\ W_{gpl_m} = 0.01;\ k_o = 0.1;\ Vf_{total_o} = 0.5;\ k_m = 0.5;\ Vf_{total_m} = 0.55;\ \alpha_b = 1$

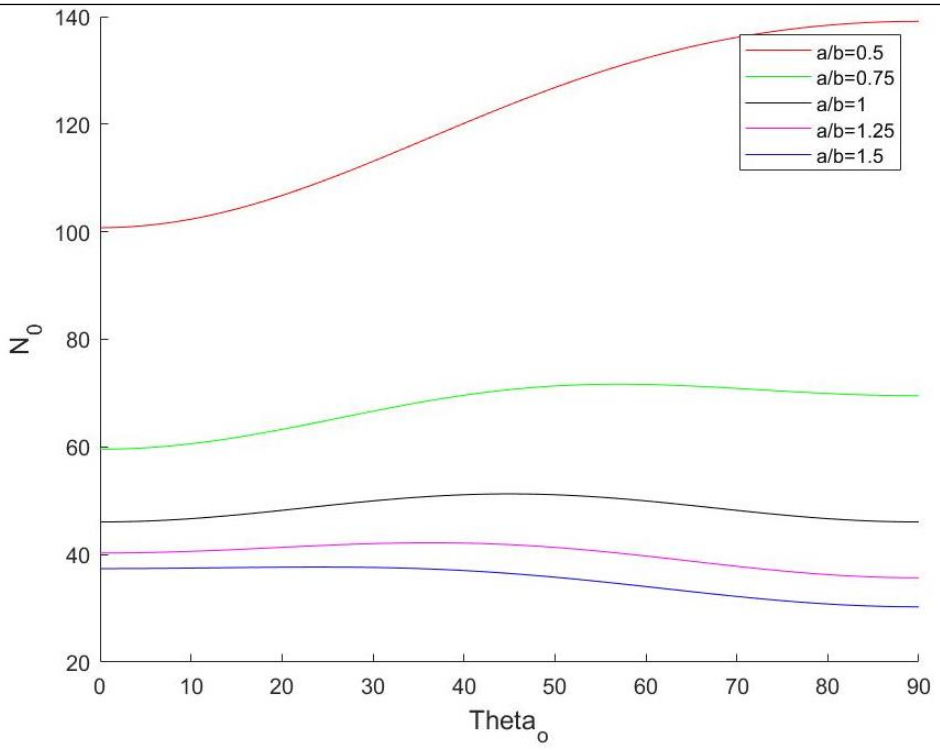

Figure 5.33 (b) $W_{gpl_o} = 0.01$

$\tau = 0.7;\ \theta_m = 0°;\ W_{gpl_m} = 0.01;\ k_o = 0.1;\ Vf_{total_o} = 0.5;\ k_m = 0.5;\ Vf_{total_m} = 0.55;\ \alpha_b = 1$

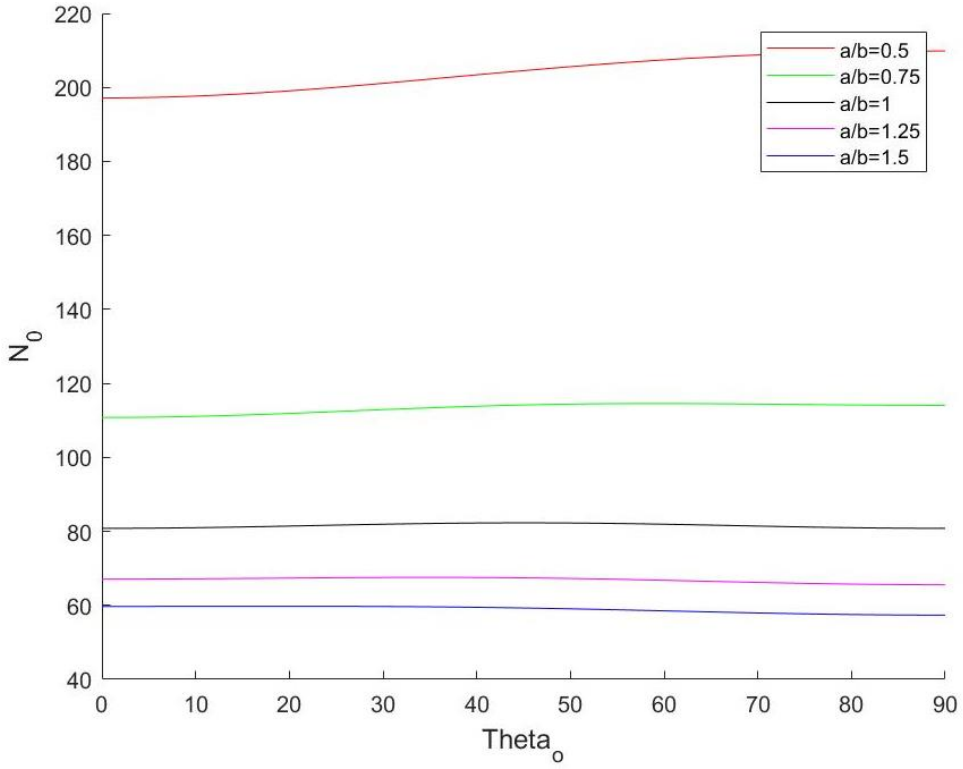

Figure 5.33 (c) $W_{gpl_o} = 0.03$

$\tau = 0.7;\ \theta_m = 0°;\ W_{gpl_m} = 0.01;\ k_o = 0.1;\ Vf_{total_o} = 0.5;\ k_m = 0.5;\ Vf_{total_m} = 0.55;\ \alpha_b = 1$

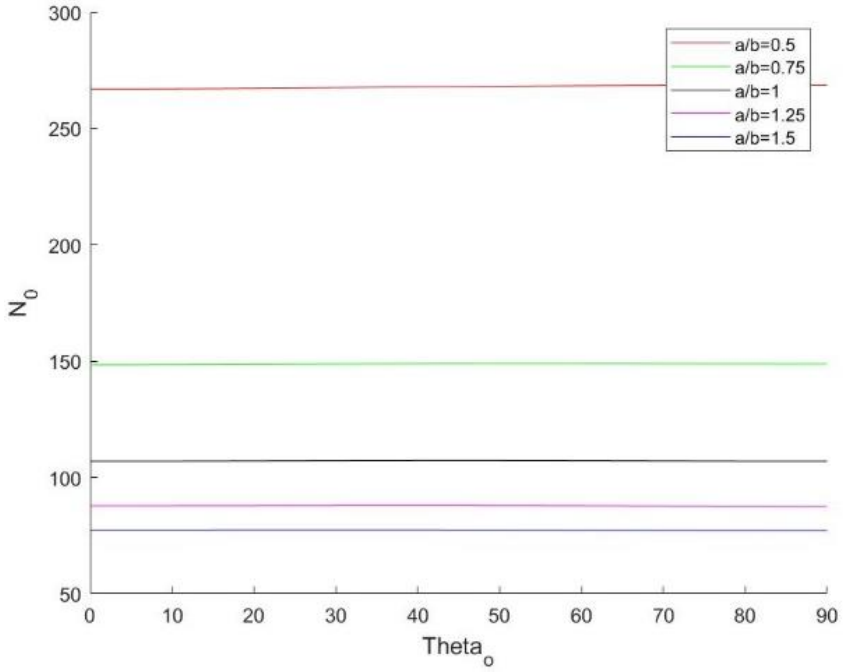

Figure 5.33 (d) $W_{gpl_o} = 0.05$

Figure 5.33: Critical buckling load vs. θ_o *for different values of* a/b

$\tau = 0.7;\ \theta_m = 0°; W_{gpl_m} = 0.01; k_o = 0.3; Vf_{total_o} = 0.5; k_m = 0.5; Vf_{total_m} = 0.55; \alpha_b = 1$

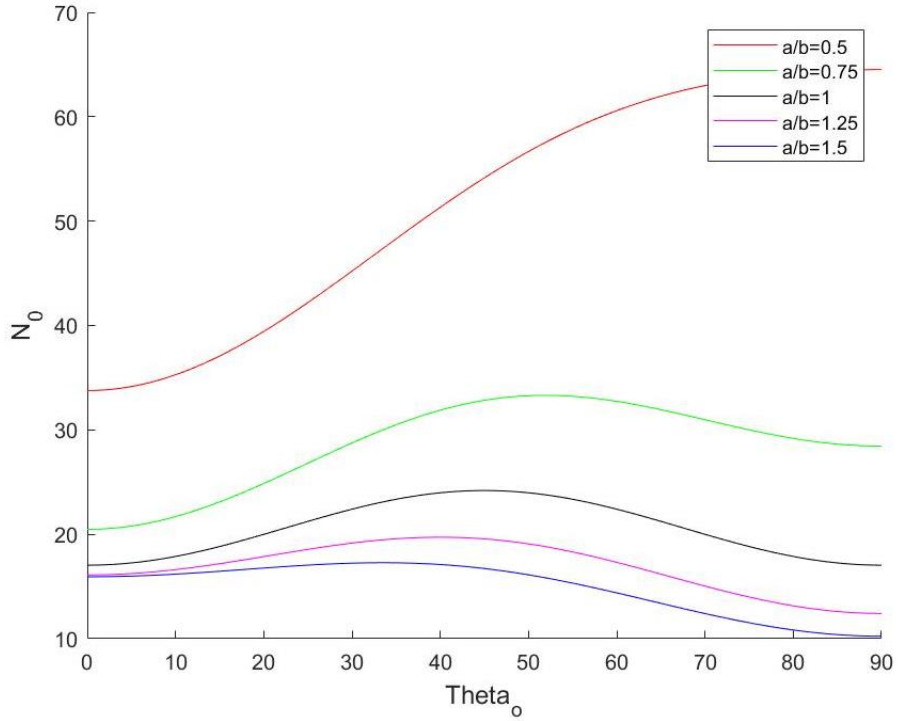

Figure 5.34 (a) $W_{gpl_o} = 0$

$\tau = 0.7;\ \theta_m = 0°; W_{gpl_m} = 0.01; k_o = 0.3; Vf_{total_o} = 0.5; k_m = 0.5; Vf_{total_m} = 0.55; \alpha_b = 1$

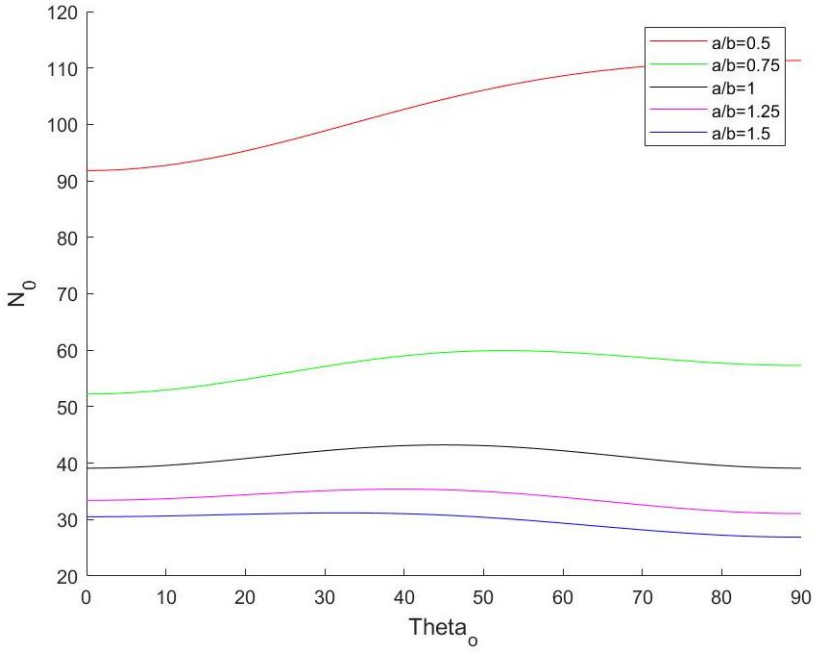

Figure 5.34 (b) $W_{gpl_o} = 0.01$

$\tau = 0.7;\ \theta_m = 0°; W_{gpl_m} = 0.01; k_o = 0.3; Vf_{total_o} = 0.5; k_m = 0.5; Vf_{total_m} = 0.55; \alpha_b = 1$

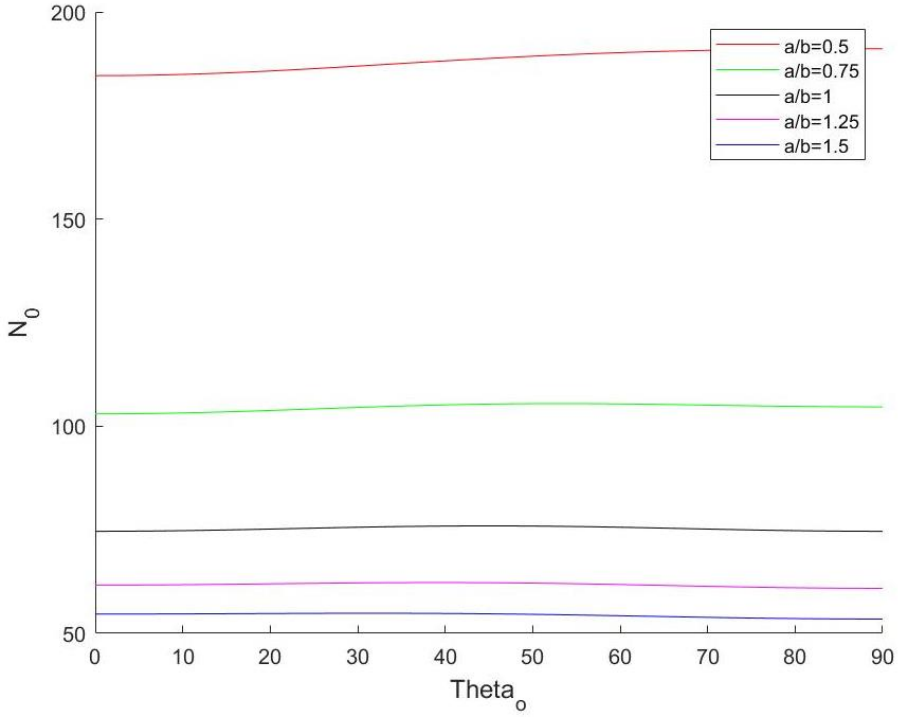

Figure 5.3416 (c) $W_{gpl_o} = 0.03$

$\tau = 0.7;\ \theta_m = 0°; W_{gpl_m} = 0.01; k_o = 0.3; Vf_{total_o} = 0.5; k_m = 0.5; Vf_{total_m} = 0.55; \alpha_b = 1$

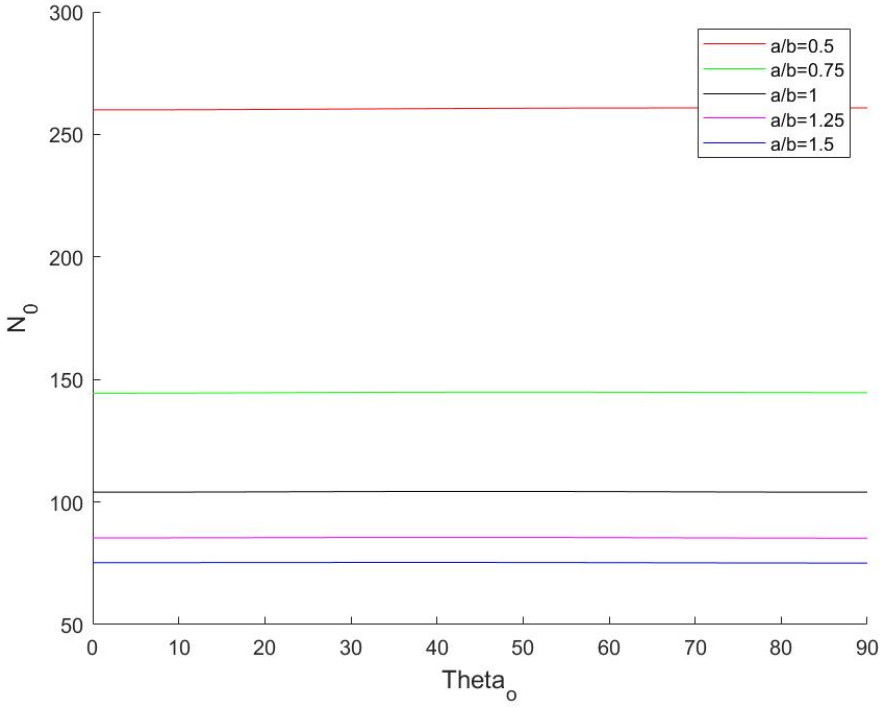

Figure 5.34 (d) $W_{gpl_o} = 0.05$

Figure 5.34: Critical buckling load vs. θ_o *for different values of* a/b

$\tau = 0.7;\ \theta_m = 0°;\ W_{gpl_m} = 0.01;\ k_o = 0.5;\ Vf_{total_o} = 0.5;\ k_m = 0.5;\ Vf_{total_m} = 0.55;\ \alpha_b = 1$

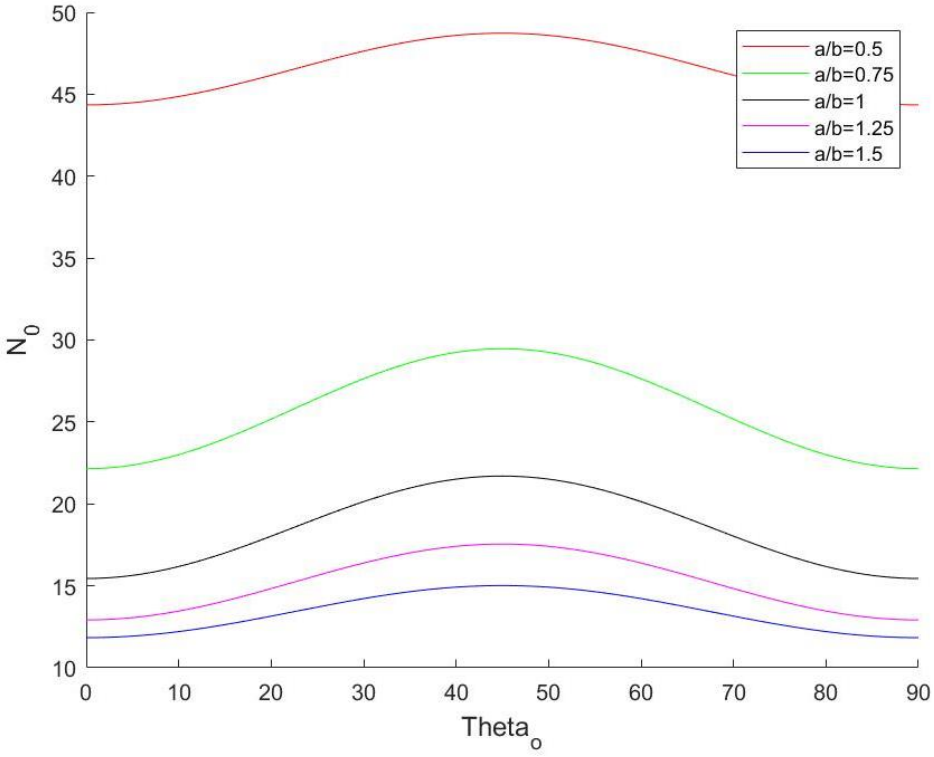

Figure 5.35 (a) $W_{gpl_o} = 0$

$\tau = 0.7;\ \theta_m = 0°;\ W_{gpl_m} = 0.01;\ k_o = 0.5;\ Vf_{total_o} = 0.5;\ k_m = 0.5;\ Vf_{total_m} = 0.55;\ \alpha_b = 1$

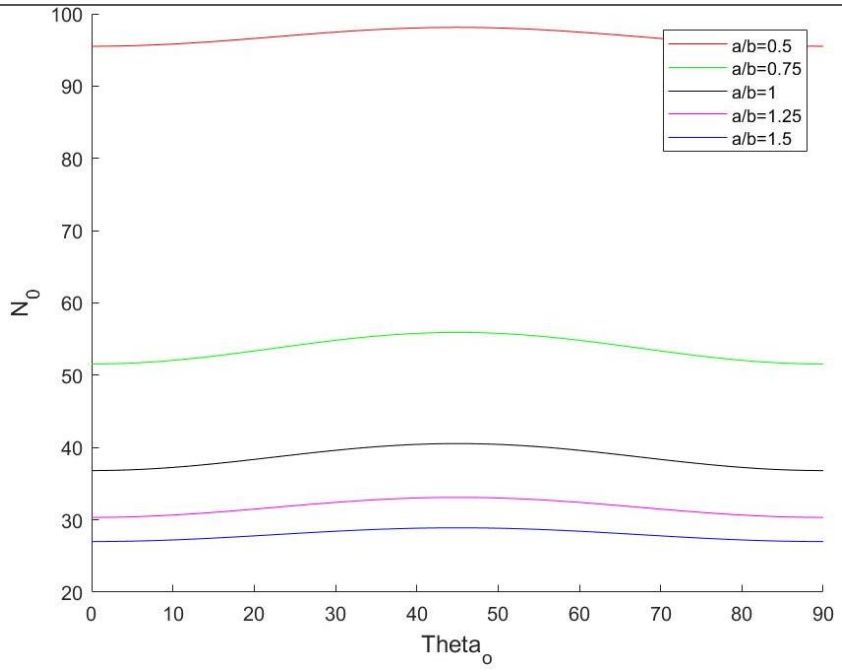

Figure 5.35 (b) $W_{gpl_o} = 0.01$

$\tau = 0.7;\ \theta_m = 0°;\ W_{gpl_m} = 0.01;\ k_o = 0.5;\ Vf_{total_o} = 0.5;\ k_m = 0.5;\ Vf_{total_m} = 0.55;\ \alpha_b = 1$

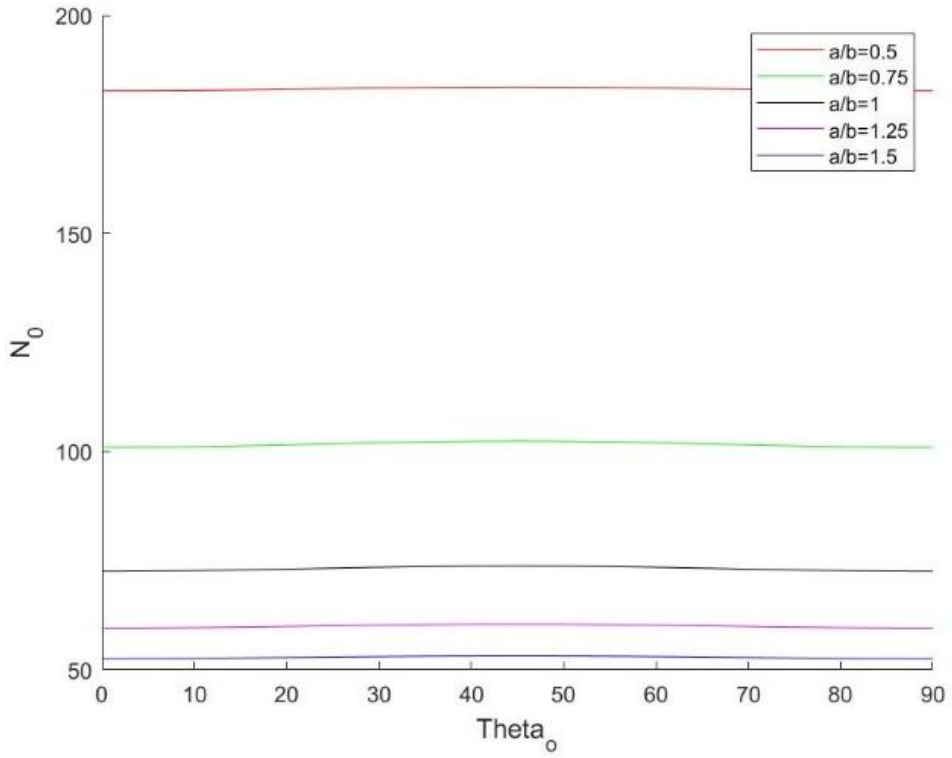

Figure 5.35 (c) $W_{gpl_o} = 0.03$

$\tau = 0.7;\ \theta_m = 0°;\ W_{gpl_m} = 0.01;\ k_o = 0.5;\ Vf_{total_o} = 0.5;\ k_m = 0.5;\ Vf_{total_m} = 0.55;\ \alpha_b = 1$

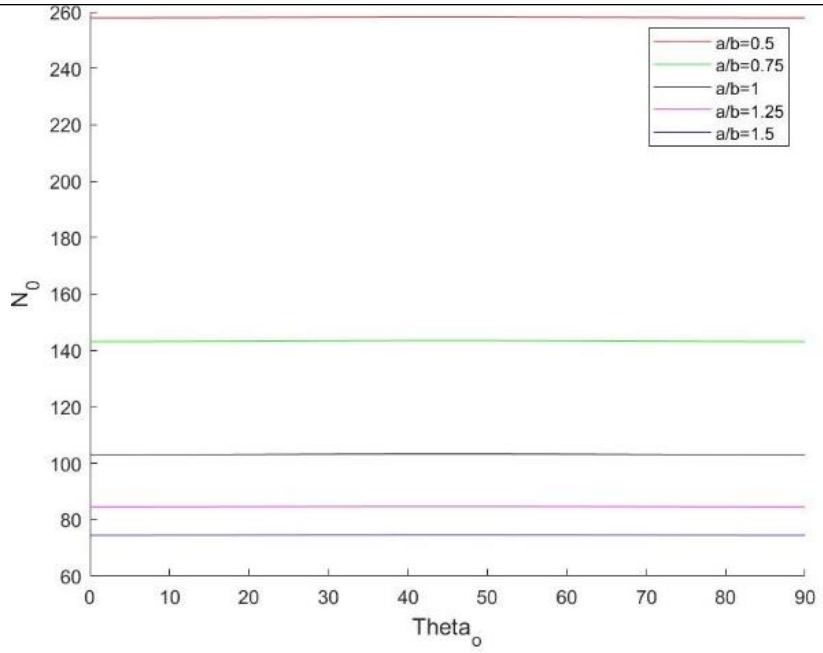

Figure 5.35 (d) $W_{gpl_o} = 0.05$

Figure 5.35: Critical buckling load vs. θ_o *for different values of* a/b

$\tau = 0.7;\ \theta_m = 0°; W_{gpl_m} = 0.01; k_o = 0.7; Vf_{total_o} = 0.5; k_m = 0.5; Vf_{total_m} = 0.55; \alpha_b = 1$

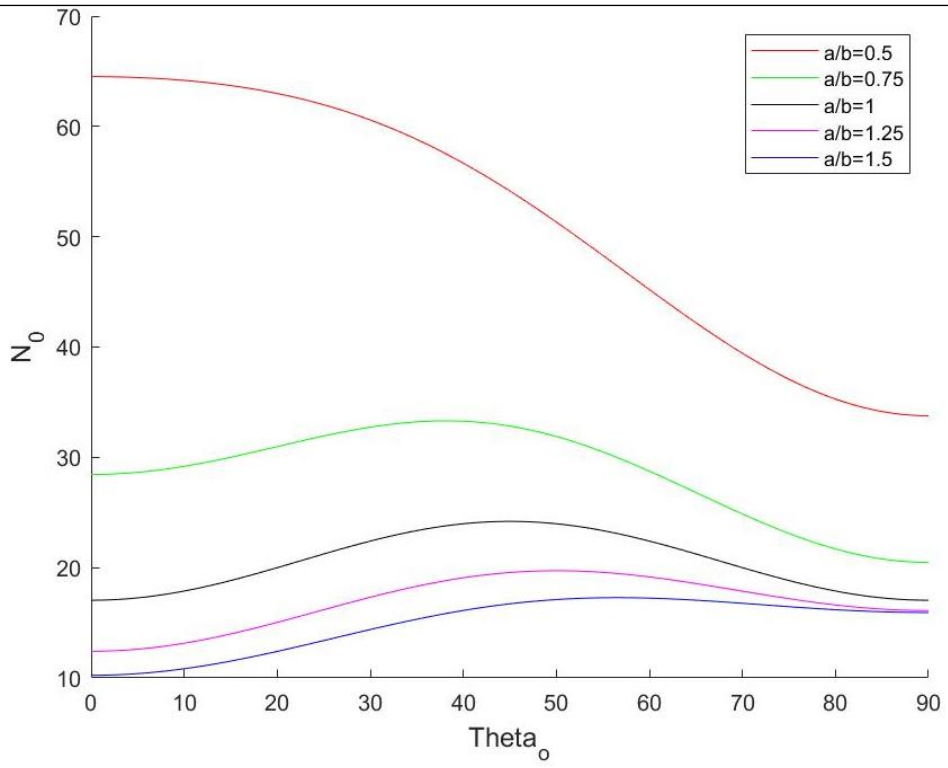

Figure 5.36 (a) $W_{gpl_o} = 0$

$\tau = 0.7;\ \theta_m = 0°; W_{gpl_m} = 0.01; k_o = 0.7; Vf_{total_o} = 0.5; k_m = 0.5; Vf_{total_m} = 0.55; \alpha_b = 1$

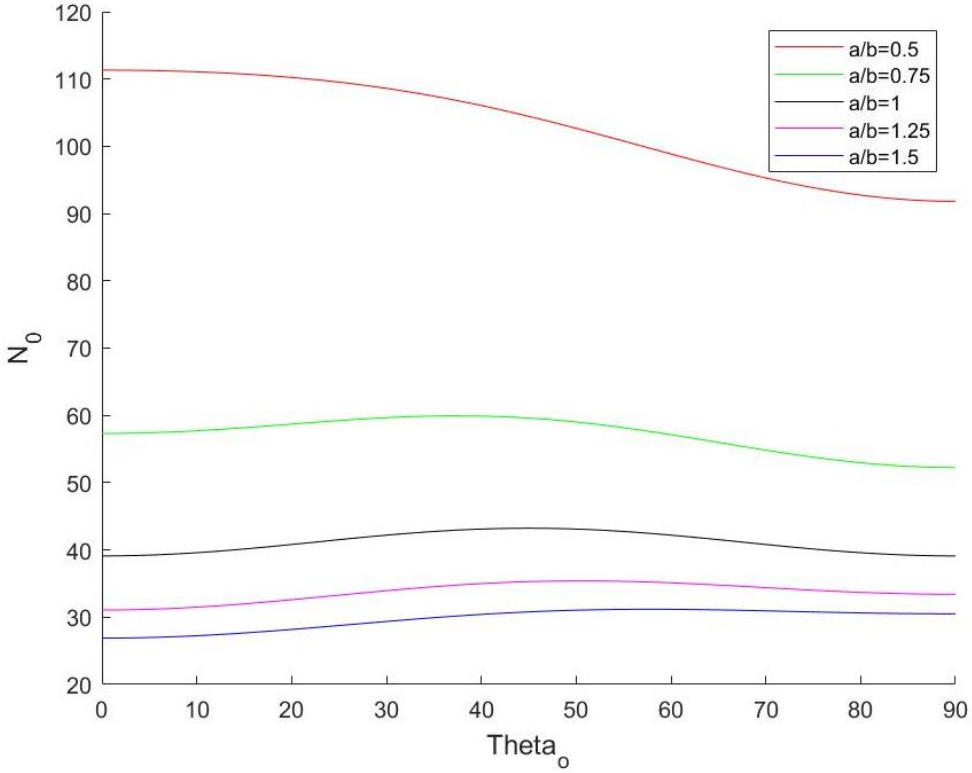

Figure 5.36 (b) $W_{gpl_o} = 0.01$

$\tau = 0.7;\ \theta_m = 0°; W_{gpl_m} = 0.01; k_o = 0.7; Vf_{total_o} = 0.5; k_m = 0.5; Vf_{total_m} = 0.55; \alpha_b = 1$

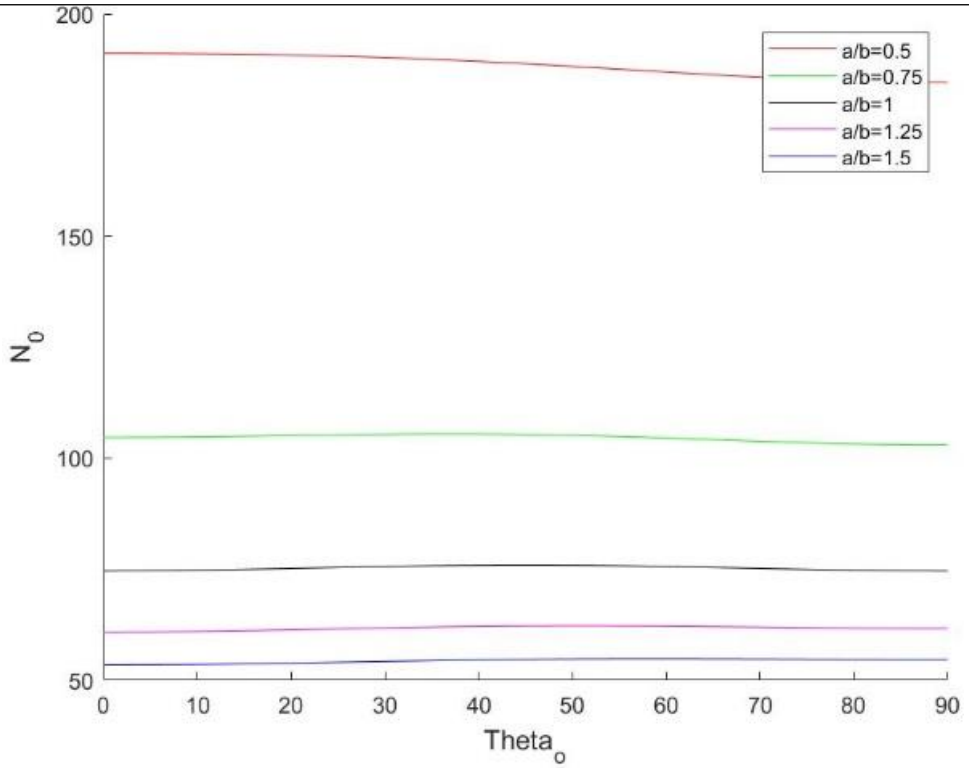

Figure 5.3617 (c) $W_{gpl_o} = 0.03$

$\tau = 0.7;\ \theta_m = 0°; W_{gpl_m} = 0.01; k_o = 0.7; Vf_{total_o} = 0.5; k_m = 0.5; Vf_{total_m} = 0.55; \alpha_b = 1$

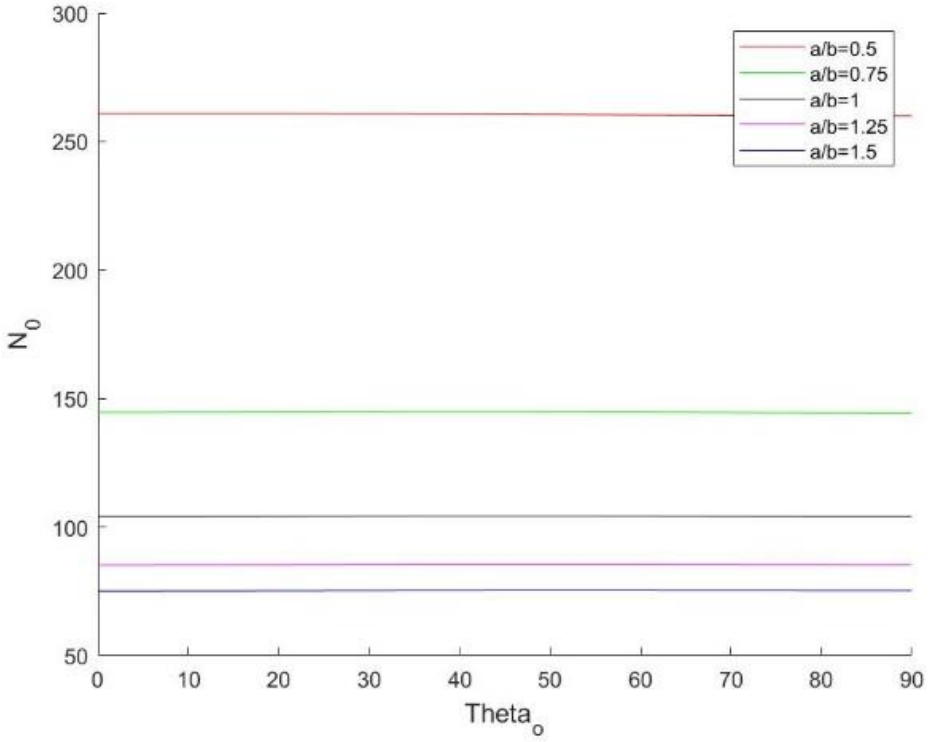

Figure 5.36 (d) $W_{gpl_o} = 0.05$

Figure 5.36: Critical buckling load vs. θ_o *for different values of* a/b

$\tau = 0.7;\ \theta_m = 0°; W_{gpl_m} = 0.01; k_o = 0.9; Vf_{total_o} = 0.5; k_m = 0.5; Vf_{total_m} = 0.55; \alpha_b = 1$

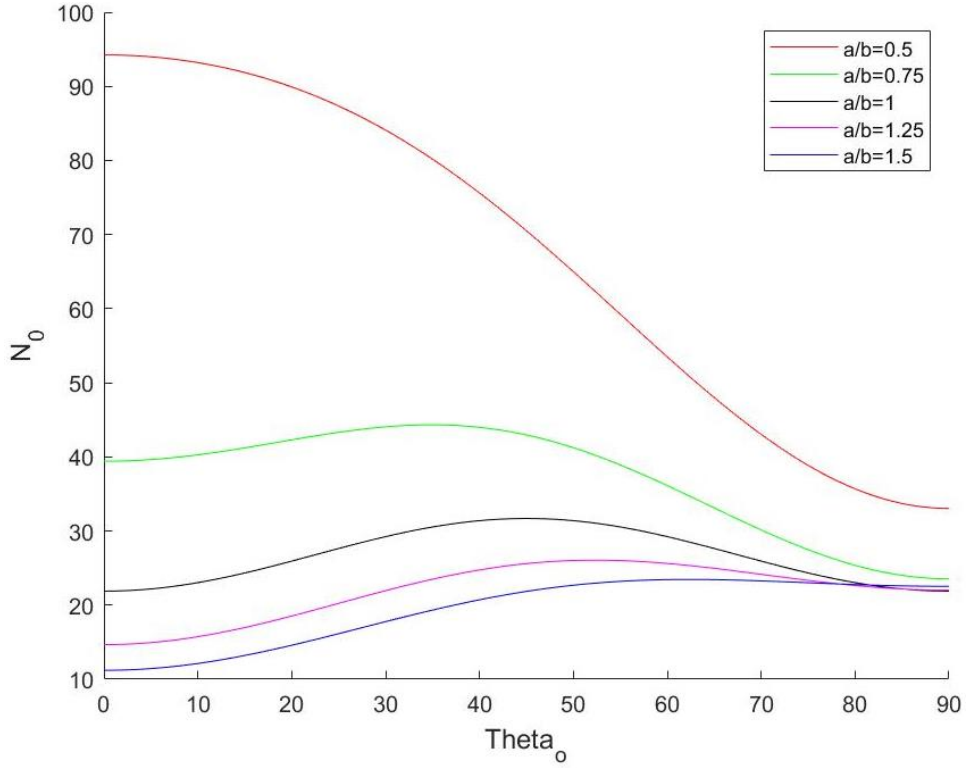

Figure 5.37 (a) $W_{gpl_o} = 0$

$\tau = 0.7;\ \theta_m = 0°; W_{gpl_m} = 0.01; k_o = 0.9; Vf_{total_o} = 0.5; k_m = 0.5; Vf_{total_m} = 0.55; \alpha_b = 1$

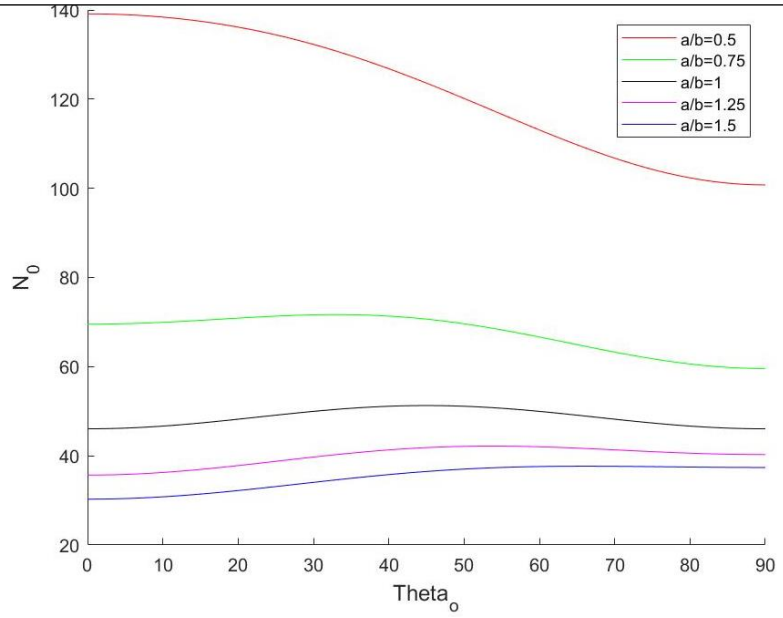

Figure 5.37 (b) $W_{gpl_o} = 0.01$

$\tau = 0.7;\ \theta_m = 0°; W_{gpl_m} = 0.01; k_o = 0.9; Vf_{total_o} = 0.5; k_m = 0.5; Vf_{total_m} = 0.55; \alpha_b = 1$

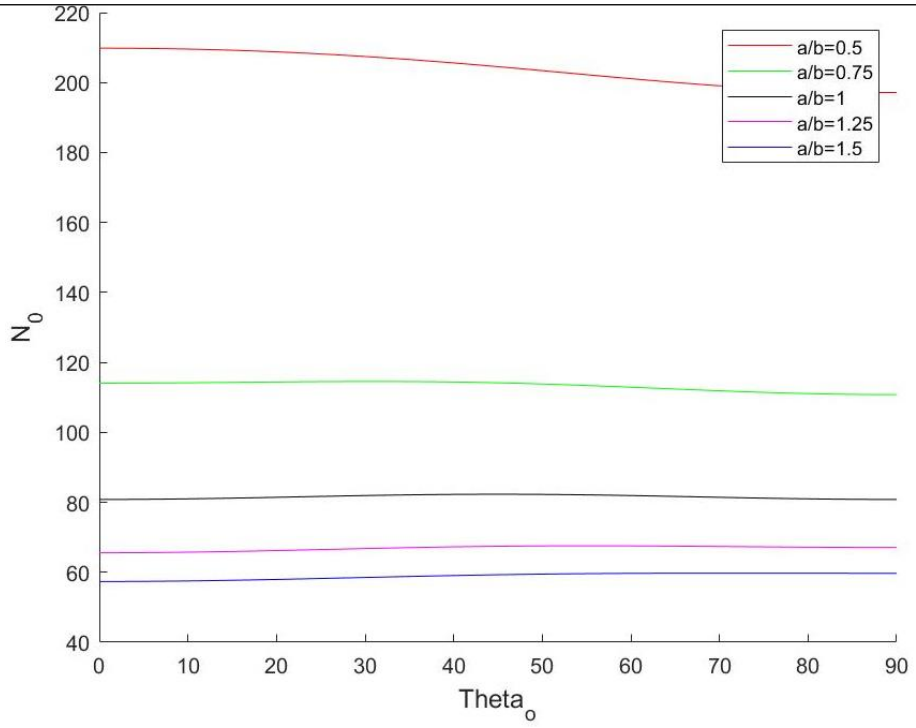

Figure 5.37 (c) $W_{gpl_o} = 0.03$

$\tau = 0.7;\ \theta_m = 0°; W_{gpl_m} = 0.01; k_o = 0.9; Vf_{total_o} = 0.5; k_m = 0.5; Vf_{total_m} = 0.55; \alpha_b = 1$

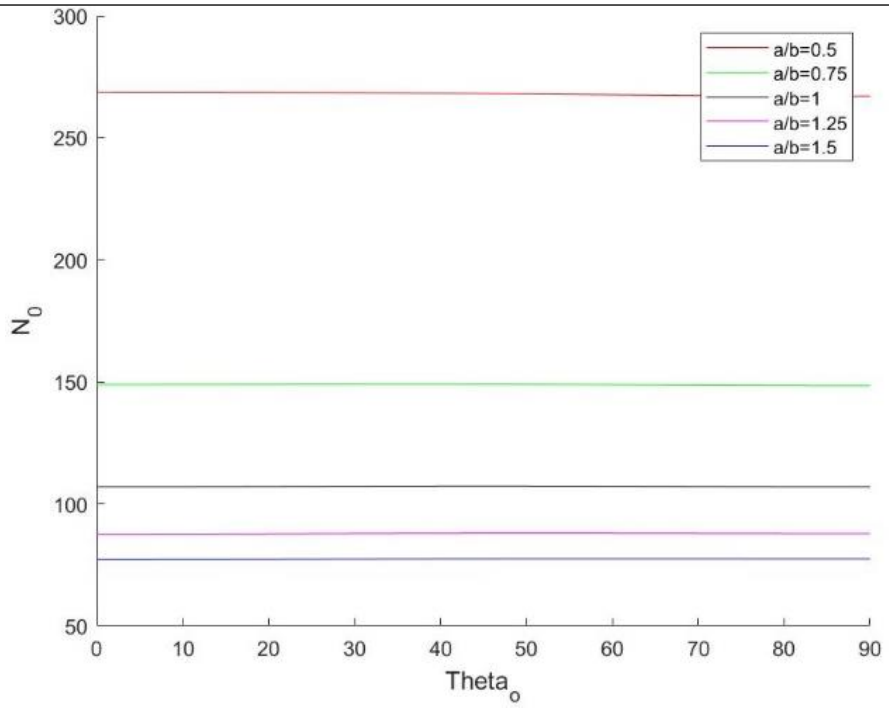

Figure 5.37 (d) $W_{gpl_o} = 0.05$

Figure 5.37: Critical buckling load vs. θ_o *for different values of* a/b

$\frac{a}{b} = 0.5;\ \tau = 0.7;\ \theta_m = 0°;\ W_{gpl_o} = 0;\ W_{gpl_m} = 0.01;\ Vf_{total_o} = 0.5;\ k_m = 0.5;\ Vf_{total_m} = 0.55;$
$\alpha_b = 1$

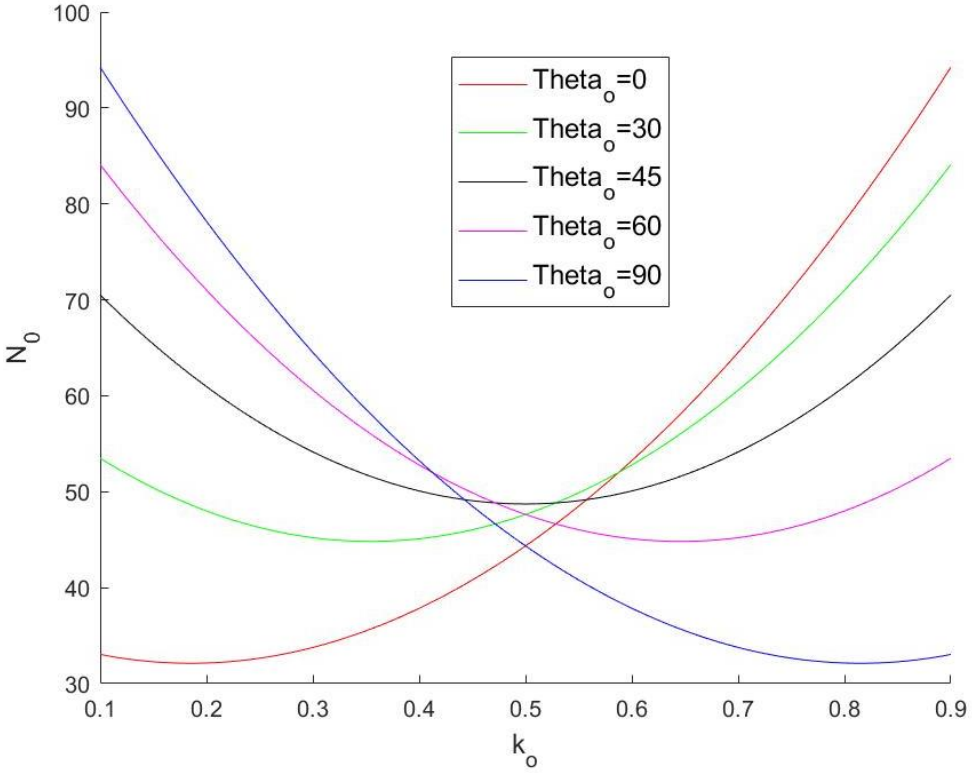

Figure 5.38: Critical buckling load vs. k_o for different values of θ_o

The combined effect of the woven fibre balancing coefficient, k_o, and the graphene platelet weight fraction, W_{gpl_o}, on the critical buckling load is more clearly seen in figure 5.39. In figures 5.39(a), 5.39(b) and 5.39(c), the aspect ratio is set to $\frac{a}{b} = 0.4$, 1 and 4 respectively. When $\frac{a}{b} = 0.4$, in figure 5.39(a), the maximum buckling load occurs at $k_o = 1$ when no graphene is present. For higher graphene weight fractions, $W_{gpl_o} \geq 0.1$ for example, the maximum buckling load occurs when k_o is closer to 0.5. In figure 5.39(b), $\frac{a}{b} = 1$ and the maximum buckling load occurs when $k_o = 0$ or 1 with no graphene present. Again, it is observed that for $W_{gpl_o} \geq 0.1$ the maximum buckling load occurs when k_o is closer to 0.5. In figure 5.39(c), $\frac{a}{b} = 4$ and the maximum buckling load occurs when $k_o = 0$ with no graphene present. Like figures 5.39(a) and 5.39(b), when $W_{gpl_o} \geq 0.1$ the maximum buckling load occurs when k_o is closer to 0.5. Thus, for higher graphene content, a more balanced fibre distribution in both the warp and weft directions is beneficial for the critical buckling load.

$\tau = 0.7;\ \theta_m = 0°; \theta_o = 0°; W_{gpl_m} = 0.01; Vf_{total_o} = 0.5; k_m = 0.5; Vf_{total_m} = 0.55; \alpha_b = 1$

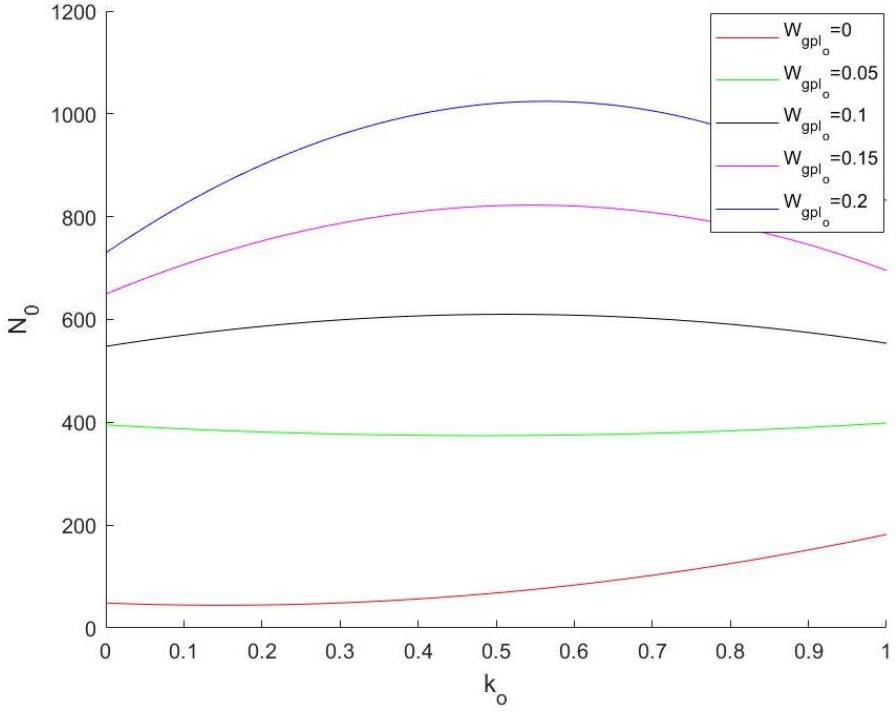

Figure 5.39 (a) $\frac{a}{b} = 0.4$

$\tau = 0.7;\ \theta_m = 0°; \theta_o = 0°; W_{gpl_m} = 0.01; Vf_{total_o} = 0.5; k_m = 0.5; Vf_{total_m} = 0.55; \alpha_b = 1$

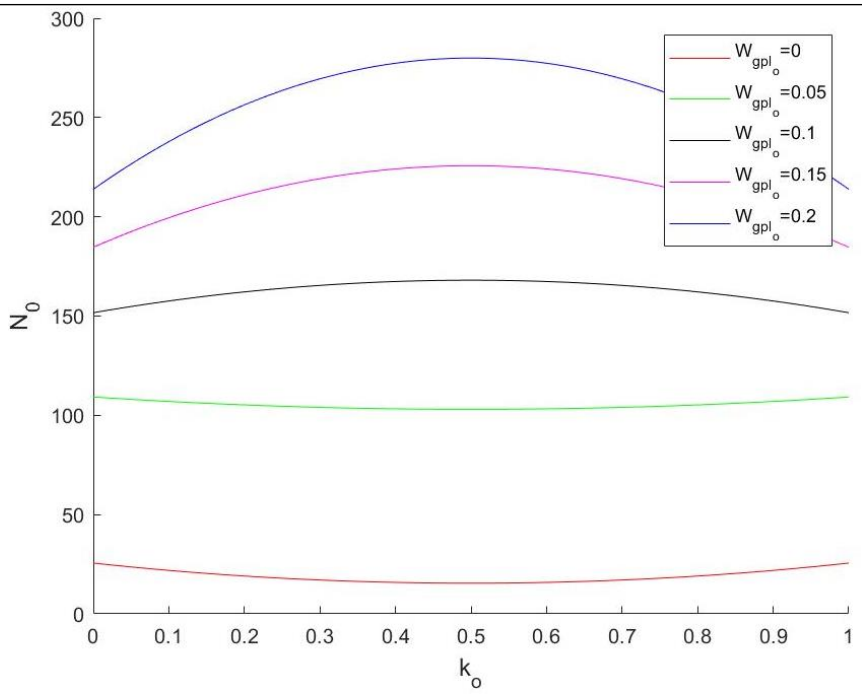

Figure 5.3918 (b) $\frac{a}{b} = 1$

$\tau = 0.7;\ \theta_m = 0°; \theta_o = 0°; W_{gpl_m} = 0.01; Vf_{total_o} = 0.5; k_m = 0.5; Vf_{total_m} = 0.55; \alpha_b = 1$

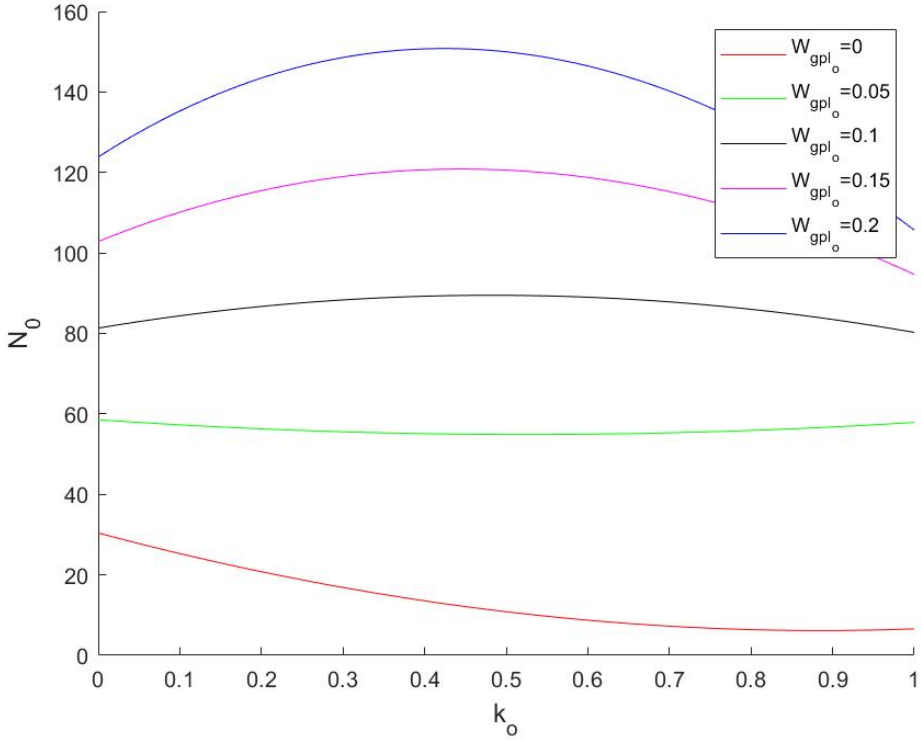

Figure 5.39 (c) $\frac{a}{b} = 4$

Figure 5.39: Critical buckling load vs. k_o *for different values of* W_{gpl_o}

5.2 Graphene platelets analysis

In this section, the effect of the specifications of the graphene platelets in a four-layer symmetric woven glass fibre and graphene platelet reinforced laminate is investigated.

5.2.1 Graphene platelet weight fraction

In this section, the effect of the graphene platelet weight fraction in the outer layers of the woven glass fibre and graphene reinforced laminate, W_{gpl_o}, on the non-dimensional critical buckling load, N_0, is investigated. This section deals with the behaviour of the critical buckling load under different values of W_{gpl_o} and the how the interaction of the graphene platelets with other laminate specifications (such as total woven glass fibre volume fraction Vf_{total_o}, woven glass fibre orientation, θ_o, woven glass fibre balancing coefficient, k_o, laminate thickness ratio, τ, and laminate aspect ratio, $\frac{a}{b}$) influences the critical buckling load.

5.2.1.1 W_{gpl_o} vs. N_0 vs. Vf_{total_o}

Figure 5.40 shows the relationship between the weight fraction of graphene in the outer layer, W_{gpl_o}, and the non-dimensional critical buckling load, N_0, for different total woven glass fibre volume fraction in the outer layer, Vf_{total_o}.

$\tau = 0.7; \frac{a}{b} = 1; \theta_o = 0°; \theta_m = 0°; W_{gpl_m} = 0.01; k_o = 0.5; k_m = 0.5; Vf_{total_m} = 0.55; \alpha_b = 1$

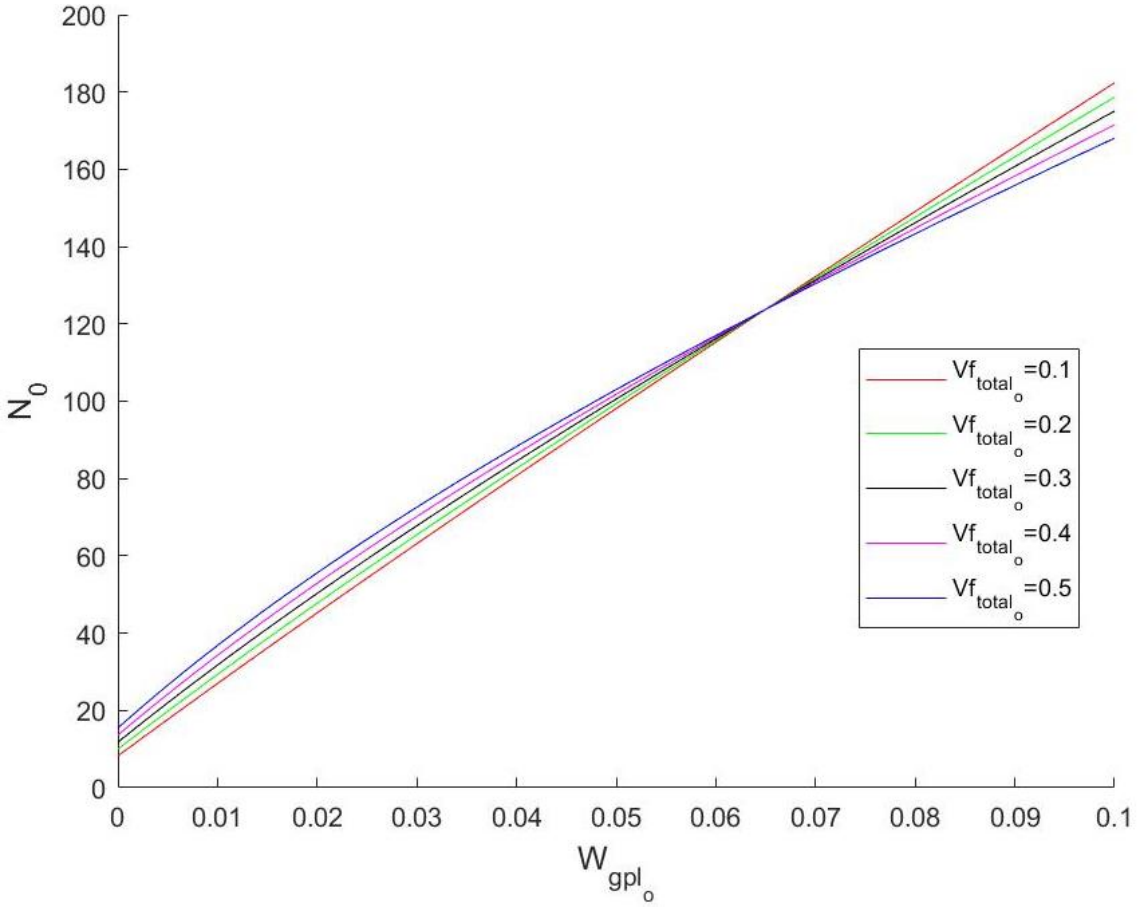

Figure 5.190: Critical buckling load vs. W_{gpl_o} for different values of Vf_{total_o}

The critical buckling load varies between approximately 0 and 190 for $0 \leq W_{gpl_o} \leq 0.1$ and $0.1 \leq Vf_{total_o} \leq 0.5$. At $W_{gpl_o} \approx 0.065$, the curves intersect and the effect of Vf_{total_o} is negligible. For values of W_{gpl_o} above 0.065, it is more beneficial for the critical buckling load when less total woven glass fibre volume is used in the laminate. For example, when $W_{gpl_o} = 10\%$, $Vf_{total_o} = 10\%$ yields a higher N_0 than $Vf_{total_o} = 50\%$.

5.2.1.2 W_{gpl_o} vs. N_0 vs. θ_o

Figure 5.41 shows the relationship between the non-dimensional critical buckling load, N_0, and the graphene weight fraction, W_{gpl_o}, in the outer layer for different fibre orientations, θ_o. The critical buckling load varies between approximately 50 and 400 for $0 \leq W_{gpl_o} \leq 0.05$ and $0° \leq \theta_o \leq 90°$. The graphene essentially increases the critical buckling load and obscures the effect of the fibre orientation on the critical buckling load. For the laminate with the specifications in figure 5.41, when $W_{gpl_o} = 0\%$, if the woven glass fibres in the outer layer are orientated at $\theta_o = 0°$, a critical buckling load, N_0, equal to approximately 90 is yielded. If the woven glass fibres are orientated at $\theta_o = 90°$, $N_0 = 50$. However,

when $W_{gpl_o} = 5\%$, the woven glass fibres can be orientated at any θ_o value and the same critical buckling load, N_0, will be yielded.

$\tau = 0.7;\ \frac{a}{b} = 0.4;\ \theta_m = 0°;\ W_{gpl_m} = 0.01;\ k_o = 0.67;\ Vf_{total_o} = 0.45;\ k_m = 0.5;\ Vf_{total_m} = 0.55;\ \alpha_b = 1$

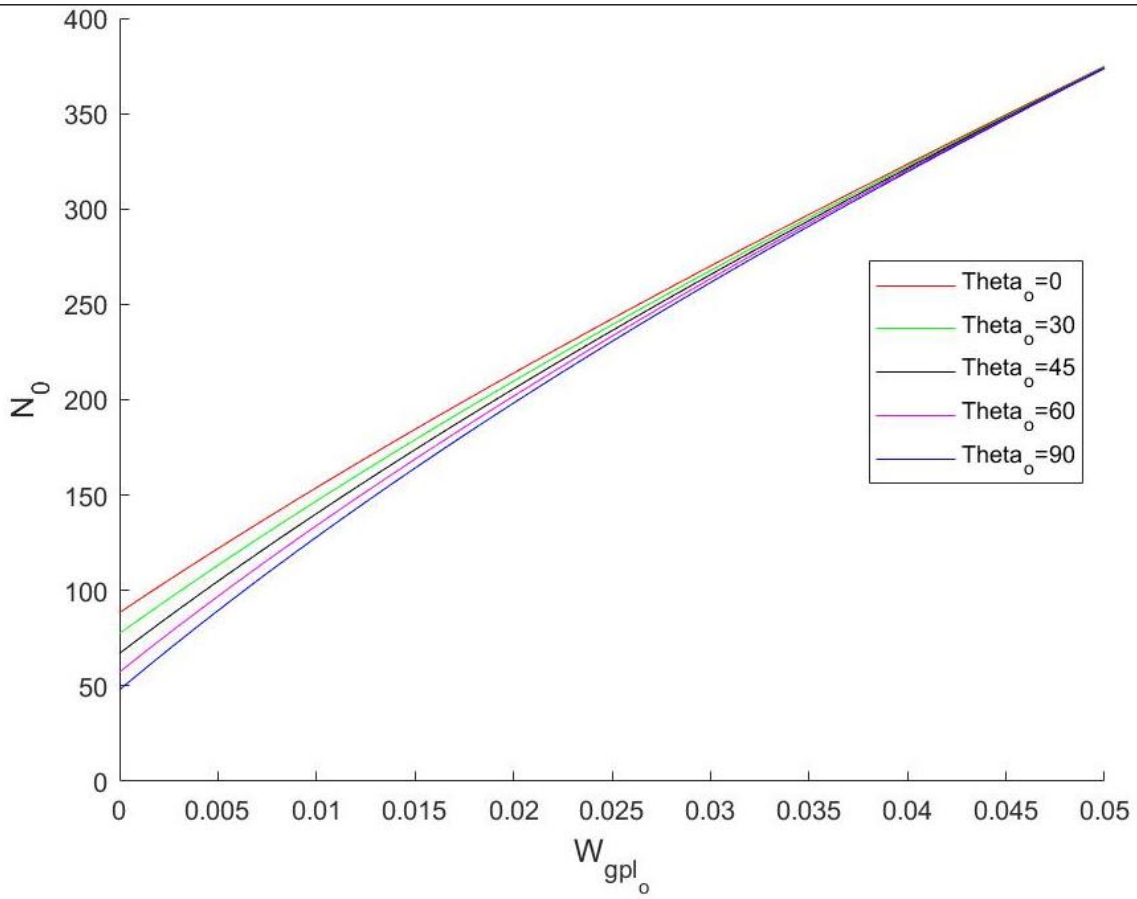

Figure 5.41: Critical buckling load vs. W_{gpl_o} for different values of θ_o

The value of θ_o at which N_0 is at its maximum value for low amounts of W_{gpl_o} in the laminate is determined by the aspect ratio. This is illustrated in figure 5.42. When $\frac{a}{b} = 0.4$ in figure 5.42, $\theta_o = 0°$ yields the maximum critical buckling load. Hence, in figure 5.41, for small amounts of W_{gpl_o} ($W_{gpl_o} < 0.05$) the maximum critical buckling load, N_0, occurs when the woven glass fibres in the outer layer are orientated at 0° ($\theta_o = 0°$). If the aspect ratio, $\frac{a}{b}$, of the laminate was set to 1, for example, the maximum N_0 would be exhibited if the woven glass fibres were orientated at 45° ($\theta_o = 45°$).

$\tau = 0.7;\ \theta_m = 0°; W_{gpl_o} = 0.005; W_{gpl_m} = 0.01; k_o = 0.67;\ Vf_{total_o} = 0.45; k_m = 0.5;$
$Vf_{total_m} = 0.55; \alpha_b = 1$

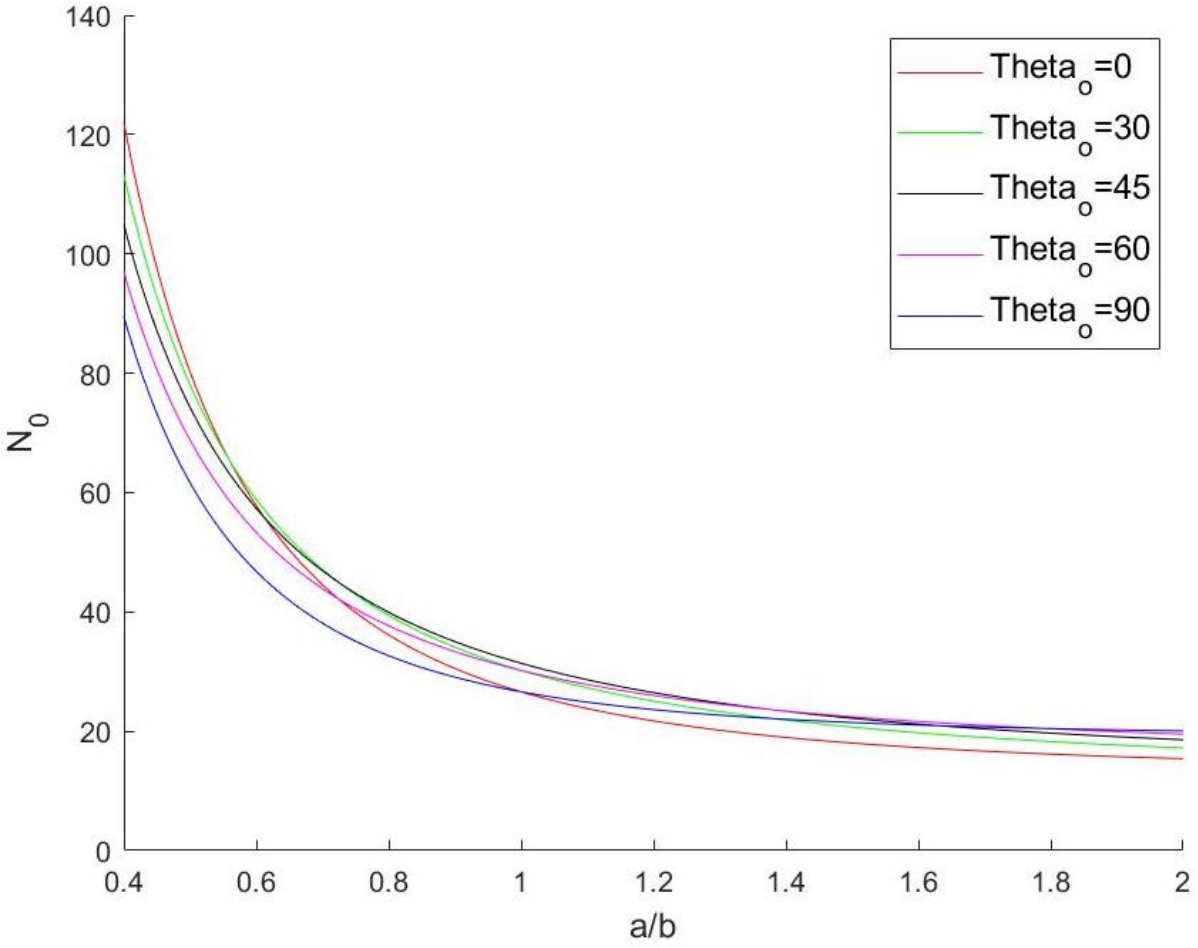

Figure 5.42: Critical buckling load vs. a/b for different values of θ_o

5.2.1.3 W_{gpl_o} vs. N_0 vs. k_o

Figures 5.43(a) and 5.43(b) show the relationship between the non-dimensional critical buckling load, N_0, and the graphene weight fraction in the outer layer, W_{gpl_o}, for different woven glass fibre balancing coefficients, k_o, with $\frac{a}{b} = 1$ and $\frac{a}{b} = 1.2$ respectively. In figure 5.43(a), the plot for $k_o = 0$ and $k_o = 1$ are identical. The same applies for $k_o = 0.25$ and $k_o = 0.75$. This is because of the square geometry of the laminate and the uniform buckling load on each axis.

For the laminate specifications in figure 5.43(a), for values of $W_{gpl_o} < 0.065$, a more concentrated glass fibre distribution in a single direction in the outer layer (either in the warp or weft direction) yields a higher critical buckling load. A balanced distribution yields the minimum critical buckling load. At $W_{gpl_o} \approx 0.065$, the curves intersect and the effect of k_o on the critical buckling load is negligible. For values of $W_{gpl_o} > 0.065$, a more balanced woven glass fibre distribution ($k_o = 0.5$) yields a higher

critical buckling load. In figure 5.43(b), $\frac{a}{b} = 1.2$. In this case, for values of $W_{gpl_o} < 0.065$, a laminate with woven glass fibres more concentrated in the weft direction ($k_o = 0$) exhibits a higher critical buckling load than a laminate with woven glass fibres balanced in both directions. For values of $W_{gpl_o} > 0.065$, a more balanced woven glass fibre distribution in the outer layer is beneficial for the critical buckling load. Thus, for high graphene content, a more balanced fibre distribution is preferred for a higher critical buckling load.

The combined effect of the aspect ratio of the laminate, $\frac{a}{b}$, and the woven glass fibre balancing coefficient, k_o, on the critical buckling load, N_0 is clearly depicted in figure 5.44. At certain points in this figure, two curves intersect each other. At these points, two different values of k_o can yield the same critical buckling load, N_0. When $\frac{a}{b} = 1$ in figure 5.44, the $k_o = 1$ curve intersects the $k_o = 0$ curve. Both these values of k_o will yield the maximum critical buckling load. This is verified in figure 5.43(a). When $\frac{a}{b} = 1.2$ in figure 5.44, $k_o = 0$ yields the maximum critical buckling load. This is verified in figure 5.43(b).

$\tau = 0.7; \frac{a}{b} = 1; \theta_o = 0°; \theta_m = 0°; W_{gpl_m} = 0.01; Vf_{total_o} = 0.5; k_m = 0.5; Vf_{total_m} = 0.55; \alpha_b = 1$

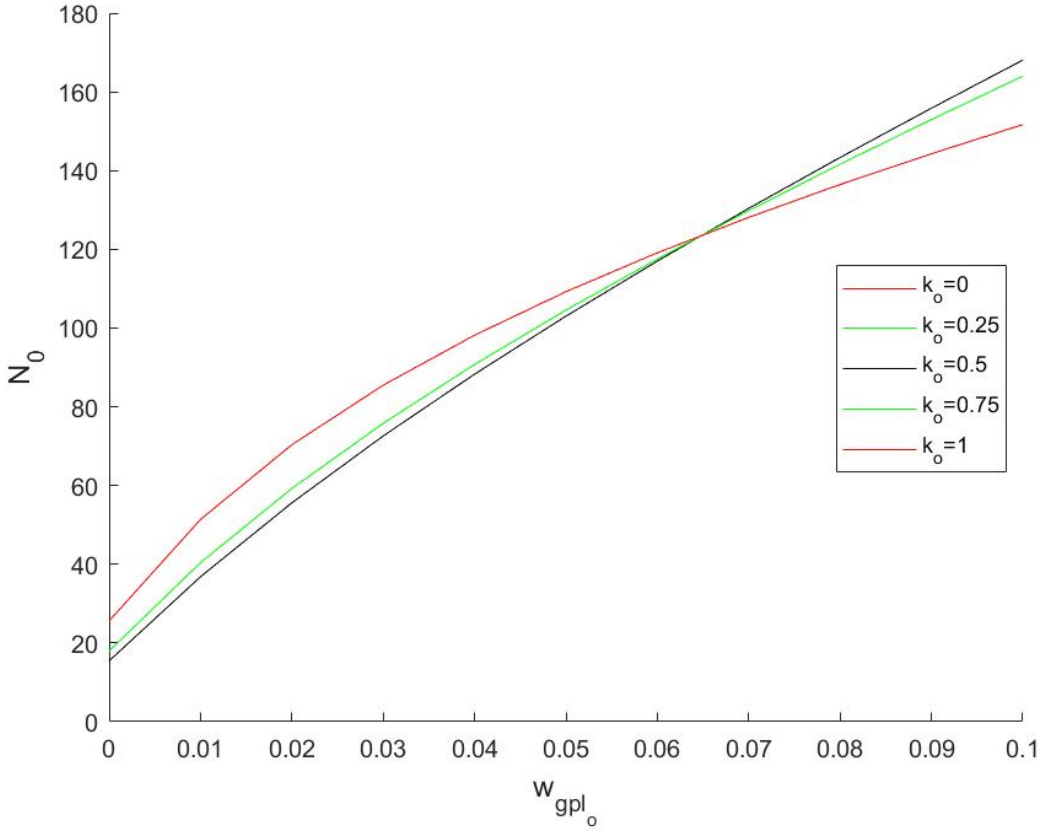

Figure 5.43 (a) $\frac{a}{b} = 1$

$\tau = 0.7; \frac{a}{b} = 1; \theta_o = 0°; \theta_m = 0°; W_{gpl_m} = 0.01; Vf_{total_o} = 0.5; k_m = 0.5; Vf_{total_m} = 0.55; \alpha_b = 1$

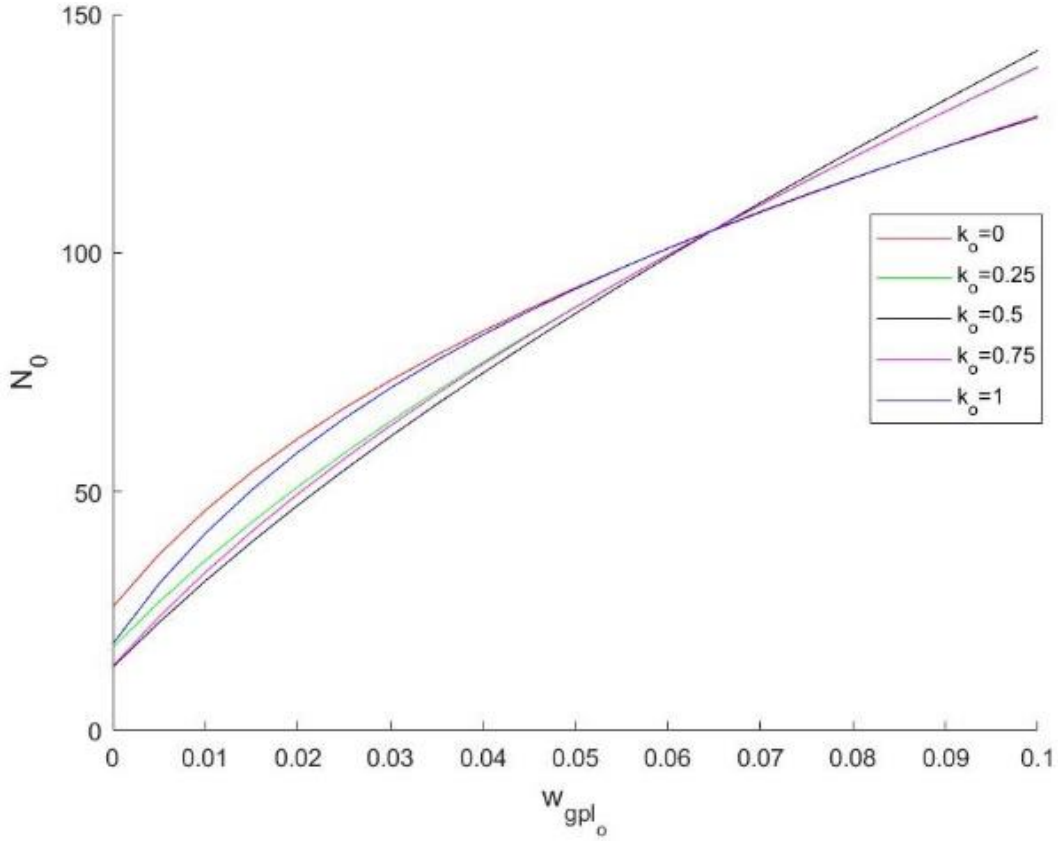

Figure 5.43 (b) $\frac{a}{b} = 1.2$

Figure 5.43: Critical buckling load vs. W_{gpl_o} *for different values of* k_o

$\tau = 0.7;\ \theta_o = 0°;\ \theta_m = 0°;\ W_{gpl_o} = W_{gpl_m} = 0.01;\ Vf_{total_o} = 0.5;\ k_m = 0.5;\ Vf_{total_m} = 0.55;$
$\alpha_b = 1$

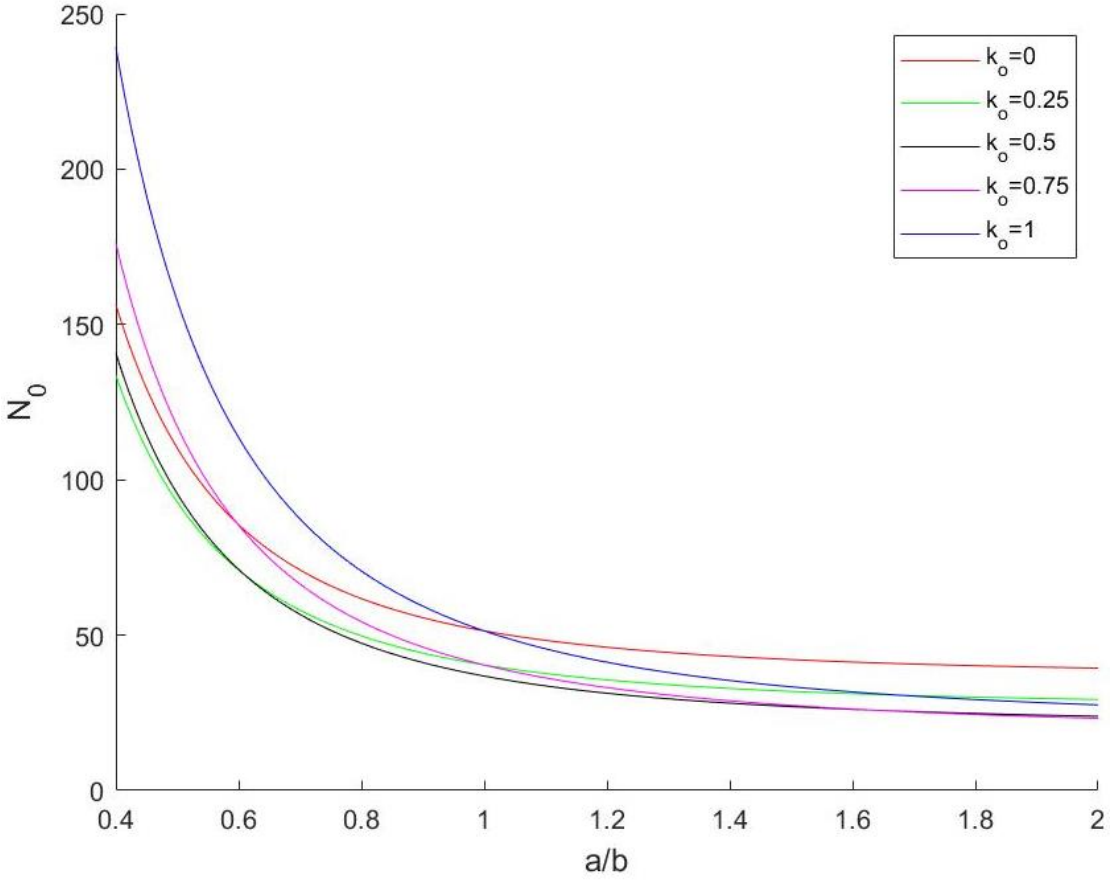

Figure 5.4420: Critical buckling load vs. a/b for different values k_o

5.2.1.4 W_{gpl_o} vs. N_0 vs. τ

Figures 5.45(a) and 5.45(b) show the relationship between the graphene weight fraction in the outer layer, W_{gpl_o}, and the non-dimensional critical buckling load, N_0, for different thickness ratios, τ, with $W_{gpl_m} = 0\%$ and $W_{gpl_m} = 1\%$ respectively. Both these figures show that if the total woven glass fibre volume and woven glass fibre balancing coefficients are identical in both the middle and outer layers, then for $\frac{a}{b} = 1$, all the thickness ratio curves intersect at the point where $W_{gpl_o} = W_{gpl_m}$. At this point, the thickness ratio has no influence on the critical buckling load. If $Vf_{total_o} = Vf_{total_m}$ and $k_o = k_m$, then for values of $W_{gpl_o} < W_{gpl_m}$, a lower thickness ratio yields a higher critical buckling load. For values of $W_{gpl_o} > W_{gpl_m}$, a higher thickness ratio yields a higher critical buckling load. Both these figures are visualized in the contour plots of figure 5.46.

$\frac{a}{b} = 1; \theta_o = 0°; \theta_m = 0°; k_o = 0.5; Vf_{total_o} = 0.55; k_m = 0.5; Vf_{total_m} = 0.55; \alpha_b = 1$

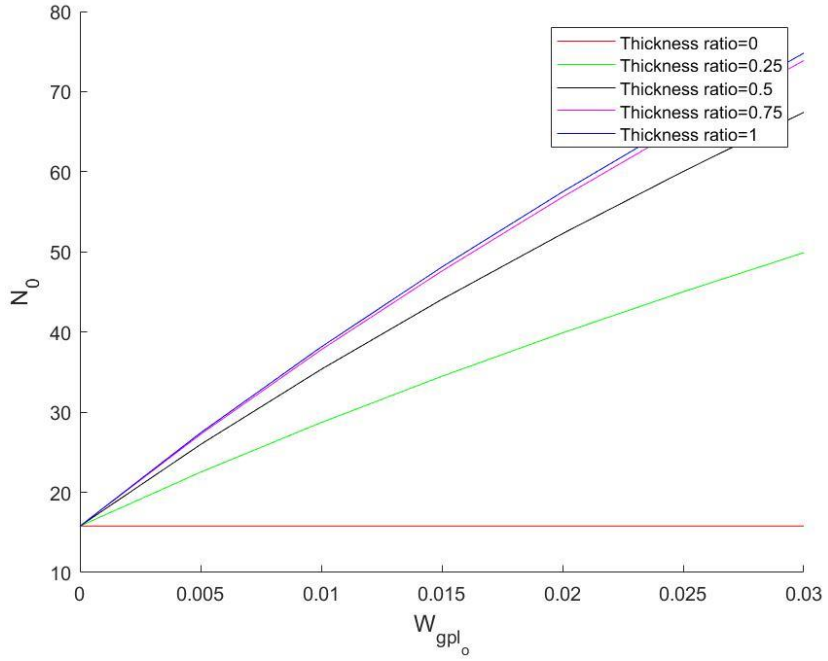

Figure 5.4521 (a) $W_{gpl_m} = 0$

$\frac{a}{b} = 1; \theta_o = 0°; \theta_m = 0°; k_o = 0.5; Vf_{total_o} = 0.55; k_m = 0.5; Vf_{total_m} = 0.55; \alpha_b = 1$

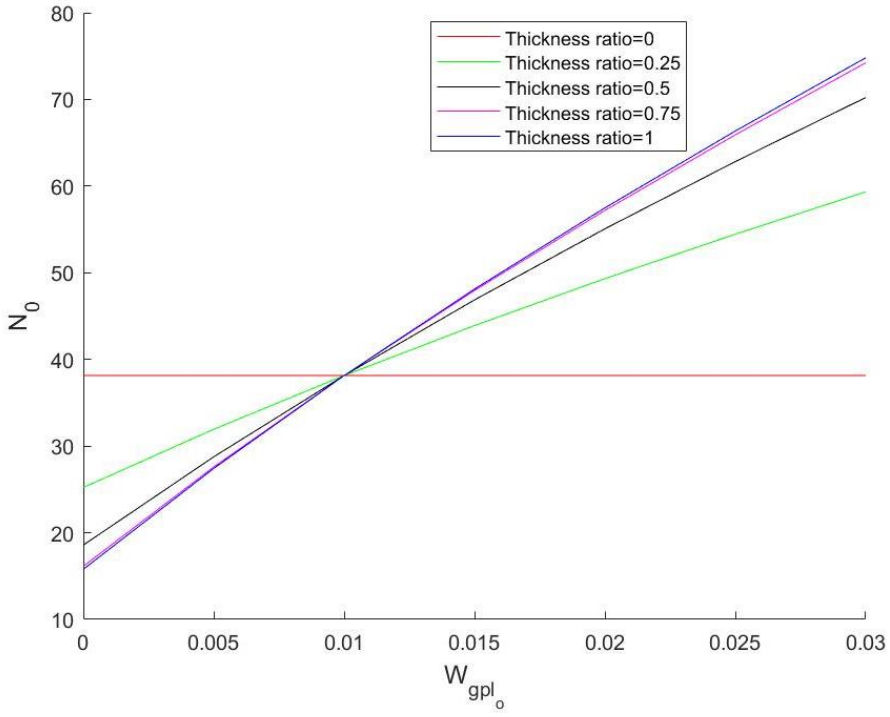

Figure 5.45 (b) $W_{gpl_m} = 0.01$

Figure 5.45: Critical buckling load vs. W_{gpl_o} *for different values of* τ

$\frac{a}{b} = 1; \theta_o = 0°; \theta_m = 0°; k_o = 0.5; Vf_{total_o} = 0.55; k_m = 0.5; Vf_{total_m} = 0.55; \alpha_b = 1$

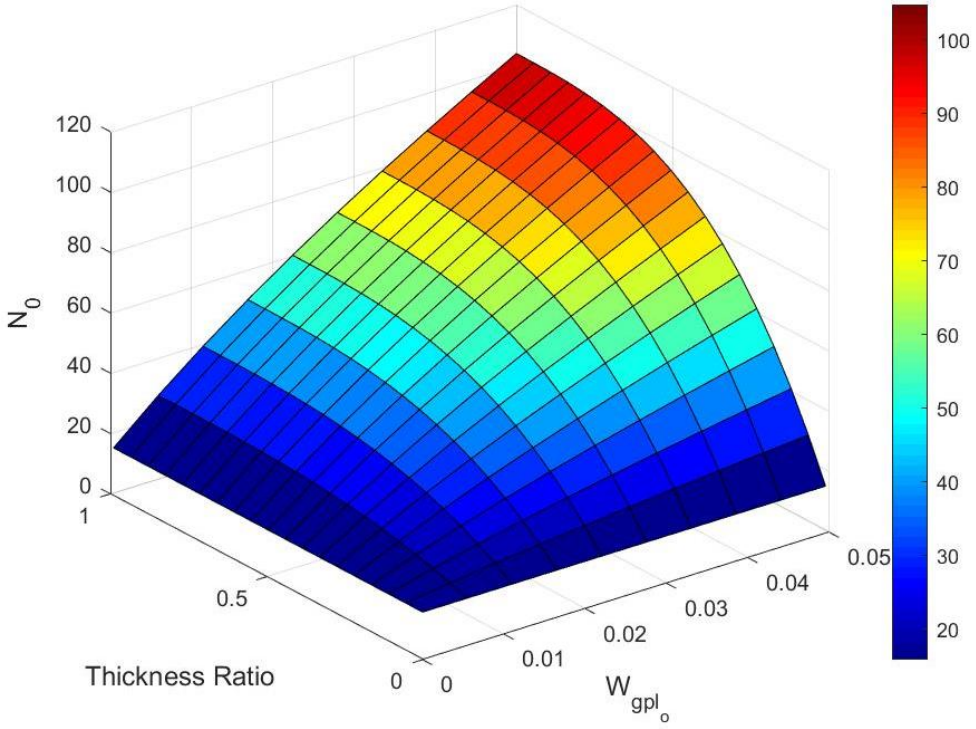

Figure 5.46 (a) $W_{gpl_m} = 0$

$\frac{a}{b} = 1; \theta_o = 0°; \theta_m = 0°; k_o = 0.5; Vf_{total_o} = 0.55; k_m = 0.5; Vf_{total_m} = 0.55; \alpha_b = 1$

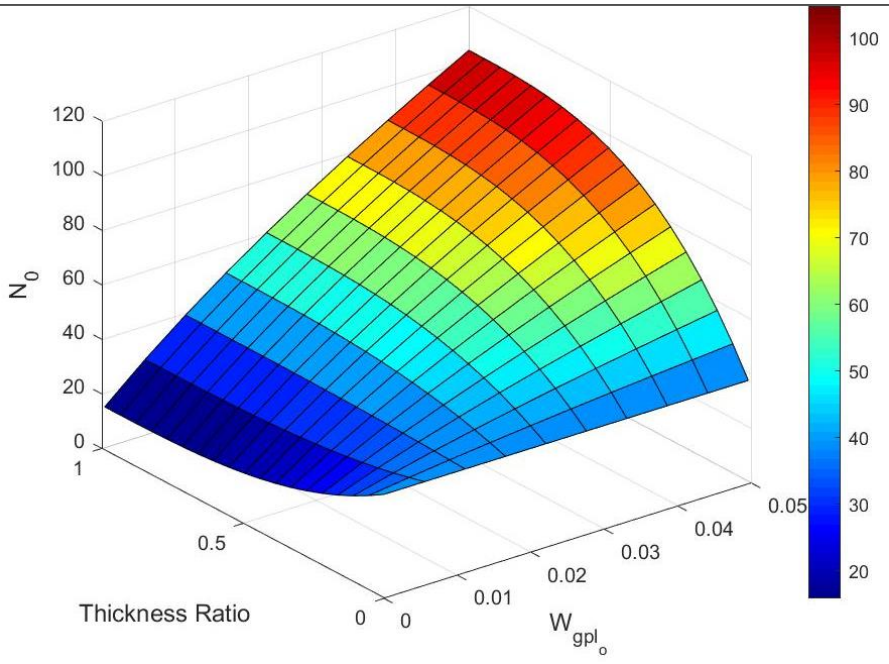

Figure 5.46 (b) $W_{gpl_m} = 0.01$

Figure 5.46: Contour plot of critical buckling load vs. W_{gpl_o} *for different values of* τ

5.2.1.5 $\mathbf{W_{gpl_o}}$ vs. $\mathbf{N_0}$ vs. $\frac{\mathbf{a}}{\mathbf{b}}$

Figure 5.47 shows the relationship between the graphene weight fraction in the outer layer, W_{gpl_o}, and the non-dimensional critical buckling load, N_0, for different values of the laminate aspect ratio, $\frac{a}{b}$. For these laminate specifications, a lower aspect ratio yields a higher critical buckling load for a laminate under biaxial, uniform compression. The rate at which N_0 increases as $\frac{a}{b}$ decreases also increases as $\frac{a}{b}$ gets smaller. For $W_{gpl_o} = 5\%$, for example, decreasing $\frac{a}{b}$ from 1.5 to 1.25 results in an increase of N_0 from approximately 50 to 60. However, decreasing $\frac{a}{b}$ from 0.75 to 0.5 results in an increase of N_0 from approximately 135 to 250.

$\tau = 0.7;\ \theta_o = 0°;\ \theta_m = 0°;\ W_{gpl_m} = 0.01;\ k_o = 0.5;\ Vf_{total_o} = 0.55;\ k_m = 0.5;\ Vf_{total_m} = 0.55;\ \alpha_h = 1$

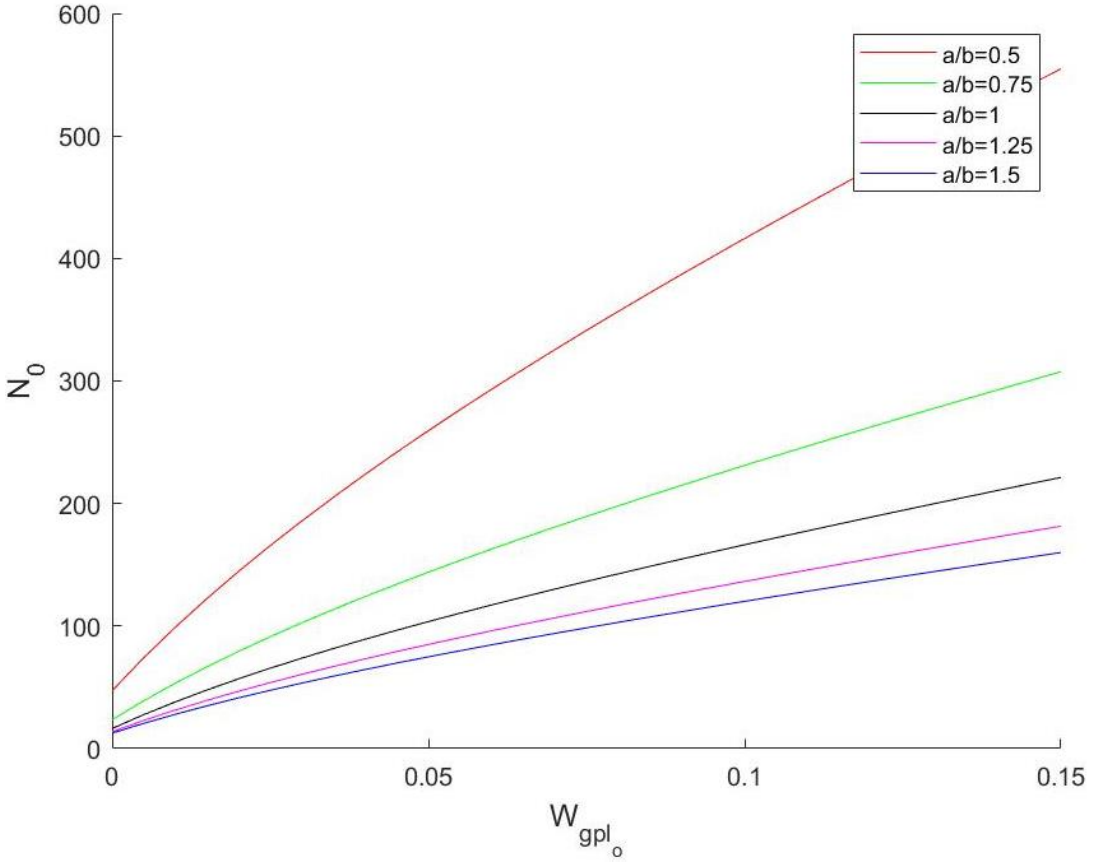

Figure 5.47: Critical buckling load vs. W_{gpl_o} for different values of a/b

6 Conclusions

This chapter concludes the investigation by summarizing the relevant results and discussing recommendations for future research.

6.1 Conclusion

The aim of this investigation was to develop an analytical model to analyse the buckling behaviour of a woven glass fibre and graphene platelet reinforced nanocomposite under compressive loading. As part of this investigation, development of a suitable software simulation programme to incorporate this analytical model was required. This was done so using Matlab. The effects of various design parameters on the critical buckling load were then investigated.

Literature was presented with various examples of the advantages of using fibre and/or nanoscopic reinforcement in composite materials. Comparisons were made between different types of fibre materials and nanoscopic materials currently used as reinforcements and their effects on the performance of composite materials. A common approach in the analysis of composite structures is to analyse the behaviour of the composite material as a laminate. To do so, the material must be analysed at a micromechanical level. This considers the interaction of the reinforcement material with the matrix material of the laminate. Various approaches exist in this regard, each with their complexities and shortcomings. Common approaches include the cylindrical cell approach based on considering a cylindrical elementary cell representing the fibre, in a cylindrical cell representing the matrix [78], and the Halpin-Tsai equations which develop a generalized formula to determine the engineering moduli in one lamina [80]. For woven fibre reinforcement laminates, a laminate analogy exists in which the laminate is modelled as an assembly of cross-ply laminates and undulation of the fibres is neglected [82]. In this analogy, the woven fibres are regarded as orientated at 90° to each other in either the warp direction or weft direction. For this investigation, this woven fibre analogy along with the Halpin-Tsai equations were adopted to analyse the woven fibre and graphene nanoplatelet nanocomposite as a laminate. An overview of classical laminate theory was presented. The governing equations of classical laminate theory, including the governing equation for buckling of a biaxially-loaded, simply-supported rectangular laminate plate, were used to determine the critical buckling load of the laminate. A non-dimensional critical buckling load was introduced as a function of the dimensionalized critical buckling load. As is often the case, the bending-twisting coupling terms in the bending stiffness matrix of classical laminate theory, D_{12} and D_{26}, were neglected in order for simple expressions of the buckling load to be developed [88].

The laminate considered for this investigation was reinforced by woven glass fibres and graphene nanoplatelets. It has 4 plies and is symmetric about its midpoint. As a result, it has two outer layers which are identical and referred to collectively as the outer layer, and two middle layers which are identical and referred to collectively as the middle layer. The reinforcement materials were non-

uniformly distributed throughout the layers and the layer thicknesses are non-uniform as well. The fibre orientations in each layer were free parameters. The thickness of the laminate was set to $5 \times 10^{-3}\ m$. The thickness ratio, τ, defined as the ratio of the width of outer layers to the width of the laminate, was set to 0.7 in cases where it is not a parameter being investigated. The buckling load ratio, defined as the ratio of the compressive force along the x direction, to the compressive force along the y direction, was set to equal 1, for uniform biaxial loading. The influences of the woven fibre volume fraction, woven fibre balancing coefficient, woven fibre orientation and graphene platelet weight fraction on the non-dimensional critical buckling load were then investigated. The investigation entailed generating 2D and 3D graphs detailing the change in buckling load with the change in the value of these variables, with different design parameters of the laminate including different aspect ratios of the laminate and different thickness ratios of the laminate.

It was found that the critical buckling load of the 4-ply, woven glass fibre and graphene platelet reinforced laminate is far more sensitive to the graphene platelet weight fraction than the woven glass fibre volume fraction. When the volume fraction of glass fibres in the outer layer was set to 50%, the non-dimensional critical buckling load was approximately 15 with no graphene and 90 with a graphene weight fraction of 4% in the outer layer.

It was found that, for the thickness ratio $\tau = 0.7$, the glass fibre volume fraction in the middle layer has an almost negligible effect on the critical buckling load. Thus, more focus should be directed to the reinforcements in the outer layer for a cost-effective laminate.

Investigating the combined influence of the woven glass fibre volume fraction and graphene nanoplatelet weight fraction in the outer layer of the laminate on the buckling load proved that once the graphene weight fraction is increased above a certain point, increasing the glass fibre volume fraction diminishes the buckling load. In this case, for a cost-effective laminate, it is more beneficial to design the laminate with a lower glass fibre volume fraction. The graphene platelets also reduce the influence of the aspect ratio of the laminate on the buckling load.

Investigating the combined influence of the woven glass fibre orientation and woven glass fibre volume fraction in the warp direction in the outer layer proved that, in most cases for a given graphene weight fraction and fibre volume in the weft direction, the optimum glass fibre orientation for buckling was either 0° for low warp-fibre volumes or 90° for high warp-fibre volumes. When graphene weight fraction in the outer layer and middle layer were equal, and aspect ratio set to 0.4, the ideal fibre orientation in the outer layer for buckling when the woven fibre balancing coefficient is close to 0.5 depends on the value of the warp-fibre volume fraction and may be anywhere between 0° and 90°. The presence of graphene also obscures the effect of the woven glass fibre orientation such that, at a certain graphene weight fraction, the woven glass fibre orientation has no effect on the buckling load. When the aspect ratio of the laminate is not 1, and no graphene is present, the ideal woven glass fibre volume

fraction in the warp direction depends on the orientation of the woven glass fibres and the laminate aspect ratio. In some cases, a woven fibre orientation may dictate that a lower warp-fibre volume fraction is required for a higher buckling load. With graphene content increased, however, this effect is obscured.

Investigating the influence of the laminate thickness ratio on the buckling load proved that, with no graphene present, a higher thickness ratio (up to 0.75) is preferred when there are more woven glass fibres in the outer layer than the middle layer. However, with graphene platelet weight fraction set to 1% in the outer layer and 0% in the middle layer, a higher thickness ratio is always preferred regardless of the woven glass fibre volume fraction. Increasing the thickness ratio above 0.75 has a negligible effect on the buckling load and is thus unnecessary for cost-effective designing.

It was also found that, for low graphene content in the outer layer, concentrating the glass fibres in a single direction results in a higher buckling load. However, for a graphene weight fraction higher than 0.065 in the outer layer, a more balanced woven glass fibre distribution in both the warp and weft directions is beneficial.

6.2 Future research recommendations

The present investigation has utilized the computer software Matlab to model the theoretical equations governing the critical buckling load of a 4-ply, symmetric woven glass fibre and graphene nanoplatelet reinforced laminate. The critical buckling load was predicted for various design parameters. The equations used in the woven fibre micromechanics neglect the undulations of the fibres and the misalignment of the threads. Other methods exist that do not neglect the fibre undulation and can improve the reliability of these results, such as the bridging model, [83]. Furthermore, the bending-twisting coupling terms of the bending stiffness matrix in classical laminate theory, D_{16} and D_{26}, were neglected in this analysis. More complex analytical models exist that do not neglect these terms and the use of these may alter the results presented here [89]. Optimization analysis of the laminate investigated in this study is also possible, whereby the laminate properties are optimized for the critical buckling load. Lastly, the woven fibres considered here were glass fibres. A hybrid laminate, consisting of glass fibres and carbon fibres woven together, and reinforced with graphene nanoplatelets may also be investigated for its buckling properties under the design parameters investigated here.

7 References

[1] D. D. Chung, Composite Materials: Science and Applications, London: Springer-Verlag London, 2010.

[2] K. K. Kar, Processing, Applications, Characterizations, Springer, 2017.

[3] A. Bunsell and J. Renard, Fundamentals of fibre reinforced composite materials, IOP Publishing, 2005.

[4] J.-K. Kim and M.-L. Sham, " Impact and delamination failure of woven-fabric composites," *Composites Science and Technology,* vol. 60, no. 5, pp. 745-761, 2000.

[5] H. Fan, L. Wang, K. Zhao, N. Li, Z. Shi, Z. Ge and Z. Jin, "Fabrication, Mechanical Properties, and Biocompatibility of Graphene-Reinforced Chitosan Composites," *Biomacromolecules ,* vol. 11, no. 9, pp. 2345-2351, 2010.

[6] F. Murat and L. Tartar, Topics in the Mathematical Modelling of Composite Materials, Birkhäuser Basel, 1997.

[7] H. Altenbach, Lecture Notes on Composite Materials: Current Topics and Achievements, Springer Netherlands, 2009.

[8] A. C. Long, Design and Manufacture of Textile Composites, Woodhead Publishing Ltd, 2005.

[9] X. Peng, "Continuous models for analyzing the mechanical behavior of reinforcements in composites," in *Composite Reinforcements for Optimum Performance*, 2011, p. 529.

[10] J. Li, Z. Wu, C. Huang and L. Li, "Multiscale carbon nanotube-woven glass fiber reinforced cyanate ester/epoxy composites for enhanced mechanical and thermal properties," *Composites Science and Technology,* vol. 104 , pp. 81-88, 2014.

[11] J. P. Carey, Handbook of Advances in Braided Composite Materials, Woodhead Publishing, 2017.

[12] S. Chatterjee, J. Wang, W. Kuo, N. Tai, C. Salzmann, W. Li, R. Hollertz, F. Nüesch and B. Chu, "Mechanical reinforcement and thermal conductivity in expanded graphene nanoplatelets reinforced epoxy composites," *Chemical Physics ,* vol. 531 , pp. 6-10, 2012.

[13] G. Mittal, V. Dhand, K. Y. Rhee, S.-J. Park and W. R. Lee, "A review on carbon nanotubes and graphene as fillers in reinforced polymer nanocomposites," *Journal of Industrial & Engineering Chemistry* , vol. 21, pp. 11-25, 2015.

[14] J. Berthelot, Composite Materials Mechanical Behaviour and Structural Analysis, Springer, 1999, p. 4.

[15] V. Çeçen, M. Sarikanat, H. Yildiz and I. H. Tavman, "Comparison of mechanical properties of epoxy composites reinforced with stitched glass and carbon fabrics: Characterization of mechanical anisotropy in composites and investigation on the interaction between fiber and epoxy matrix," *Polymer Composites* , vol. 29, no. 8, pp. 840-853, 2008.

[16] T. J. Reinhart, "Overview of Composite Materials," in *Handbook of Composites*, S. Peters, Ed., London, Chapman & Hall, 1998, pp. 21-33.

[17] R. M. Jones, Mechanics of Composite Materials, 2 ed., New York: Taylor & Francis Group, 1999.

[18] K. K. Chawla, Composite Materials: Science and Engineering, 3 ed., Alabama: Springer, 2006.

[19] F. L. Matthews and R. D. Rawlings, Composite Materials: Engineering and Science, Florida: Woodhead Publishing, 2006.

[20] A. K. Kaw, Mechanics of Composite Materials, 2 ed., Florida: CRC Press; Taylor & Francis Group, 2006.

[21] T. W. Clyne and D. Hull, An Introduction to Composite Materials, 3 ed., Cambridge: Cambridge University Press, 2019.

[22] S. R. Reid and G. Zhou, Impact Behaviour of Fibre-Reinforced Composite Materials and Structures, Florida: Woodhead Publishing, 2000.

[23] H. Pihtili, "An experimental investigation of wear of glass fibre–epoxy resin and glass fibre–polyester resin composite materials," *European Polymer Journal*, vol. 45, no. 1, pp. 149-154, 2009.

[24] A. Gopinath, M. S. Kumar and A. Elayaperumal, "Experimental Investigations on Mechanical Properties Of Jute Fiber Reinforced Composites with Polyester and Epoxy Resin Matrices," *Procedia Engineering 97* , p. 2052 – 2063 , 2014.

[25] M. Rosso, “Ceramic and metal matrix composites: Routes and properties,” *Journal of Materials Processing Technology*, vol. 175, pp. 364-375, 2006.

[26] I. Ibrahim, F. A. Mohamed and E. Lavernia, “Particulate reinforced metal matrix composites — a review,” *Journal of Materials Science*, vol. 26, no. 5, pp. 1137-1156, 1991.

[27] K. U. Kainer, Metal Matrix Composites, Wiley, 2006.

[28] J. W. S. Hearle, “Glass Fibres,” in *High-Performance Fibres*, Florida, Woodhead Publishing, 2000, p. 193.

[29] W. Watt, “Production and Properties of High Modulus Carbon Fibres,” *Proceedings of the Royal Society*, vol. 319, pp. 5-15, 1970.

[30] J. Summerscales and D. Short, “Carbon fibre and glass fibre hybrid reinforced plastics,” *Composites*, vol. 9, no. 3, pp. 57-166, 1978.

[31] B. Fiedler, F. H. Gojny, M. H. Wichmann, M. C. Nolte and K. Schulte, “Fundamental aspects of nano-reinforced composites,” *Composites Science and Technology*, vol. 66, pp. 3115-3125, 2006.

[32] M. Raffie, X. Q. He, S. Mareishi and K. M. Liew, “MODELING AND STRESS ANALYSIS OF SMART CNTs/FIBER/POLYMER MULTISCALE COMPOSITE PLATES,” *International Journal of Applied Mechanics*, vol. 6, no. 3, p. 1450025, 2014.

[33] M. Ahmadi, R. Ansari and H. Rouhi, “Multi-scale bending, buckling and vibration analyses of carbon fiber/carbon nanotube-reinforced polymer nanocomposite plates with various shapes,” *Physica E: Low-dimensional Systems and Nanostructures*, 2017.

[34] Z. Shen, S. Bateman, D. Y. Wu, P. McMahon, M. Dell’Olio and J. Gotama, “The effects of carbon nanotubes on mechanical and thermal properties of woven glass fibre reinforced polyamide-6 nanocomposites,” *Composites Science and Technology*, vol. 69, pp. 239-244, 2009.

[35] B. Fiedler, F. H.Gojny, M. H.G.Wichmann, M. C. Nolte and K. Schulte, “Fundamental aspects of nano-reinforced composites,” *Composites Science and Technology*, vol. 66, no. 16, pp. 3115-3125, 2006.

[36] E. Bekyarova, E. T. Thostenson, A. Yu, H. Kim, J. Gao, J. Tang, H. T. Hahn, T. Chou, M. E. Itkis and R. C. Haddon, “Multiscale Carbon Nanotube-Carbon Fiber Reinforcement for Advanced Epoxy Composites,” *Langmuir*, vol. 23, pp. 3970-3974, 2007.

[37] J. A. King, D. R. Klimek, I. Miskioglu and G. M. Odegard, “Mechanical Properties of Graphene Nanoplatelet/Epoxy Composites,” *Journal of Applied Polymer Science* , vol. 128, no. 6, pp. 4217-4223, 2013.

[38] M. Shokrieh, M. Esmkhani, Z. Shokrieh and Z. Zhao, “Stiffness prediction of graphene nanoplatelet/epoxy nanocomposites by a combined molecular dynamics–micromechanics method,” *Computational Materials Science,* vol. 92, pp. 444-450, 2014.

[39] X. Zhao, Q. Zhang, D. Chen and P. Lu, “Enhanced Mechanical Properties of Graphene-Based Poly(vinyl alcohol) Composites,” *Macromolecules,* vol. 43, no. 5, pp. 2357-363, 2010.

[40] J. Cho, J. Chen and I. Daniel, “Mechanical enhancement of carbon fiber/epoxy composites by graphite nanoplatelet reinforcement,” *Scripta Materialia,* vol. 56, no. 8, pp. 685-688, 2007.

[41] C. Feng, S. Kitipornchai and J. Yang, “Nonlinear bending of polymer nanocomposite beams reinforced with non-uniformly distributed graphene platelets (GPLs),” *Composites Part B: Engineering,* vol. 110 , pp. 132-140, 2017.

[42] M. Song, J. Yang, S. Kitipornchai and W. Zhu, “Buckling and postbuckling of biaxially compressed functionally graded multilayer graphene nanoplatelet-reinforced polymer composite plates,” *International Journal of Mechanical Sciences* , 2017.

[43] M. Song, S. Kitipornchai and J. Yang, “Free and forced vibrations of functionally graded polymer composite plates reinforced with graphene nanoplatelets,” *Composite Structures* , 2016.

[44] M. A. Rafiee, J. Rafiee, Z. Wang, H. Song, Z.-Z. Yu and N. Koratkar, “Enhanced Mechanical Properties of Nanocomposites at Low Graphene Content,” *ACS Nano* , vol. 3, no. 2, pp. 3884-3890, 2009.

[45] S.-Y. Yang, W.-N. Lin, Y.-L. Huang, H.-W. Tien, J.-Y. Wang, C.-C. M. Ma, S.-M. Li and Y.-S. Wang, “Synergetic effects of graphene platelets and carbon nanotubes on the mechanical and thermal properties of epoxy composites,” *Carbon Volume,* vol. 803, no. 3, p. 793, 2011.

[46] W. Li, A. Dichiara and J. Bai, “Carbon nanotube–graphene nanoplatelet hybrids as high-performance multifunctional reinforcements in epoxy composites,” *Composites Science and Technology,* vol. 74, no. 24, pp. 221-227, 2013.

[47] C. Soutis, “Fibre reinforced composites in aircraft construction,” *Progress in Aerospace Sciences,* vol. 1, no. 2, pp. 143-151, 2005.

[48] C. Scarponi and M. Messano, “Comparative evaluation between E-Glass and hemp fiber composites application in rotorcraft interiors,” *Composites Part B: Engineering,* vol. 69, pp. 542-549, 2015.

[49] S. Ramakrishna, J. M. E. Wintermantel and K. W. Leong, “Biomedical applications of polymer-composite materials: a review,” *Composites Science and Technology,* vol. 61, no. 9, pp. 1189-1224, 2001.

[50] M. Zhang and J. P. Matinlinna, “E-Glass Fiber Reinforced Composites in Dental Applications,” *Silicon,* vol. 4, no. 1, pp. 73-78, 2012.

[51] F. W. Wendt, H. Liebowitz and N. Perrone, Mechanics of Composite Materials: Proceedings of the Fifth Symposium on Naval Structural Mechanics, Philadelphia: Pergamon Press Ltd, 1967.

[52] U. K. Vaidya, F. Samalot, S. Pillay, G. M. Janowski, G. Husman and K. Gleich, “Design and Manufacture of Woven Reinforced Glass/Polypropylene Composites for Mass Transit Floor Structure,” *Journal of Composite Materials,* 2004.

[53] K. N. Shivakumar, G. Swaminathan and M. Sharpe, “Carbon/Vinyl Ester Composites for Enhanced Performance in Marine Applications,” *Journal of Reinforced Plastics and Composites,* 2006.

[54] P. Shrotriya and N. R. Sottos, “Creep and relaxation behavior of woven glass/epoxy substrates for multilayer circuit board applications,” *The Joint American Society of Mechanical Engineers (ASME), American Society of Civil Engineers (ASCE), Society of Engineering Science (SES) Summer Meeting,* 15 April 2004.

[55] J. Schutz, “Properties of composite materials for cryogenic applications,” *Cryogenics,* vol. 38, no. 1, pp. 3-12, 1998.

[56] R. T. Haftka and J. L. Walsh, “Stacking-sequence optimization for buckling of laminated plates by integer programming,” *AIAA,* vol. 30, no. 3, p. 814, 2012.

[57] N. Pagano and R. B. Pipes, “The Influence of Stacking Sequence on Laminate Strength,” *Journal of Composite Materials,* vol. 5, no. 1, pp. 50-57, 1971.

[58] C. Toscano and C. Vitiello, “Influence of the stacking sequence on the porosity in carbon fiber composites,” *Journal of Applied Polymer Science,* vol. 122, no. 6, pp. 3583-3589, 2011.

[59] L.-R. Tsau, Y.-H. Chang and F.-L. Tsao, “The design of optimal stacking sequence for laminated FRP plates with inplane loading,” *Computers & Structures,* vol. 55 , no. 4, pp. 565-580, 1995.

[60] B. Liu, R. T. Haftka, M. A. Akgün and A. Todoroki, “Permutation genetic algorithm for stacking sequence design of composite laminates,” *Computer Methods in Applied Mechanics and Engineering ,* vol. 186 , no. 2-4, pp. 357-372, 2000.

[61] Z. Y. Han, Z. L. Cao and H. Y. Fu, “Buckling analysis of laminated composite plates with variable fibre orientation angle,” *Materials Research Innovations,* vol. 19, no. S5, pp. 836-842, 2015.

[62] F. Matthews and T. Tester, “The influence of stacking sequence on the strength of bonded CFRP single lap joints,” *International Journal of Adhesion and Adhesives ,* vol. 5, no. 1, pp. 13-18, 1985.

[63] P. Jackson and D. Cratchley, “The effect of fibre orientation on the tensile strength of fibre-reinforced metals,” *Journal of the Mechanics and Physics of Solids ,* vol. 14, no. 1, pp. 49-64, 1966.

[64] A. Bernasconi, P. Davoli, A. Basile and A. Filippi, “Effect of fibre orientation on the fatigue behaviour of a short glass fibre reinforced polyamide-6,” *International Journal of Fatigue,* vol. 29 , no. 2, pp. 199-208, 2007.

[65] G. Giare and R. Newcomb, “Effects of slight orientation of fibre on fracture toughness of unidirectional fibre reinforced composites in mode II,” *Engineering Fracture Mechanics,* vol. 23, no. 4, pp. 667-679, 1986.

[66] A. Muc, “Optimal fibre orientation for simply-supported, angle-ply plates under biaxial compression,” *Composite Structures ,* vol. 9 , no. 2, pp. 161-172, 1988.

[67] H. Bhatt, K. Y. Donaldson, D. P. H. Hasselman, K. Chyung and M. P. Taylor, “Effect of fibre orientation on the thermal conductivity of a uniaxial carbon fibre-reinforced aluminoborosilicate glass-matrix composite for various specimen geometries,” *Journal of Materials Science Letters,* vol. 10, no. 21, pp. 1267-1270, 1991.

[68] H. M. Cheng, A. Kitahara, K. Kobayashi and B. L. Zhou, “Hybridization with SiC particulates to control the fibre volume fraction and improve the longitudinal tensile strength of carbon fibre-reinforced aluminium composites,” *Journal of Materials Science Letters ,* vol. 10, no. 13, pp. 795-797, 1991.

[69] M. Allah, E. M. Abdin, A. Selmy and U. Khashaba, “Effect of fibre volume fraction on the fatigue behaviour of GRP pultruded rod composites,” *Composites Science and Technology,* vol. 56, no. 1, pp. 23-29, 1996.

[70] P. Davies, P. Casari and L. Carlsson, “Influence of fibre volume fraction on mode II interlaminar fracture toughness of glass/epoxy using the 4ENF specimen,” *Composites Science and Technology,* vol. 65, no. 2, pp. 295-300, 2005.

[71] T. Peijs, S. Garkhail, R. Heijenrath, M. van Den Oever and H. Bos, “Thermoplastic composites based on flax fibres and polypropylene: Influence of fibre length and fibre volume fraction on mechanical properties,” *Macromolecular Symposia,* vol. 127, no. 1, pp. 193-203, 1998.

[72] A. S. Swapnil, B. SatheSandip, P. ChaudhariBapu and S. J. Vishal, “Experimental Investigation of Mechanical Properties of Glass Fibre/Epoxy Composites with variable volume fraction,” *Materials Today: Proceedings* , vol. 4, no. 9, pp. 9487-9490, 2017.

[73] J. Thomason and M. Vlug, “Influence of fibre length and concentration on the properties of glass fibre-reinforced polypropylene: 1. Tensile and flexural modulus,” *Composites Part A: Applied Science and Manufacturing,* vol. 27, no. 6, pp. 477-484, 1996.

[74] A. Weinberg and P. Schwartz, “Effect of fibre volume fraction on the strength of Kevlar-29/epoxy strands,” *Journal of Materials Science Letters,* vol. 6, no. 2, pp. 183-184, 1987.

[75] J. D. Eshelby, “ The Determination of the Elastic Field of an Ellipsoidal Inclusion, and Related Problems,” *Proceedings Mathematical Physical & Engineering Sciences,* vol. 241, no. 1226, pp. 376-396, 1957.

[76] Z. Hashin, “On elastic behaviour of fibre reinforced materials of arbitrary transverse phase geometry,” *Journal of the Mechanics and Physics of Solids,* vol. 13 , no. 3, pp. 119-134, 1965.

[77] R. Hill, “Theory of mechanical properties of fibre-strengthened materials: I. Elastic behaviour,” *Journal of the Mechanics and Physics of Solids* , vol. 12, no. 4, pp. 199-212, 1964.

[78] Z. Hashin, “Viscoelastic fiber reinforced materials,” *AIAA Journal* , vol. 4, no. 8, pp. 1411-1417, 1966.

[79] R. Christensen and K. Lo, “ Solutions for effective shear properties in three phase sphere and cylinder models,” *Journal of the Mechanics and Physics of Solids* , vol. 27, no. 4, pp. 315-330, 1979.

[80] J. Halpin, “Effects of Environmental Factors on Composite Materials,” Air Force Materials Laboratory, Ohio, 1969.

[81] J. C. Halpin and J. L. Kardos, “The Halpin-Tsai equations: A review,” *Polymer Engineering & Science*, vol. 16, no. 5, pp. 344-352, 1976.

[82] T. Chou and T. Ishikawa, “One-dimensional micromechanical analysis of woven fabric composites,” *AIAA Journal,* vol. 21, no. 12, pp. 1714-1721, 1983.

[83] T. Ishikawa and T. -W. Chou, “Stiffness and strength behaviour of woven fabric composites,” *Journal of Materials Science ,* vol. 17, no. 11, pp. 3211-3220, 1982.

[84] N. Naik and P. Shembekar, “Elastic Behavior of Woven Fabric Composites: I--Lamina Analysis,” *Journal of Composite Materials,* vol. 26, no. 15, pp. 2196-2225, 1992.

[85] C. Casavola, A. Cazzato, V. Moramarco and C. Pappalettere, “Orthotropic mechanical properties of fused deposition modelling parts described by classical laminate theory,” *Materials & Design* , vol. 90, pp. 453-458, 2016.

[86] C. Casavola, A. Cazzato, V. Moramarco and C. Pappalettere, “ Orthotropic mechanical properties of fused deposition modelling parts described by classical laminate theory,” *Materials & Design* , vol. 90 , pp. 453-458, 2016.

[87] C. Kasapoglou, Design and Analysis of Composite Structures: With Applications to Aerospace Structures, John Wiley and Sons, 2010.

[88] J. M. Whitney, “Midplane Symmetric Laminates,” in *Structural Analysis of Laminated Anisotropic Plates*, Pennsylvania, Technomic Publishing Company, 1987.

[89] J. L. Grenestedt, “A study on the effect of bending-twisting coupling on buckling strength,” *Composite Structures* , vol. 12, no. 4, pp. 271-290, 1989.

[90] D. Kumar and S. Singh, “Effects of boundary conditions on buckling and postbuckling responses of composite laminate with various shaped cutouts,” *Composite Structures* , vol. 92, no. 3, pp. 769-779, 2010.

[91] X. Cheng, L. Gong and X. Fu, “Thermal Bend of Concrete Rectangular Thin Plate: Two Adjacent Clamped Edges, One Simply Supported Edge, One Free Edge,” *Arabian Journal for Science and Engineering* , 2018.

[92] MathWorks, “Matlab Overview,” 2019. [Online]. Available: https://www.mathworks.com/products/matlab.html. [Accessed November 2019].

[93] F. Cribari-Neto and M. J. Jensen, “MATLAB as an econometric programming environment,” *Journal of Applied Econometrics,* vol. 12, no. 6, pp. 735-744, 1997.

[94] Y. Huang, Z. Yang, A. Liu and J. Fu, “Nonlinear Buckling Analysis of Functionally Graded Graphene Reinforced Composite Shallow Arches with Elastic Rotational Constraints under Uniform Radial Load,” *Materials* , vol. 11, no. 6, p. 910, 2018.

[95] W. M, R. T and A. S, “A Procedure to Select the Best Material CObinations and Optimally Design Hybrid COmposite Plates for Minimum Weight and Cost,” *Engineering Optimization* , vol. 29, no. 1, pp. 65-83, 1997.

[96] S. Banerjee and B. V. Sankar, “Mechanical properties of hybrid composites using finite element method based micromechanics,” *Composites Part B: Engineering,* vol. 58, pp. 318-327, 2014.

[97] S. Choi, “Micromechanical Analysis of Composite Laminates at Cryogenic Temperatures,” *Journal of Composite Materials* , vol. 40 , no. 12, pp. 1077-1091, 2005.

[98] J. W. S. Hearle, “Glass Fibres,” in *High-Performance Fibres,* Florida, Woodhead Publishing, 2000, p. 194.

[99] S. Choi and B. V. Sankar, “Micromechanical Analysis of CompositeLaminates at Cryogenic Temperatures,” *Journal of Composite Materials,* vol. 00/2005, 2005.

[100] M. Song, J. Yang, S. Kitipornchai and W. Zhu, “Buckling and postbuckling of biaxially compressed functionally graded multilayer graphene nanoplatelet-reinforced polymer composite plates,” *International Journal of Mechanical Sciences,* vol. 131132, pp. 345-355, 2017.

Appendix A: Matlab script and report

```
%% Matlab Script (Buckling)

clear;
clc;

%%---- Define path for subroutines
path(path,'./Four Layer Micromechanics')
path(path,'./Four Layer Buckling')

%%---- The laminate consists of 4 layers numbered 1-4 from the bottom, up.
%% Given data for outer layers (1,4)

% WARP MATERIAL PROPERTIES
%fprintf(2,'\nLAYER 1 WARP MATERIAL PROPERTIES\n')
T_wpo=1000*10^-6; %tex
%fprintf(2,'\nNumber of Rovings\n')
%eta_wpo= 600;
%fprintf(2,'\nDensity\n')
rho_wpo= 2600; %kg/m^3
%fprintf(2,'\nYoung's Modulus\n')
E_wpo= 73*10^9; %GPa
%fprintf(2,'\nPoisson's Ratio\n')
ni_wpo= 0.22;
%fprintf(2,'\nShear Modulus\n')
G_wpo=(E_wpo/(2*(1+ni_wpo)));
%fprintf(2,'\nVolume Fraction\n')
%Vf_wpo=0.275; %Volume Fraction of Warp Material

% WEFT MATERIAL PROPERTIES
%fprintf(2,'\nLAYER 1 WEFT MATERIAL PROPERTIES\n')
T_wfo= 2400*10^-6; %tex
%fprintf(2,'\nNumber of Rovings\n')
eta_wfo= 200;
%fprintf(2,'\nDensity\n')
rho_wfo= 2600;
%fprintf(2,'\nYoung's Modulus\n')
E_wfo= 73*10^9; %GPa
%fprintf(2,'\nPoisson's Ratio\n')
ni_wfo= 0.22;
%fprintf(2,'\nShear Modulus\n')
G_wfo=(E_wfo/(2*(1+ni_wfo)));
%fprintf(2,'\nVolume Fraction\n')
%Vf_wfo=0.275; %Volume Fraction of Weft Material

%% Given data for middle layers (2&3)

% WARP MATERIAL PROPERTIES
%fprintf(2,'\nLAYER 2 WARP MATERIAL PROPERTIES\n')
T_wpm=1000*10^-6; %tex
%fprintf(2,'\nNumber of Rovings\n')
eta_wpm= 600;
%fprintf(2,'\nDensity\n')
rho_wpm= 2600; %kg/m^3
```

```
%fprintf(2,'\nYoung's Modulus\n')
E_wpm= 73*10^9; %GPa
%fprintf(2,'\nPoisson's Ratio\n')
ni_wpm= 0.22;
%fprintf(2,'\nShear Modulus\n')
G_wpm=(E_wpm/(2*(1+ni_wpm)));
%fprintf(2,'\nVolume Fraction\n')
Vf_wpm=0.275; %Volume Fraction of Warp Material

% WEFT MATERIAL PROPERTIES
%fprintf(2,'\nLAYER 2 WEFT MATERIAL PROPERTIES\n')
T_wfm= 2400*10^-6; %tex
%fprintf(2,'\nNumber of Rovings\n')
eta_wfm= 200;
%fprintf(2,'\nDensity\n')
rho_wfm= 2600;
%fprintf(2,'\nYoung's Modulus\n')
E_wfm= 73*10^9; %GPa
%fprintf(2,'\nPoisson's Ratio\n')
ni_wfm= 0.22;
%fprintf(2,'\nShear Modulus\n')
G_wfm=(E_wfm/(2*(1+ni_wfm)));
%fprintf(2,'\nVolume Fraction\n')
Vf_wfm=0.275; %Volume Fraction of Weft Material


%% Given data for matrix
% MATRIX MATERIAL PROPERTIES
%fprintf(2,'\nMATRIX MATERIAL PROPERTIES\n')
%fprintf(2,'\nDensity\n')
rho_m=1200; %kg/m^3
%fprintf(2,'\nYoung's Modulus\n')
E_m= 3*10^9; %GPa
%fprintf(2,'\nPoisson's Ratio\n')
ni_m= 0.35;
%fprintf(2,'\nShear Modulus\n')
G_m=(E_m/(2*(1+ni_m)));

%% Graphene nanoplatelets

% Graphene's Young's Modulus
E_gpl=1010e9 %(N)

% Graphene's Poisson's ratio
ni_gpl=0.186

% Weight fraction
w_gplo=0.02 % Outer layer%%%%%%%%%%%%%%%%%%%%1
w_gplm=0.01 % Middle layer

% Mass density
rho_gpl=1060 % kg/m3

% Graphene nanoplatelets length, widht, thickness
length_gpl=2.5e-6 % m
```

```
width_gpl =1.5e-6
thick_gpl =1.5e-9

%% Laminate Properties
%fprintf(2,'\nLaminate Total Thickness\n')
H= 5*10^-3; %m

%fprintf(2,'\nLaminate Thickness Ratio\n')
thick_ratio=0.7;

%fprintf(2,'\nBalancing Coefficients\n')
%ko=0.5;
%km=0.5;

%fprintf(2,'\nm and n for Buckling and Vibration Frequency\n')
m=1;  % for fundamental frequency, m,n=1
n=1;

%fprintf(2,'\nLoad Ratio for Buckling\n')
alpha_b=1;

%fprintf(2,'\nPlate Dimensions\n')
a=1;
b=1;
R=a/b;

%fprintf(2,'\nOuter and Inner Load Angle\n')
theta_o=0;
theta_m=0;
%%%%%%%%%%%%%%%%%%%%%%%%%%%%%%%%%%%%%%%%%%%%%%%%%%%%%%%%%%%%%%%%%%%%%%%%%%%%%%%%
%

%% Output
% Output data
Output=[];
dim=[]; % Dimensions of the external and the internal loop
      % (matrix Nx2, where N is the number of the external loops, first column indicates
      % the external loop iterations and second column the numbering of internal loops)

% % Alternative way for output: pre-allocation of size
% % Number of points per diagram (it depends on the internal loop)
% diag_p=11;
% % Number of diagrams (it depends on the external loop)
% diag_n=5;
% Output=zeros(diag_p*diag_n,2); % diag_p points per diagram, for diag_n variations.

% LOOP
count_1=0;
count_2=0;

for i_ext=0.1:0.1:0.5

Vf_wfo=i_ext;
count_1=count_1+1;
```

```
for i_int=0:0.01:0.5

Vf_wpo=i_int;
count_2=count_2+1;

%% Micromechanics

% fprintf(2,'\nGraphene volume content\n');
v_gplo=graphenecontent(w_gplo,rho_gpl,rho_m) % Outer layer
v_gplm=graphenecontent(w_gplm,rho_gpl,rho_m) % Middle layer

% ksi
[ksi_l,ksi_w]=ksi(length_gpl,width_gpl,thick_gpl)

% eta
[eta_l,eta_w]=eta(E_gpl,E_m,ksi_l,ksi_w)

% fprintf(2,'\nGraphene reinforced matrix: Elasticity modulus\n');
E_gmo=Graphene_rein_matrix(ksi_l,ksi_w,eta_l,eta_w,v_gplo,E_m) % Outer layer
E_gmm=Graphene_rein_matrix(ksi_l,ksi_w,eta_l,eta_w,v_gplm,E_m) % Middle layer

% fprintf(2,'\nGraphene reinforced matrix: Poisson ratio\n');
ni_gmo=Graphene_rein_matrix2(ni_gpl,ni_m,v_gplo) % Outer layer
ni_gmm=Graphene_rein_matrix2(ni_gpl,ni_m,v_gplm) % Middle layer

% fprintf(2,'\nGraphene reinforced matrix: Shear modulus\n');
G_gmo=Graphene_rein_matrix3(E_gmo,ni_gmo) % Outer layer
G_gmm=Graphene_rein_matrix3(E_gmm,ni_gmm) % Middle layer


%fprintf(2,'\nBalancing Co-efficient\n')
[ko, km] = balancing_coefficient(Vf_wpo,Vf_wfo,Vf_wpm,Vf_wfm)

%fprintf(2,'\nLayer Thicknesses\n')
[eo, em] = layerthicknesses(thick_ratio,H)

%fprintf(2,'\nWarp Longitudinal Modulus\n')
[EL_wpo,EL_wpm]=warpmodulus__EL_wp(E_wpo,Vf_wpo,E_gmo,E_gmm,E_wpm,Vf_wpm)

%fprintf(2,'\nWeft Longitudinal Modulus\n')
[EL_wfo,EL_wfm]=weftmodulus__EL_wf(E_wfo,Vf_wfo,E_gmo,E_gmm,E_wfm,Vf_wfm)

%fprintf(2,'\nWarp & Weft Poisson's Ratio\n')
[niLT_wpo, niLT_wfo,niLT_wpm,
niLT_wfm]=nifibers__niLT(ni_wpo,Vf_wpo,ni_gmm,ni_gmo,ni_wfo, Vf_wfo,ni_wpm,Vf_wpm,
ni_wfm, Vf_wfm)

%fprintf(2,'\nWarp & Weft Shear Modulus\n')
[GLT_wpo,GLT_wfo,GLT_wpm,GLT_wfm]=fibers__GLT(G_wpo, G_wfo, G_gmm, G_gmo,
Vf_wpo, Vf_wfo, G_wpm, G_wfm, Vf_wpm, Vf_wfm)

%fprintf(2,'\nStiffnesses\n')
[smallk_gmm, smallk_gmo, smallk_wpo, smallk_wfo, smallk_wpm, smallk_wfm] =
stiffness(E_gmm,E_gmo, E_wpo, E_wfo, ni_gmm, ni_gmo, ni_wpo, ni_wfo, E_wpm, E_wfm,
ni_wpm, ni_wfm)
```

```
%fprintf(2,'\nLateral Compression Moduli\n')
[K_gmm, K_gmo, K_wpo, K_wfo, K_wpm, K_wfm] = lateralcompression(E_gmm,E_gmo, E_wpo,
E_wfo, ni_gmm, ni_gmo, ni_wpo, ni_wfo, E_wpm, E_wfm, ni_wpm, ni_wfm)

%fprintf(2,'\nK_L for Warp and Weft\n')
[KL_wpo, KL_wfo, KL_wpm, KL_wfm] = fibers__KL(K_gmm,K_gmo, smallk_gmm, smallk_gmo,
smallk_wpo, smallk_wfo, G_gmm, G_gmo, Vf_wpo, G_wpo, Vf_wfo, G_wfo, smallk_wpm,
smallk_wfm, Vf_wpm, G_wpm, Vf_wfm, G_wfm)

%fprintf(2,'\nWarp & Weft Transverse Shear Modulus\n')
[GTT_wpo, GTT_wfo, GTT_wpm, GTT_wfm] = transverseshear__GTT(smallk_gmm, smallk_gmo,
G_gmm, G_gmo, Vf_wpo, G_wpo, Vf_wfo, G_wfo, Vf_wpm, G_wpm, Vf_wfm, G_wfm)

%fprintf(2,'\nWarp & Weft Transverse Young's Moduli\n')
[ET_wpo, ET_wfo, ET_wpm, ET_wfm] = transversemoduli(KL_wpo, KL_wfo, GTT_wpo,
GTT_wfo, niLT_wpo, niLT_wfo, EL_wpo, EL_wfo, KL_wpm, KL_wfm, GTT_wpm, GTT_wfm,
niLT_wpm, niLT_wfm, EL_wpm, EL_wfm)

%fprintf(2,'\nWarp & Weft Alpha for Micromechanics\n')
[alpha_wpo, alpha_wfo, alpha_wpm, alpha_wfm] = alphafibers(ET_wpo, ET_wfo, EL_wpo, EL_wfo,
niLT_wpo, niLT_wfo, ET_wpm, ET_wfm, EL_wpm, EL_wfm, niLT_wpm, niLT_wfm)

%fprintf(2,'\nAlpha for Micromechanics Equations\n')
[alpha_ko, alpha_km] = alphak(ko, alpha_wpo, niLT_wpo, ET_wpo, alpha_wfo, niLT_wfo, ET_wfo,
EL_wpo, EL_wfo, km, alpha_wpm, niLT_wpm, ET_wpm, alpha_wfm, niLT_wfm, ET_wfm,
EL_wpm, EL_wfm)

%fprintf(2, '\nOVERALL ENGINEERING CONSTANTS FOR LAMINATE\n')

%fprintf(2,'\nLongitudinal Young's Modulus\n')
[ELo, ELm] = overallEL(ko, alpha_wpo, alpha_wfo, alpha_ko, ET_wfo, EL_wpo, km, alpha_wpm,
alpha_wfm, alpha_km, ET_wfm, EL_wpm)

%fprintf(2,'\nTransverse Young's Modulus\n')
[ETo, ETm] = overallET(ko, alpha_wpo, alpha_wfo, alpha_ko, ET_wpo, EL_wfo, km, alpha_wpm,
alpha_wfm, alpha_km, ET_wpm, EL_wfm)

%fprintf(2,'\nPoisson's Ratio\n')
[niLTo, niLTm] = overallNI(ko, alpha_wpo, alpha_wfo, ET_wpo, ET_wfo, EL_wfo, niLT_wpo,
niLT_wfo, km, alpha_wpm, alpha_wfm, ET_wpm, ET_wfm, EL_wfm, niLT_wpm, niLT_wfm)

%fprintf(2,'\nShear Modulus\n')
[GLTo, GLTm] = overallGLT(ko, GLT_wpo, GLT_wfo, km, GLT_wpm, GLT_wfm)

%fprintf(2,'\nModuli with varied load angle\n')
[E_thetaL,E_thetaT] = Angle_varied_modulus(ELo,theta_o,GLTo,ETo,niLTo)
%% Output (Buckling and Vibration)
%fprintf(2, '\nCritical Buckling Load\n')
[Ncr,N0] = Four_layer_buckling(ELo, ELm, ETo, ETm, niLTo, niLTm, GLTo, GLTm,
theta_o,theta_m,eo,em,H,alpha_b,R,a,b,m,n)

Output(count_2,:)=[i_int N0]; % Diagram of i_int = x axis (defined at the beginning of internal loop)
vs Buckling load
                % Variations of the diagram according to external loop are recorded.
```

```
end

dim=[dim; [count_1 count_2]];

end

Colours_diag = {'red','green','black','magenta','blue','yellow','cyan',[.5 .6 .7],[.8 .2 .6]}; % Colours for
the diagrams below
figure('Units', 'pixels', 'Position', [100 100 640 480]);
hold on;
% line={'-','--','-o',':','-.'};
for i=1:size(dim(:,1)) % Number of diagrams=number of external loops

x1 = Output(dim(i,2)-dim(1,2)+1:dim(i,2),1);
y1 = Output(dim(i,2)-dim(1,2)+1:dim(i,2),2);

plot(x1,y1,'color',Colours_diag{i})

end

%% Choose Diagram

% Buckling Diagram
% if Output(count_2,:)==[i_int Ncr]
 legend('Vf_{wf_o}=0.1','Vf_{wf_o}=0.2','Vf_{wf_o}=0.3','Vf_{wf_o}=0.4','Vf_{wf_o}=0.5')
 xlabel('Vf_{wp_o}','FontSize',12)
 ylabel('N_{0}','FontSize',12)
```

Appendix B: Influence of woven glass fibre balancing coefficient and laminate thickness ratio

$H = 0.005; \frac{a}{b} = 1; \theta_o = 0°; \theta_m = 0°; Vf_{total_o} = 0.5; k_m = 0.36; Vf_{total_m} = 0.55; \alpha_b = 1$

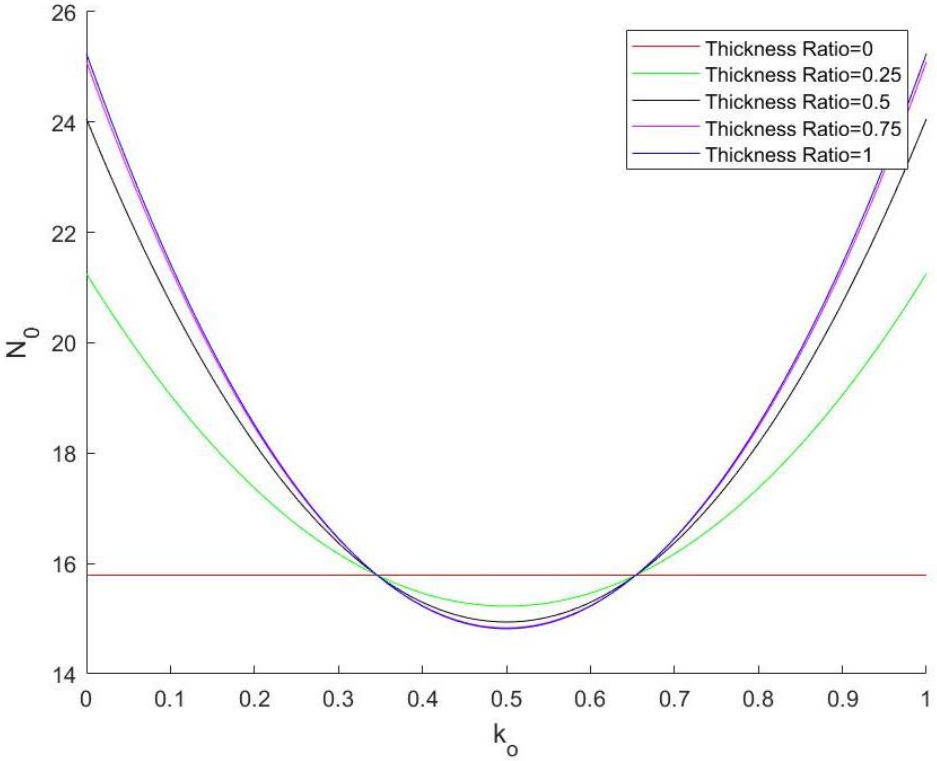

Figure B.1 (a) $W_{gpl_o} = W_{gpl_m} = 0$

$H = 0.005; \frac{a}{b} = 1; \theta_o = 0°; \theta_m = 0°; Vf_{total_o} = 0.5; k_m = 0.36; Vf_{total_m} = 0.55; \alpha_b = 1$

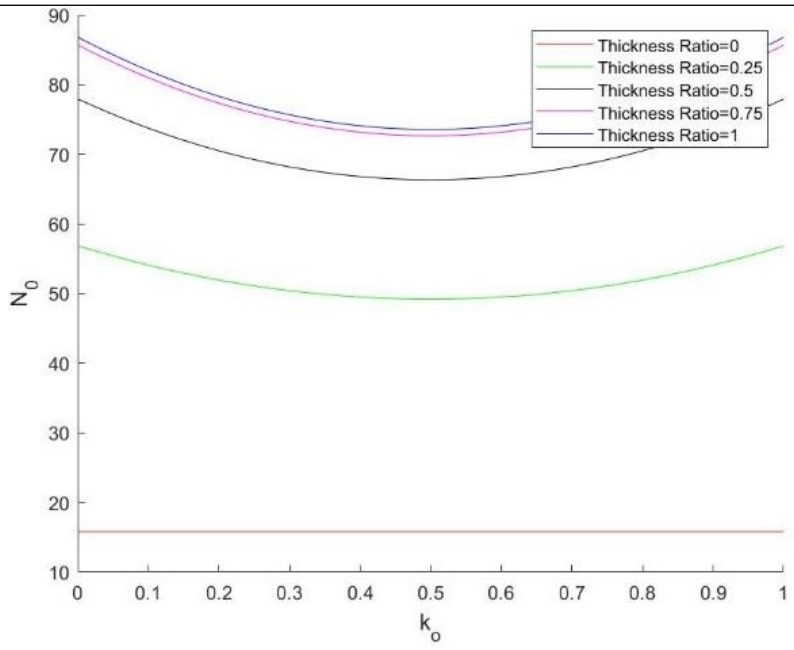

Figure B.1 (b) $W_{gpl_o} = 0.03; W_{gpl_m} = 0$

$H = 0.005; \frac{a}{b} = 1; \theta_o = 0°; \theta_m = 0°; Vf_{total_o} = 0.5; k_m = 0.36; Vf_{total_m} = 0.55; \alpha_b = 1$

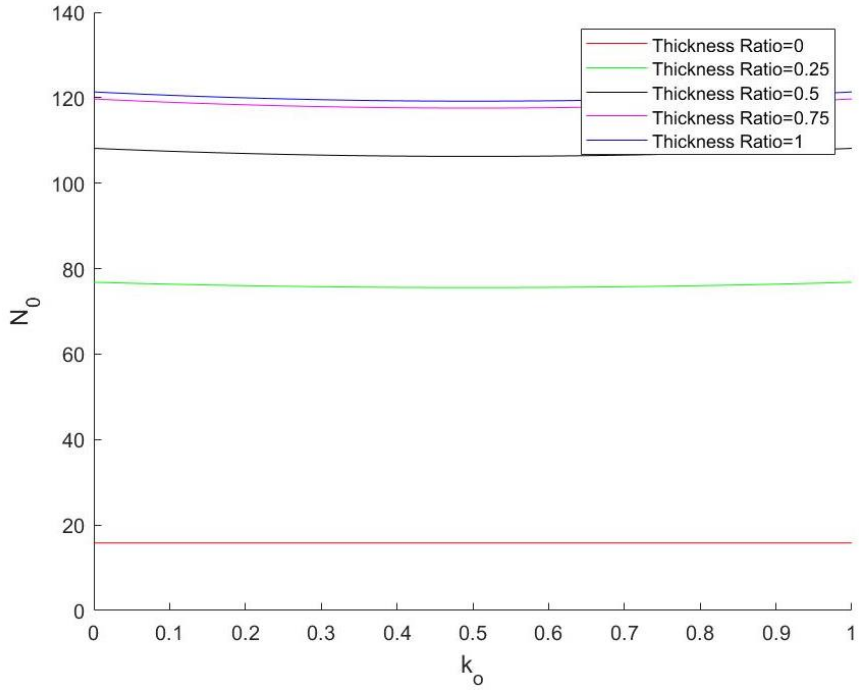

Figure B.1 (c) $W_{gpl_o} = 0.06; W_{gpl_m} = 0$

$H = 0.005; \frac{a}{b} = 1; \theta_o = 0°; \theta_m = 0°; Vf_{total_o} = 0.5; k_m = 0.36; Vf_{total_m} = 0.55; \alpha_b = 1$

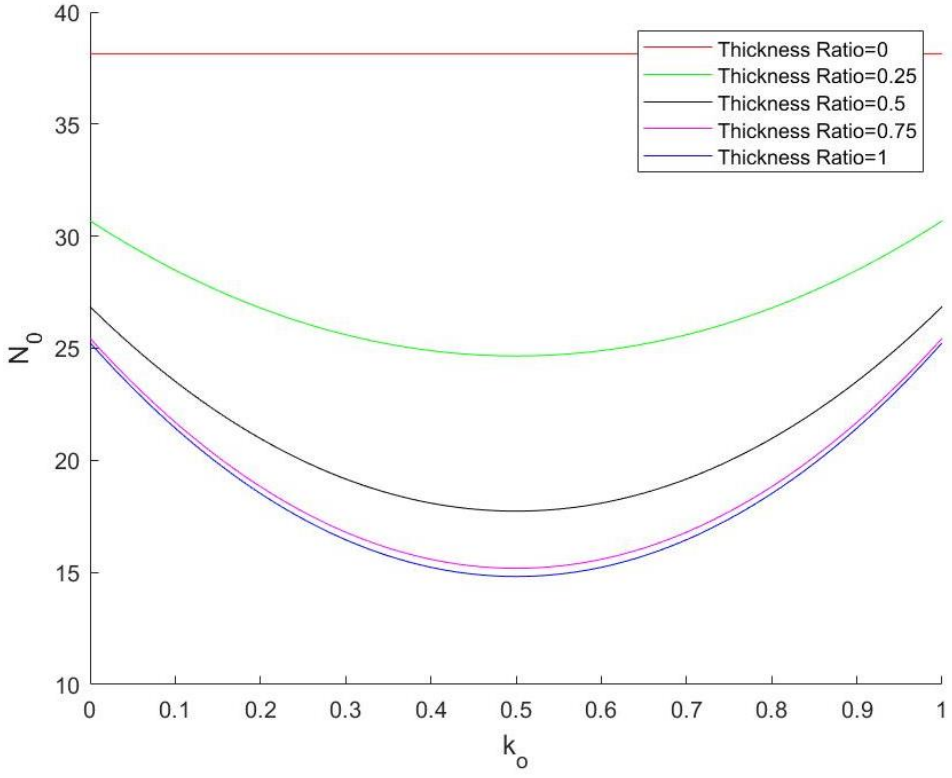

Figure B.1 (d) $W_{gpl_o} = 0; W_{gpl_m} = 0.01$

$$H = 0.005; \frac{a}{b} = 1; \theta_o = 0°; \theta_m = 0°; Vf_{total_o} = 0.5; k_m = 0.36; Vf_{total_m} = 0.55; \alpha_b = 1$$

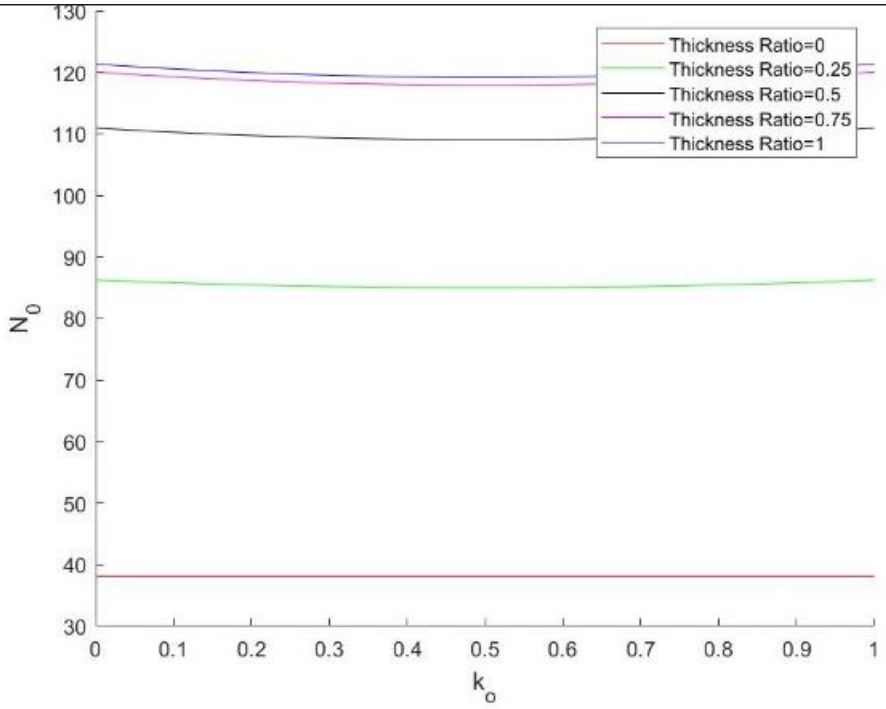

Figure B.1 (e) $W_{gpl_o} = 0.06$*;* $W_{gpl_m} = 0.01$

Figure B.1: Critical buckling load vs. k_o *for different values of* τ

$H = 0.005; \frac{a}{b} = 0.4; \theta_o = 0°; \theta_m = 0°; Vf_{total_o} = 0.5; k_m = 0.36; Vf_{total_m} = 0.55; \alpha_b = 1$

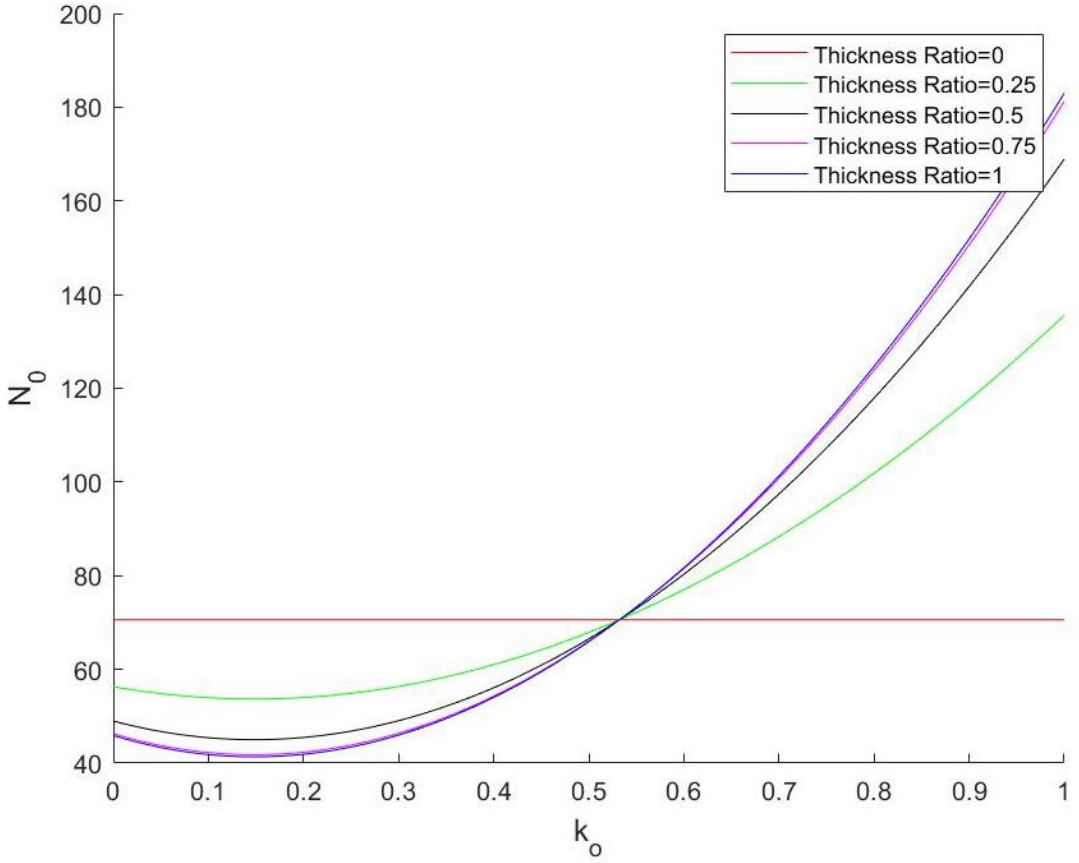

Figure B.2 (a) $W_{gpl_o} = W_{gpl_m} = 0$

$H = 0.005; \frac{a}{b} = 0.4; \theta_o = 0°; \theta_m = 0°; Vf_{total_o} = 0.5; k_m = 0.36; Vf_{total_m} = 0.55; \alpha_b = 1$

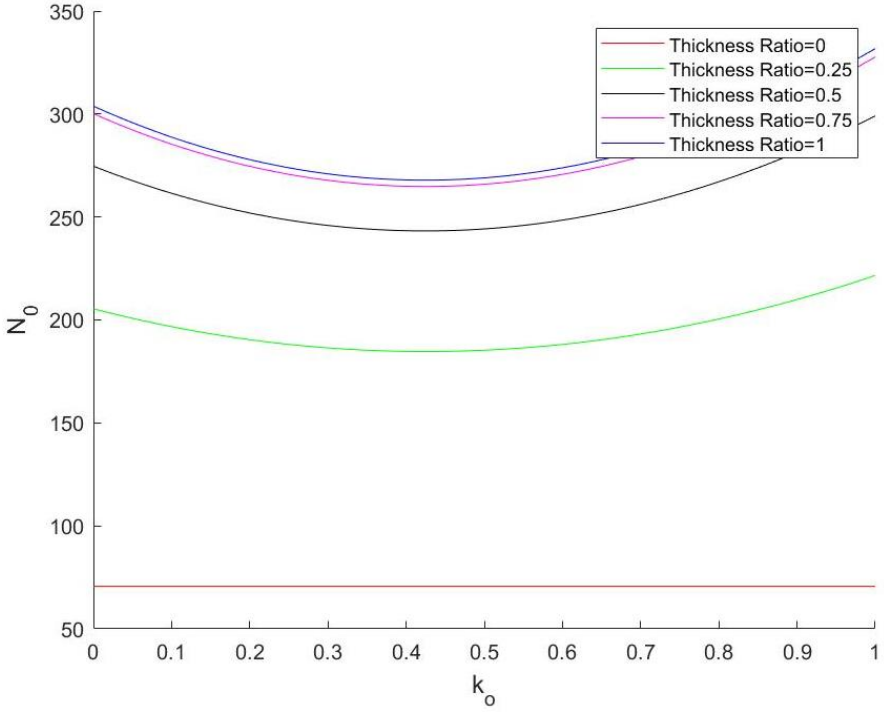

Figure B.2 (b) $W_{gpl_o} = 0.03; W_{gpl_m} = 0$

$H = 0.005; \frac{a}{b} = 0.4; \theta_o = 0°; \theta_m = 0°; Vf_{total_o} = 0.5; k_m = 0.36; Vf_{total_m} = 0.55; \alpha_b = 1$

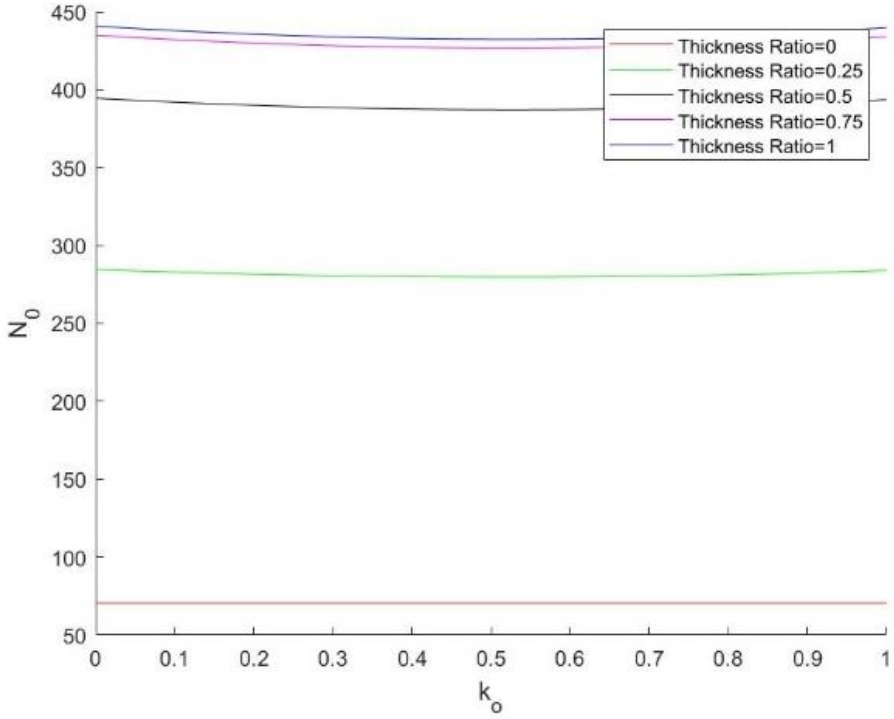

Figure B.2 (c) $W_{gpl_o} = 0.06; W_{gpl_m} = 0$

$H = 0.005; \frac{a}{b} = 0.4; \theta_o = 0°; \theta_m = 0°; Vf_{total_o} = 0.5; k_m = 0.36; Vf_{total_m} = 0.55; \alpha_b = 1$

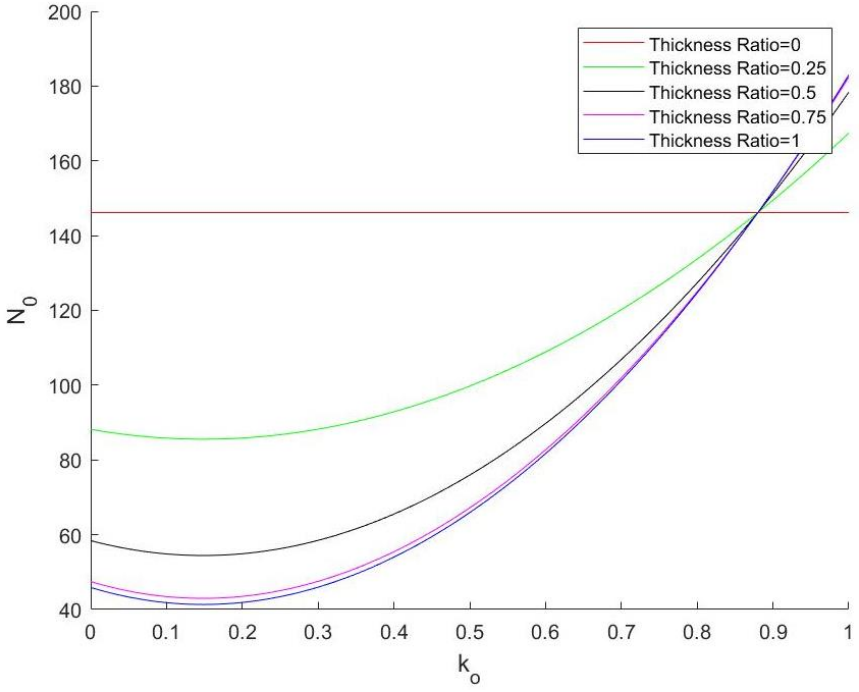

Figure B.2 (d) $W_{gpl_o} = 0; W_{gpl_m} = 0.01$

$H = 0.005; \frac{a}{b} = 0.4; \theta_o = 0°; \theta_m = 0°; Vf_{total_o} = 0.5; k_m = 0.36; Vf_{total_m} = 0.55; \alpha_b = 1$

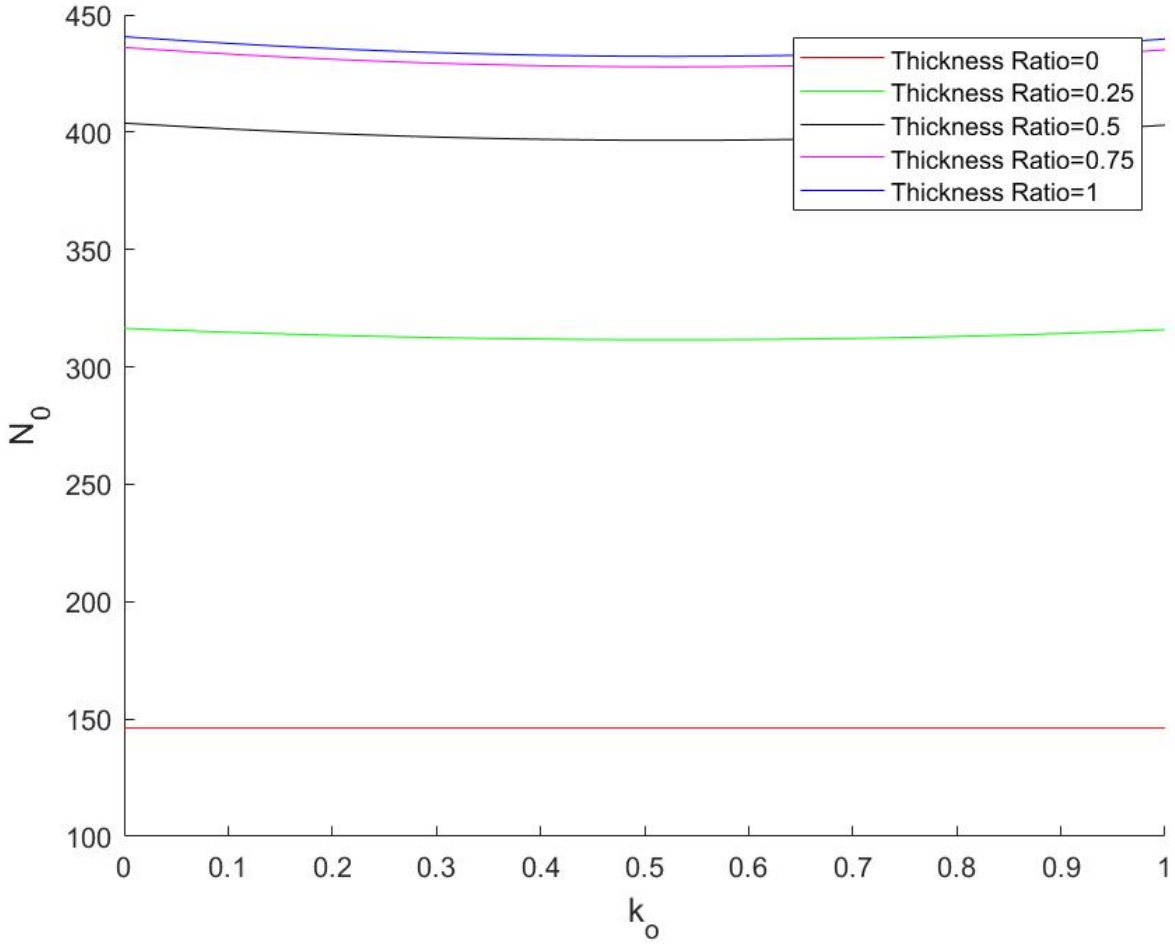

Figure B.2 (e) $W_{gpl_o} = 0.06$*;* $W_{gpl_m} = 0.01$

Figure B.2: Critical buckling load vs. k_o *for different values of* τ

$H = 0.005; \frac{a}{b} = 4; \theta_o = 0°; \theta_m = 0°; Vf_{total_o} = 0.5; k_m = 0.36; Vf_{total_m} = 0.55; \alpha_b = 1$

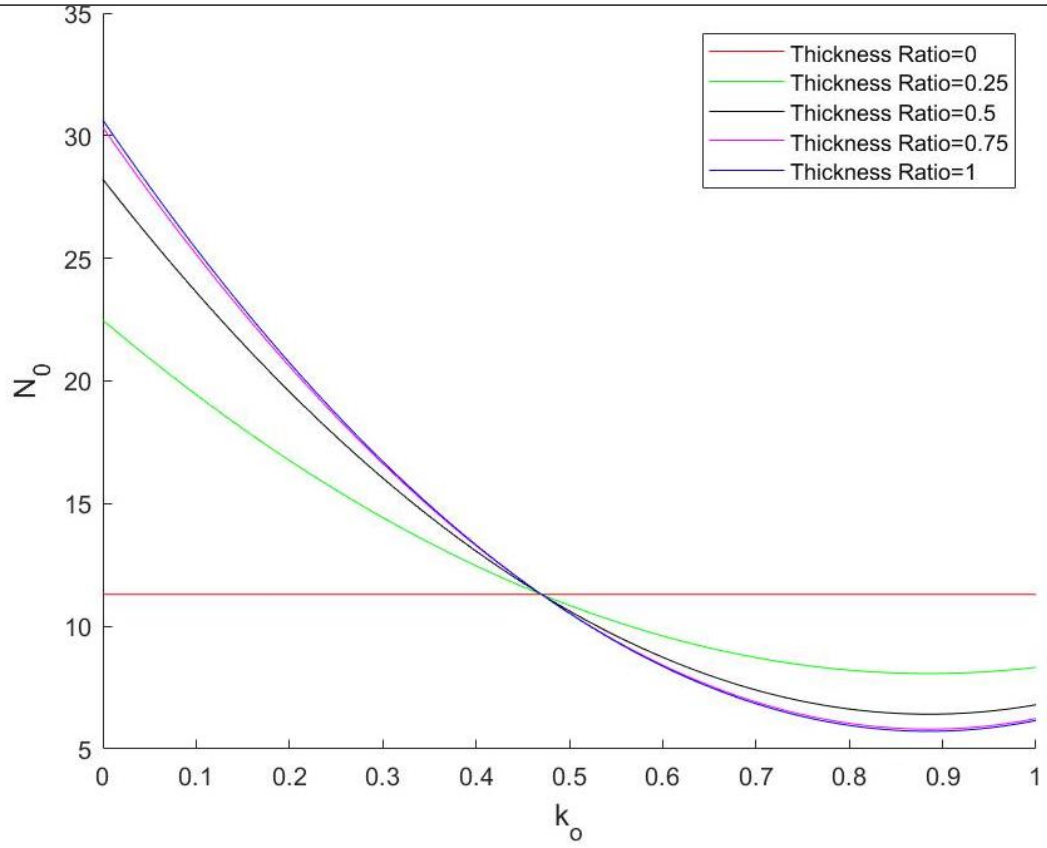

Figure B.3 (a) $W_{gpl_o} = W_{gpl_m} = 0$

$H = 0.005; \frac{a}{b} = 4; \theta_o = 0°; \theta_m = 0°; Vf_{total_o} = 0.5; k_m = 0.36; Vf_{total_m} = 0.55; \alpha_b = 1$

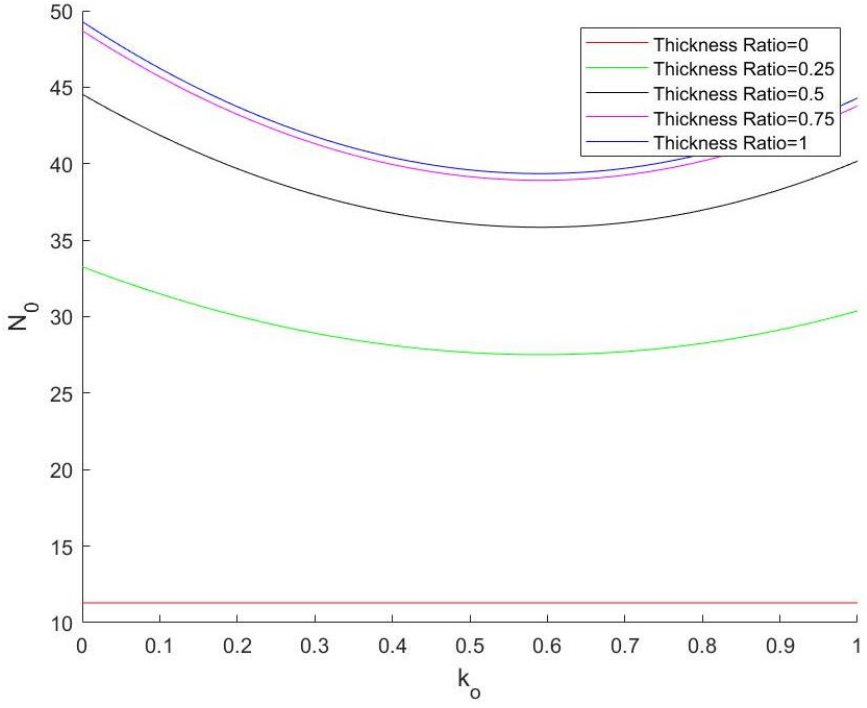

Figure B.3 (b) $W_{gpl_o} = 0.03; W_{gpl_m} = 0$

$H = 0.005; \frac{a}{b} = 4; \theta_o = 0°; \theta_m = 0°; Vf_{total_o} = 0.5; k_m = 0.36; Vf_{total_m} = 0.55; \alpha_b = 1$

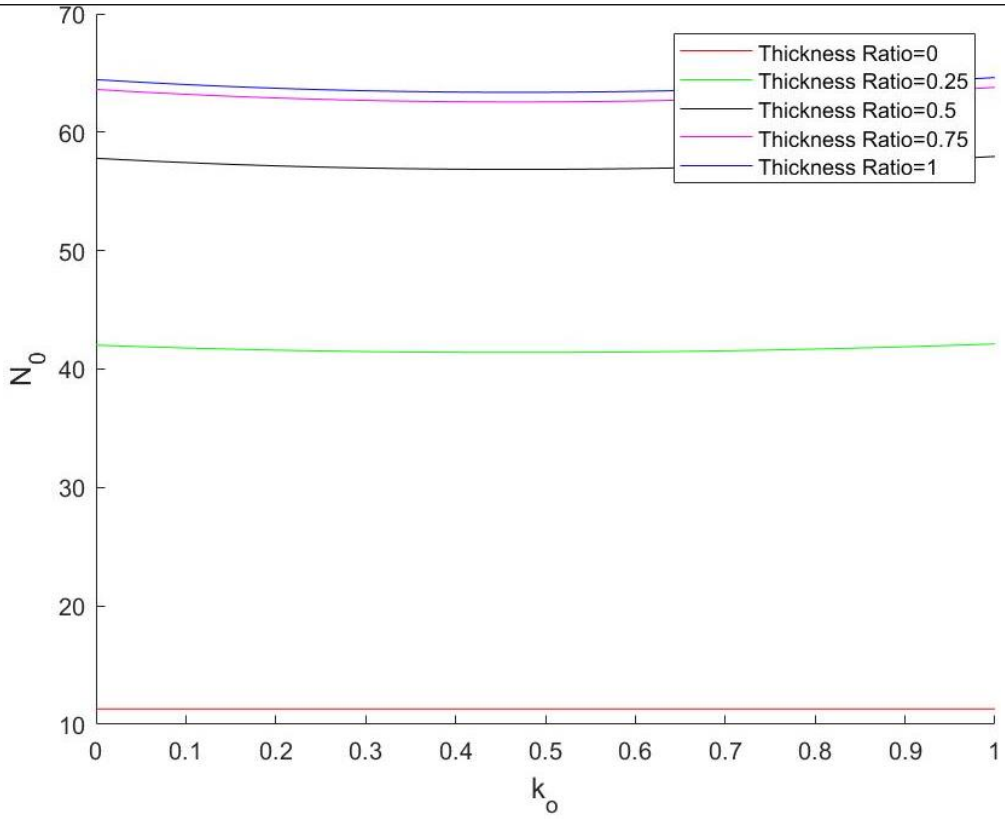

Figure B.33 (c) $W_{gpl_o} = 0.06$*;* $W_{gpl_m} = 0$

$H = 0.005; \frac{a}{b} = 4; \theta_o = 0°; \theta_m = 0°; Vf_{total_o} = 0.5; k_m = 0.36; Vf_{total_m} = 0.55; \alpha_b = 1$

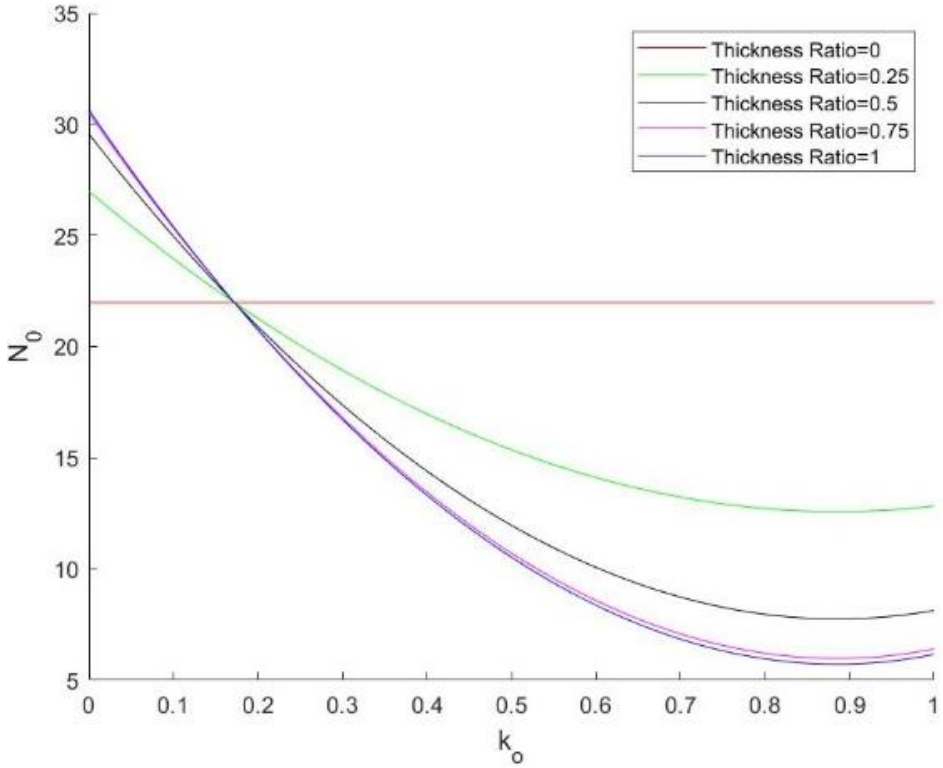

Figure B.3 (d) $W_{gpl_o} = 0$*;* $W_{gpl_m} = 0.01$

$H = 0.005; \frac{a}{b} = 4; \theta_o = 0°; \theta_m = 0°; Vf_{total_o} = 0.5; k_m = 0.36; Vf_{total_m} = 0.55; \alpha_b = 1$

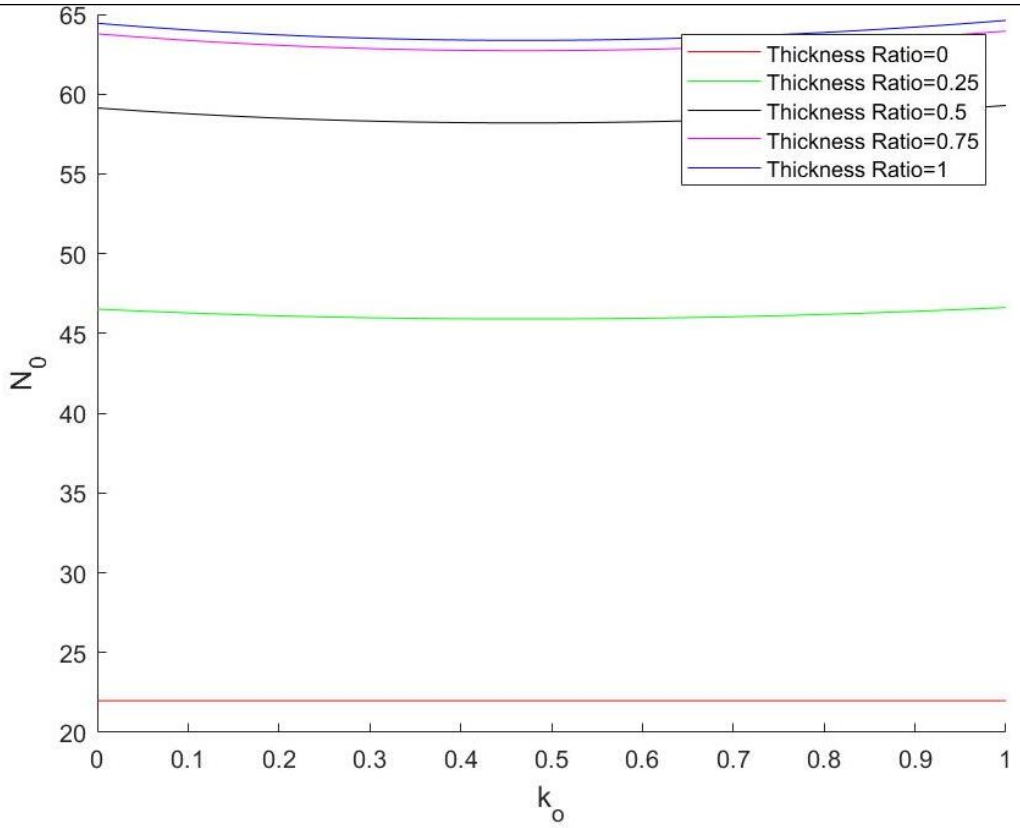

Figure B.34 (e) $W_{gpl_o} = 0.06$*;* $W_{gpl_m} = 0.01$

Figure B.3: Critical buckling load vs. k_o *for different values of* τ

Appendix C: Influence of laminate aspect ratio and woven glass fibre orientation

$\tau = 0.7$; $\theta_m = 0°$; $W_{gpl_m} = 0$; $Vf_{wp_o} = 0.5$; $Vf_{wf_o} = 0.275$; $k_m = 0.5$; $Vf_{total_m} = 0.55$; $\alpha_b = 1$

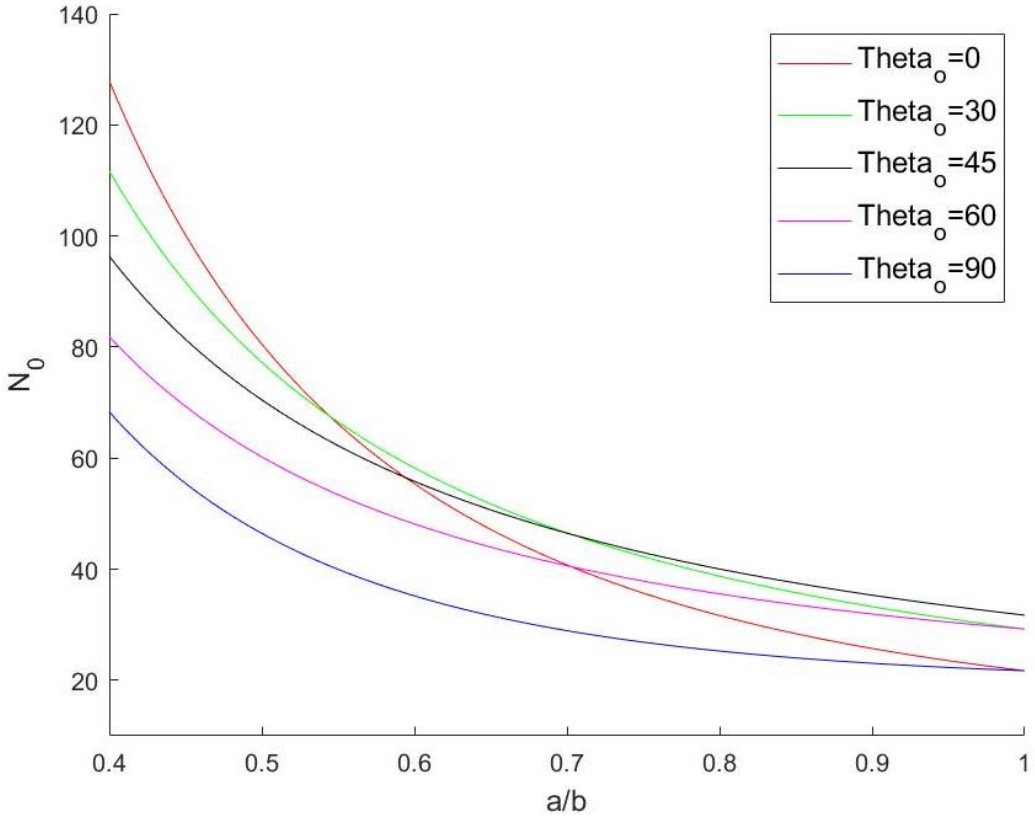

Figure C.1 (a) $W_{gpl_o} = 0$; $0.4 \leq a/b \leq 1$

$\tau = 0.7$; $\theta_m = 0°$; $W_{gpl_m} = 0$; $Vf_{wp_o} = 0.5$; $Vf_{wf_o} = 0.275$; $k_m = 0.5$; $Vf_{total_m} = 0.55$; $\alpha_b = 1$

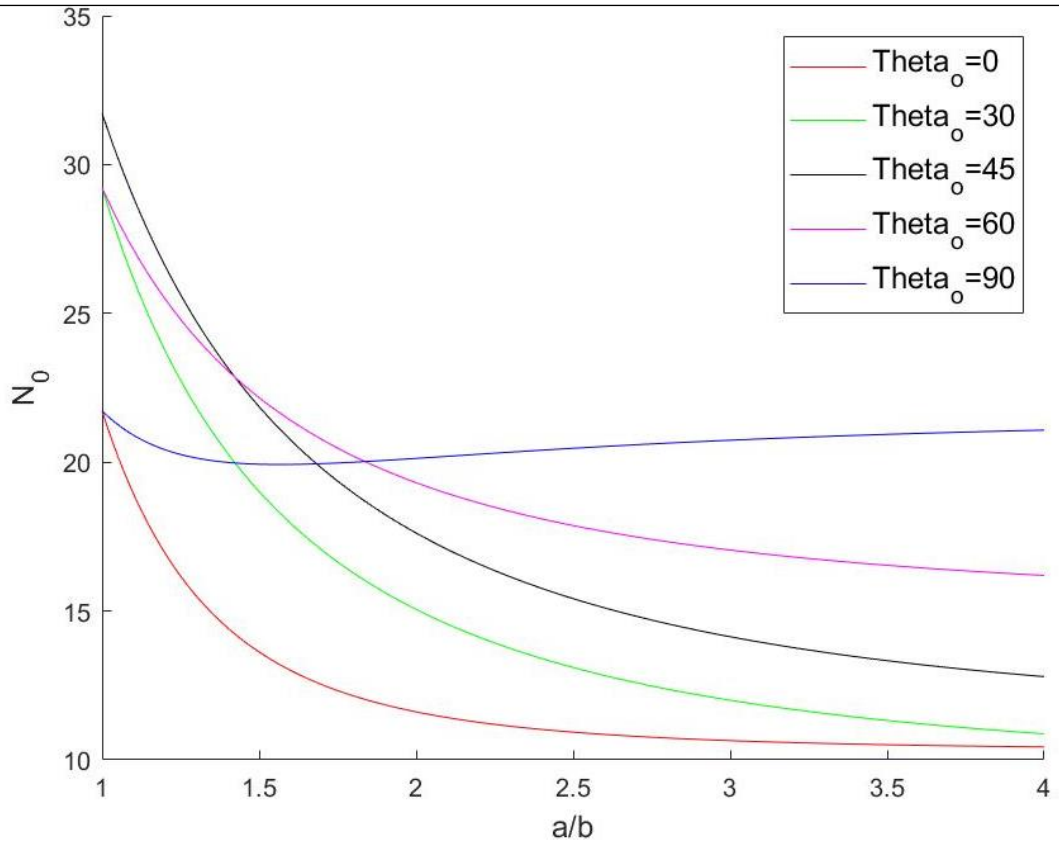

Figure C.1 (b) $W_{gpl_o} = 0; 1 \leq a/b \leq 4$

$\tau = 0.7; \theta_m = 0°; W_{gpl_m} = 0; Vf_{wp_o} = 0.5; Vf_{wf_o} = 0.275; k_m = 0.5; Vf_{total_m} = 0.55; \alpha_b = 1$

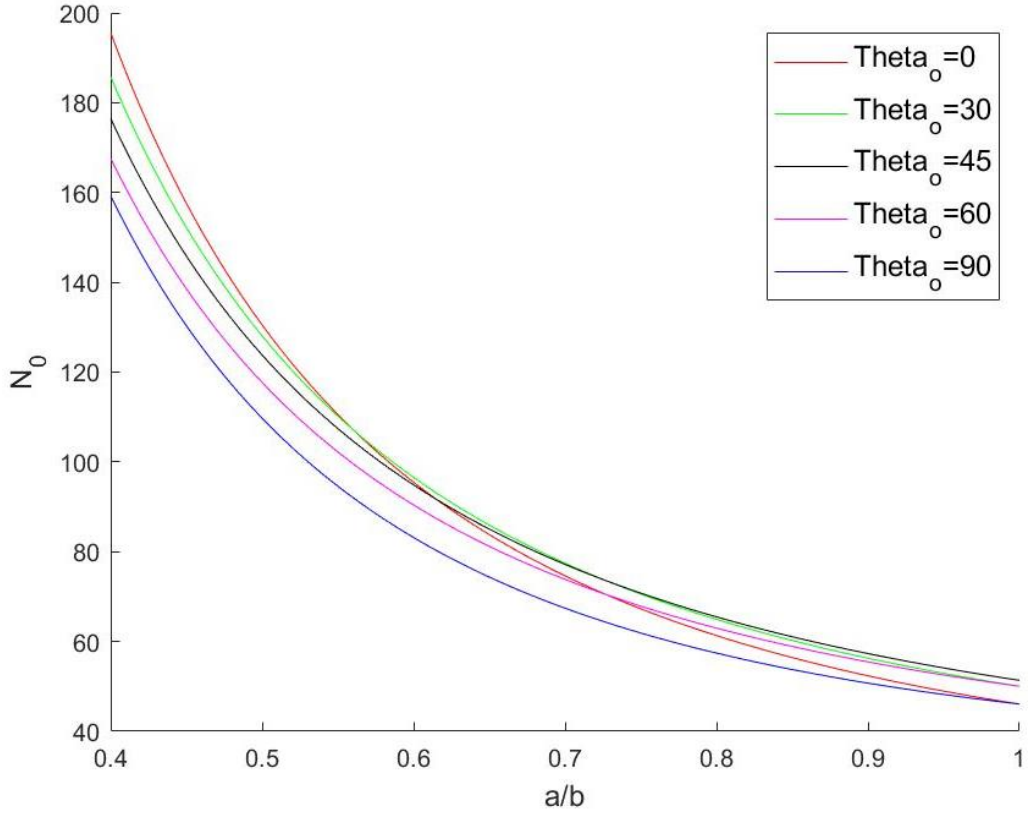

Figure C.1 (c) $W_{gpl_o} = 0.01; 0.4 \leq a/b \leq 1$

$\tau = 0.7; \theta_m = 0°; W_{gpl_m} = 0; Vf_{wp_o} = 0.5; Vf_{wf_o} = 0.275; k_m = 0.5; Vf_{total_m} = 0.55; \alpha_b = 1$

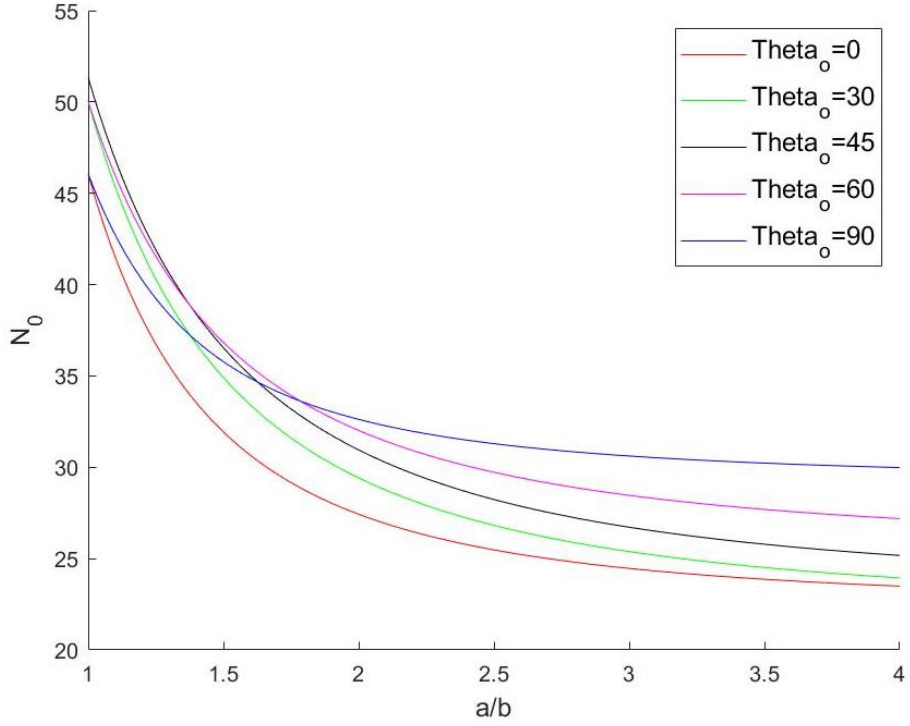

Figure C.1 (d) $W_{gpl_o} = 0.01; 1 \leq a/b \leq 4$

$\tau = 0.7; \theta_m = 0°; W_{gpl_m} = 0; Vf_{wp_o} = 0.5; Vf_{wf_o} = 0.275; k_m = 0.5; Vf_{total_m} = 0.55; \alpha_b = 1$

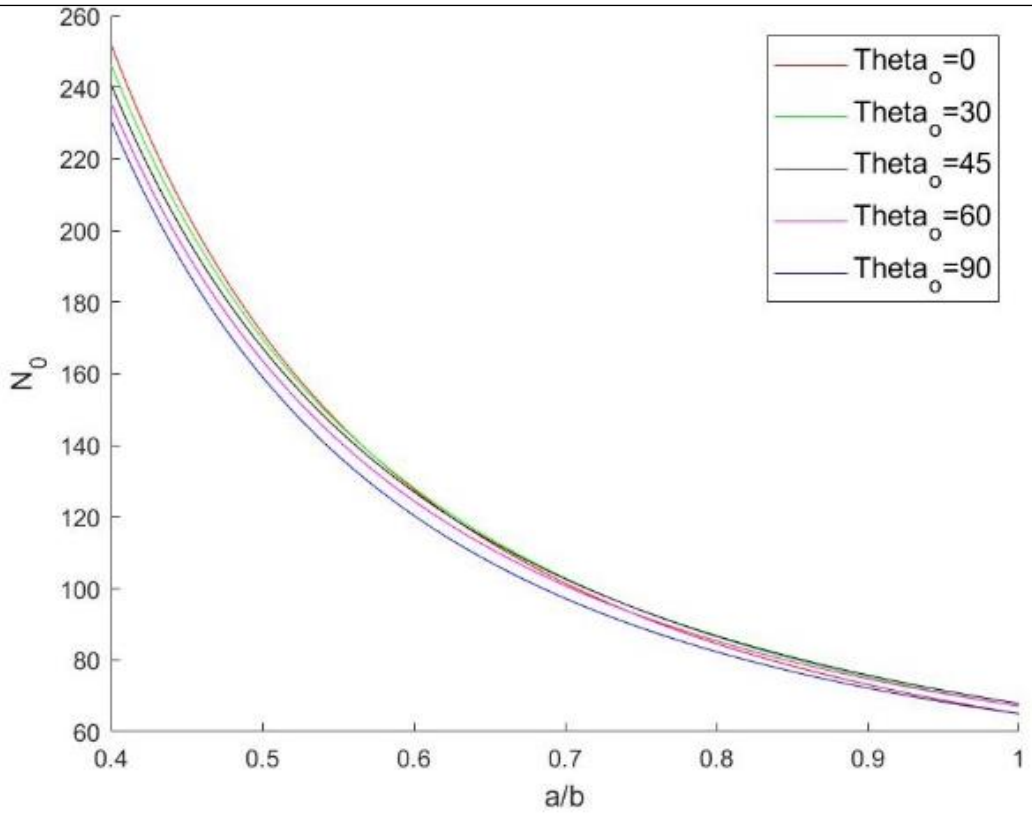

Figure C.1 (e) $W_{gpl_o} = 0.02; 0.4 \leq a/b \leq 1$

$\tau = 0.7; \theta_m = 0°; W_{gpl_m} = 0; Vf_{wp_o} = 0.5; Vf_{wf_o} = 0.275; k_m = 0.5; Vf_{total_m} = 0.55; \alpha_b = 1$

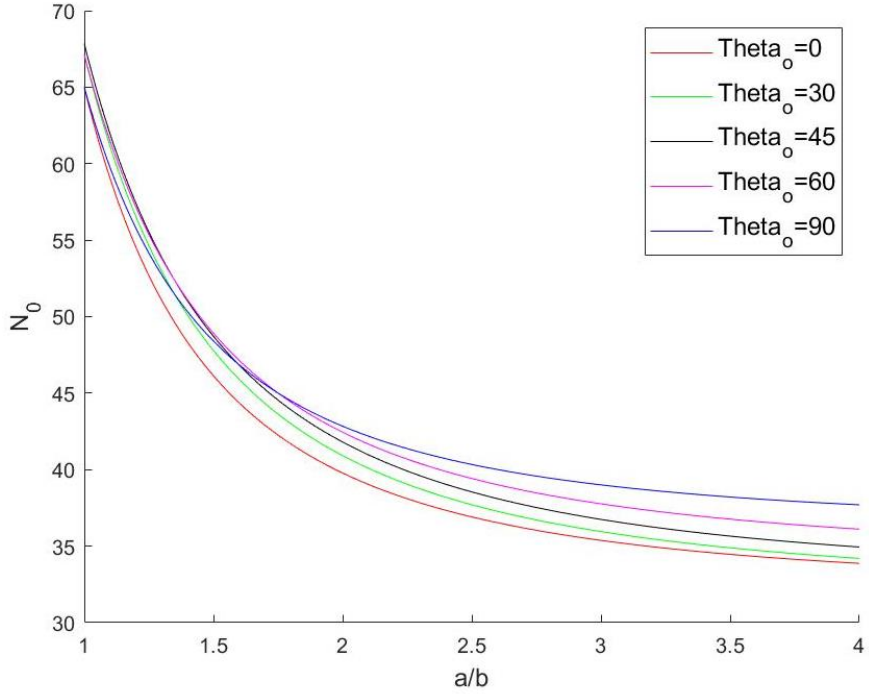

Figure C.1 (f) $W_{gpl_o} = 0.02; 1 \leq a/b \leq 4$

Figure C: Critical buckling load vs. a/b *for different values of* θ_o

Appendix D: Influence of laminate aspect ratio and glass warp-fibre volume fraction

$\tau = 0.7;\ \theta_m = 0°;\ W_{gpl_o} = 0;\ W_{gpl_m} = 0;\ Vf_{wf_o} = 0.275;\ k_m = 0.5;\ Vf_{total_m} = 0.55;\ \alpha_b = 1$

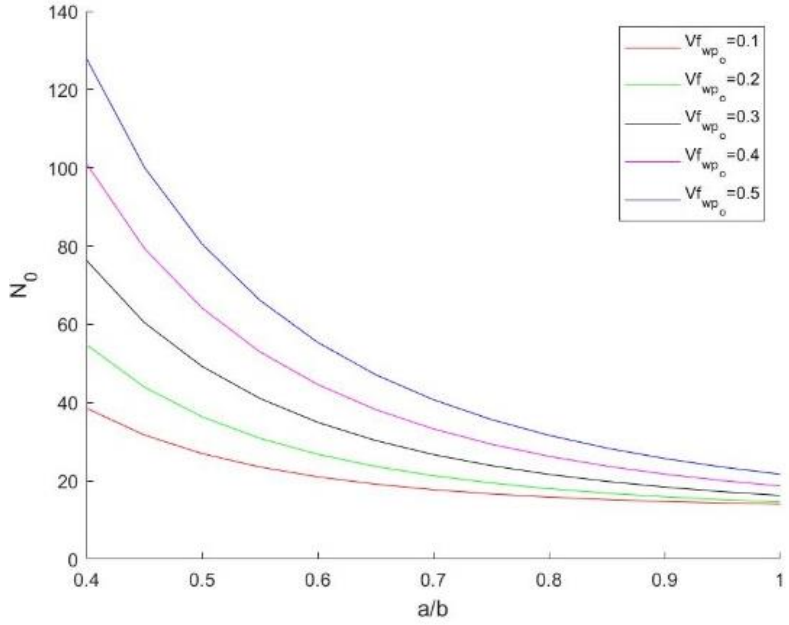

Figure D.1 (a) $\theta_o = 0;\ 0.4 \leq a/b \leq 1$

$\tau = 0.7;\ \theta_m = 0°;\ W_{gpl_o} = 0;\ W_{gpl_m} = 0;\ Vf_{wf_o} = 0.275;\ k_m = 0.5;\ Vf_{total_m} = 0.55;\ \alpha_b = 1$

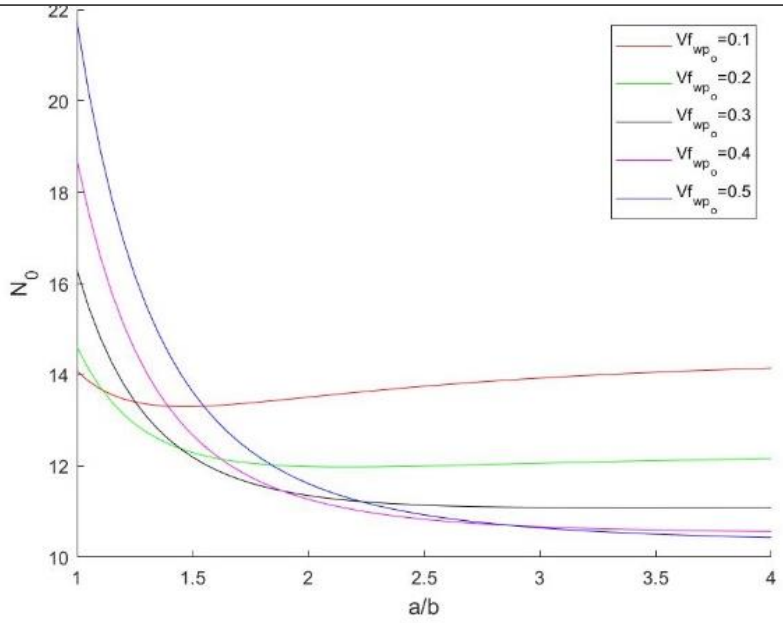

Figure D.1 (b) $\theta_o = 0;\ 1 \leq a/b \leq 4$

$\tau = 0.7; \theta_m = 0°; W_{gpl_o} = 0; W_{gpl_m} = 0; Vf_{wf_o} = 0.275; k_m = 0.5; Vf_{total_m} = 0.55; \alpha_b = 1$

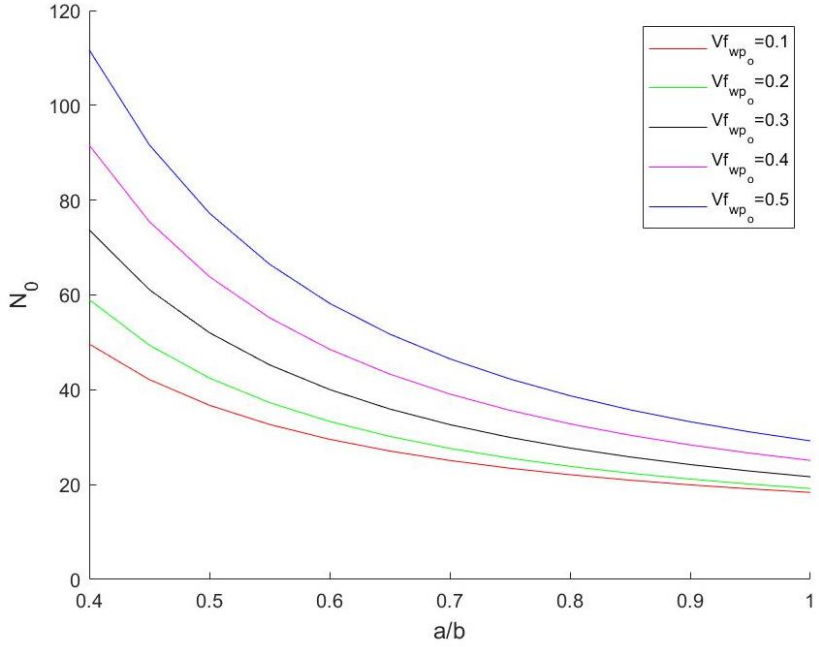

Figure D.1 (c) $\theta_o = 30;\ 0.4 \leq a/b \leq 1$

$\tau = 0.7; \theta_m = 0°; W_{gpl_o} = 0; W_{gpl_m} = 0; Vf_{wf_o} = 0.275; k_m = 0.5; Vf_{total_m} = 0.55; \alpha_b = 1$

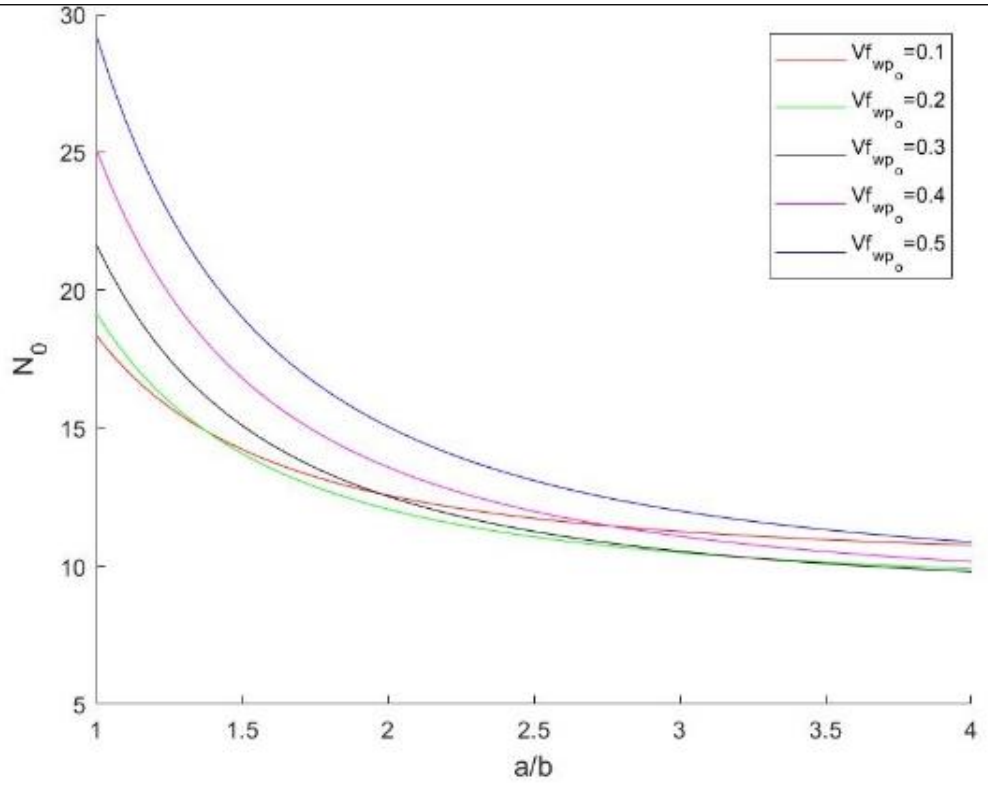

Figure D.1 (d) $\theta_o = 30;\ 1 \leq a/b \leq 4$

Figure D.1: Critical buckling load vs. a/b *for different values of* Vf_{wp_o}

$\tau = 0.7;\ \theta_m = 0°;\ W_{gpl_o} = 0;\ W_{gpl_m} = 0;\ Vf_{wf_o} = 0.275;\ k_m = 0.5;\ Vf_{total_m} = 0.55;\ \alpha_b = 1$

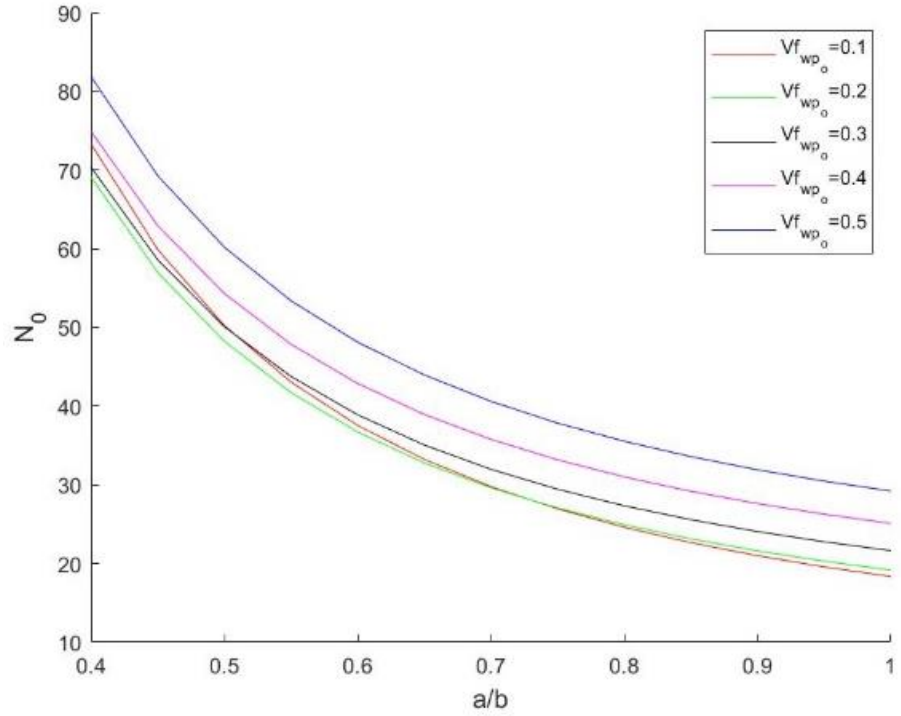

Figure D.2 (a) $\theta_o = 60;\ 0.4 \leq a/b \leq 1$

$\tau = 0.7;\ \theta_m = 0°;\ W_{gpl_o} = 0;\ W_{gpl_m} = 0;\ Vf_{wf_o} = 0.275;\ k_m = 0.5;\ Vf_{total_m} = 0.55;\ \alpha_b = 1$

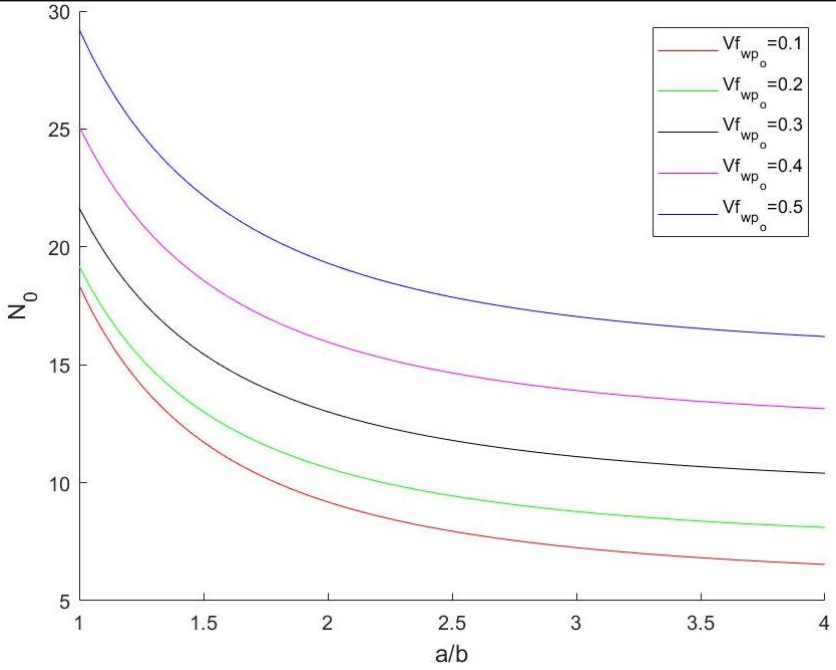

Figure D.2 (b) $\theta_o = 60;\ 1 \leq a/b \leq 4$

$\tau = 0.7; \theta_m = 0°; W_{gpl_o} = 0; W_{gpl_m} = 0; Vf_{wf_o} = 0.275; k_m = 0.5; Vf_{total_m} = 0.55; \alpha_b = 1$

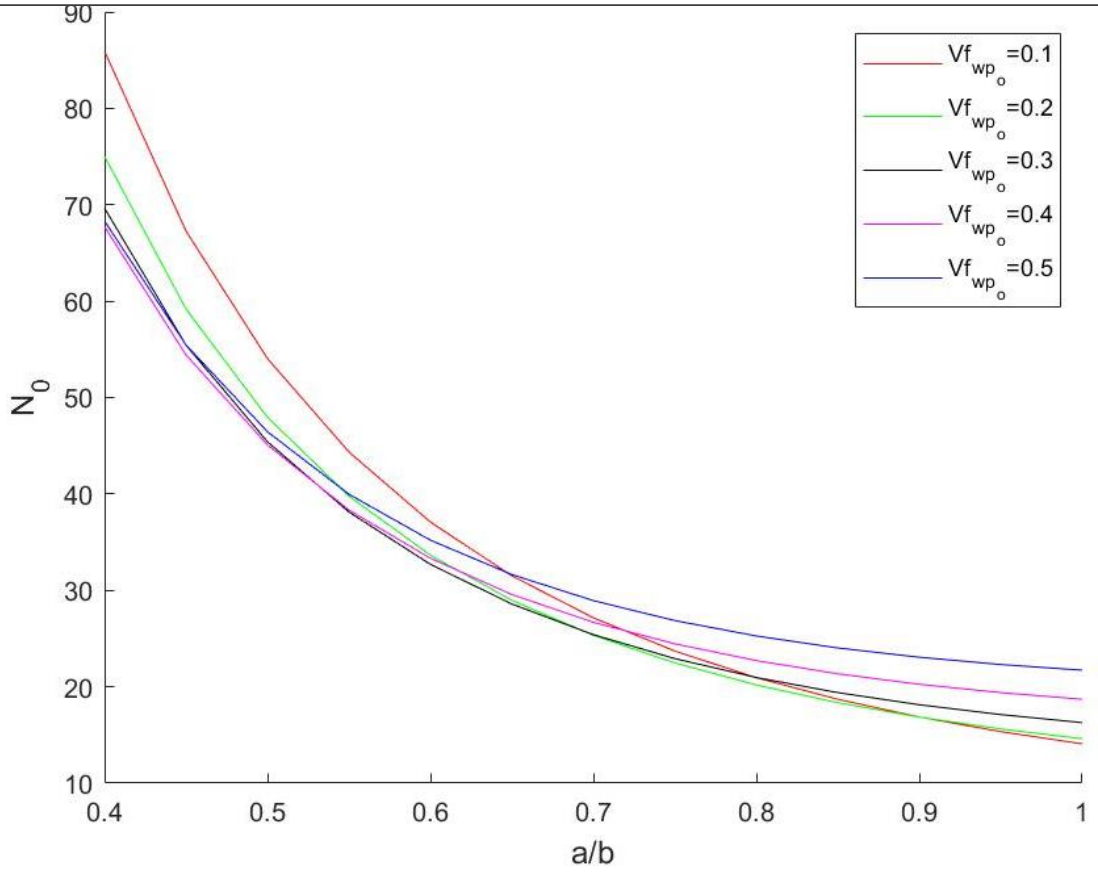

Figure D.2 (c) $\theta_o = 90; 0.4 \leq a/b \leq 1$

$\tau = 0.7; \theta_m = 0°; W_{gpl_o} = 0; W_{gpl_m} = 0; Vf_{wf_o} = 0.275; k_m = 0.5; Vf_{total_m} = 0.55; \alpha_b = 1$

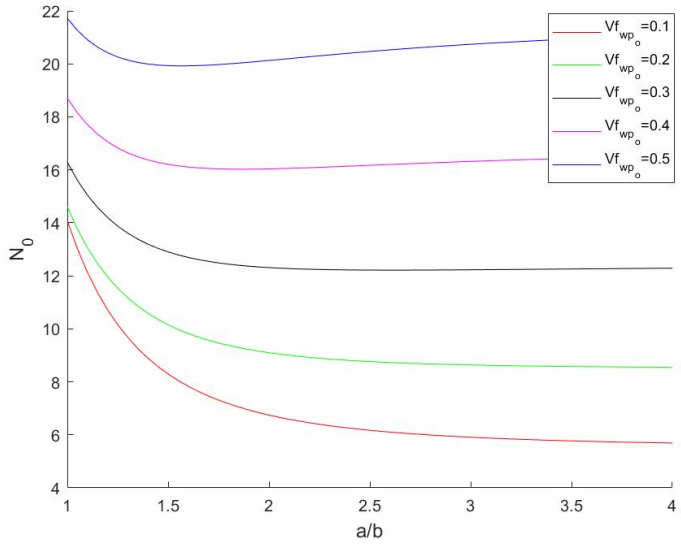

Figure D.2 (d) $\theta_o = 90; 1 \leq a/b \leq 4$

Figure D.2: Critical buckling load vs. a/b *for different values of* Vf_{wp_o}

$\tau = 0.7;\ \theta_m = 0°;\ W_{gpl_o} = 0.01;\ W_{gpl_m} = 0;\ Vf_{wf_o} = 0.275;\ k_m = 0.5;\ Vf_{total_m} = 0.55;\ \alpha_b = 1$

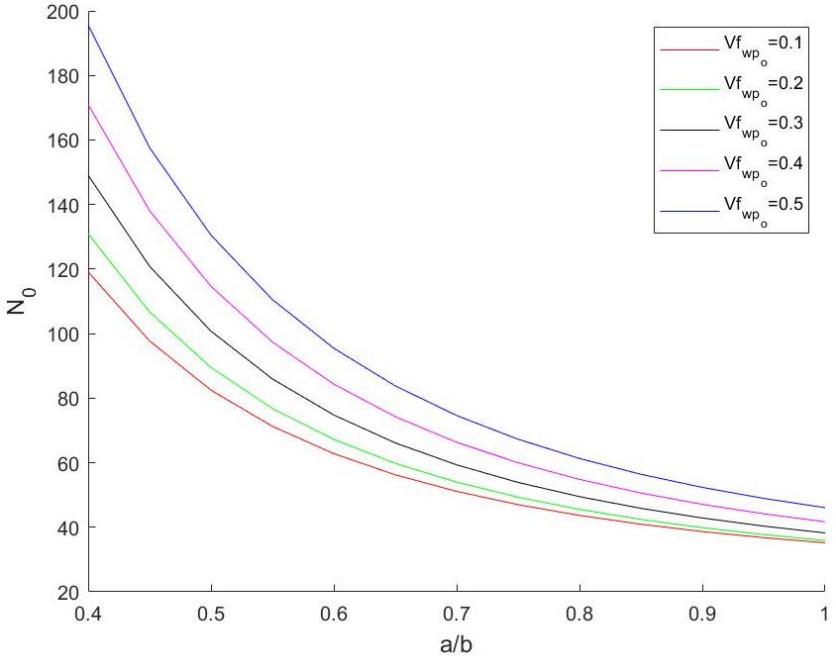

Figure D.3 (a) $\theta_o = 0;\ 0.4 \leq a/b \leq 1$

$\tau = 0.7;\ \theta_m = 0°;\ W_{gpl_o} = 0.01;\ W_{gpl_m} = 0;\ Vf_{wf_o} = 0.275;\ k_m = 0.5;\ Vf_{total_m} = 0.55;\ \alpha_b = 1$

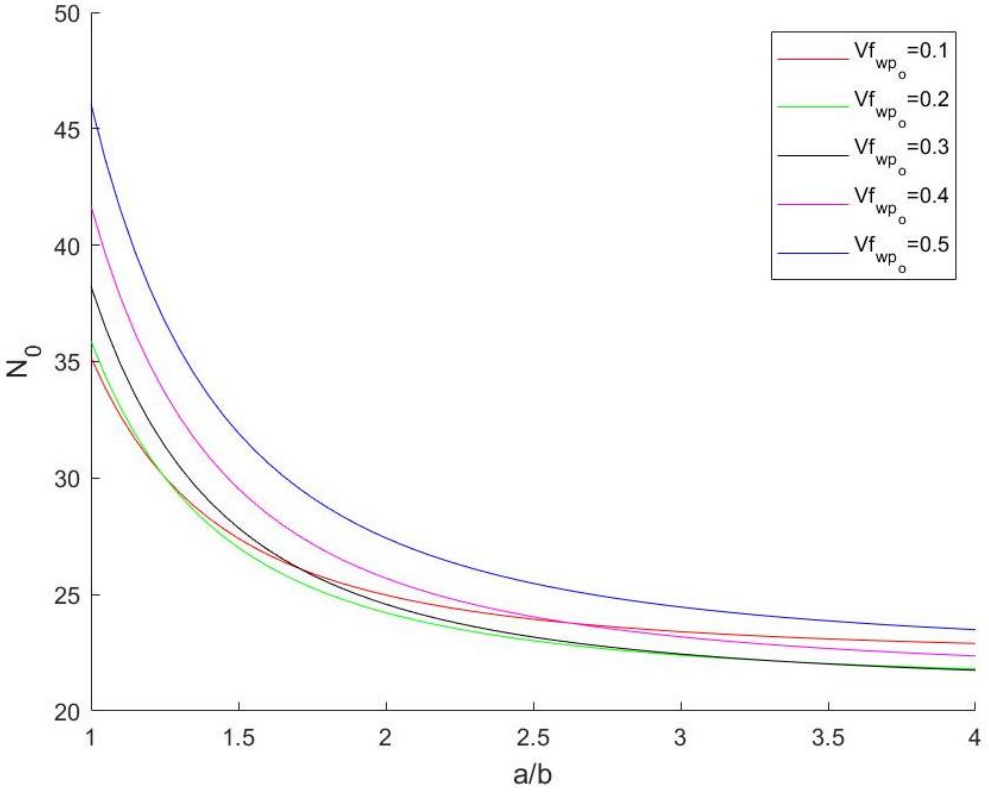

Figure D.3 (b) $\theta_o = 0;\ 1 \leq a/b \leq 4$

$\tau = 0.7;\ \theta_m = 0°;\ W_{gpl_o} = 0.01;\ W_{gpl_m} = 0;\ Vf_{wf_o} = 0.275;\ k_m = 0.5;\ Vf_{total_m} = 0.55;\ \alpha_b = 1$

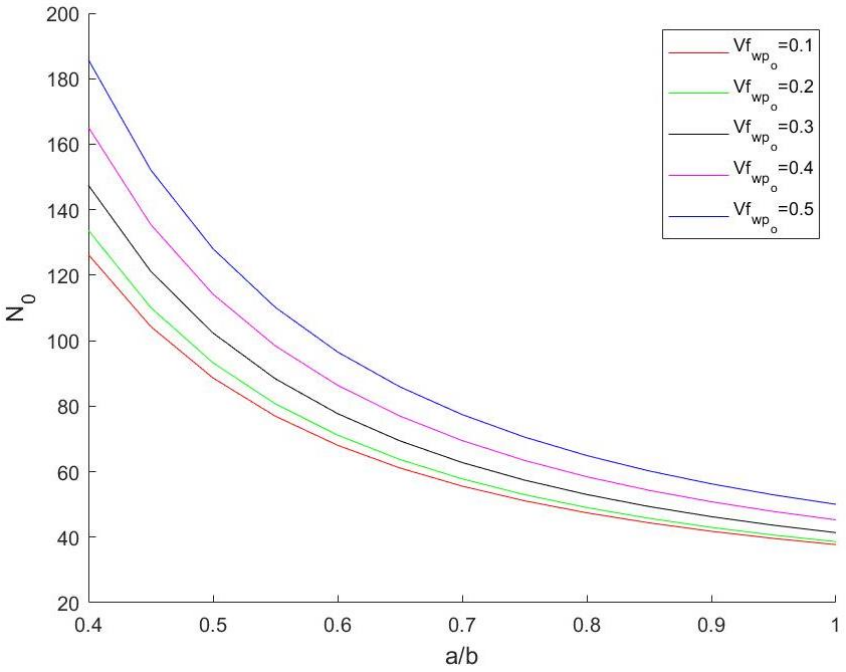

Figure D.3 (c) $\theta_o = 30;\ 0.4 \leq a/b \leq 1$

$\tau = 0.7;\ \theta_m = 0°;\ W_{gpl_o} = 0.01;\ W_{gpl_m} = 0;\ Vf_{wf_o} = 0.275;\ k_m = 0.5;\ Vf_{total_m} = 0.55;\ \alpha_b = 1$

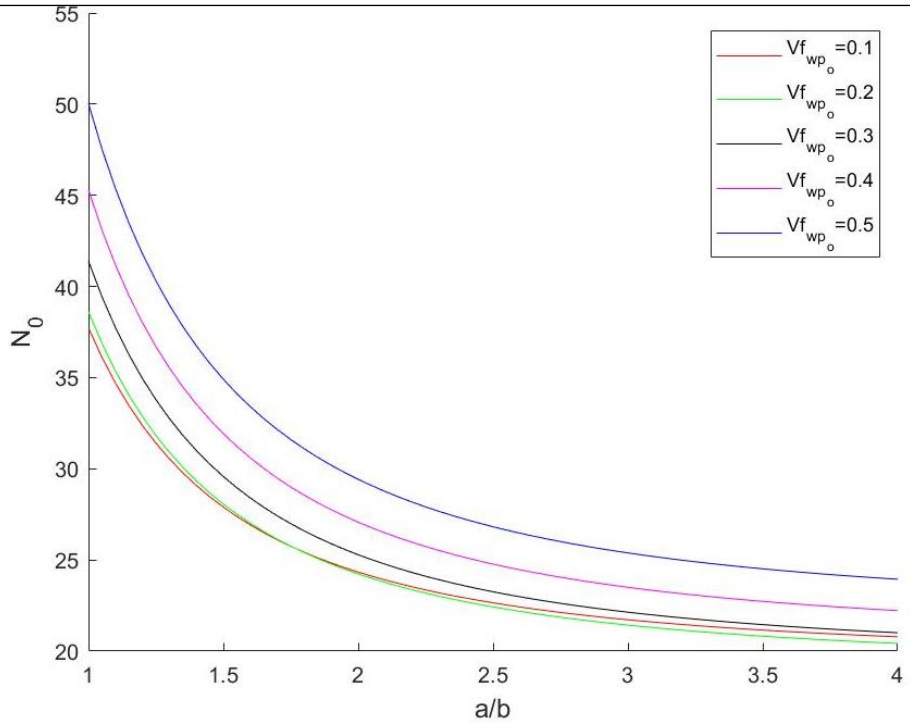

Figure D.3 (d) $\theta_o = 30;\ 1 \leq a/b \leq 4$

Figure D.3: Critical buckling load vs. a/b *for different values of* Vf_{wp_o}

$\tau = 0.7;\ \theta_m = 0°;\ W_{gpl_o} = 0.01;\ W_{gpl_m} = 0;\ Vf_{wf_o} = 0.275;\ k_m = 0.5;\ Vf_{total_m} = 0.55;\ \alpha_b = 1$

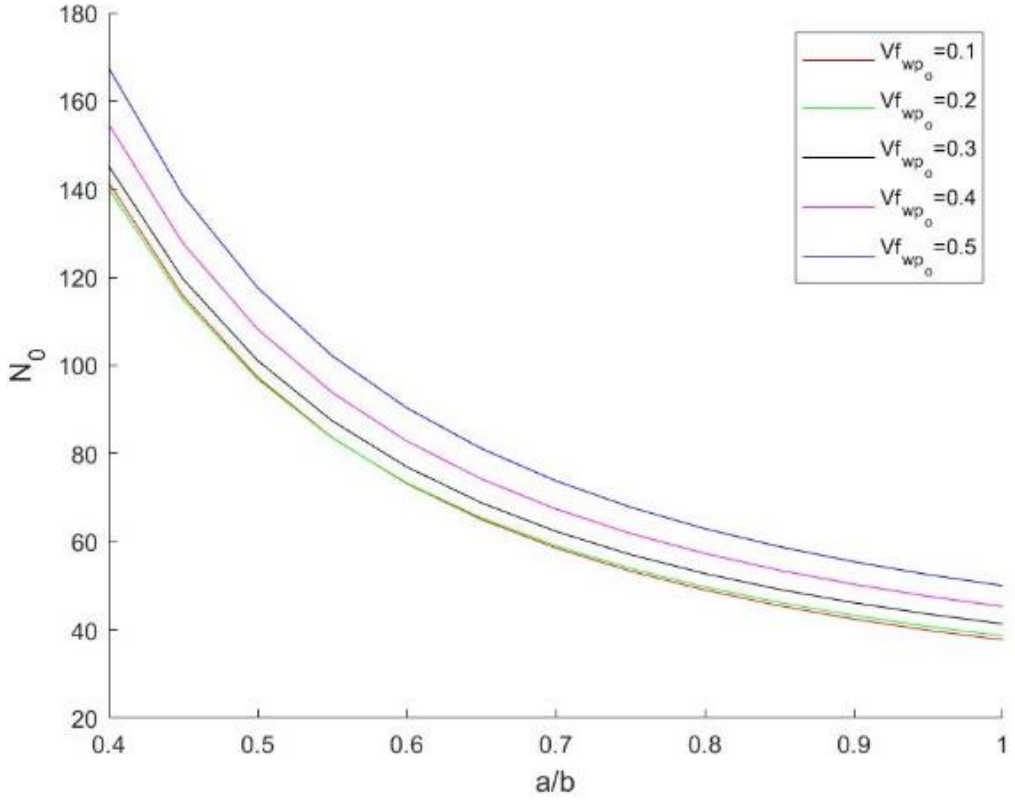

Figure D.4 (a) $\theta_o = 60;\ 0.4 \leq a/b \leq 1$

$\tau = 0.7;\ \theta_m = 0°;\ W_{gpl_o} = 0.01;\ W_{gpl_m} = 0;\ Vf_{wf_o} = 0.275;\ k_m = 0.5;\ Vf_{total_m} = 0.55;\ \alpha_b = 1$

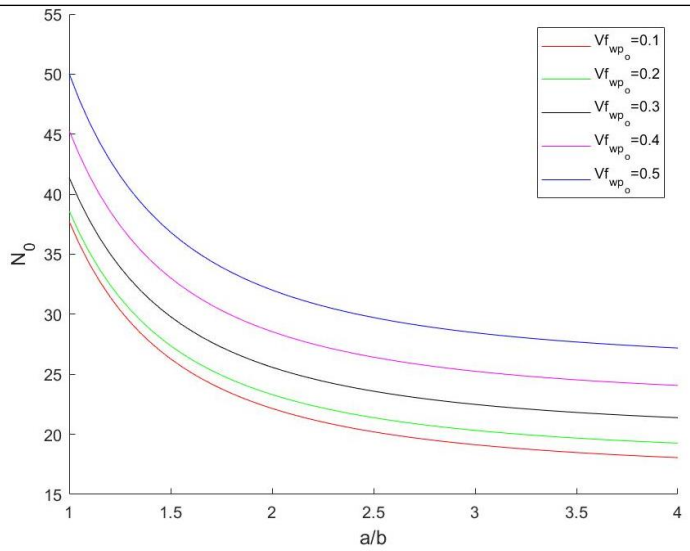

Figure D.4 (b) $\theta_o = 60;\ 1 \leq a/b \leq 4$

$\tau = 0.7; \theta_m = 0°; W_{gpl_o} = 0.01; W_{gpl_m} = 0; Vf_{wf_o} = 0.275; k_m = 0.5; Vf_{total_m} = 0.55; \alpha_b = 1$

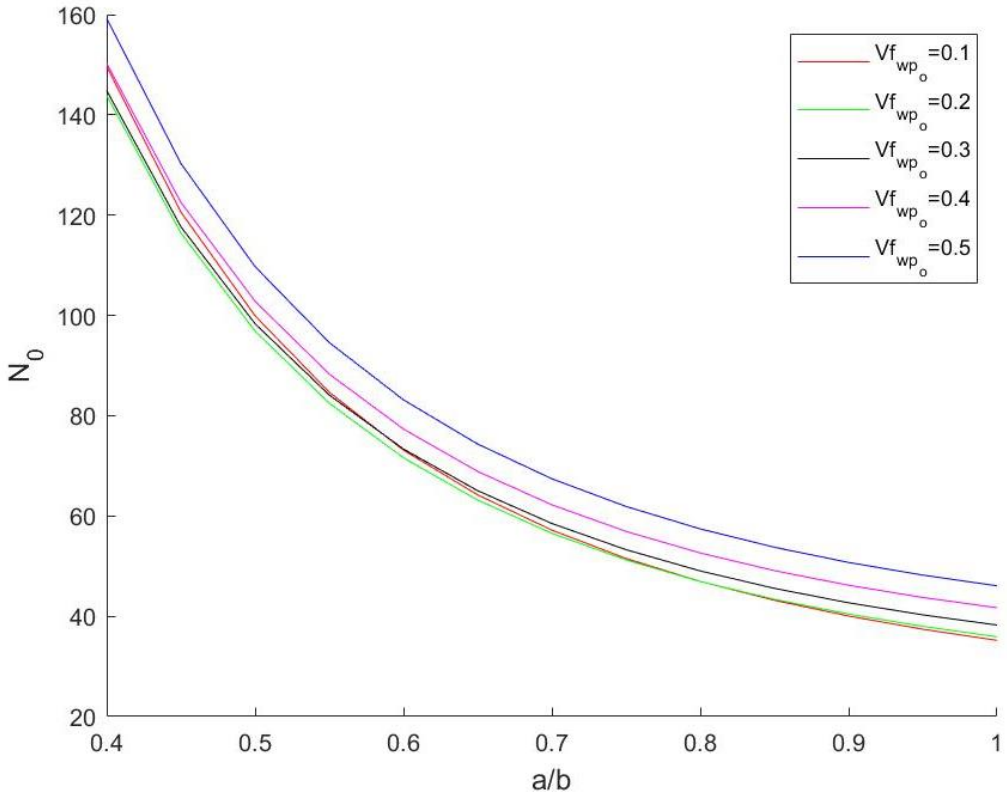

Figure D.4 (c) $\theta_o = 90;\ 0.4 \leq a/b \leq 1$

$\tau = 0.7; \theta_m = 0°; W_{gpl_o} = 0.01; W_{gpl_m} = 0; Vf_{wf_o} = 0.275; k_m = 0.5; Vf_{total_m} = 0.55; \alpha_b = 1$

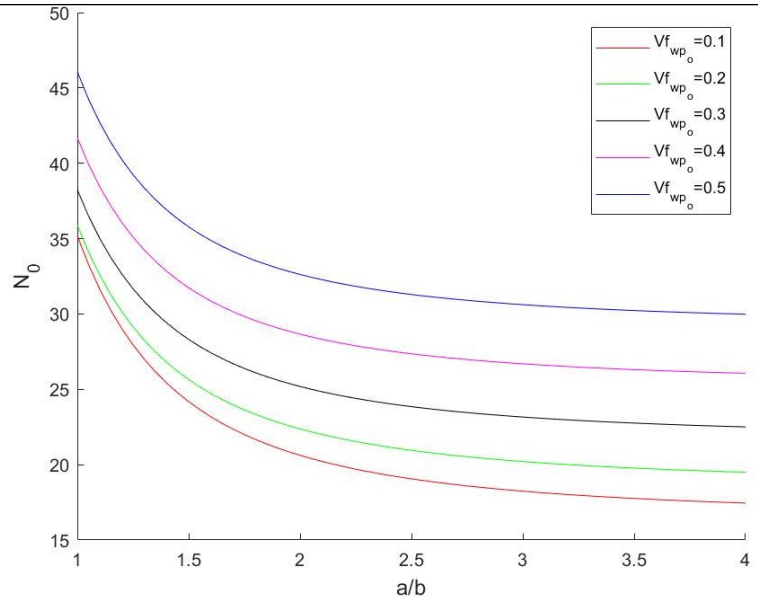

Figure D.4 (d) $\theta_o = 90;\ 1 \leq a/b \leq 4$

Figure D.4: Critical buckling load vs. a/b *for different values of* Vf_{wp_o}